Applications of solid-state NMR spectroscopy to a reactively processed polyether-polyamide block copolymer

Stefan Friebel

To

Robert and Ingrid
Silvia, Jonas and Niklas

Applications of Solid-State NMR Spectroscopy to a Reactively Processed Polyether-Polyamide Block Copolymer

by
Stefan Friebel
1995

Supervisor
Professor Robin K. Harris

University of Durham
South Road
Science Laboratories
Durham, DH1 3LE

Abstract

Solid-state NMR has become a powerful tool for studies of structural and physical properties of polymers. This thesis investigates a technically produced block copolymer by means of solid-state NMR. The properties which are of principal interest are the heterogeneity on various scales ranging from molecular (unit cell) to macroscopic (morphology), and molecular motion in solids.

The important question of cross polarisation is addressed. Quantification of depolarisation experiments will bring some more insight into the origins of the polarisation transfer. Basically a model by Müller, Kumar and Ernst has been used to describe the polarisation transfer. Novel results are reported in this area.

^{1}H spin-lattice relaxation measurements, both in the laboratory and on-resonance rotating frames of resonance are applied to the block copolymer. An attempt is made to address the relation of the observed relaxation times and the macroscopic properties. The behaviour of the observed and the intrinsic properties of the various regions of the heterogeneous system in the presence of spin diffusion is investigated. The system is simulated by a computer model, which allows quantification of the dimensions of the different regions. Comparison with small-angle X-ray diffraction measurements illustrates the accuracy of this new powerful technique.

Acknowledgements

I would like to express my gratitude to my supervisor Professor Robin Harris, for his help and encouragement during the past three years. In particular, without his efforts to find finances for my support, I would not have been able to take the opportunity to carry out my Ph.D. work here in Durham. Also, I thank Professor A. Johnson and Dr. S-W Tsui for helpful technical discussions and for providing the material I studied in this collaborative work. Other thanks go to Dr. Alan Kenwright and Barry Say for the endless discussions and the time they spent with me (also for tuition in how to make jokes-mainly about me);
to Peter Clarke for being sane in my first year and for his patient help in my most difficult time in England;
to David Apperley and Nicola Davis for the spectra acquired on the VXR300; to Race Yeung, reducing my pile of data sheets, by applying a neat graphic-routine on the Archimedes computer; to Elizabeth Wood for the prompt development of my photo prints;
to Graham Almond and Abdul Khaliq for all the chat and insight to Islam;
to the SERC and IRC for grants to me, and to everyone else who helped me along the way.

Chapter 1

1. Introduction

1.1. The Scope of the Work

In the last fifteen years solid-state nuclear magnetic resonance (NMR) has become an important tool for structural and morphological analysis in solids. This is largely because of the development of new techniques which allow the observation of high-resolution spectra of solids. In favourable circumstances these techniques can yield spectra which appear similar to those previously available from non-viscous liquids and solutions. Since the apparent physical nature of solids is naturally more complex in NMR terms than that in liquids, the experimental demands to obtain high-resolution spectra are higher than those in liquids.

In this thesis a polyetheramide block polymer produced by a Rejection Injection Moulding (RIM) process is investigated. This technique is very important nowadays, because of its low production cost of the polymers. The work will show that solid-state NMR is capable of looking at a completely unknown, highly complex polymer system. Known standard, modified and novel techniques have been used to show that solid-state NMR can be a standard method for analysis in solids. The work has been carried out under the Interdisciplinary Research Centre (IRC) scheme, in collaboration with the University of Bradford. Professor Anthony Johnson and Dr. S-W. Tsui were responsible for producing the material and for standard analytical work, like Differential Scanning Calorimetry

(DSC), DTMA and optical microscopy measurements. Additionally Small-angle X-ray scattering experiments were carried out in Durham. The results from these measurements were used as additional information, and brought in conjunction with the solid-state NMR results. The aim was to select as much data as possible from the material so as to obtain a fairly accurate model of the polymer system, of which hardly was anything known, although it is already used in the automotive industry.

Chapter 2

2. Theory

2.1 Introduction

The detection of nuclear magnetic resonance by Bloch et al. [1] and Purcell and co-workers [2] in 1946 has led to the development of one of the most powerful spectroscopic techniques known today. The reason is that, besides the applied external magnetic field, a nuclear spin also experiences extra local magnetic fields, which are due to surrounding electron clouds and other spins, leading to a chemical shift. These local fields differ for nuclei located at chemically different positions in a molecule. The result is that a NMR spectrum often consists of several lines, which can be considered to be fingerprints of the material under investigation and also assist in clarifying its molecular structure.

NMR has been especially successful in liquids and liquid-like materials, where fast molecular tumbling averages out the anisotropies in the local fields, resulting in well-resolved isotropic NMR resonances. NMR for liquids has become a standard routine analytical technique, which can be found in nearly every research laboratory nowadays.

Initially the development of solid-state NMR was less dramatic. Originally, for reasons of sensitivity, attention was focused mainly on ^{1}H-NMR. However, problems arise because the anisotropies in the local fields, which are no longer averaged out, broaden the spectral line to

such an extent that no spectral resolution is observed. The resulting spectra often consist of a single broad, featureless line, which, except for special cases, such as isolated spin pairs or methyl groups, does not provide much information. Therefore initial solid-state NMR investigations concentrated on the measurement of nuclear relaxation times as a function of the external field and/or the temperature. These types of study provide information on the mobility of a part of the molecule such as the rotation of methyl groups or motion of parts of the molecular chains in polymers.

2.2. The Problem of obtaining High-resolution Spectra of Solids

The problem of obtaining a high-resolution ^{13}C NMR spectrum for a typical organic solid is essentially two-fold. The following considerations are, of course, valid for all rare spin-$\frac{1}{2}$ nuclei. The first part of the problem is to remove those interactions present in a solid-state system which lead to broadening of the ^{13}C resonances. Considering an ^{1}H-atom attached to a carbon-13 atom, the main source of line broadening is the ^{13}C-^{1}H dipolar coupling, which is generally of the order of $\approx 10^4$ Hz. Even for carbons with no directly-bonded protons, long-range ^{13}C,^{1}H dipolar interactions (i.e. from the next-nearest neighbours) can cause a frequency spread of up to 5 kHz measured for a single carbon atom.

Another interaction contributing to line broadening is, as mentioned above, the chemical shift anisotropy. This

interaction also can cause line broadening up to 100 ppm. Note that the origin of chemical shift anisotropy is only due to the different relative orientations of the molecular axes to the $\vec{B}_0$-field.

The second part of the problem is to overcome the inherently-low ^{13}C sensitivity and typically-long (1-100s) ^{13}C spin-lattice relaxation times, which make the direct acquisition of ^{13}C-spectra of solids prohibitively time-consuming in many cases. To achieve more insight in those interactions causing line broadening it is necessary to understand their nature. The following section will explain them in more detail.

2.3. Basic Interactions of a Spin-½ System in a Solid

It is assumed that the interactions of the spins with the external magnetic field dominate all other interactions (*high-field approximation*) and that the energy associated with the lattice temperature is large compared to the Zeeman energy (*high-temperature approximation*).

The nuclei of a spin system under investigation are characterised by their magnetic moment $\vec{\mu}$, angular momentum operator $\hbar\hat{I}$, gyromagnetic ratio γ_I, and Larmor frequency ω_I. If this spin system is interacting with another spin-½ system, which is not measured, the respective parameters of this system will be $\vec{\mu}_S, \vec{S}, \gamma_S, \omega_S$.. If the solid is placed in an external magnetic field, $\vec{B}_0$, directed along

the z-axis of the laboratory frame, then the spin Hamiltonian, H, describing the interactions of the I-spins with $\vec{B}_0$ and their surroundings is given by

$$H = H_Z + H_{CS} + H_{D,II} + H_{D,IS} + H_J + H_{rf} \qquad (2.1)$$

were H_Z represents the Zeeman interaction, H_{CS} the chemical shift, $H_{D,II}$ the dipolar interaction among I-spins, $H_{D,IS}$ the dipolar interaction between the I- and S-spins, H_J the indirect (electron-mediated) interaction, and H_{rf} the interaction with the applied rf field.

2.3.1. Zeeman Interaction

The Zeeman interaction occurs between the magnetic moment of the nucleus and the applied magnetic field B_0, yielding $2I+1$ energy levels (where $\hbar\hat{I}$ is the nuclear spin quantum number) of separation $h\omega_0 = \gamma h\vec{B}_0$. The Hamiltonian may be written as

$$H_Z = -\sum_{k=1}^{N} \gamma_{Ik}\hbar\hat{I}\vec{B}_0 \qquad (2.2)$$

were γ_{Ik} denotes the gyromagnetic ratio of spin k and N is the total number of I spins.

The interaction is linear with the applied magnetic field. Therefore a larger separation of the energy levels occurrs at higher fields with a corresponding increase in the population difference between them and an increase in the signal/noise ratio (S/N) of the spectrum.

2.3.2. Chemical Shift, H_{CS}

The chemical shift arises from loop currents in the electron clouds surrounding the nuclei that are induced by the external field $\vec{B}_0$. The currents produce a secondary field at the site of a nucleus with a magnitude proportional to $\vec{B}_0$. The corresponding Hamiltonian can be written as

$$H_{CS} = \gamma_I \hbar \vec{I} \hat{\sigma} \vec{B}_0 \qquad (2.3)$$

Where $\hat{\sigma}$ is the chemical shift tensor.

Since this interaction involves the surrounding electrons, it is the most sensitive interaction to the geometry and identity of the other atoms in the vicinity of a particular nucleus and will usually be the most important measurable in NMR studies.

2.3.3. Indirect (Spin-Spin) Interaction H_J

The spin-spin coupling interaction between a pair of spins may represented as

$$H_{J,II} = \sum_{i>j} \hbar \hat{I}_i \hat{J}_{II_{ij}} \hat{I}_j \qquad (2.4)$$

For unlike spins I and S, $H_{J,IS}$ is given by

$$H_{J,IS} = \sum_i \hbar \hat{I}_i \hat{J}_{IS_i} \hat{S}_i \qquad (2.5)$$

The interaction is field independent and is usually smaller than the other interactions under consideration.

2.3.4. Dipolar Interaction

Because of the importance of the dipolar interaction in solid-state NMR, this interaction will be explained in more detail.

Any two dipole moments will interact directly through space to produce mutually perturbed energy states. The strength of this interaction is inversely proportional to the cube of the distance between the origins of the moments. Therefore only dipoles which are relatively adjacent in space will have a significant interaction.

The classical interaction energy E between two magnetic moments $\vec{\mu}_1$ and $\vec{\mu}_2$ is

$$E = \frac{\mu_0}{4\pi}\left[\frac{\vec{\mu}_1\vec{\mu}_2}{\vec{r}^3} - \frac{3(\vec{\mu}_1\vec{r})(\vec{\mu}_2\vec{r})}{\vec{r}^5}\right] \qquad (2.6)$$

were $\vec{r}$ is the radius vector from $\vec{\mu}_1$ and $\vec{\mu}_2$, μ_0 is the permeability of free space, and $\vec{\mu}_i$ is the i^{th} dipole moment.

In any real system involving many nuclei, it is necessary to sum the interactions over all pairs [3]. This extension is straightforward. For the quantum mechanical Hamiltonian eqn. (2.2) is simply taken and $\vec{\mu}_1$, $\vec{\mu}_2$ are treated as operators as usual:

$$\hat{\mu}_i = \gamma_i \hbar \hat{I}_1 \qquad (2.7)$$

were $\hbar\hat{I}$ is the spin angular momentum operator of the nucleus. The general dipolar contribution to the Hamiltonian for N spins then becomes

$$H_D = \frac{1}{2}\frac{\mu_0}{4\pi}\sum_{j=1}^{N}\sum_{k=1}^{N}\left[\frac{\hat{\mu}_j\hat{\mu}_k}{\bar{r}^3} - \frac{3(\hat{\mu}_j\bar{r}_{jk})(\hat{\mu}_k\bar{r}_{jk})}{\bar{r}^5}\right] \tag{2.8}$$

were the $\frac{1}{2}$ is needed, since the sums over j and k would count each pair twice and where, of course, terms with j=k were excluded.

By writing $\bar{\mu}_1$ and $\bar{\mu}_2$ in component form and omitting the subscripts from $\bar{r}$ it follows from Eqn. (2.2) that the dipolar Hamiltonian will contain terms such as

$$\begin{aligned}&\gamma_1\gamma_2\hbar^2\hat{I}_{1x}\hat{I}_{2x}\frac{1}{\bar{r}^3}\\ &\gamma_1\gamma_2\hbar^2\hat{I}_{1x}\hat{I}_{2x}\frac{xy}{\bar{r}^5}\end{aligned} \tag{2.9}$$

Expressing $\hat{I}_{1x}$ and $\hat{I}_{1y}$ in terms of the raising and lowering operators $\hat{I}_1^+$ and $\hat{I}_1^-$, respectively, and the rectangular coordinates x,y,z in terms of spherical coordinates $\bar{r}$, θ, ϕ, (Fig. 2.1.)

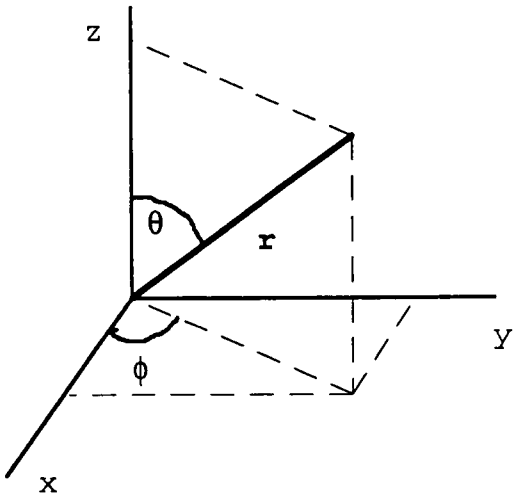

Fig. 2.1 Relationship between rectangular coordinates x,y,z (describing the position of nucleus 2 relative to nucleus 1) and the polar coordinates $\bar{r}$, θ, ϕ

the Hamiltonian can be written in a form that is particular convenient for computing matrix elements [3].

$$H_D = \frac{\mu_0}{4\pi}\frac{\gamma_1\gamma_2\hbar^2}{\vec{r}^3}(A + B + C + D + E + F) \tag{2.10}$$

where

$$\begin{aligned} A &= \hat{I}_{1Z}\hat{I}_{2Z}\left(1 - 3\cos^2\theta\right) \\ B &= -\frac{1}{4}\left(\hat{I}_1^+\hat{I}_2^- + \hat{I}_1^-\hat{I}_2^+\right)\left(1 - 3\cos^2\theta\right) \\ C &= -\frac{3}{2}\left(\hat{I}_1^+\hat{I}_{2Z} + \hat{I}_{1Z}\hat{I}_2^+\right)\sin\theta\cos\theta e^{-i\phi} = D^* \\ E &= -\frac{3}{4}\hat{I}_1^-\hat{I}_2^-\sin^2\theta e^{2i\phi} = F^* \end{aligned} \tag{2.11}$$

In the above expressions

$$\begin{aligned} \hat{I}_+ &= \hat{I}_X + i\hat{I}_Y \\ \hat{I}_- &= \hat{I}_X - i\hat{I}_Y \end{aligned} \tag{2.12}$$

The constant $d = \frac{\mu_0}{4\pi}\frac{\gamma_1\gamma_2\hbar^2}{\vec{r}^3}$ is known as the dipolar coupling constant. Each of the terms A to F contains a spin factor and a geometrical factor. The time-average values of the terms C to F are all zero for random thermal motion of molecules in liquids. These terms do not therefore lead to the splitting or broadening of NMR line in liquids, but are active in nuclear relaxation.

Further, terms A and B contain the geometrical factor $\left(1 - 3\cos^2\theta\right)$. This term vanishes too for random thermal motion of molecules, because the time average $\left\langle 1 - 3\cos^2\theta\right\rangle = 0$, with the result that in liquids the whole dipolar interaction is averaged to zero.

To determine the effects of dipolar interactions in solids, it is necessary to calculate the eigenvalues of the total Hamiltonian

$$H = H_Z + H_D \tag{2.13}$$

The exact way of doing so would be to diagonalise the sum of matrix representations. However, it is more appropriate to use time-independent perturbation theory and treat H_D as a small perturbation on the Zeeman Hamiltonian. It is necessary to consider two distinct cases:

1. $\gamma_1 = \gamma_2$, which means the two spins are identical. This is the so-called homonuclear case
2. $\gamma_1 \neq \gamma_2$, the heteronuclear case

However, perturbation theory is only legitimate when all eigenvalues of H_Z are much larger than the eigenvalues of H_D .

In order to truncate the Hamiltonian H_D, it has to be considered which terms in (2.11) contribute to each of the elements of the matrix $\{H_D\}$. A straightforward calculation shows that in the interaction frame A and B remain time-independent, resulting in first-order energy shifts [4] and that the C to F terms become time-dependent with frequencies ω_I (C,D) and ω_I (E,F), respectively causing second-order admixtures of eigenfunctions and/or relaxation transitions.

It follows from (2.11) that the B term is responsible for the so-called flip-flop transitions, where spin I flips, e.g., from a state parallel to $\vec{B}_0$, simultaneously accompanied by a flop of spin 2 in the opposite direction. Especially for abundant spin species, where the like-spin dipolar interactions are strong, the flip-flop term gives

rise to efficient spin-diffusion and homogeneous line-broadening.

However, the magnitude of the perturbation produced by each term is inversely dependent on the energy difference between the Zeeman spin-states it affects. Thus, to a good approximation it is only necessary to consider those terms which affect iso-energetic Zeeman spin-states. This will, strictly speaking, include only term A, which affects only discrete spin states. It could also include term B if the spin states $/\alpha\beta\rangle$ and $/\beta\alpha\rangle$ are iso-energetic. This, of course, will only occur if the two nuclei are of the same isotope. The truncated form of the dipolar Hamilonian thus obtained is called the secular Hamiltonian. The first-order secular part of the heteronuclear $H_{D,12}$, $H_{D,12}^{sec}$ is determined by the A term only [5]

$$H_{D,12}^{sec} = \frac{\mu_0}{4\pi}\frac{\gamma_1\gamma_2\hbar^2}{\bar{r}^3}\hat{I}_{1Z}\hat{I}_{2Z}\left(1 - 3\cos^2\theta\right) \qquad (2.14)$$

Analoguous considerations for the homonuclear case yield

$$H_{D,12}^{sec} = \frac{\mu_0}{4\pi}\frac{\gamma_1\gamma_2\hbar^2}{\bar{r}^3}\left[\hat{I}_{1Z}\hat{I}_{2Z} + \frac{1}{4}\left(\hat{I}_{1+}\hat{I}_{2-} + \hat{I}_{1-}\hat{I}_{2+}\right)\right]\left(1 - 3\cos^2\theta\right) \qquad (2.15)$$

because now the B term also operates between iso-energetic Zeeman spin-states

2.3.5. Shielding Anisotropy

Shielding anisotropy might be a problem in high-resolution solid-state NMR, because of its line-broadening character, but on the other hand it contains valuable

structural information on the molecule under investigation.

The resonance frequency of a particular nucleus depends on both the type of nucleus (^{1}H, ^{13}C, ^{29}Si, etc.) and the electronic environment of that nucleus. The surrounding electrons shield the nucleus from the external magnetic field. The electronic environment is usually spatially dependent in a molecule, and therefore induces different shieldings for different directions in the molecule. The single-valued chemical shifts observed in solution are in reality isotropic averages of anisotropic shieldings resulting from rapid molecular tumbling.

In solids, however, this interaction is usually not averaged because of the restricted mobility. The shielding at a given nucleus may be expressed in terms of a shielding tensor, $\hat{\sigma}$, where

$$B_{loc} = \hat{\sigma}\vec{B} \qquad (2.16)$$

The orientation dependence of $\vec{B}_{loc}$ is implicit in $\hat{\sigma}$.
In the general case the observed shielding constant is denoted $\hat{\sigma}_{zz}$ and is a linear combination of the principal components, $\hat{\sigma}_{jj}$

$$\hat{\sigma}_{zz} = \sum_{j=1}^{3} \hat{\sigma}_{jj} \cos^2 \theta_j \qquad (2.17)$$

where θ_j are the angles between $\hat{\sigma}_{jj}$ and $\vec{B}_0$. In solutions, with fast isotropic molecular tumbling, substantial averaging of $\hat{\sigma}$ occurs, so that only one third of the

trace, $\hat{\sigma}_{zz} = \frac{1}{3}(\sigma_{11} + \sigma_{22} + \sigma_{33})$, is observed. Eqn. (2.17) can be rewritten [8]

$$\hat{\sigma}_{zz} = \frac{1}{3} Tr\hat{\sigma} + \frac{1}{3} \sum_{j=1}^{3} \left(3 \cos^2 \theta_j - 1\right)\sigma_{jj} \qquad (2.18)$$

where Tr stands for trace. In the case of axial symmetry, the corresponding equation is

$$\hat{\sigma}_{zz} = \frac{1}{3}\left[Tr\hat{\sigma} + \left(3 \cos^2 \theta_{II} - 1\right)(\sigma_{II} - \sigma_{\perp})\right] \qquad (2.19)$$

where $Tr\hat{\sigma}$ is $(\sigma_{II} + 2\sigma_{\perp})$ and $(\sigma_{II} - \sigma_{\perp})$ is referred to as the shielding anisotropy. As a consequence of these facts, for a single crystal containing nuclei which are all in translationally equivalent positions, the NMR spectrum will consist of only one line whose frequency varies with the orientation of the crystal in $\vec{B}_0$. Consequently, for a microcrystalline powder sample, this will lead to a range of frequencies corresponding to all possible orientations between σ_{II} and $\sigma_{\perp}$, which may cover several tens of parts per million.

2.4. Magic-Angle Spinning

As pointed out in the previous sections the two main origins of line broadening in solid-state NMR are the dipolar interaction and the shielding anisotropy. The question of removing from the final spectrum broadening due to those effects relies on the application of one general principle of NMR, namely that if a spin system can exist in two or more states the effect of those states can

be averaged to a single value when the rate of transitions or exchange between the states exceeds the energy difference between them. That means, if an interaction gives rise to a frequency spread of $\Delta\nu$ for a given transition, the effects of the interaction may be removed from the spectrum if an exchange of the states can be induced at a rate greater than $\Delta\nu$. This does not mean only interactions involving a change of the spin-state, but also frequency differences induced by changes in the environment, as is the situation in the case of chemical exchange or jumping between inequivalent crystallographic sites.

In the case of non-viscous liquids, rapid molecular tumbling averages all anisotropic interactions such as dipolar coupling and shielding anisotropy to leave only the isotropically averaged chemical shift and the isotropic part of the indirect dipolar coupling ("J-coupling") [8].

In solids, however, molecular motion is generally too restricted for significant averaging to take place. Therefore, some form of artificial averaging has to be applied. The first successful technique was developed in 1958 by Andrew, Bradbury and Eades [9] and led to independent recognition by both Andrew [10] and Lowe [11] of the fact that sufficiently rapid rotation of a powdered sample about an axis inclined at 54°44' ("the magic angle") to the applied $\vec{B}_0$ would result in isotropic averaging of the direct dipolar interaction.

The following discussion will explain the theoretical background of magic-angle spinning, because the averaging

effect is not obvious. Consider rotation of a powdered sample about an axis $\vec{s}$ inclined at an angle β to the applied field $\vec{B}_0$ as defined in Fig. (2.2).

Let $\vec{r}$ be the principal vector for the interaction of interest, making an angle θ with $\vec{B}_0$, and let the angle between $\vec{r}$ and $\vec{s}$ be χ.

In the case of rotation, at rate ω, the angle $\phi = \omega t$ if $\vec{r}$ is in the plane of $\vec{B}_0$ and $\vec{s}$ at time t=0. Thus at a subsequent time, t

$$\cos\theta = \cos\chi\cos\beta + \sin\chi\sin\beta\cos\omega t \tag{2.20}$$

Thence

$$\begin{aligned}\langle\cos^2\theta\rangle = {} & \cos^2\chi\cos^2\beta + 2\sin\chi\cos\chi\sin\beta\cos\beta\langle\cos\omega t\rangle \\ & + \sin^2\chi\sin^2\beta\langle\cos^2\omega t\rangle\end{aligned} \tag{2.21}$$

Also

$$\langle\cos^2\omega t\rangle = 0 \text{ and } \langle\cos^2\omega t\rangle = \frac{1}{2}$$

Eqn. (2.21) reduces to

$$\begin{aligned}\langle\cos^2\theta\rangle &= \cos^2\chi\cos^2\beta + \frac{1}{2}\sin^2\chi\sin^2\beta \\ &= \cos^2\chi\cos^2\beta + \frac{1}{2}(1-\cos^2\chi)(1-\cos^2\beta) \\ &= \frac{1}{3} + \frac{1}{6}(3\cos^2\chi - 1)(3\cos^2\beta - 1) \\ \langle 3\cos^2\theta - 1\rangle &= \frac{1}{2}(3\cos^2\chi - 1)(3\cos^2\beta - 1)\end{aligned} \tag{2.22}$$

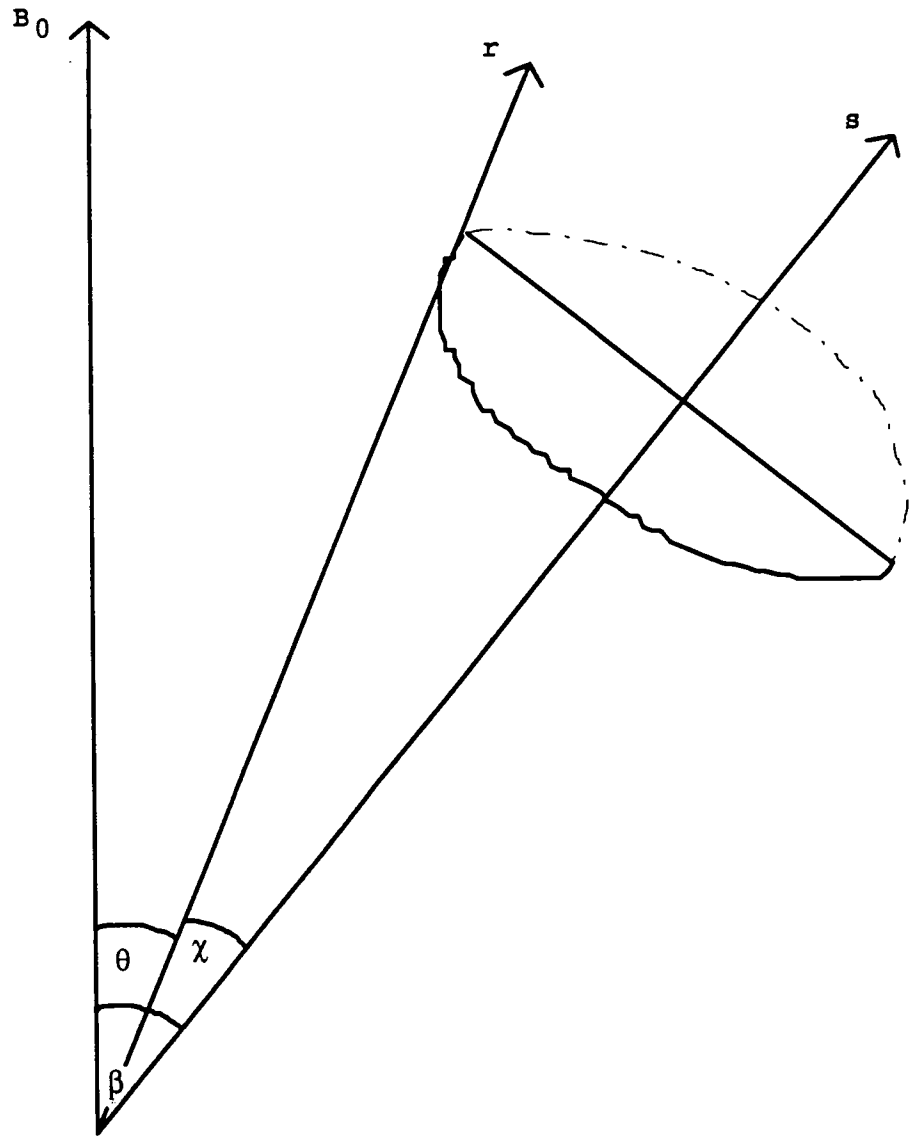

Fig. 2.2 Geometrical Representation for the effect of rotation

Both parameters θ and χ are fixed for a rigid solid, though they take all possible values if the material is a powder. The term $\frac{1}{2}\left(3\cos^2\beta - 1\right)$ therefore acts as a scaling factor on a dipolar powder pattern.

Fortunately the angle β is under the control of the experimentalist. If $\beta = 0^0$, i.e. $\vec{r}$ is parallel to the applied magnetic field $\vec{B}_0$, $\frac{1}{2}\left(3\cos^2\beta - 1\right) = 1$, so there is no effect on the spectrum. If $\beta = 90^0$, i.e. rotation about

an axis perpendicular to $\vec{B}_0$, the powder pattern is scaled down by a factor of 2 and reversed in direction. The most interesting case, for solid-state NMR spectroscopists, is when $\cos^2\beta = \frac{1}{3}$ (β=55°44'), since then $\cos\beta = 1/\sqrt{3}$ and $\frac{1}{2}\left(3\cos^2\beta - 1\right) = 0$, so that $\frac{1}{2}\left(3\cos^2\theta - 1\right) = 0$ for all orientations, i.e. for any χ.

Basically, rapid rotation about an angle of 55°44' to $\vec{B}_0$, will average out all effects due to anisotropic interactions, just as for isotropic tumbling in non-viscous liquids.

In all the above discussions, the assumption that the time- averaged value of this interaction over a rotation will be observed is implicit.

However, as has been previously stated, for observation of simple average values, the rate of mixing of states, i.e. in this case the rate of sample spinning, must be greater than the frequency spread produced by the anisotropic interactions. Since the interactions under consideration will often be in the range of 10^2 - 10^5 Hz, it is obviously not always possible to achieve a spinning rate high enough to satisfy this condition. If the spinning rate is smaller than the frequency spread, then there are two classes of interaction to be considered.

These two interactions have been christened "heterogeneous" and "homogeneous" by Porties [12] and were theoretically discussed by Maricq and Waugh [13]. Considering firstly homogeneous interactions such as homonuclear dipolar interactions in a spatially homogeneous solid, there will be no narrowing of the line

observed if the rotation rate is less than the dipolar linewidth because adjacent pairs of spins, being of the same isotope, are continually undergoing energy-conserving radiationless mutual transitions, caused by the coupling of the $\alpha\beta$- and $\beta\alpha$-states of the adjacent pair of nuclei by the "B"-term in Eqn. (2.11), which effects the secular homonuclear dipolar Hamiltonian in Eqn. (2.15).

These "flip-flop" transitions produce a fluctuating magnetic field at a given nucleus, with a characteristic correlation frequency υ, which is of the same order as the frequency spread caused by this interaction.

The resulting effect of rotation with a rate less than the frequency spread in the spectrum, will be opposed by a Fourier component of the fluctuating field, and no averaging will take place.

If the interaction is inhomogeneous, e.g. heteronuclear dipolar coupling and shielding anisotropy, then the interactions at various sites are not coupled and behave independently. Maricq and Waugh [13] showed that at spinning speeds less than the frequency spread of the shielding anisotropy interaction, the static lineshape will break up into a series of discrete lines, one of which will represent the isotropic average resonance whereas the others will be separated from it by multiples of ν_r (the rotor frequency). The lines are so-called spinning side-bands.

However, another problem is the homogeneous dipolar interactions. Since these interactions are homogeneous, magic-angle spinning has very little effect, if the spinning rate does not exceed the equivalent line-

broadening due to the homogeneous dipolar interaction. This interaction can easily produce a line broadening upto 100 kHz in the spectrum. These spinning rates cannot be achieved with the present techniques of magic-angle spinning.

To overcome this problem Bloch [14] suggested a technique, today generally known as dipolar decoupling. In this techique the mixing of the states is achieved by transitions between proton spin-states induced by powerful rf irradiation at the appropriate proton Larmor frequency. The criterion for effective averaging in this case is that the amplitude of the magnetic component of the rf radiation expressed in frequency units ($\nu = \frac{\gamma}{4\pi} \vec{B}_1^{1H}$), should exceed the dipolar linewidth. It should be pointed out that such irradiation will average both the anisotropic and isotropic part of the indirect dipolar interaction. The latter is the basis of the solution-state heteronuclear decoupling technique used to remove J-coupling from spectra.

Both techniques mentioned are in principle capable of leading to high-resolution ^{13}C-spectra of solids. However, there is still the problem of the low sensivity of ^{13}C (1.1 %) and the normally relatively long longitudinal relaxation times of ^{13}C in solids.
To overcome these problems a third technique is required.

2.5 Cross Polarisation

The main idea of the cross polarisation technique is to use the magnetic properties of an abundant spin species,

like ^1H, to obtain a high-resolution spectrum of the rare spins.

It was introduced first in 1960 by Hartman and Hahn [15]. The classical analysis of the method has been given by Hartman and Hahn using the general density matrix technique and was developed by Lurie and Slichter [17] using a thermodynamic treatment. The technique relies on the transfer of energy in the form of spin polarisation from the abundant S spins to the rare I spins.

The proper way to describe such a system is in a double rotation frame representation [16,17]. In this representation, each of the two spin species can be made to sense a different effective field. The effective Zeeman splittings of the two species can be made equal, thereby allowing rapid polarisation transfer from the abundant S-spins to the rare I-spins. This condition of equal effective field splittings is called the *Hartman-Hahn* condition. The experimental requirement to fulfil this condition is

$$\gamma_S \vec{B}_{1S} = \gamma_I \vec{B}_{1I} \qquad (2.23)$$

where $\vec{B}_1$ is the effective radiofrequency magnetic field at nucleus I or S. At this condition both I and S nuclei in their respective rotation frames of reference will precess about their respective $\vec{B}_1$'s at the same frequency and therefore are able to exchange energy.

A more quantitative description of the rate of transfer of polarisation under such conditions is complicated. It has been extensively studied both theoretically [18,19]

and experimentally [20-22]. Without going into detail, it can be stated that polarisation transfer will normally occur so as to approach an equilibrium value via an inverted exponential decay curve for carbons weakly coupled to protons. When the carbons are strongly coupled to the protons the polarisation will be frequently modulated by the strong ^{13}C-^{1}H dipolar coupling, and the overall initial signal built up is better described by a gaussian function [22].

This process is termed *cross relaxation* and for the ^{13}C in the presence of ^{1}H the symbol of the polarisation time constant is usually termed as T_{CH} .

It should be pointed out that since in practice the protons are usually spin locked during the process of cross polarisation, they will be undergoing spin-lattice relaxation in the rotating frame ($T_{1\rho}^{H}$) simultaneously. In other words the whole process of cross polarisation is built up from two competing processes occurring at the same time. If the relaxation rate is sufficiently fast the proton polarisation reservoir may become severely depleted, and the magnetisation will begin to flow back from the ^{13}C reservoir to the ^{1}H reservoir if the contact in continued. The resulting function of a cross polarisation experiment with successively increasing contact times therefore is expected to have a maximum magnetisation at a certain time depending on the polarisation transfer rate and the relaxation rate of the nuclei under investigation.

The combined techniques, dipolar decoupling and cross polarisation, were first used by Pines, Gibby and Waugh in

1972 [23,24,25]. Ignoring $T_{1\rho}^{H}$-relaxation, the gain in S-spin polarisation is $\gamma_S/\gamma_I \cong 4$ for S = ^1H and I = ^{13}C. This fact and the shorter longitudinal relaxation time of the protons, compared to the carbon relaxation time constant, which shortens the recycle time between two acquisitions, are responsible for the importance of the cross polarisation technique.

The combined use of cross polarisation, magic-angle spinning and dipolar decoupling to obtain high-resolution solid-state spectra was further studied by Stejskal and Schaefer [26] and made solid-state NMR a valued technique for analytical purposes.

The experiment consists of an initial 90° pulse to the protons followed by immediate spin-locking and CP. After the spin-locking the ^{13}C-FID is acquired with simultaneously proton decoupling.

Thus, the experiment as normally performed may be represented in a schematic diagram (Fig. 2.3)

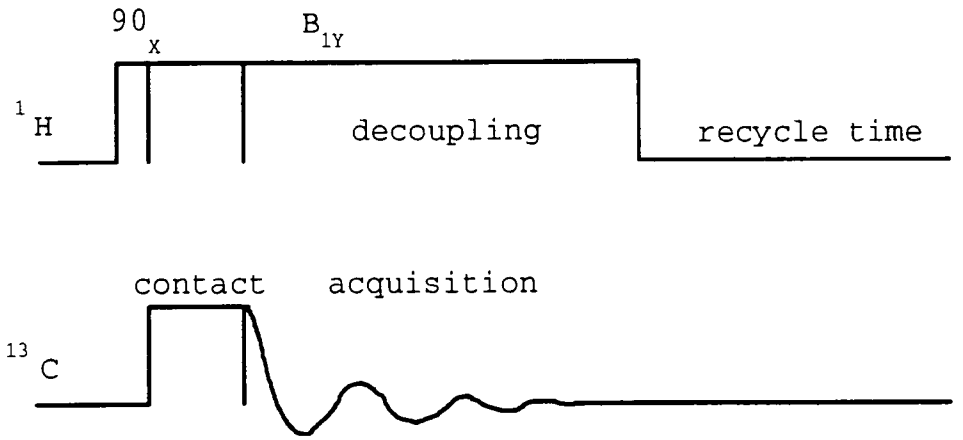

Fig. 2.3 Standard cross polarisation pulse sequence

The dynamics of the polarisation transfer were described theoretically by Mehring [27], looking at an abundant spin system S (e.g. ^1H) and a rare spin system (e.g. ^{13}C), with an infinite heat capacity of the S-spins. $T_{1\rho}^H$ relaxation should also be included. A useful expression for the time dependence of the cross-polarisation experiment in such a case can be written as

$$M(\tau) = \frac{M_0}{1-\lambda}\left[1 - \exp\left\{-\frac{(1-\lambda)\tau}{T_{CH}}\right\}\right]\exp\left(-\frac{\tau}{T_{1\rho}^H}\right) \qquad (2.24)$$

where M_0: is the maximum magnetisation possible without any relaxation

$T_{1\rho}^H$: is the relaxation time in the rotating frame

τ: is the contact time

$M(\tau)$: is the magnetisation at some subsequent time τ

$$\lambda = \frac{T_{CH}}{T_{1\rho}^H} - \frac{T_{CH}}{T_{1\rho}^C}$$

This function shows the exponential behaviour of the polarisation transfer. The second exponential takes the rotating frame relaxation of the abundant spins into account. The cross polarisation behaviour is schematically shown in Fig. 2.4. It should be noted that for ideal cases this technique is able to discriminate between CH and CH_2 carbons in one molecule. The rate of cross polarisation is theoretically for CH atoms lower than for CH_2 carbons of the same mobility. The ideal case would result a maximum polarisation ratio at short contact times of 2:1. The CH_3 carbons behave differently because of their rapid rotation and therefore partially averaged dipolar interactions. The

cross polarisation time constant is usually larger for CH_3 than for CH or CH_2 carbons.

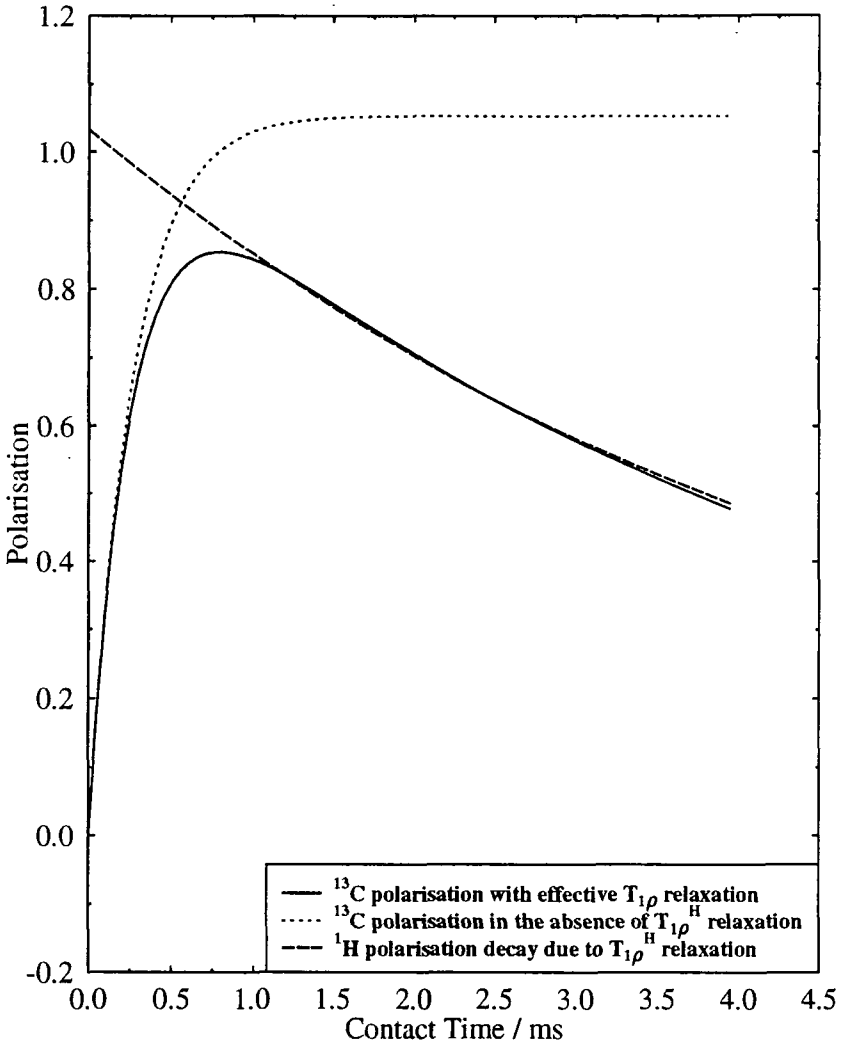

Fig. 2.4: ^{13}C magnetisation as a function of cross polarisation contact time

2.6 Relaxation

The preceding section has shown that relaxation characteristics may play an important part in NMR. The different kinds of relaxation mechanism, which are of considerable importance, will be briefly explained.

Firstly, attention will be drawn to longitudinal and transverse relaxation, T_1 and T_2, respectively. Qualitatively, T_1 and T_2 relaxation can be understood using the concept of a fluctuating magnetic field $\vec{B}_2$. When the fluctuations are due to random thermal motion in a liquid, there will be almost certainly be some frequency components of $\vec{B}_2$ around the Larmor frequency. This gives rise to random transitions between various x,y components of the magnetisation.

For random motions in liquids, all frequencies up to a certain limit are equally probable. Therefore the random field $\vec{B}_2(t)$ can be characterised by an autocorrelation function $G(t)$

$$G(t) = \frac{\vec{B}_2(t+\tau)\cdot\vec{B}_2(t)}{\vec{B}_2(t)} \qquad (2.25)$$

$G(t)$ describes the memory of the molecule at the time $t+\tau$ for its orientation or position at time t. In fact, $G(t)$ is always taken as an ensemble average over a large number of molecules. It is therefore stationary and can be written as an exponentially decaying function.

$$G(t) = \exp\left(-\frac{|\tau|}{\tau_c}\right) \qquad (2.26)$$

The correlation time τ_c is a measure of the time scale in which molecule motions can occur in the system under study. The shorter τ_c is, the faster the molecule moves. Solomon [28] derived equations for T_1 and T_2 relaxation for dipole-dipole relaxation caused by molecular diffusive rotation:

$$\frac{1}{T_1} = \frac{2}{5}\frac{\gamma^4\hbar^2}{r^6} I(I+1)\tau_c\left[\frac{1}{1+\omega^2\tau_c^2} + \frac{4}{1+4\omega^2\tau_c^2}\right]$$
$$\frac{1}{T_2} = \frac{1}{5}\frac{\gamma^4\hbar^2}{r^6} I(I+1)\tau_c\left[3 + \frac{5}{1+\omega^2\tau_c^2} + \frac{2}{1+4\omega^2\tau_c^2}\right] \qquad (2.27)$$

For small molecules (τ_c very small, of the order of 10^{-11}s) an increase in spin-lattice relaxation (decrease in T_1) with τ_c is observed until a minimum is reached for $\omega\tau_c \cong 1$. If the molecules are larger and slower, i.e. systems with high viscosity, the lack of frequency components at the Larmor frequency ω_0 eventually leads to an increase in T_1 when τ_c increases further. The fluctuations that cause spin-lattice relaxation are also in part responsible for T_2 relaxation. However, frequency components far below the Larmor frequency will still cause dephasing of the x,y-magnetisation and therefore cause T_2 relaxation, although these low-frequency fluctuations no longer contribute to T_1 relaxation. This is the reason why T_2 keeps decreasing with increasing correlation time without going to a minimum. It can be shown from a quantitative treatment of the spin-lattice relaxation, that in the case of extreme-narrowing $(\omega\tau_c << 1)$, the relaxation rates, T_1 and T_2, are equal. For homonuclear dipolar relaxation of I=1/2 nuclei and $\omega\tau_c << 1$ Eqn. (2.27) reduces to

$$\frac{1}{T_1} = \frac{1}{T_2} = \frac{3}{2}\gamma^4\hbar^2\tau_c\frac{1}{r^6} \qquad (2.28)$$

In solids, however, the situation is much more complicated. The lack of fast motions can lead to T_1

values of minutes, while T_2 can no longer be readily related to the shape of the resonance line.

The width of the proton resonance is now a superposition of resonances, broadened by intramolecular as well as intermolecular dipolar interactions between protons. The lineshape may be Gaussian rather than Exponential [29]. The relaxation rate as a function of τ_c is shown in Fig. 2.5 for various proton Larmor frequencies.

Also, when a molecule with chemical shift anisotropy is subjected to random motions, the effective magnetic field at the nucleus is changing rapidly, and this may cause the spins to relax.

However, for ^1H in an insulating organic solid at room temperature, the dominant mechanism is almost certain to be fluctuations in the homonuclear dipole-dipole interactions due to molecular motion. Since the fluctuations in the dipolar interaction which constitute the relaxation mechanism are due to molecular motion, the relaxation behaviour will reflect the molecular motions present in the system, particularly (for T_1) those around the resonant frequency of interest [30,31].

The spin-lattice relaxation may be monitored by the rate of re-growth of magnetisation in the +z direction following perturbation. The re-establishment of equilibrium population distribution by energy exchange between the spin's magnetic energy and other degrees of freedom of the system such as molecular rotations and translation, is entirely dependent of the Larmor frequency

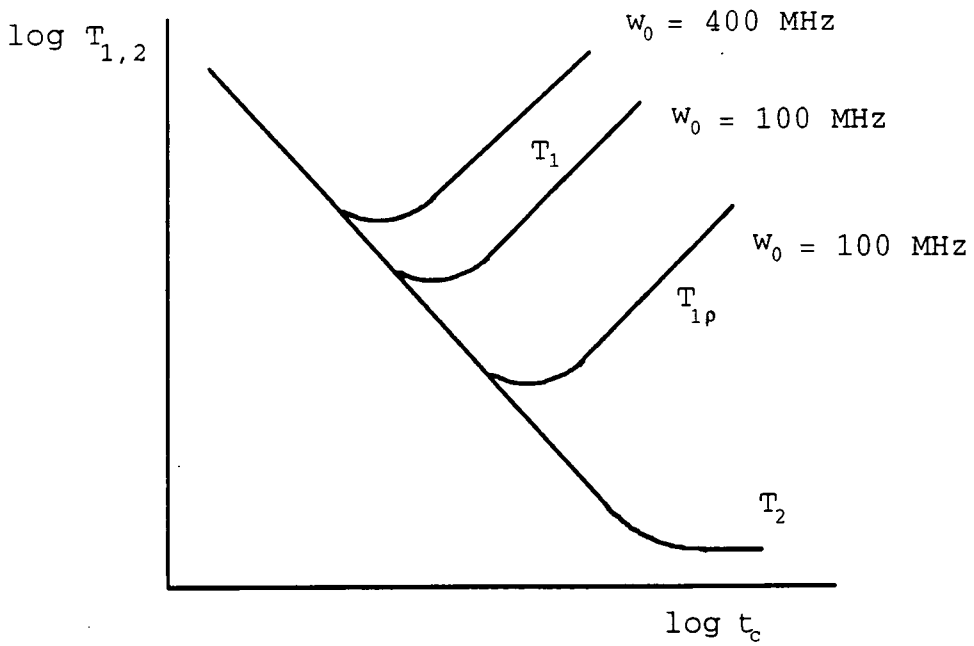

Fig. 2.5: Relaxation times as a function of the correlation time

of the nucleus in the applied magnetic field B_0 (for protons typically 60-600 MHz). However, other frequency ranges can be probed by measurements of other manifestations. The other most important relaxation time is the decay of magnetisation spin-locked in the rotating frame. In this case the motional frequencies of interest will be of the same order as the frequency of the applied rf radiation used for the spin-locking, which is typically $10^4 - 10^5$ Hz. This relaxation time is termed as *spin-lattice relaxation in the rotating frame*.

It is found that, for a discrete, homogeneous spin system, the rate of relaxation follows an exponential law:

$$M_0 - M(t) = M_0 - M(0)\exp\left(-\frac{t}{T_1}\right) \qquad (2.29)$$

Where M_0 is the equilibrium value of the measured magnetisation

$M(0)$ is the magnetisation value initially after the rf perturbation

$M(t)$ is the value of the measured magnetisation at some subsequent time t

T_1 is the characteristic relaxation time constant

In macroscopically heterogeneous systems, however, this simple behaviour of relaxation is not found. Rather, spin-lattice relaxation can be represented as a superposition of exponential processes. A reasonable model for a heterogeneous system would be to consider it as a mixture of several discrete homogeneous subsystems, each following the rules for exponential relaxation in (2.29). It follows that the overall relaxation behaviour of the mixture can be decribed by

$$M_0 - M(t) = M_0 - M(0) \sum_{i=1}^{n} P(i) \exp\left(- \frac{t}{T_1(i)} \right) \qquad (2.30)$$

where $P(i)$ is the proportion of component i

$T_1(i)$ is the time constant of component i

In principle it should be possible to extract information about the constituent components in such a system. However, non-exponential behaviour is often found in systems where the heterogeneity is structural, or chemical on a microscopic level. Block-copolymers, for instance, are often built from microscopic domains, where naive analysis of the relaxation data in term of constituent

components can yield to misleading results because of the phenomenon of *spin-diffusion* [29,32,33,34].

2.7 Spin Diffusion

The nature of the spin diffusion can be explained with the homonuclear secular dipolar Hamiltonian. The B-term in Eqn. (2.11) allows energy conserving simultaneous radiationless transitions for a pair of adjacent nuclei. This is the mechanism by which spin diffusion occurs. Spin diffusion allows transportation of polarisation from one part of the lattice to another, thereby tending to even out the polarisation throughout the lattice. Obviously, for a tightly coupled lattice in a heterogeneous system, where chemically or physically different domains in that system would yield a non-uniform distribution of polarisation during the process of relaxation, spin diffusion may greatly modify the overall observed relaxation behaviour from that expected from the intrinsic relaxation properties of the various sites, and quantitative interpretation becomes difficult or impossible. It can readily be shown [29] that this transportation takes the form of a diffusion equation

$$\frac{dM}{dt} = Wa^2\nabla^2 M \qquad (2.31)$$

where M is the polarisation at a given site

W is the flip-flop transition probability

a is the inter-nuclear distance to the nearest neighbour in the lattice

The quantity Wa^2 is given the symbol D, and referred to as the *spin diffusion coefficient*.

In such cases, the observed relaxation behaviour will now depend not only on the intrinsic relaxation properties of the various regions, but also on their sizes, their spatial distribution and morphology and finally of the spin diffusion within the various domains.

However, this equation in principle enables one to extract domain sizes and morphology in heterogeneous systems. A straight forward experiment uses the well-known Goldman-Shen [35] pulse sequence, that measures polarisation transfer from one region to another. All attempts in the past to extract the domain size and the morphology of heterogeneous systems, especially polymers, failed due to the neglect of relaxation during the polarisation transport. Many attempts have been made to cancel (minimise) the so called "T_1-effect" [36,37,38]. In fact Packer et al. [39,40] showed that it is in principle impossible to cancel this effect

In order to describe such a system, another model is necessary. A general equation that takes the intrinsic relaxation parameters and spin-diffusion modulation into account could be written in a form [41,42]

$$\frac{d\vec{M}(\vec{r},t)}{dt} = D(\vec{r})\nabla^2\vec{M}(t) + R(\vec{r})\left(\vec{M}_0 - M(t)\right) \qquad (2.32)$$

where $\vec{M}(t)$ is the magnetic polarisation after time t

D is the spin-diffusion coefficient

R is the spin-relaxation rate constant

$\vec{r}$ is the positional vector

$D(\bar{r})$ and $R(\bar{r})$ are assumed to be isotropic and constant within the given region. An equation of this type is reported in a subsequent chapter as the basis of a computer model to investigate domain sizes, intrinsic relaxation properties and the morphology of heterogeneous systems.

References to Chapter 2

[1] F. Bloch, W.W. Hansen, M. Packard, Phys. Rev. **69** (1946) 127

[2] E.M. Purcell, H.C. Torrey, R.V. Pound, Phys. Rev. **69** (1946) 37

[3] C.P. Slichter; "*Principles of Magnetic Resonance*", 2nd Edition, Springer Verlag, Berlin (1978)

[4] Ed. Alexander I. Popov and Klaas Hallenga, Practical Spectroscopy Series, Vol. 11, "*Modern NMR Techniques and Their Application in Chemistry*", Marcel Dekker, New York (1991)

[5] Jacek W.Hennel, Jacek Klinowski, "*Fundamentals of Nuclear Magnetic Resonance*", Longman Scientific & Technical (1993)

[6] A. Abragam, "*The Principles of Nuclear Magnetism*", Clarenden Press: Oxford (1961)

[7] U. Haeberlen, "*High Resolution NMR in Solids*", Springer Verlag, Berlin

[8] R.K. Harris, "*Nuclear Magnetic Resonance Spectroscopy*", Longman Scientific & Technican (1987)

[9] E.R. Andrew, A. Bradbury, R.G. Eades, Nature, **182** (1958) 1659

[10] E.R. Andrew, Arch Sci. (Geneva) **12** (1958) 103

[11] I.J. Lowe, Phys. Rev. Lett., **2** (1959) 285

[12] A.M. Porties, Phys. REv., **91** (1953) 1971

[13] M.M. Maricq, J.S. Waugh, J. Chem .Phys., **70** (1979) 3300

[14] F. Bloch, Phys. Rev., **111** (1958) 841

[15] S.R. Hartman and E.C. Hahn, Bull. Am. Phys. Soc., **5**

(1960) 498

[16] S.R. Hartman and E.C. Hahn, Phys. Rev., **128**, (1962) 2042

[17] F.M. Lurie, C.P. Slichter, Phys. Rev., **133** (1964) A1108

[18] A. Pines, M.G. Gibby, J.S. Waugh, J. Chem. Phys., **59** (1973) 565

[19] D.E. Demco, T. Tegenfeld, J.S. Waugh, Phys. Rev., **111** (1975) B4133

[20] L.B. Alemany, D.M. Grant, R.J. Pugmire, T.G. Alger, K.W. Zilm, J. Amer. Chem. Soc., **105** (1983) 2192

[21] L.B. Alemany, D.M. Grant, T.G. Alger, R.J. Pugmire, J. Amer. Chem. Soc., **105** (1983) 6697

[22] E.O. Stejskal, J. Schaefer, J.S. Waugh, J. Magn. Res., **28** (1978) 105

[23] A.Pines, M.G. Gibby, J.S. Waugh, J. Chem. Phys., **56** (1972) 1776

[24] A.Pines, M.G. Gibby, J.S. Waugh, Chem. Phys. Lett., **15** (1972) 373

[25] A.Pines, M.G. Gibby, J.S. Waugh, J. Chem. Phys., **59** (1973) 569

[26] J. Schaefer, E.O. Stejskal, J. Amer. Chem. Soc., **98**, (1976) 1031

[27] M. Mehring, "*High Resolution NMR in Solids*", 2nd Ed., Springer Verlag, Berlin (1983)

[28] I. Solomon, Phys. Rev., **99** (1955) 559

[29] A. Abragam, "*The Principles of Nuclear Magnetism*", Clarenden Press: Oxford (1961)

[30] N. Bloembergen, E.M. Purcell, R.V. Pound, Phys. Rev., **73** (1948) 679

[31] C.P. Poole, H.A. Farach, *"Relaxation in Magnetic Resonance"*, Academic Press, London (1972)

[32] M. Goldman, "spin temperature and Nuclear Magnetic Resonance in Solids", OUP, London

[33] G.P. Jones, Phys. Rev., **148** (1966) 332

[34] H. Wennerstrom, J. Magn. Res., **11** (1973) 219

[35] M. Goldman, L. Shen, Phys. Rev., **144** (1966) 321

[36] T.T.P. Cheung, B.C. Gernstein, J. Appl. Phys., **52** (1981) 5517

[37] S. Zhang, M. Mehring, Chem. Phys. Lett., **160** (1989) 644

[38] R.H. Newman, Chem. Phys. Lett., **180** (1991) 301

[39] A.M. Kenwright, K.J. Packer, B.J. Say, J. Magn. Res., **69** (1986) 426

[40] A.M. Kenwright, K.J. Packer, Chem. Phys. lett., **173** (1990) 471

[41] T.T.P. Cheung, Phys. Rev., **B23** (1981) 1404

[42] K.J. Packer, J.M. Pope, R.R. Yeung, M.E.A. Cudby, J. Polym. Sci, Polym. Phys. Ed., **22** (1984) 589

Chapter 3

3.1 Introduction

Nylon-6 block copolymers (NBC) are a relatively new class of Reaction Injection Moulding (RIM) systems, covering a broad range of morphologies and properties. RIM is a low-cost easy-to-handle process for preparing polyurethanes, and was first mentioned in 1941 [1,2,3]. It is now also available for nylon-6 block copolymers, since Monsanto began their exploratory research in base-catalysed polymerisation of lactams in 1955 [4] and subsequently developed a RIM system for nylon-6 block copolymers as described by Hedrick and Gabbert [5]. Very rapid polymerisation occurred at temperatures between 80 °C and 180 °C, well below the temperature required for the thermal initiation (≈200 °C). In this work, NBC have been produced by anionic polymerisation of caprolactam with end-functionalised soft-block components involving polyether fragments. This gives rise to linear segmented block copolymers with alternating polyamide (hard block) and polyether-polyesteramide prepolymer (soft block) components.

A prominent factor distinguishing block copolymers from random copolymers is the frequent, though not invariable, separation of the materials of their constituent blocks into microphases or domains, resulting in a supramolecular texture that is specific to block copolymers and which has an important influence upon their properties and uses. Nylon-6 on its own is insufficient for most applications,

in particular in the automotive industry because of its toughness. Copolymerisation, e.g. with a polyether, improves the fracture resistance significantly and the impact strength can be increased severalfold. This even compensates for the decrease in flexural modulus and tensile strength.

3.2 Synthesis of Polyamide-6 (Nylon-6)

Nylon-6 was prepared by an acyllactam-initiated anionic polymerisation. A recipe by Powell [6] has been used to prepare nylon-6:

250 mg caprolactam were weighted into an oven-dried glass vial. 3 µL of N-acetylcaprolactam was added to the caprolactam. The vial was placed in an oil bath at 160 °C and purged with a slow steam of dry nitrogen. Sodium hydride (10 mg of a 60 % dispersion in mineral oil) was added all at once to the molten solution. The polymerisation was allowed for five minutes. The vial was then removed from the bath and allowed to cool to room temperature. The vial was crushed, and the product was powdered, extracted overnight with hot methanol and finally dried at 60 °C under vacuum.

3.3 Mode of Formation of Polyamide-6 (Nylon-6)

Joyce and Ritter [1] obtained in 1941 a patent on the base-catalysed polymerisation of caprolactam. It was a thermally initiated anionic polymerisation. A small amount of sodium or other alkali metal in caprolactam was reacted to produce sodium caprolactam. The rapid, exothermic polymerisation of caprolactam to nylon-6 takes place at 200 °C. The nylon-6 prepared under this condition is usually of high molecular weight, which is not a function of the sodium caprolactam concentration. It was postulated that polymerisation occurs not only due to ring-opening but also by cross-linking reactions within the chains. Figures 3.1 and 3.2 show the reactions.

H.K. Hall [7] of DuPont subsequently proposed an analogous mechanism which was published in 1958. A pre-formed acyllactam was added to caprolactam containing sodium caprolactam at 160 °C. Very rapid polymerisation and a solid nylon-6 casting resulted in four to five minutes. In the absence of acyllactam the polymerisation did not occur. The polymerisation results again in a very high molecular weight nylon-6, but this time with a acylamino end group rather than the amino end group from the thermally initiated polymerisation. The mechanism for the acyllactam initiated caprolactam polymerisation is presented in Fig. 3.3.

Initiation

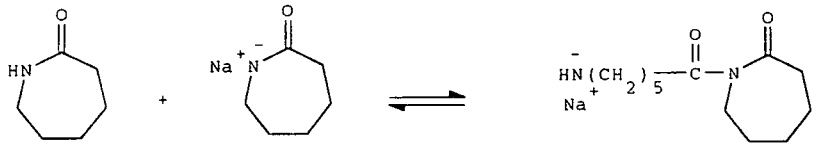

Catalyst Regeneration

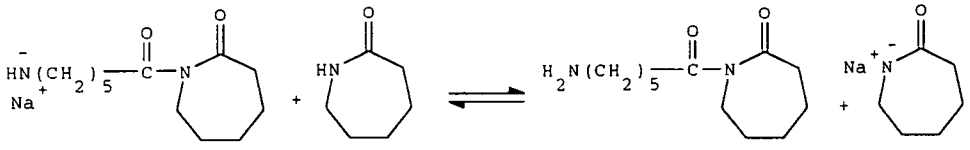

Propagation

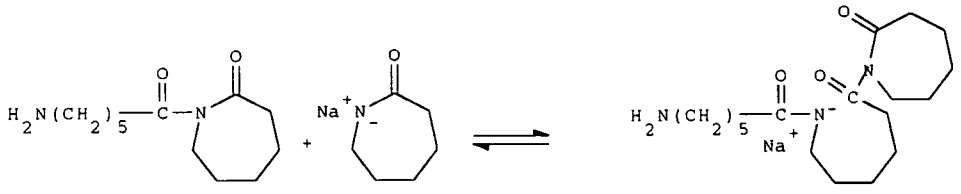

Polymer

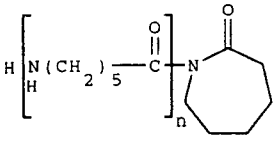

Nylon-6

Fig. 3.1 Proposed mechanism for the thermally initiated anionic polymerisation of caprolactam

In this case the initiator concentration controls the number of chains started and thus the molecular weight, provided the temperature is below of that for thermally initiated polymerisation. The same kind of branching reaction as pointed out in Fig. 3.2 takes place because of the high molecular weight of the nylon-6.

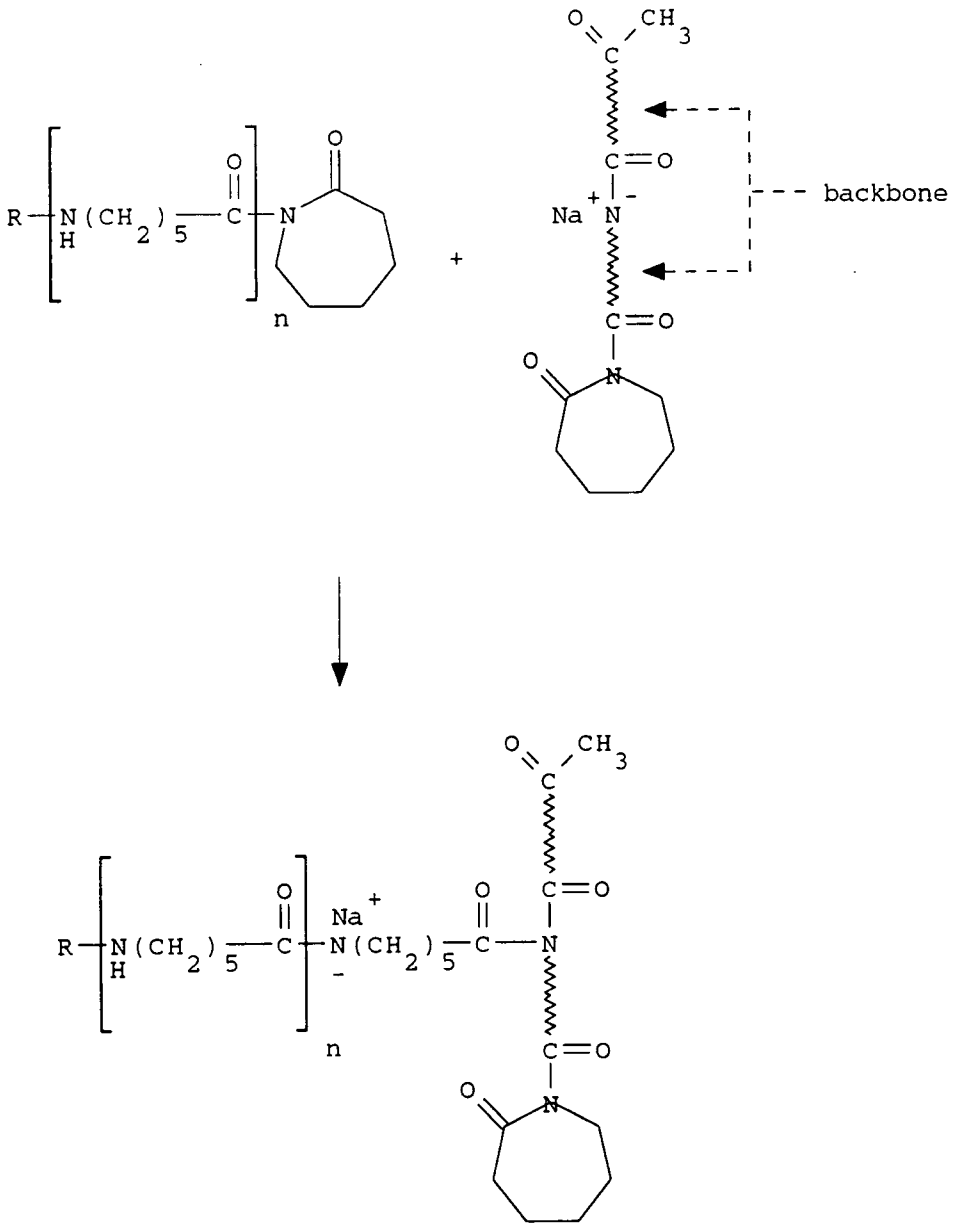

Fig. 3.2 A branching reaction in anionic initiated lactam polymerisation
R=H for thermally initiated polymerisation
R=acetyl for acyllactam initiated polymerisation

3.4 Mode of Formation of Polyether-polyesteramide (Prepolymer)

Very little is known about the polyether-polyesteramide prepolymer used for the copolymerisation with caprolactam. It is a technically-produced low molecular weight polymer. It appears as a brown, sticky, highly-viscous liquid as purchased from DSM. This section will give a summary of

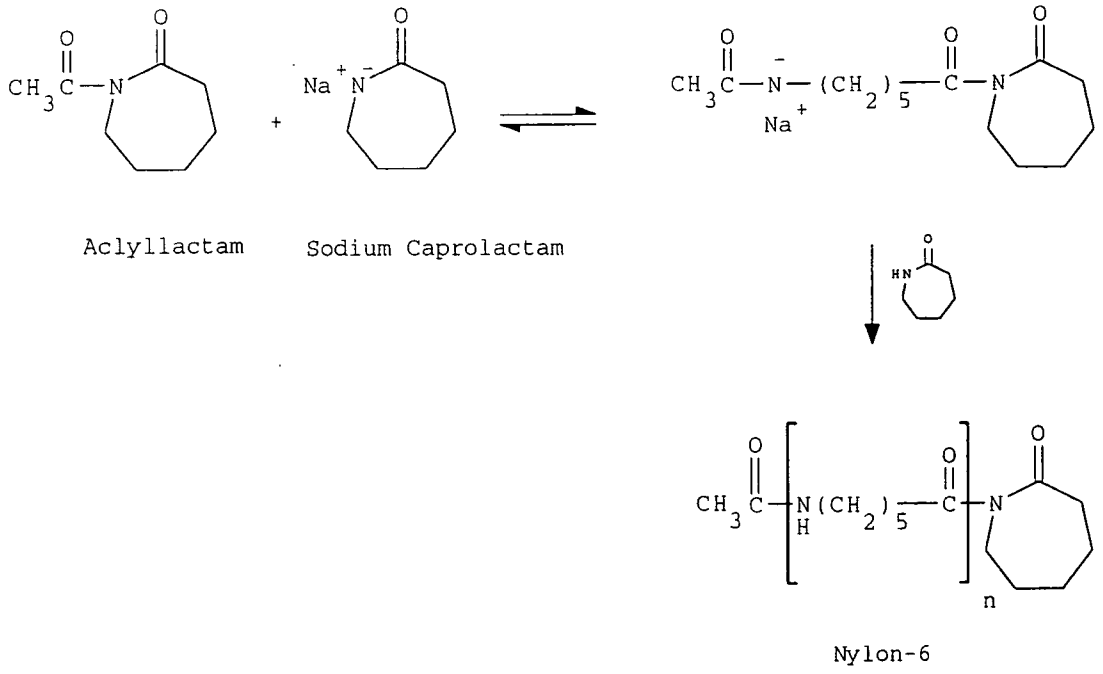

Fig. 3.3 Acyllactam initiated anionic polymerisation of caprolactam

the literature available dealing with the synthesis and structure of the polyether polyesteramide[4,5,8,9,10]. The prepolymer formation was done using a multi-functional bis-acyllactam which normally acts as initiator for caprolactam polymerisation. In this reaction it functions to combine with the poly(ethylene oxide) (PEO) end-functionalised poly(propylene oxide)(PPO) moieties. The molecular weight of the polyether is about 2000 g/mol according to the manufacturers. The total molecular weight is also unknown, but according to [4] *x* in fig. 3.4 is about 9, resulting in a total molecular weight of about 20000 g/mol. The ratio of PPO to PEO is not quoted by the manufacturers but was determined by solid-state NMR to ≈ 7:1 (see chapter 4.2.2). An excess of acyllactam was used to ensure the prepolymer is terminated by acyllactam. The reaction is completed within seconds in the presence of an

alkaline catalyst. Unfortunately no paper mentioned the catalyst used, nor what kind of bis-acyllactam. An early work by Hedrick and Gabbert [4] used a phenyl-bis-acyllactam. The reaction is as follows:

3.5 Synthesis of Polyether-polyesteramide Block Copolymer

The nylon-6 block copolymers were prepared by a simulated reaction injection moulding (RIM) process. The block copolymer was made by Dr. S.W.-Tsui at the University of Bradford. Therefore the reaction components were divided into two parts in a weight ratio of about 1:1. They were placed into two beakers which were then covered with cotton wool which prevented the moisture in the air from deactivating the catalyst. No nitrogen atmosphere has been introduced.

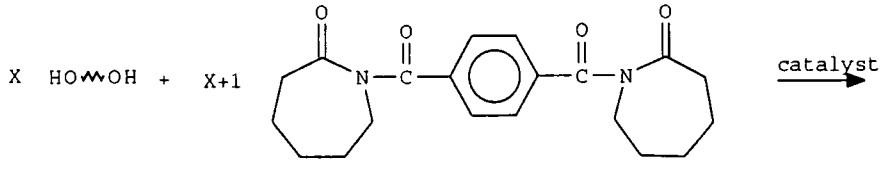

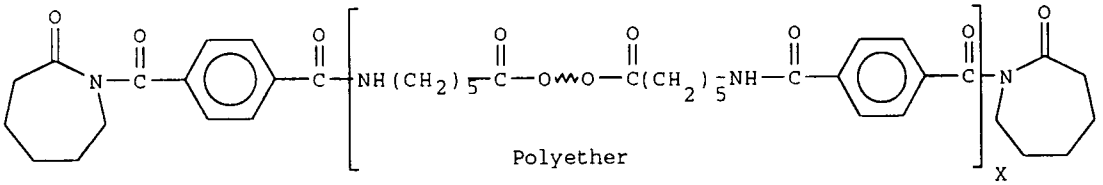

polyesteramide prepolymer

Fig. 3.4 Prepolymer formation

Beaker A, which contained the prepolymer and a part of the total amount of caprolactam, was heated to a temperature of 90 °C. This temperature was maintained until all the caprolactam was melted. The remaining caprolactam in beaker B was heated to a temperature of 110 °C. The catalyst (caprolactam magnesium bromide) was then poured into the beaker. The temperature was maintained until the catalyst was well dissolved into the caprolactam. The temperature was then lowered to about 90 °C, and the contents of beaker A and B were finally mixed together for copolymerisation into a preheated (140 °C) mould. The polymerisation was allowed to proceed at 140 °C for 5 min before demoulding. Impurities, like starting material or oligomers were removed with hot methanol followed by drying at 60 °C under vacuum.

3.6 Mode of Formation of Polyether-polyesteramide Block Copolymer

Polymerisation of the polyether polyesteramide with caprolactam suggests that either an ABA or an alternating AB block structure is possible, where A is the polyamide and B is the polyether-polyester block. At first glance it appears that caprolactam polymerisation from each end of the prepolymer would lead to an ABA structure. However, it is known that ester and amide linkages in the prepolymer can function as initiation and transfer sites [4,11,12]. Polyamide chains can be formed and incorporated into the prepolymer unit at these sites, leading to an alternating structure shown in figure 3.5. Of course, the resulting

polyamide block length would decrease by a factor of x, the number of polyether units in the prepolymer, provided the incorporation of polyamide will be equally distributed in the block copolymer. The homogeneity of the polyamide phase was investigated and confirmed by Hedrick and Gabbert [4]. Kurz [9] has shown that the molecular weight of polyamide units matches better to an alternating structure than to the ABA structure by selective degeneration of the soft blocks. An example of his work showed that the number average molecular weight of the polyamide blocks is 2400 g/mol which is in agreement to the calculated AB structure, rather than 17200 g/mol as expected for an ABA structure. Considering the definition of the number average molecular weight

$$\bar{M}_n = \frac{\sum_i w_i}{\sum_i n_i} \qquad (3.1)$$

where w_i is the mass of the ith fraction in the specimen

n_i is the number of moles of the ith fraction in the specimen

the average number of polyamide units is 21 and 152 respectively for the above mentioned molecular weights. For the alternating structure in 3.5 this means that the indices a, b, c and d are equal to 21 lactam units.

This structure was also proposed by the workers who have developed that system [4,8]. However, the final structure has a significant effect on the domain sizes of the polyamide blocks and therefore the morphology of the system. One would strongly expect larger domain sizes of polyamide in an ABA than in an AB block copolymer. It

should be pointed out that the prepolymer has a given molecular weight and consequently could be considered as a constant. For different molecular weights of the polyether, the domain sizes of the polyamide are expected to be smaller with decreasing molecular weight of the polyether because the number of active end-groups in the prepolymer is increasing. In a later chapter the structure and morphology will be studied by obtaining the domain sizes of the different blocks by means of proton solid-state NMR. Conclusions about the morphology and chemical structure obtained by this technique will be discussed in chapter 5.

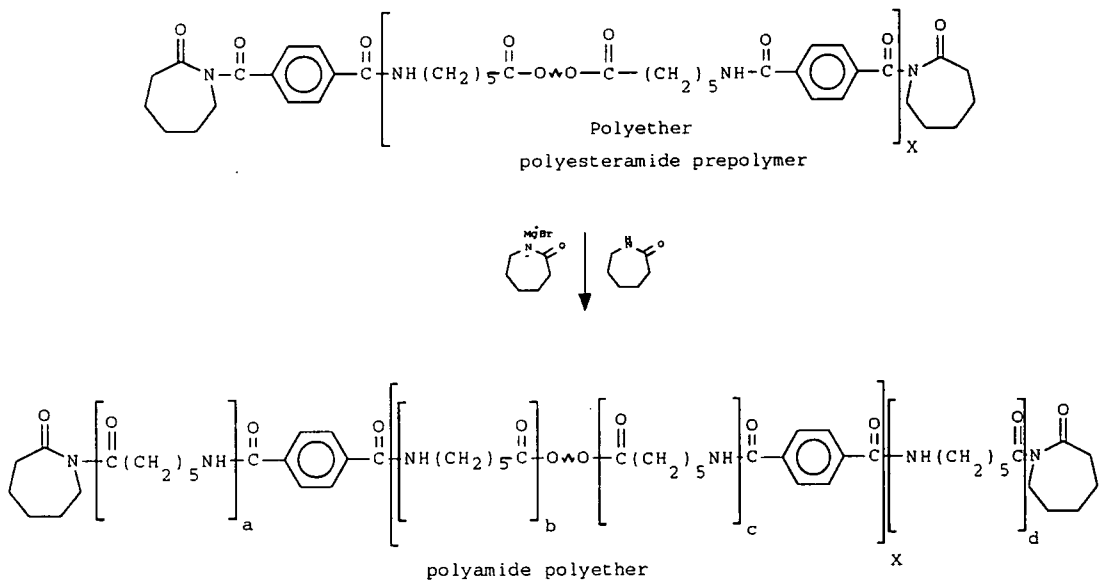

Fig. 3.5 Copolymer formation

3.7 Spectrometer Systems

Three spectrometer systems, a Bruker CXP-200, a Varian VXR-300 and a custom built WRAC, were used for the majority of the work outlined in this thesis. The CXP-200

is equipped with a 4.7 Tesla wide-bore (89.5 mm) magnet, with a proton resonance frequency of 200.13 MHz and 50.322695 MHz for ^{13}C. Two broad-band, dual-channel double-bearing probes were usually used on the CXP-200 spectrometer. The double-bearing probes provided a very stable spinning system for magic-angle spinning studies. The spinning speed of the rotor could be up to 5 kHz.

The VXR-300 is a spectrometer equipped with a 7.1 Tesla narrow-bore (89 mm) magnet with a proton resonance frequency of 299.95 MHz. The probe used for the CP/MAS experiments was a double-bearing Doty Scientific 7 mm. The rotor material was zirconia, with Kel-F end-caps. The bearing/spin gas for low-temperatures was nitrogen, cooled through a heat exchanger placed in liquid nitrogen and then heated to the required temperature by the probe heater, or just air for high-temperature experiments.

The ^{1}H relaxation time measurements and the spin-diffusion measurements were performed on a custom-built spectrometer, which has a proton resonance frequency of 60.00 MHz. It was especially designed for static proton relaxation measurements. It is controlled by a BBC 8 bit computer with a custom-built pulse programmer. The relaxation data analysis was carried out on an Archimedes microcomputer to which the data were transferred after acquisition.

References to Chapter 3

[1] Hanford, W.E and Joyce, R.M., U.S. Patent 2,241,322, 1941

[2] Joyce, R.M., Ritter, D.M., U.S. Patent 2,551,519,1941

[3] Hanford, W.E and Joyce, R.M., J. Polym. Sci., **3** (1948) 167

[4] Monsanto, Italien Patent 580,069 (1958)

[5] Hedrick, K.M. und Gabbert,J.D., "A New RIM System From Nylon 6 Block Copolymers Chemistry" AIChE **14** (1981) 1

[6] Powell, D.G., Mathias,L.J., J. Am. Chem. Soc., **112** (1990) 669

[7] Hall, H.K., J. Am. Chem. Soc., **80** (1958) 6404

[8] Gabbert, J.D., Hedrick,R.M., Polym. Proc. Eng., **4**(2) (1986) 359

[9] Kurz, J.E., Polym. Proc. Eng. **3**(1) (1985) 7

[10] Hedrick, R.M., Gabbert, J.D. und Wohl, M.H., ACS Symposium Series, "Reaction Injection Moulding", ed. Kresta, J.E., **270** (1985) 135

[11] Goodman, I., Developments in Block Copolymers, Vol. 1, ed. Goodman, I., Applied Science Publishers, London (1982)

[12] Goodman, I., Hurworth, N.R., British Patent 1099 184, 1968

Chapter 4

4. High-resolution ^{13}C Cross-polarisation Magic-angle Spinning (CP/MAS)

4.1 Introduction

This chapter will illustrate the power of high-resolution CP/MAS in examining the NYRIM system. The work concentrates on the structural elements of the NYRIM, but qualitative results of local mobilities in the polymeric material will be dealt with as well. Another topic is the cross-polarisation dynamics. Only little attention has been given to polarisation-transfer in heterogeneous materials, that is governed by spin-diffusion. This thesis will at least try to understand the basic rules involved in this matter.

The interesting fact of this thesis is that it deals not with "ideal" samples which suit a certain solid-state NMR technique. NYRIM is entirely a commercial product. All the results obtained in this thesis will be compared with other standard analytical methods and prove or disprove the capability of solid-state NMR for investigating commercial materials.

4.2 The Solid-state High-resolution CP/MAS Spectrum of NYRIM and Nylon-6

The CP/MAS spectra presented were all acquired on the Bruker CXP200 spectrometer unless otherwise stated, using a spectral width of 20 kHz. The other parameters, like

number of transients, data points acquired, recycle delay and contact time, are stated on the spectra. The spectral assignments are made by comparison with the solid-state Nylon-6 spectrum which is described in the literature and with solution-state work on poly(propylene oxide), which has been intensively studied by Schilling and Tonelli [1]. Some examples of annealed and quenched samples will be given. In actual fact *annealed* in this thesis means a sample that has been allowed to cool down to ambient temperature without applying any external temperature. A quenched sample has been prepared as a thin film and then rapidly cooled in liquid nitrogen.

The structure of the Nylon-6 block copolymer was studied by means of simple C-13 CP/MAS spectroscopy. Dynamical properties were studied indirectly and qualitatively by means of selective $T_{1\rho}^{H}$-measurements and cross-polarisation dynamics.

Firstly the variation of ^{13}C-CP/MAS of NYRIM with different compositions will be shown. Figures 4.1 to 4.4 present spectra for Nylon-6 and a selection of NYRIM materials. Tables 4.1 and 4.2 give relevant chemical shift data both from the literature and from the present work. It has to be mentioned that figures 4.1 to 4.3a and tables 4.1 and 4.2 were already presented for my German Diploma degree. Nylon-6 is known to exist in two crystalline forms. The thermodynamically more stable form is called the α-phase and consists of molecules in an extended chain conformation, with hydrogen bonds between anti-parallel chains [2,3]. A representation of the two crystalline forms of nylon-6 is given in figure 4.5. In figure 4.5,

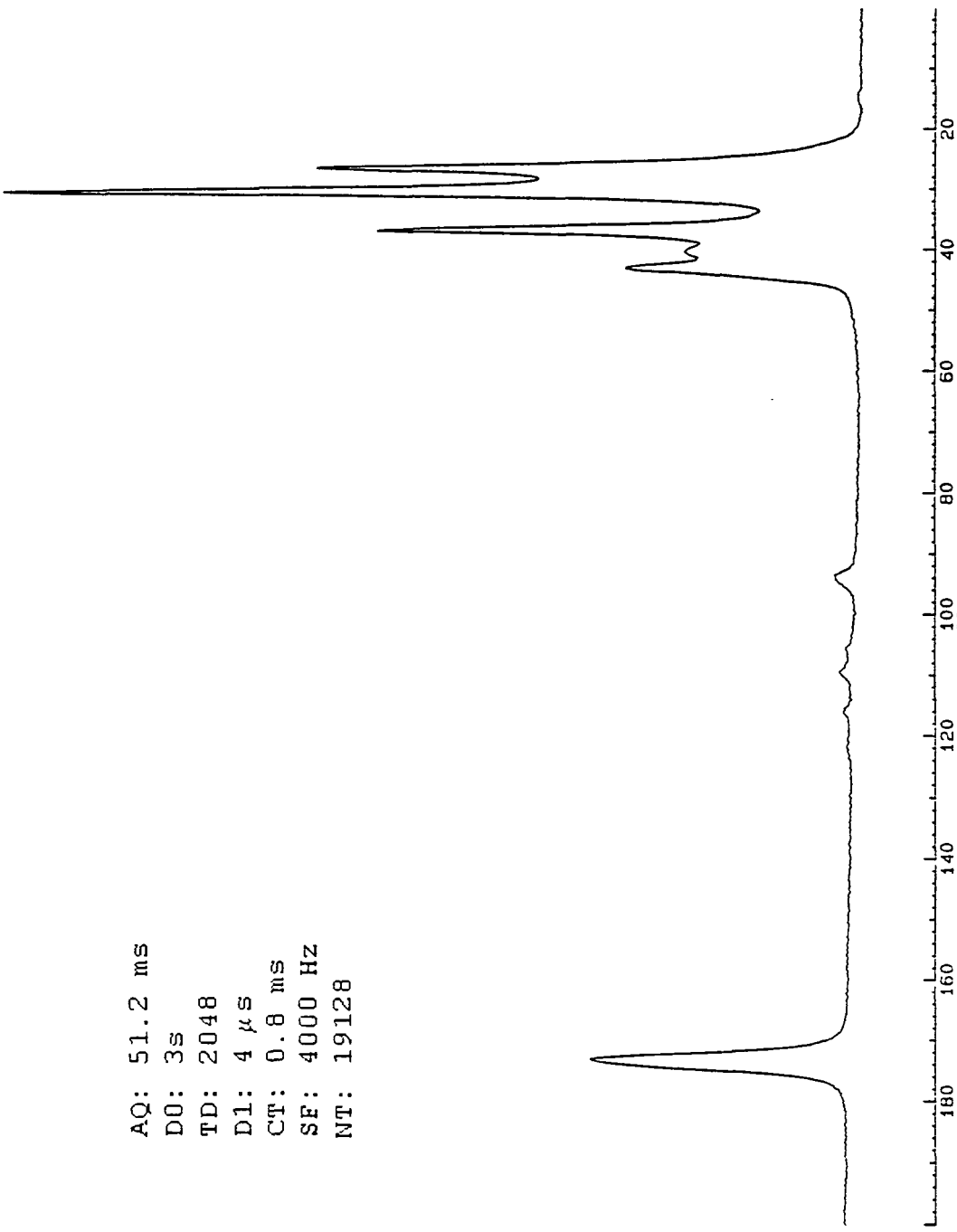

Figure 4.1 C-13 CP/MAS spectrum of nylon-6

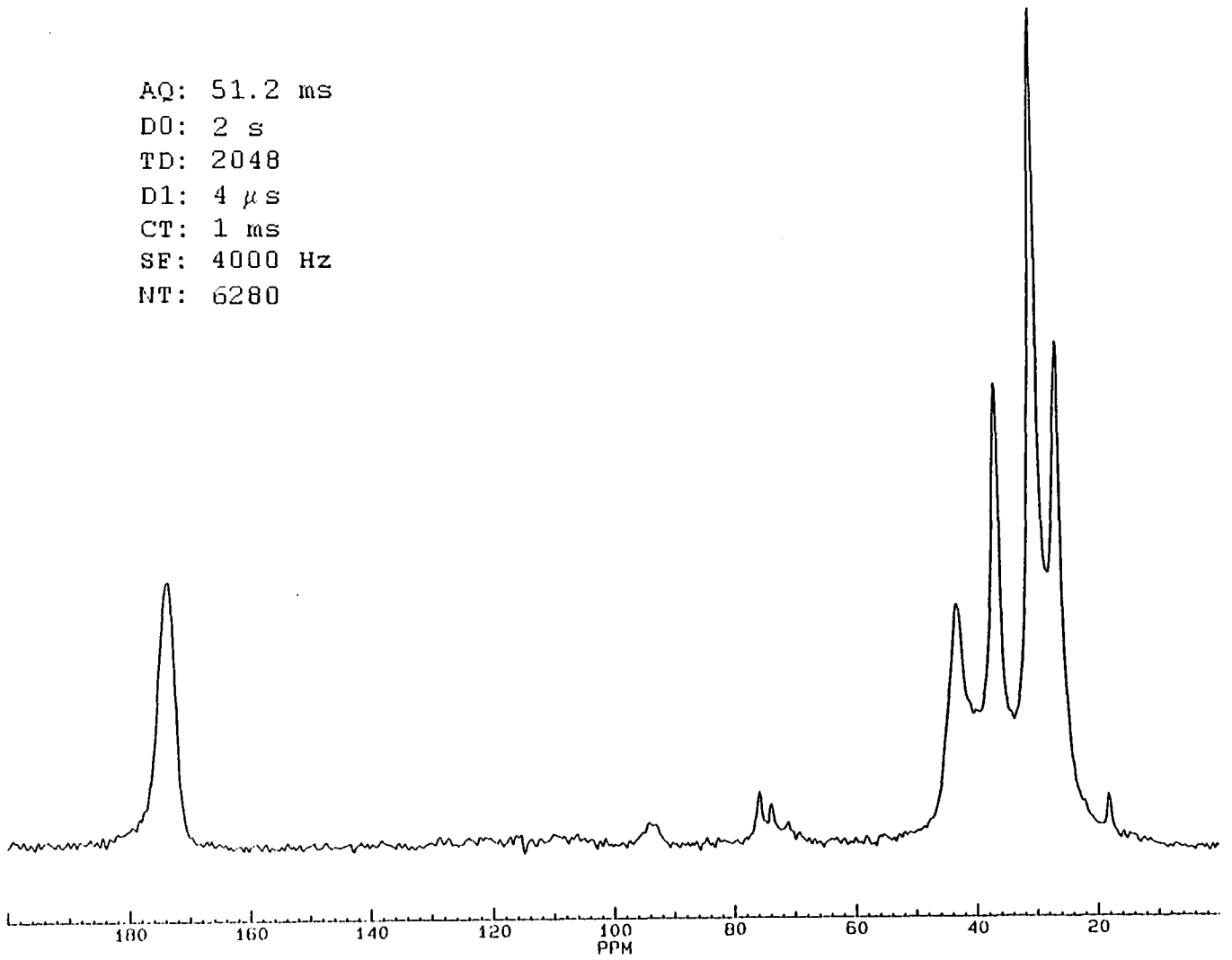

Figure 4.2 C-13 CP/MAS spectrum of nylon-6 + 20% prepolymer

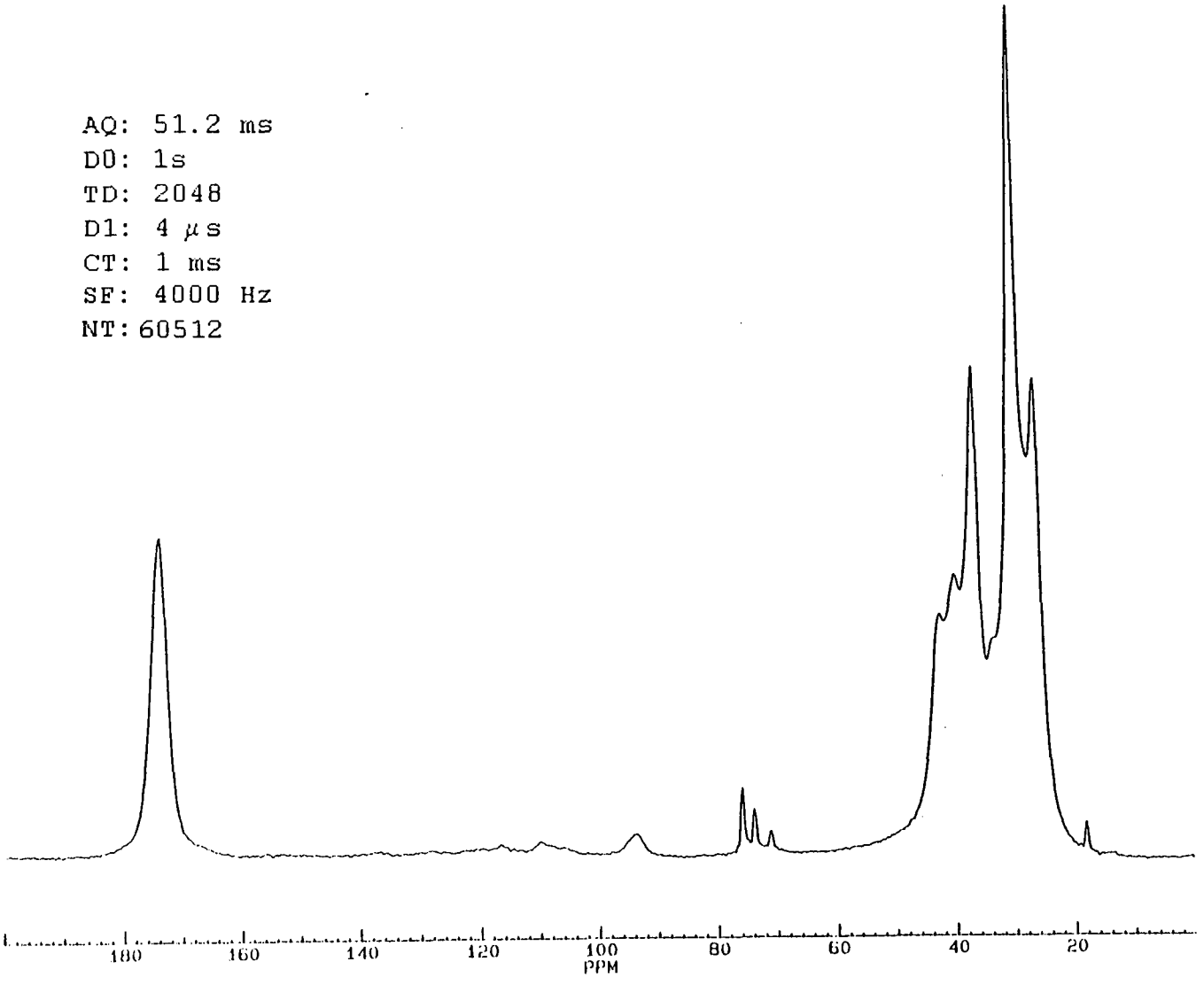

Figure 4.3 C-13 CP/MAS spectrum of quenched Nylon-6 + 20% Prepolymer

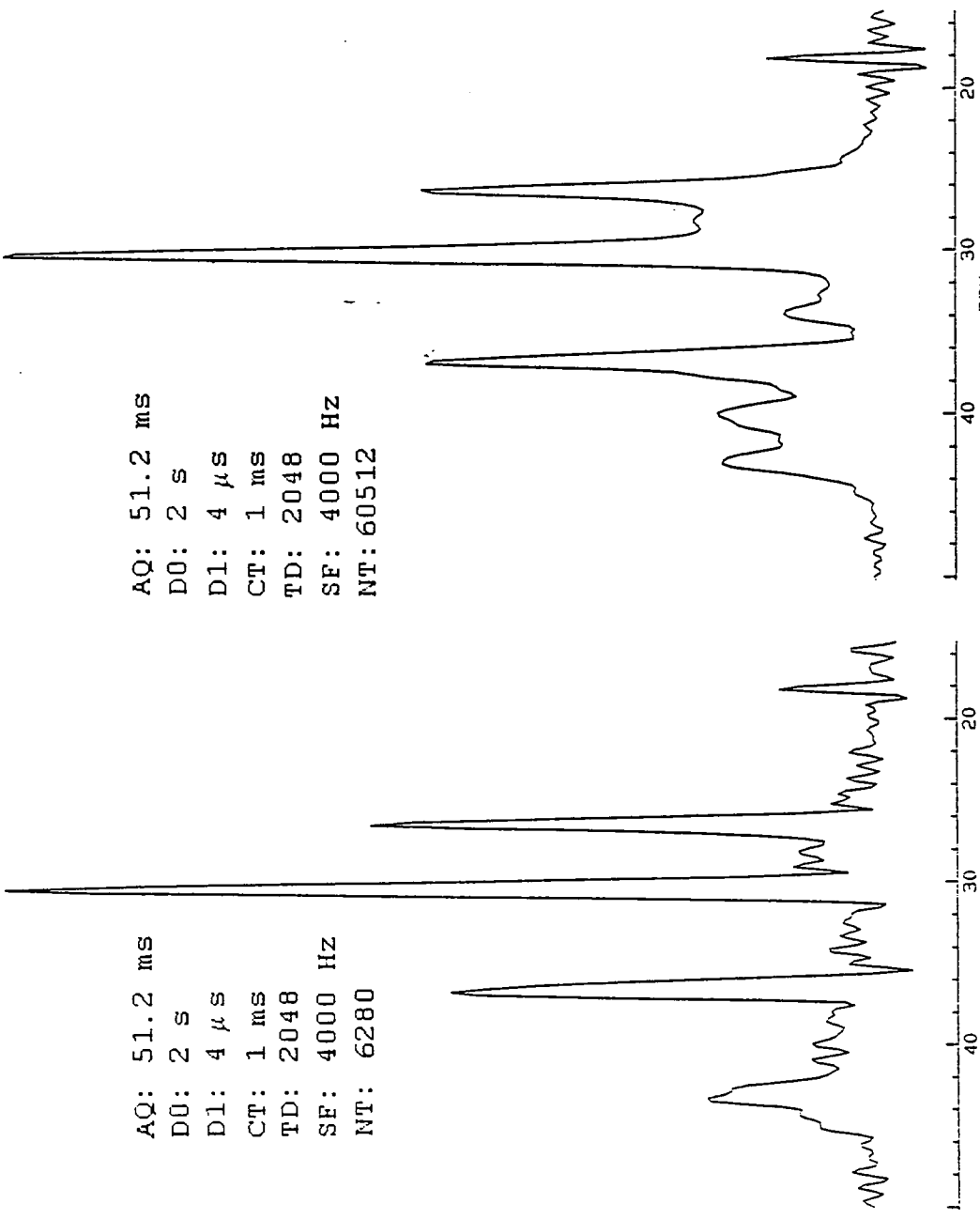

Figure 4.3a CP/MAS C-13 spectrum of Nylon-6 + 20% Prepolymer (left annealed, right quenched, resolution enhanced GB: 0.99, LB: -100 Hz)

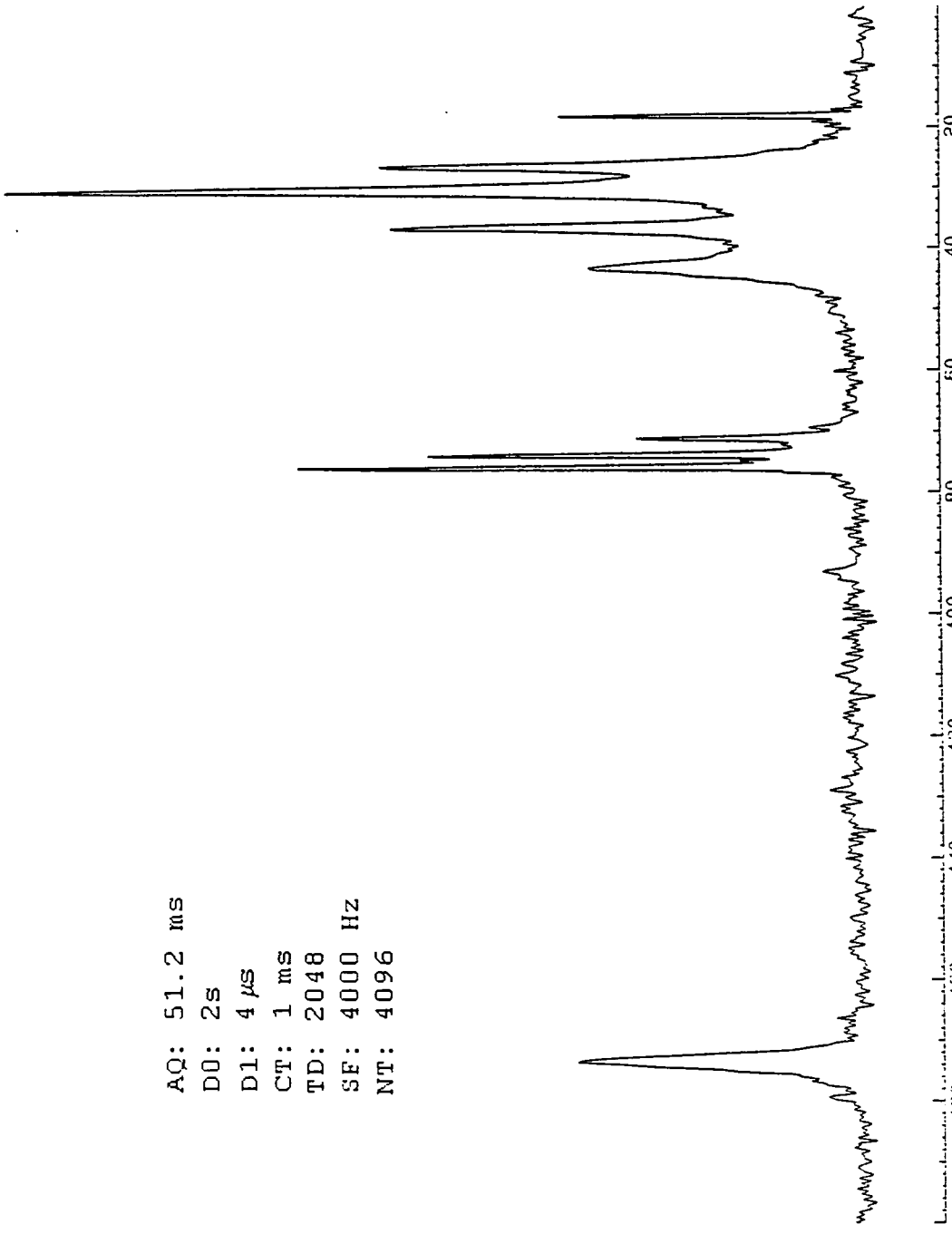

Figure 4.4 C-13 CP/MAS spectrum of nylon-6 + 70% prepolymer

the black filled circles represent carbon-atoms, the grey filled circles represent oxygen-atoms and the open circles are nitrogen-atoms. Very little is known about the structure of the amorphous phase. The nature of the hydrogen bonding plays a key-role for the physical properties of nylon-6. The hydrogen-bonding creates delocalisation in electron density at both the carbonyl and the amide sites, resulting in each nucleus becoming deshielded, and the C-13 carbonyl and N-15 amide chemical shifts are expected to move to higher frequency.

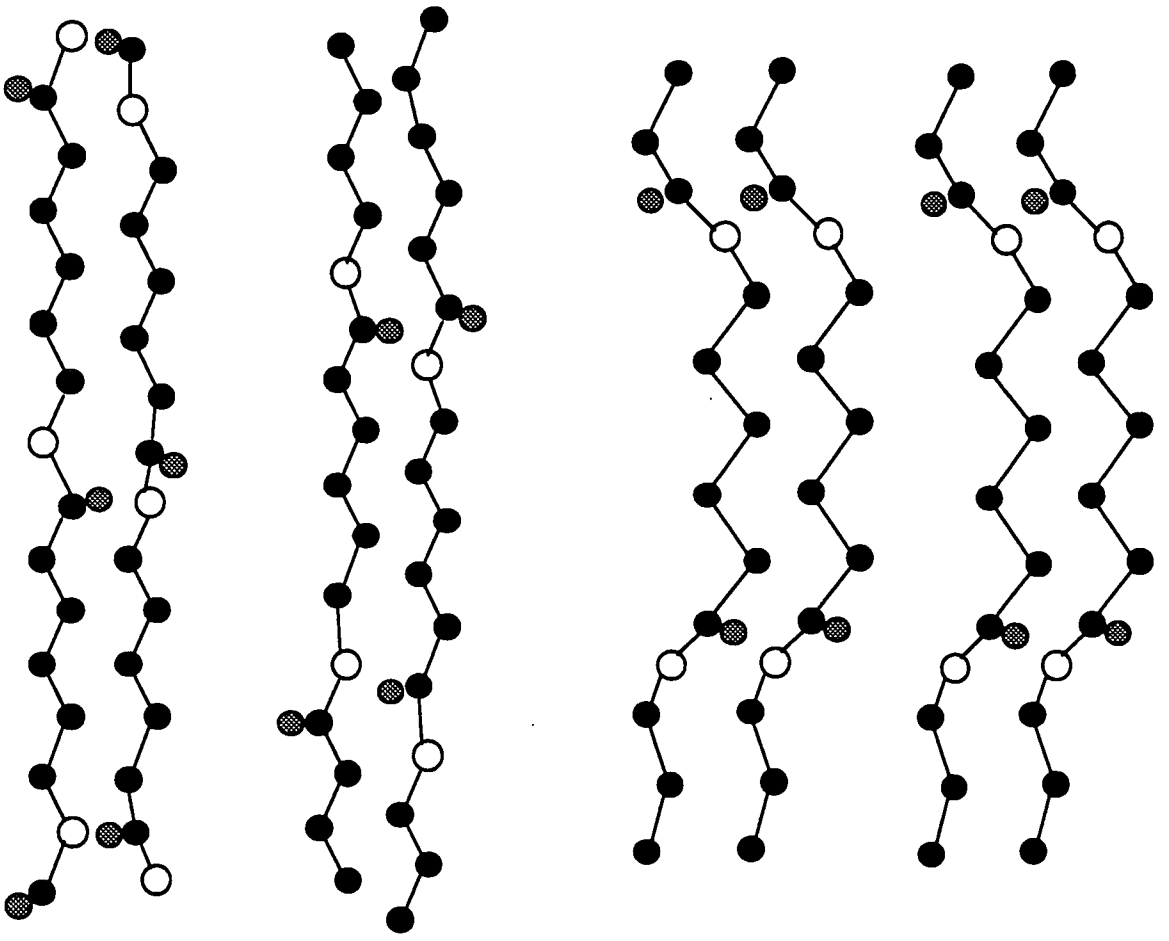

Nylon-6 (α)

Nylon-6 (γ)

Figure 4.5 Conformations of Nylon-6

Hatfield et al. [4] found N-15 CP/MAS to be a very sensitive tool for investigating the conformational changes in molecules. According to the N-15 chemical shift they found, they came to the conclusion that the hydrogen-bond is strongest in the γ-, followed by the amorphous- and finally the α-phase. This conclusion was confirmed by infra-red and X-ray data [7]. This is a surprising result, because it suggests that the γ- and amorphous phases are more strongly hydrogen-bonded than the thermodynamically more stable α-phase. It also implies that the thermodynamical stability of the α-phase relative to the γ – phase arises from interactions other than, or in addition to, hydrogen bonding. These could be e.g. interactions like Van der Waals and/or electrostatic interactions. However, the resonances of the carbonyl carbons do not confirm these results. Table 4.1 shows the C-13 chemical shifts of the polyamide-6 phase and figure 4.6 shows the numbering of the nylon-6 carbons used for assignment.

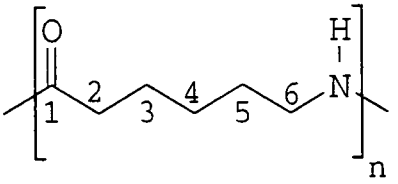

Nylon-6

Figure 4.6 Numbering of the carbons in nylon-6

According to the chemical shift of the carbonyl carbon, the hydrogen bond is equally strong in all three phases. Until today there is no conclusive explanation for the

^{13}C-chemical shifts in the α- and γ-phases. One explanation that accounts for the apparent discrepancy in the α- and γ-phase carbonyl shifts is that other factors are compensating for the hydrogen bonding effect on the ^{13}C-shifts in the crystalline phases of nylon-6. Several possibilities exist including, among others, hyper-conjugation and chain-packing effects. Note from table 4.1 that the ^{13}C-shifts for carbons C3, C5, and C6 are substantially different in the α- and γ-phase. This undoubtedly reflects the structural differences between the two phases. The deshieldings for C3 and C5 in the γ-phase relative to the α-phase were explained by Okada [8] by hyperconjugative effects. In the α-phase, the methylene chain is fully extended, while in the γ-phase the amide-group is rotated out of the plane. The dihedral angles θ between the π-orbital and the σ(C2-C3) bond are about 30° in the γ-phase, judging from the X-ray study [8]. This conformation is very advantageous for hyperconjugation or $\sigma - \pi$ conjugation. It is expected that the C2-C3 σ-bond can overlap with the π-orbitals of the carbonyl-group, allowing a transfer of electron density into the carbonyl-group (see figures 4.7 and 4.8). This should qualitatively deshield C3 and C1. The shielding of C1 might compensate for the deshielding effect from the hydrogen-bonding. Okada [8] applied the same argument to explain the deshielding of C5 through hyperconjugation with the p-orbital of the amide nitrogen as illustrated in figure 4.8. Hyperconjugation would not seem to apply here since the nitrogen p-orbital is filled and one would not expect effective electron transfer to occur from the C6-C5 σ-bond

towards the amide group. Further, hyperconjugation would increase the charge density at nitrogen and would be expected to cause a shielding effect on the ^{15}N chemical shift. This is in disagreement with the result found by Hatfield [4] for the ^{15}N chemical shift in nylon-6. Hatfield also claims that simple electronic effects cannot account for these differences, as semiempirical MNDO and ab initio calculations on model alkyl amides reveal no trends that correlate directly with the observed differences between the α- and γ-phase in nylon-6. A possible explanation could be found from the intermolecular crystal forces for the observed shifts. An obvious benefit of a clear understanding of the chemical shifts of polyamides is the potential for modelling amorphous phase structures. The knowledge of how these two phases are packed in the α- and γ-phase might suggest an answer. However, this is not an easy task, since the amorphous structure is still mysterious. The amorphous phase shows a substantially low-frequency shift for C4 (-3.0 ppm) and C6 (-3.3 ppm) compared to the α-phase and a low-frequency shift for C2 (-0.9 ppm), C3 (-3.9 ppm), C4 (-2.7 ppm) and C5 (-4.1 ppm) relative to the γ-phase [4]. This suggests that the amorphous chains prefer an extended conformation about the amide moiety. Kubo et al. [9] assigns a γ-gauche effect for the shielding of C6 in the amorphous phase, which happens to be present in vinyl polymers [10]. But this would also include a shielding for C3, which is not observed. Instead, this shift suggests a deshielding effect, possibly related to packing. More recent research has been carried out by

Sample	Phase	C-1	C-2	C-3	C-4	C-5	C-6
Reference [5]							
Nylon-6	α-crystalline	173.4	36.8	26.5	30.1	30.1	42.8
	γ-crystalline[a]	173.4	33.9	26.7	30.0	30.0	39.9
	amorphous[b]	173.4	36.3	26.2	27.9	29.8	40.1
Reference [6]							
Nylon-6	α-crystalline[a]	173.4	36.7	26.5	30.4	30.4	43.6
	γ-crystalline[b]	173.0	37.8	30.1	30.1	34.1	39.9
	amorphous	174.5	36.9	26.2	27.4	30.0	40.3
	solution[c]	177.8	37.2	26.4	27.1	29.5	40.7
Reference [8]							
Nylon-6	α-crystalline[d]	171.1	34.4	24.3	28.1	28.1	41.1
	γ-crystalline[d]	171.0	35.4	28.2	28.2	32.0	37.9
	solution[d]	176.4	34.6	24.4	25.0	27.2	39.2

[a] CP/MAS at room temperature

[b] Bloch decay / MAS at 100°C

[c] dilute solution in trifluoroethanol

[d] external reference: glycine carbonyl signal (176.03 ppm)

Table 4.1a ^{13}C Chemical shift assignment for nylon-6 / ppm (literature)

Sample	Phase	C-1	C-2	C-3	C-4	C-5	C-6
Nylon 6	α-crystalline	173.1	36.6	26.5	30.4	30.4	43.3
Nylon-6	amorphous[e]	174.2	36.8	26.2	28.2	30.4	40.0
NBC20	α-crystalline	173.2	36.4	26.1	30.1	30.1	43.0
NBC20							
(quenched)	α-crystalline	173.2	36.4	26.1	30.1	30.1	43.0
	γ-crystalline	na	35.0	na	na	33.8	na
	amorphous	173.2	36.4	26.1	28.1	30.1	40.0

na: chemical shifts overlap with chemical shifts of α-crystalline nylon-6

[e] Bloch/MAS decay at room temperature

Table 4.1b ^{13}C Chemical shift assignment for nylon-6 and the polyamide part in NYRIM / ppm

PPO			PEO
CH	CH_2	CH_3	CH_2
75.8	73.9	18.2	71.2

Table 4.2 ^{13}C Chemical shift assignment of the polyether part in NYRIM / ppm

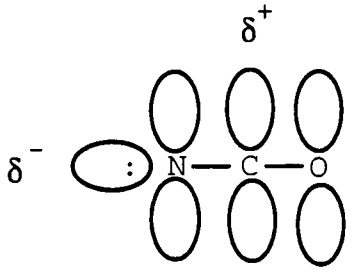

Figure 4.7 Polarisation of amide of hydrogen-bonded nylon-6

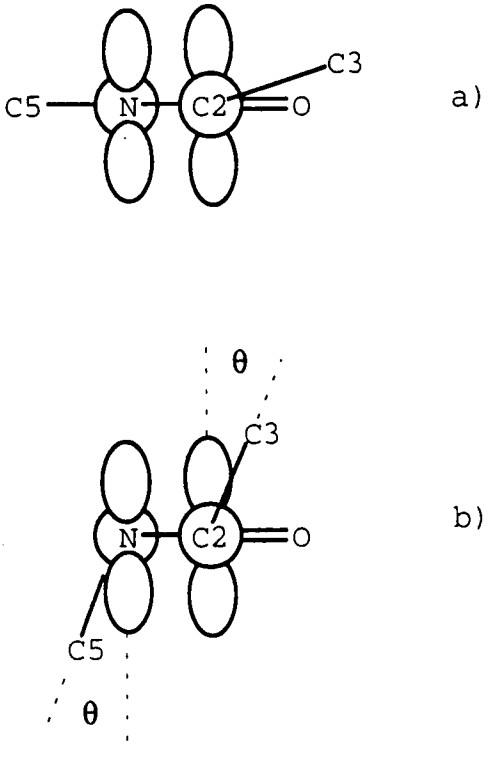

Figure 4.8 Hyperconjugative effects in nylon-6:

a) α-form; b) γ-form

Powell and Mathias [11]. They used ^{15}N-labelled α-nylon-6 to investigate ^{15}N spin-lattice relaxation times. For the crystalline phase they found as expected a very long T_1^N (416 s). However, for the amorphous phase they found two different relaxation times (29 s and 1.9 s). They assigned the short relaxation time to a liquid-like mobile region and the longer relaxation time to a noncrystalline interface region with restricted motion. Unfortunately, the authors did not give the proportion of the two populations, but from the graphical representation they presented in their publication I found that the "interface" region makes about 30% of the total amorphous fraction, which I consider is too high to be an interfacial region. From my own measurements I could not detect an interfacial region of that extent between the amorphous and the crystalline region in nylon-6 (see chapter 5) and therefore I cannot confirm the results found by Powell and Mathias.

However, the ^{13}C spectrum of the polyamide carbons of the block-copolymer shows in principle the same features as the ^{13}C spectrum of nylon-6. A very interesting observation was made by comparing the carbon resonances of the annealed and the quenched nylon-6 phase. Undoubtedly the annealed material does not show the resonances at 40 ppm and 28 ppm that the quenched material reveals (figure 4.3a). The single-pulse spectrum of annealed NBC50 (figure 4.41a), however, shows strong, intense but mainly unresolved signals of the amorphous nylon-region. As DSC results reveal (see chapter five), the crystallinity of the nylon-phase is only about 35% in the annealed

material, which explains the intense resonances of the amorphous region in the single-pulse experiment. But it remains a question as to why the CP efficiency of the amorphous region is so small. If the proton free-induction decay is taken as a measure of the dipolar strength, then this cannot be the reason for the low CP efficiency, because the time constant of the FID, T_2, is not distinguishable between the crystalline and amorphous phases (see e.g. figures 5.19 and 5.20 in chapter five). Additionally, for quenched NBC20 the same cross-polarisation characteristics were found for the amorphous phase as for the crystalline phase (see figure 4.9). Another point which could be responsible for the low CP efficiency, is $T_{1\rho}^H$ relaxation. A variable contact-time experiment the purpose of which it was to check the $T_{1\rho}^H$ value of the amorphous region is depicted in figure 4.9. The resonances of the amorphous and the crystalline regions are strongly overlapping, therefore only C6 for the amorphous region can be used to compare the relaxation characteristics. The cross-polarisation dynamics show that the signal maximum of the amorphous phase agrees with that of the crystalline phase, indicating their same CP-characteristics. The signal decay, which is responsible for the $T_{1\rho}^H$ relaxation, only shows a slightly faster relaxation for the amorphous region compared to the crystalline region, as seen in figure 4.9. However, as discussed in a later section, the variable contact-time experiment only detects long-time component relaxation. Whether the amorphous region is dominated by a short-time

component relaxation cannot be said for certain, but the results strongly suggest this.

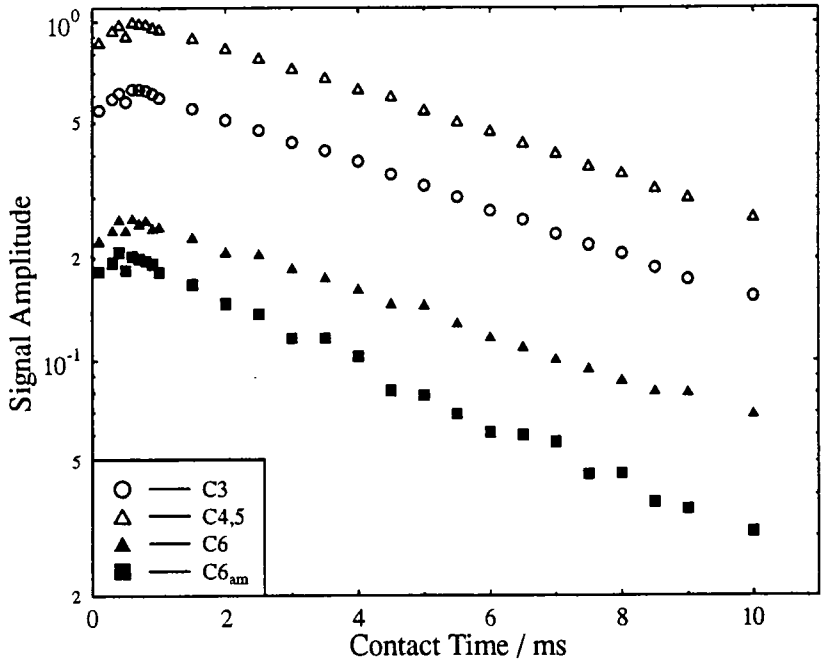

Figure 4.9 Time-dependence for the intensity of C-13 signals in a powder sample (nylon-6 carbons) of nylon-6 + 20% prepolymer in the variable contact-time cross-polarisation experiment (D0=2 s, AQ=25.6 ms, TD=512, NT=2048, SW= 10000 Hz, rotor spinning frequency: 4000 Hz) am: amorphous region

4.3 Cross-polarisation Dynamics

4.3.1 Introduction

Cross-polarisation in connection with magic-angle spinning and high-power decoupling (CP/MAS) is now well-established as a routine technique for the spectroscopic investigation of solids [12]. The understanding of the time-dependence of magnetisation transfer between two unlike nuclei is, however, not a fully understood problem. This section tries to summarise the different theories and applies them to the NYRIM-system.

4.3.2 Theory

Suppose we have a system of abundant I- and rare S-spins. Each spin-system is coupled to the lattice and approaches the lattice temperature (in terms of spin-temperature β) with the spin-lattice relaxation time T_{1I} and T_{1S} respectively, as is shown in figure 4.10. If the dipolar interactions among the protons are strong, then spin-diffusion, symbolised by the isotropic spin-diffusion operator Γ, is effective. In general spin-diffusion is negligibly small among the carbons because of their low abundance. The I and S spins may be coupled by some interactions represented by the cross-relaxation time T_{IS}. This is the case if the Hartmann-Hahn (eqn. 4.1) condition is fulfilled.

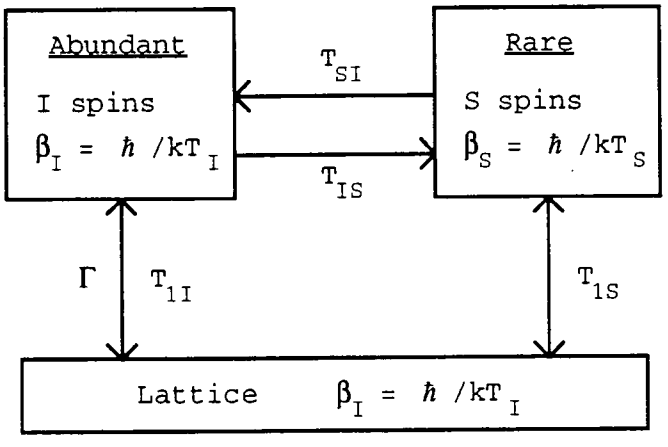

Figure 4.10 Schematic representation of an abundant I spin reservoir, which is coupled to the lattice by their spin-lattice relaxation times T_{1I} and T_{1S} and spin-diffusion Γ among the abundant I spins. The coupling between the two reservoirs is represented by the cross-relaxation T_{SI} and T_{IS} that can be varied in direction by suitable application of rf-fields (depolarisation and polarisation of S spins)

$$\omega_{1I} = \gamma_I B_{1I} = \gamma_S B_{1S} = \omega_{1S} \qquad (4.1)$$

Where B_{1I} and B_{1S} are the rf-fields in the rotating frame of the I and S spins respectively and ω_{1I}, ω_{1S} are the precession frequencies of the I and S spins in their respective rotating frames of reference on resonance. Since the I spins are cold and the S spins are hot, there will be a calorimetric effect [13] and energy exchange may proceed with a time constant T_{IS}. It should be noted that only if $T_{IS} << T_{1I}, T_{1\rho I}$ is this energy exchange considerable and can be utilised for a double resonance effect.

To describe the variation of the inverse spin temperature β_I and β_S of the I and S spins respectively while these two spin-systems are in contact, it is assumed that the initial inverse S-spin temperature is zero $(\beta_S = 0)$. If the Hartmann-Hahn match is fulfilled then:

$$\beta_I = \beta_L \frac{B_0}{B_{1I}} \qquad \text{spin-locking} \quad B_{1I} >> B_{LI} \qquad (4.2)$$

where B_{IL} is the field of the lattice. Invoking energy conservation in the rotating frame it can be written

$$\frac{d}{dt}\beta_I + \varepsilon' \frac{d}{dt}\beta_S = 0 \qquad (4.3)$$

where $\varepsilon' = \varepsilon\alpha^2 = \frac{N_S S(S+1))}{N_I I(I+1))}\alpha^2$ and $\alpha = \frac{\gamma_S B_{1S}}{\gamma_I B_{1I}}$ (Hartmann-Hahn mismatch parameter).

The S-spin temperature β_S is relaxed with the time constant T_{IS} towards the instantaneous I-spin temperature which results in the following coupled differential equations:

$$\frac{d}{dt}\beta_S = -\frac{1}{T_{IS}}(\beta_S - \beta_I) - \frac{1}{T_{1\rho}^S}\beta_S$$
$$\frac{d}{dt}\beta_I = -\frac{\varepsilon'}{T_{IS}}(\beta_I - \beta_S) - \frac{1}{T_{1\rho}^I}\beta_I \qquad (4.4)$$

The last terms on the right hand side have been added to account for relaxation in the rotating frame which may occur if $T_{1\rho} \cong T_{IS}$. Mehring [14] gave some solutions for special cases. From those one, will be pointed out: If $\varepsilon = 0$ (vanishing heat capacity of the S spins) and $T_{IS}/T_{1\rho}^S \neq 0$, the solution of the coupled differential equation is:

$$\beta_S(t) = \frac{1}{1-\lambda}\left(1 - e^{-(1-\lambda)t/T_{IS}}\right)e^{-t/T_{1\rho}}\beta_{I0}$$
$$\beta_I(t) = e^{-t/T_{1\rho}}\beta_{I0} \qquad (4.5)$$

where $\lambda = T_{IS}/T_{1\rho}^I + T_{IS}/T_{1\rho}^S$

This equation is particular useful for a quantitative analytical description of a time-dependent cross-polarisation experiment without dominant heterogeneous dipolar interaction, a case that will be discussed next. Note that this equation is only valid under exact Hartmann-Hahn condition ($\alpha = 1$).

As was described by McArthur et al. [15] the ^{19}F resonance of CaF_2 shows transient oscillations in the rotating frame in the double-resonance experiment. These oscillations were confirmed by Ernst and co-workers [16] for a ferrocene single-crystal. They used a simple thermodynamic picture based on the spin-temperature concept [17-20]. As Hartmann and Hahn showed previously [21], transient oscillation can be observed for cross-

polarisation experiments in liquids. It is caused by coherent off-diagonal elements of the density operator which are produced by the scalar spin-spin interaction between the I and S spins. An oscillatory polarisation transfer can also be observed for solids if there is a dominant dipolar interaction which causes a non-Gaussian line or even a line with fine structure. Ernst and co-workers developed a theory based on the following assumptions:

1. The dipolar interactions of the isolated S spins with I spins are only important for coupling to the directly-bonded I spins
2. The interaction of a particular I spin with the remaining I spins is taken into account in a phenomenological manner and is described by an isotropic spin-diffusion process with rate R
3. Spin-lattice relaxation is neglected
4. The concentration of the rare S spins is sufficient low to consider the I-spin system as an infinite energy reservoir

This model leads to a two-stage magnetisation transfer in cross-polarisation experiments as shown in figure 4.12. The density operator equation in a doubly-rotating frame, rotating with the frequencies of the applied rf fields B_{1I} and B_{1S}

$$\dot{\sigma} = -(i/\hbar)[H, \sigma] - \Gamma(\sigma - \sigma_0) \qquad (4.6)$$

can be solved with the following assumptions:

$\Delta\omega_I = \Delta\omega_S = 0$, $|\lambda_I B_{1I} + \lambda_S B_{1S}| >> |b| >> R$

where $\Delta\omega_I = \omega_{0I} - \omega_I$ and $\Delta\omega_S = \omega_{0S} - \omega_S$ are the resonance offsets of the rf-fields,

$b = \frac{1}{2}\left(\lambda_I \lambda_S \hbar / r_{C-H}^2\right) x \left(3\cos^2\Theta - 1\right)$, the dipolar coupling,

Θ is the angle between the axis of the free molecular rotation and the static magnetic field,

$\Gamma(\sigma)$ is the isotropic spin-diffusion operator,

H is the dipolar Hamiltonian:

$H/\hbar = \Delta\omega_I I_Z - \gamma_I B_{1I} I_X + \Delta\omega_S S_Z - \gamma_S B_{1S} S_X + b I_Z S_Z$,

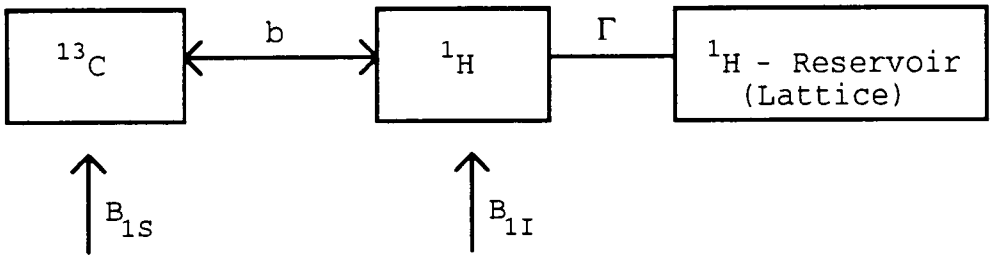

Figure 4.11 Schematic representation of the two-stage magnetisation transfer process in CP-experiments with the dipolar coupling b and the spin-diffusion operator Γ

Ernst et al. gave an expression for the time evolution of the density operator under the exact Hartmann-Hahn condition for a static powder sample:

$$M_{SX}(\tau) = Tr\left[\sigma(\tau) S_X\right] = \frac{1}{4}\beta\hbar\omega_{0I}\left(1 - \frac{1}{2}e^{-R\tau} - \frac{1}{2}e^{-3R\tau/2}\cos\frac{1}{2}b\tau\right) \qquad (4.7)$$

The oscillating frequency of the magnetisation is given by $\omega_{osc} = b / 2$. If we consider a rapidly rotating solid powder (MAS) instead of a single crystal, we have to sum over all orientations of the crystallites. The dipolar modulation of each carbon-13 spin by the local protons can be expected to follow a $\cos\omega\tau$ dependence. Therefore in

the short time limit the higher-order terms in the expansion vanish, and M shows a quadratic dependence on time.

$$\begin{aligned} M &= \sum_i M_{0i} \cos \omega_i \\ &= \sum_i M_{0i} \left(1 - \frac{\omega_i^2 \tau^2}{2!} + \frac{\omega_i^4 \tau^4}{4!} - + \ldots \right) \\ &\equiv M_0 - \sum_i \frac{M_{0i} \omega_i^2}{2} \tau^2 \end{aligned} \qquad (4.8)$$

When the carbons are very strong coupled to the protons, the signal decay frequently is modulated by the strong ^{13}C–^{1}H dipolar coupling. The overall decay of the signal in the short-time limit is described by a Gaussian function:

$$\begin{aligned} M &= M_0 e^{-\tau^2/2T_2^2} \\ &= M_0 \left(1 - \frac{\tau^2}{2T_2^2} + \frac{\tau^4}{2^2 2! T_2^4} - + \ldots \right) \\ &= M_0 - \frac{\tau^2}{2T_2^2} \end{aligned} \qquad (4.9)$$

In such a short-time limit, T_2 is related to ω_i [22]:

$$\frac{1}{T_2^2} = \sum_i \frac{M_{0i} \omega_i^2}{M_0} = \sum_i \frac{M_{0i} \left(b/2 \right)^2}{M_0} \qquad (4.10)$$

$1/T_2$ can be considered to be a root-mean-square average of ω_i, weighted by the fraction M_{0i}/M_0 of molecules with a given orientation having the dipolar modulation frequency ω_i. Summing over all orientations yields destructive interference between crystallites that rapidly attenuates the signal. With eqn. 4.9 and eqn. 4.10 it follows for the polarisation of a CH carbon [23]:

$$M_S(\tau) = M_{S0} \left(1 - \frac{1}{2} e^{-R\tau} - \frac{1}{2} e^{-3R\tau/2} e^{-\tau^2/2T_2^2} \right) \qquad (4.11)$$

Hahn et al. [24] pointed out that, for a dynamical energy-transfer process between two dissimilar nuclei, in principle three situations are important:

1. The system under investigation shows negligible spin-diffusion effects and rapid modulation of the dipolar coupling between rare and abundant nuclear spins. The A-B nuclear coupling is weak, i.e., $T_{AB} >> T_{2A}$. Such a process exhibits a simple exponential rate behaviour
2. If the rare spins have a considerably greater nuclear moment than the abundant spins, giving $\langle M_2 \rangle_{AB} T_{2A}^2 > 1$, where $\langle M_2 \rangle_{AB}$ is the Van Vleck [25] second moment of the magnetic resonance-line, then this simple rate-behaviour will only occur if $\omega_{eB} T_{2A} >> 1$. At lower frequencies, ω_{eB}, the oscillating behaviour will merge with the cross-relaxation process.
3. This picture will be further complicated by spin-diffusion limitations, which will become severe in a case where $T_{AB} < T_{2A}$

4.3.3 The CP-Depolarisation Experiment

Basically two different types of experiment have been carried out to investigate the cross-polarisation dynamics.

1. The depolarisation experiment
2. The polarisation experiment with variable contact-time

The depolarisation experiment that has been applied to monitor the cross-polarisation dynamics is illustrated in figure 4.12. It is a simple modification of the standard

CP pulse sequence. Two additional time-intervals t_d and t_{CP_2} are inserted between the usual polarisation time t_{CP_1} and the acquisition time. As usual, during t_{CP_1} ^1H-magnetisation is locked along B_{1H}, while a polarised ^{13}C-magnetisation is created along B_{1C}. During the time t_d the irradiation of the ^1H-channel is switched off, while the ^{13}C-magnetisation remains spin-locked. Now the ^1H-magnetisation is gradually destroyed by spin-spin relaxation, but the polarisation of the ^{13}C is hardly effected because $T_{1\rho}^C >> T_{CH}$ (for experimental proof see later section). During t_{CP_2}, when the ^1H-irradiation is turned on again, the polarisation transfer happens again but in the reverse direction with respect to that during t_{CP_1}. All depolarisation measurements were carried out at room temperature. The samples were dried over night at 70 °C under vacuum in order to accomplish the same thermal history for all samples.

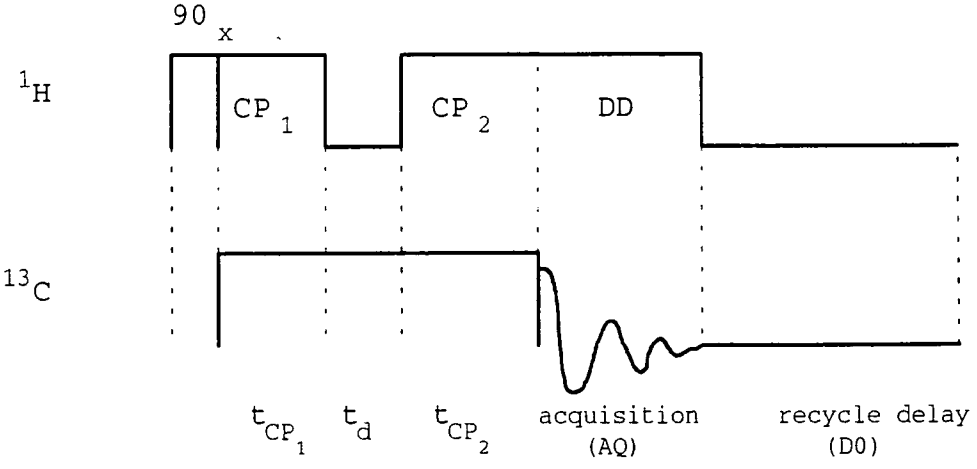

Figure 4.12 Pulse sequence for a C-13 CP/MAS depolarisation experiment, where t_{CP_1} is the polarisation time for the S spins, t_d is the dephasing time for the I spins, and t_{CP_2} is the depolarisation time for the S spins

The spectral-width of all measurements was 10 kHz and the transmitter-offset 5 kHz. The other important acquisition parameters are on the spectra. (NT: number of transients; TD: number of recorded data-points; SF: spinning-frequency of the rotor; for further symbol definitions see figure 4.13)). For the sake of resolution-enhancement, before fourier-transformation the FID was multiplied with an exponential term $\exp(LB \cdot AQ)$, where LB is the line-broadening factor. In all depolarisation experiments a line-broadening of 25 Hz has been applied. Each individual fourier-transformed spectrum has been baseline-corrected in order to accomplish the best reproducible results possible. The Hartmann-Hahn match was carefully set with adamantane as an external reference sample by finding the optimum signal. The only exceptions are the experiments NBC70(3) and NBC70(4) where the match was set to the first maximum signal of the polyether carbon resonances in the NYRIM sample.

4.3.4 Results and Discussion

The time-dependence of the ^{13}C magnetisation as a function of depolarisation time t_d was simulated by using the model suggested by Müller et al. Therefore the experimental data were simulated by a non-linear least-squares fit using equation 4.11 as the basic model. It is easy to obtain an expression for depolarised ^{13}C magnetisation under otherwise-identical conditions.

$$M_S(\tau) = M_{S0}\left(\frac{1}{2}e^{-R\tau} + \frac{1}{2}e^{-3R\tau/2}e^{-\tau^2/2T_2^2}\right) \qquad (4.12)$$

This expression describes the depolarisation of ^{13}C in a CH-group. Assuming that the ^{13}C-H dipolar interactions in CH_2 are twice as strong as in CH, depolarised magnetisation for CH_2 can be described as:

$$M_S(\tau) = M_{S0}\left(\frac{1}{3}e^{-R\tau} + \frac{2}{3}e^{-3R\tau/2}e^{-\tau^2/2T_2^2}\right) \qquad (4.13)$$

The optimised parameters from the analysis of the nylon-6 carbons using equation 4.13 are listed in tables 4.4a and 4.4b. The experimental and the simulated data are illustrated in figures 4.13a to 4.21. Figure 4.13a illustrates the depolarisation of the methylene carbons of nylon-6. Note that C2 is not plotted, because it depolarisation curve interferes with the one of C3. For this reason and because its depolarisation curve shows the same characteristics as the ones for the other carbons, it will not be plotted in the other graphs. The depolarisation of the carbonyl carbon has been depicted in a separate figure (fig. 4.13b). The features of this curve are not changing by varying the polyether concentration, thus it will not be plotted for the other experiments. A numerical analysis of the depolarisation dynamics according to the above-mentioned model could only be done for the nylon carbons. The depolarisation behaviour of the methylene carbons will be discussed first. The two-stage behaviour of the Hartmann-Hahn cross relaxation is depicted in figures 4.13 to 4.21. The short-time behaviour is mediated by the dipolar interactions between an individual ^{13}C and its directly-bonded protons. The $^{13}CH_2$-group can be considered as a subsystem in the whole lattice because of the low natural abundance of ^{13}C

(0.11%). These dipolar interactions are caused by coherent off-diagonal elements of the density operator which are produced by scalar spin-spin interaction between the ^1H and ^{13}C spins [21]. The coherent polarisation transfer may be, as mentioned before, oscillatory in nature. The long-time behaviour can be described by an exponential expression. It is determined by spin-diffusion, which is mediated by interactions of a $^{13}CH_2$-subsystem with the remote H-spins in the lattice. Both polarisation transfer mechanisms depend on dipolar interactions, $b_{het} = \frac{\mu_0}{4\pi} \frac{\gamma_H \gamma_C \hbar^2}{\bar{r}^3_{C-H}} \frac{1}{2} \left(3 \cos^2 \Theta - 1\right)$ for the heterogeneous case, and $b_{homo} = \frac{\mu_0}{4\pi} \frac{\gamma_H^2 \hbar^2}{\bar{r}^3_{H-H}} \frac{1}{2} \left(3 \cos^2 \Theta - 1\right)$ for the homonuclear case, which are proportional to the gyromagnetic ratios of the two nuclei and inversely proportional to the cube of their internuclear distance. The ^{13}C–^1H bond-distance is smaller than the nearest-neighbour distance between two protons. For this reason, and because $\gamma_H = 4\gamma_C$, the polarisation transfer rate of the second stage is much lower than the coherent polarisation transfer. In the following, the cross relaxation of the polyamide methylene carbons shown in the figures will be investigated. The experiments in figures 4.13 to 4.15 show the expected and previously-observed two-feature behaviour [22, 23, 26, 27]. The two-stage feature signifies that the cross relaxation between protonated ^{13}C and protons belongs to the diffusion bottleneck limit [21], so that the proton spin system is not always describable by a single-spin temperature. An interesting observation is the oscillatory behaviour seen in figures 4.16a, 4.17, 4.19a, 4.19b and 4.21. This

behaviour cannot be explained by any simple theory. The analysis of the cross-relaxation data does not show any significant change in the coherent magnetisation transfer time, T_2. The spin-diffusion rates are between 2.91 ms^{-1} and 4.2 ms^{-1} for the different composites. It must be mentioned that data-analysis with equation 4.13 was not always possible for the depolarisation curves with oscillations. The presented theoretical line in the appropriate figures was than obtained by fitting the first part of the curve using only the datapoints until the oscillations start using a Gaussian function, $M(\tau) = M_0 \exp\left(-\tau^2/T_2^2\right)$, and using an exponential expression, $M(\tau) = M_0 \exp(-R\tau)$, for the second stage of the depolarisation.

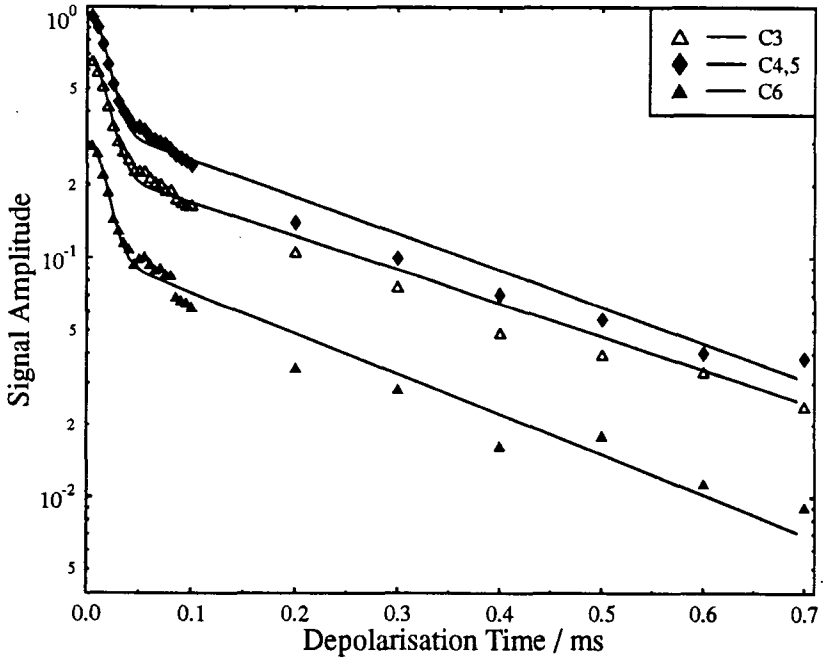

Figure 4.13a Time-dependence of the intensity of C-13 signals in a powder sample of nylon-6 in the depolarisation experiment (t_{CP_1}=800 μs, t_d=100 μs, D0=5 s, AQ=25.6 ms, TD=512, rotor spinning frequency: 4000 Hz)

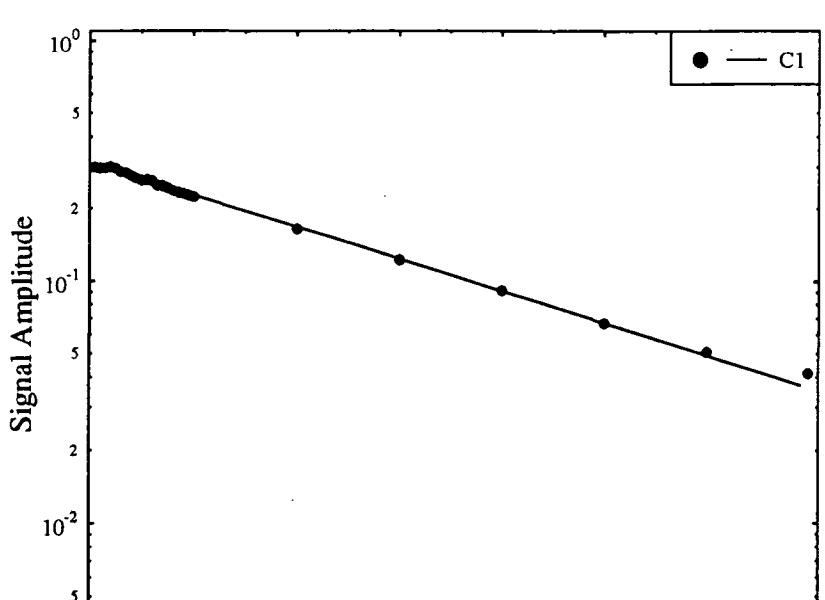

Figure 4.13b Time-dependence of the intensity of C-13 signals in a powder sample of nylon-6 in the depolarisation experiment
(only the carbonyl carbon of the nylon block is presented)
(t_{CP_i}=800 μs, t_d=100 μs, D0=5 s, AQ=25.6 ms, TD=512, rotor spinning frequency: 4000 Hz)

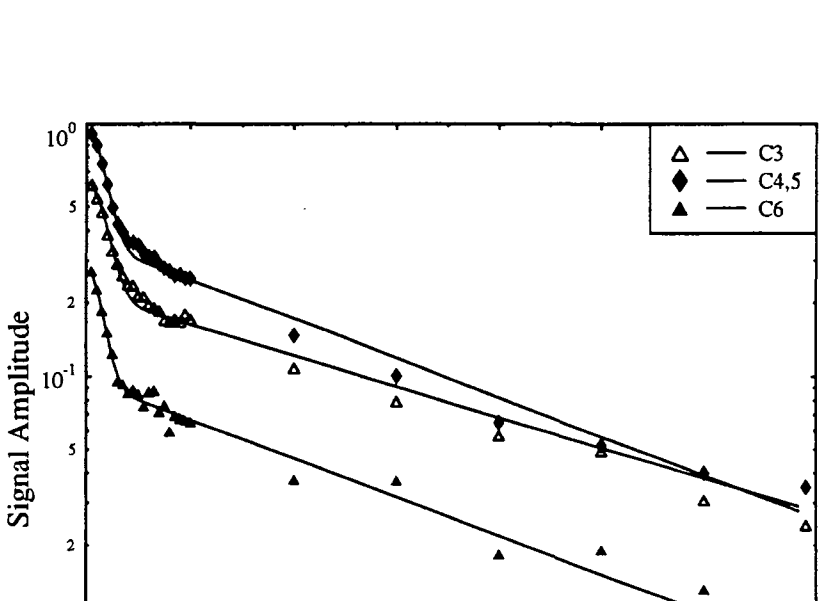

Figure 4.14 Time-dependence of the intensity of C-13 signals in a powder sample of nylon-6 + 20% prepolymer (NBC20(1)) in the depolarisation experiment
(only the methylene carbons of the nylon block are presented)
(t_{CP_i}=1000 μs, t_d=1000 μs, D0=3 s, AQ=51.2 ms, TD=1024, NT=770, rotor spinning frequency: 4000 Hz)

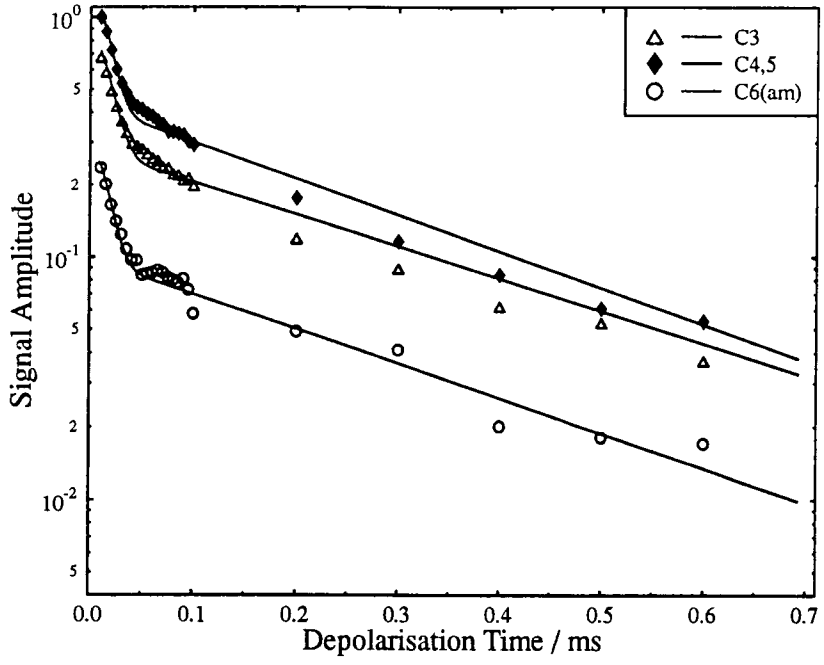

Figure 4.15 Time-dependence of the intensity of C-13 signals in a powder sample of nylon-6 + 20% prepolymer (RIM, quenched, NBC20(2)) in the depolarisation experiment (only the methylene carbons of the nylon block are presented) (t_{CP_1}=1000 μs, t_d=1000 μs, D0=3 s, AQ=25.6 ms, TD=512, NT=1024, rotor spinning frequency: 4000 Hz)

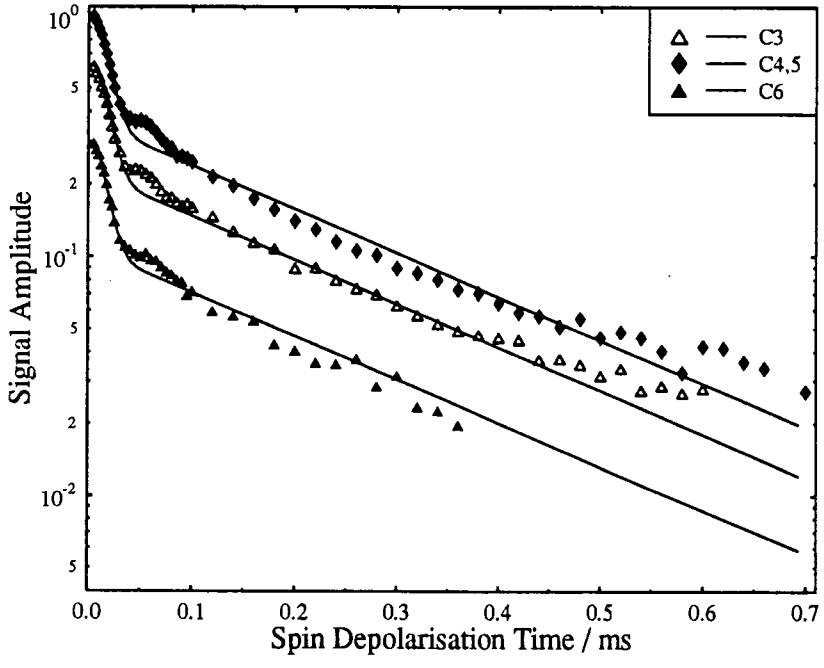

Figure 4.16a Time-dependence of the intensity of C-13 signals in a powder sample of nylon-6 + 30% prepolymer (NBC30) in the depolarisation experiment (only the methylene carbons of the nylon block are presented) (t_{CP_1}=1000 μs, t_d=1000 μs, D0=3 s, AQ=51.2 ms, TD=1024, NT=1024, rotor spinning frequency: 3000 Hz)

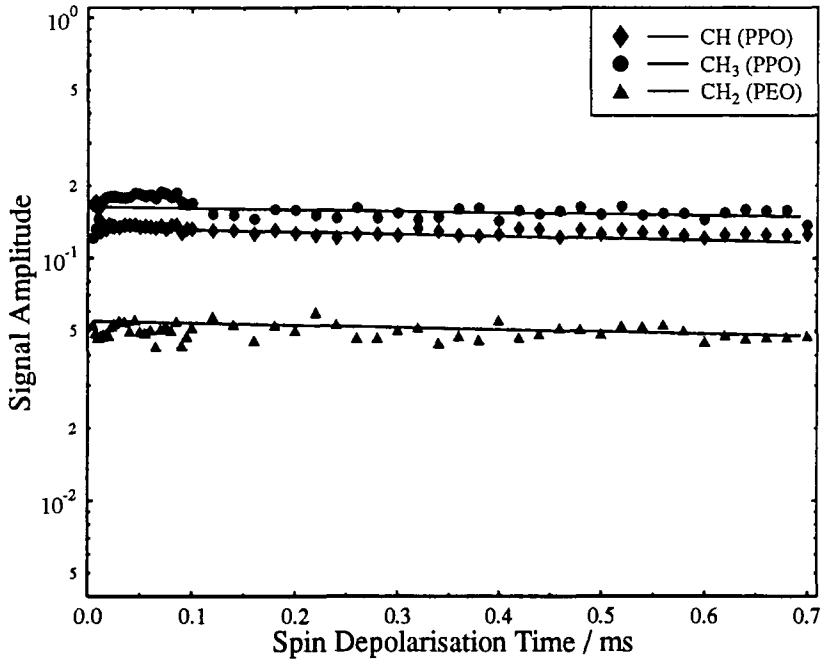

Figure 4.16b Time-dependence of the intensity of C-13 signals in a powder sample of nylon-6 + 30% prepolymer (NBC30) in the depolarisation experiment (only the polyether carbons are presented) (t_{CP_1}=1000 μs, t_d=1000 μs, D0=3 s, AQ=51.2 ms, TD=1024, NT=1024, rotor spinning frequency: 3000 Hz)

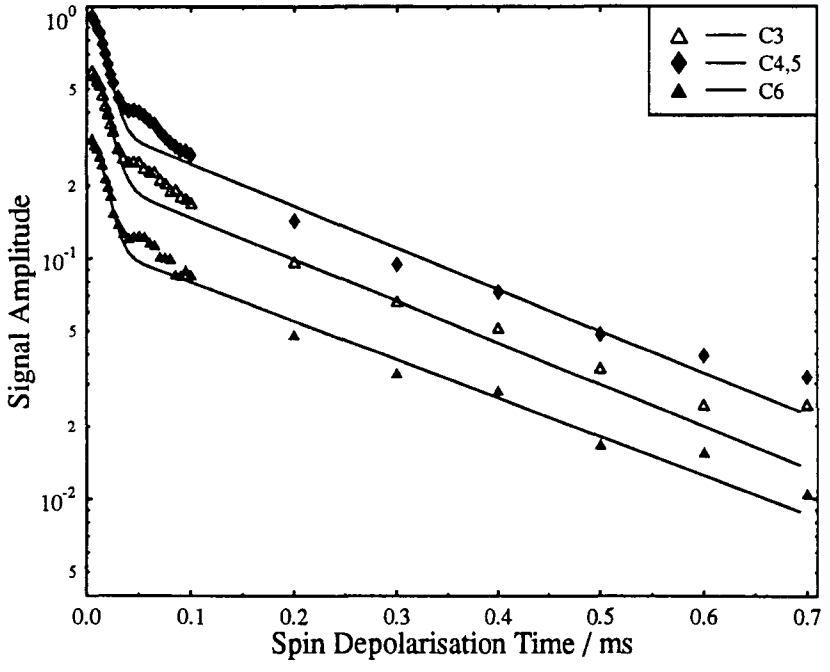

Figure 4.17 Time-dependence of the intensity of C-13 signals in a powder sample of nylon-6 + 40% prepolymer (NBC40(2)) in the depolarisation experiment (only the methylene carbons of the nylon block are presented) (t_{CP_1}=1000 μs, t_d=2000 μs, D0=3 s, AQ=51.2 ms, TD=1024, NT=1024, rotor spinning frequency: 3000 Hz)

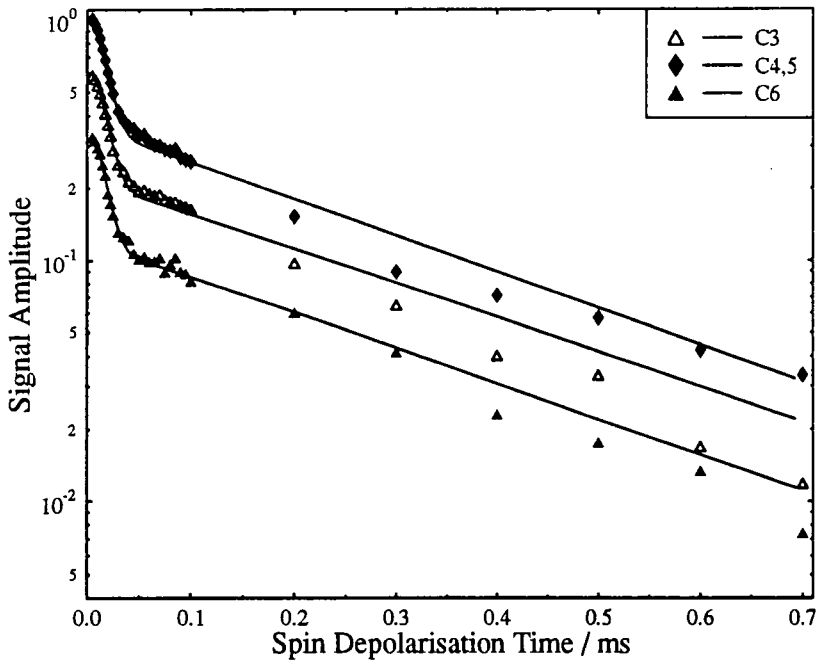

Figure 4.18 Time-dependence of the intensity of C-13 signals in a powder sample of nylon-6 + 70% prepolymer (NBC70(1)) in the depolarisation experiment (only the methylene carbons of the nylon block are presented) (t_{CP_i}=1000 μs, t_d=2000 μs, D0=2 s, AQ=51.2 ms, TD=1024, NT=1024, rotor spinning frequency: 4000 Hz)

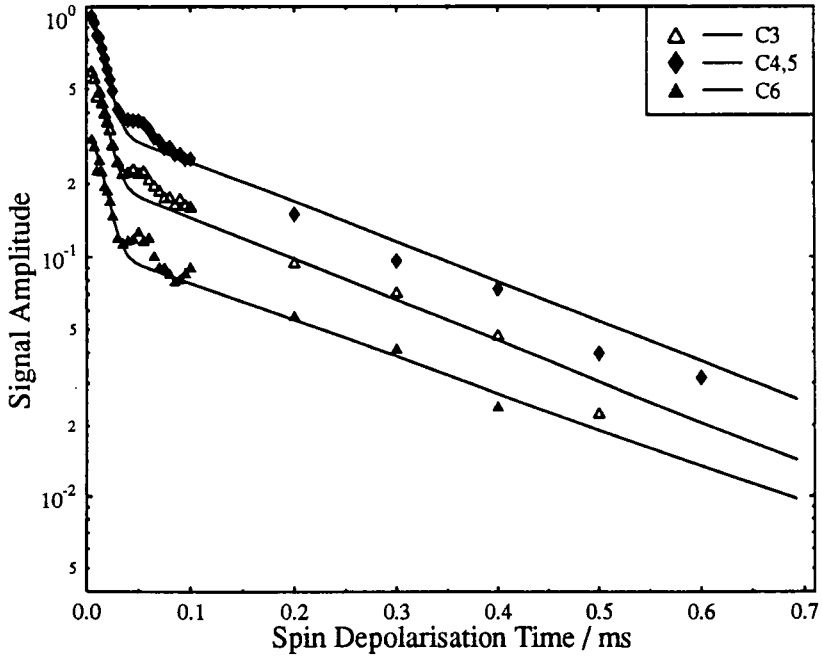

Figure 4.19a Time-dependence of the intensity of C-13 signals in a powder sample of nylon-6 + 70% prepolymer (NBC70(2)) in the depolarisation experiment (only the methylene carbons of the nylon block are presented) (t_{CP_i}=1000 μs, t_d=2000 μs, D0=2 s, AQ=51.2 ms, TD=1024, NT=1024, rotor spinning frequency: 3000 Hz)

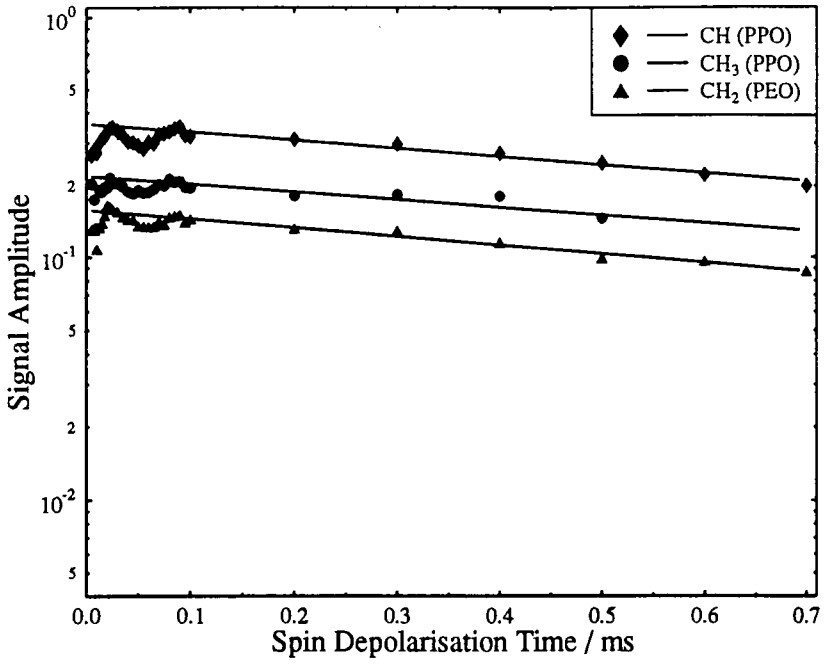

Figure 4.19b Time-dependence of the intensity of C-13 signals in a powder sample of nylon-6 + 70% prepolymer (NBC70(2)) in the depolarisation experiment (only the polyether carbons are presented) (t_{CP_1}=1000 μs, t_d=2000 μs, D0=2 s, AQ=51.2 ms, TD=1024, NT=1024, rotor spinning frequency: 3000 Hz)

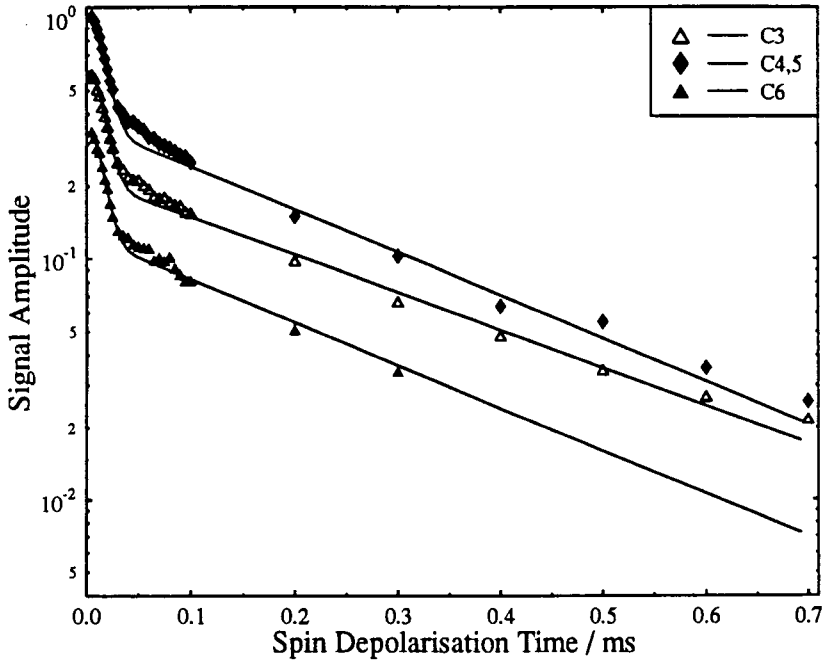

Figure 4.20a Time-dependence of the intensity of C-13 signals in a powder sample of nylon-6 + 70% prepolymer (NBC70(3)) in the depolarisation experiment (off Hartmann-Hahn match) (only the methylene carbons of the nylon block are presented) (t_{CP_1}=1000 μs, t_d=2000 μs, D0=2 s, AQ=51.2 ms, TD=1024, NT=1024, rotor spinning frequency: 4000 Hz)

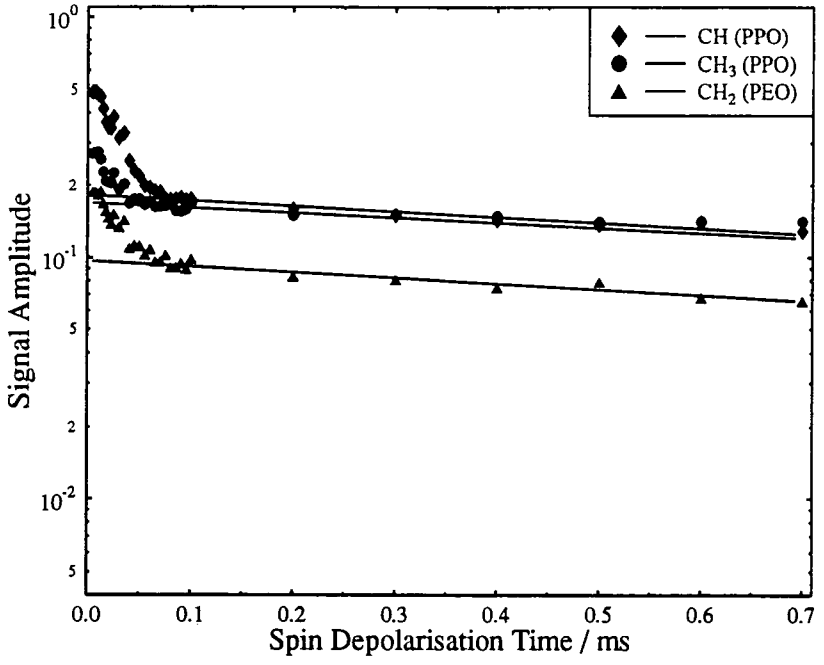

Figure 4.20b Time-dependence of the intensity of C-13 signals in a powder sample of nylon-6 + 70% prepolymer (NBC70(3)) in the depolarisation experiment (off Hartmann-Hahn match) (only the polyether carbons presented)
(t_{CP_1}=1000 μs, t_d=2000 μs, D0=2 s, AQ=51.2 ms, TD=1024, NT=1024, rotor spinning frequency: 4000 Hz)

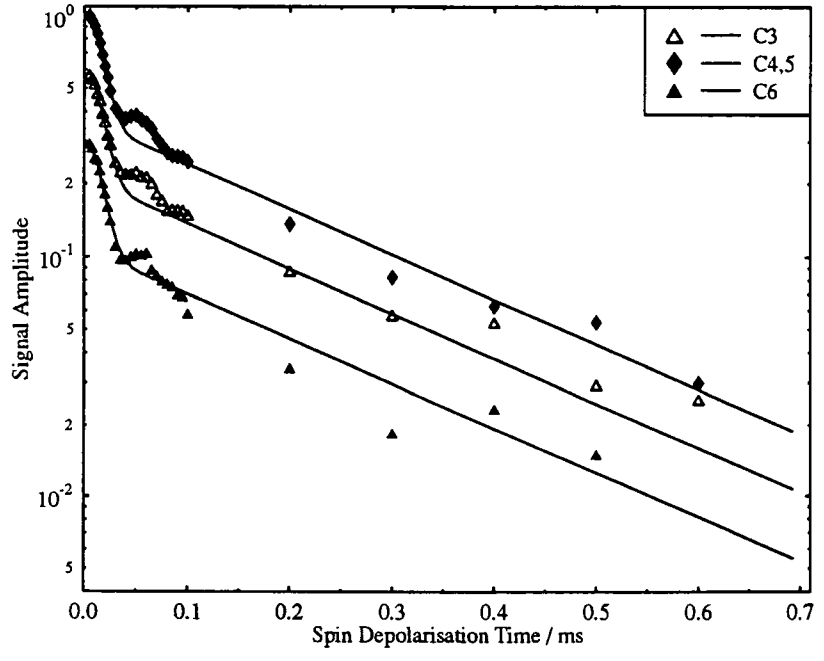

Figure 4.21 Time-dependence of the intensity of C-13 signals in a powder sample of nylon-6 + 70% prepolymer (NBC70(5)) in the depolarisation experiment (only the methylene carbons of the nylon block are presented)
(t_{CP_1}=1000 μs, t_d=2000 μs, D0=2 s, AQ=51.2 ms, TD=1024, NT=1024, rotor spinning frequency: 2500 Hz)

The parameters obtained were set into equation 4.13 and plotted against the experimental data. It should be noted that the values M_0 are related to the signal height, where the signal height of carbons 4 and 5 of nylon-6 was set to 1 and the other signal intensities were related to that. The area of the signal could not be taken because the signals were overlapping, making the integration of the signals impossible. The question arises as to why some samples show transient oscillations and some not. An exact solution for this problem would require correlation functions of the dynamical variables. This is in general not possible for strongly-coupled many-body systems because such calculations raise conceptual and mathematical problems in which the "self-energy"-effects due to the interactions are large compared to the "unperturbed" single-particle energies. Although it was not subject of this thesis to apply or develop such a theory, it should be mentioned, without deeper explanation, that two main approaches have been elaborated. One involves an attack on the microscopic problem from first principles, making appropriate mathematical approximations [28-31]. The other procedure is to adopt what amounts to a fitting scheme [32-38] in which one postulates a certain plausible and perhaps defensible shape (e.g. Gaussian) for some suitable function (a spin correlation function, a memory function) and adjusts parameters to fit certain rigorously calculable quantities such as moments. Demco et al. [39] showed that exact knowledge of a few moments, together with a Gaussian memory function, reproduces a wide variety

of unexplained experimental results. However, to explain cross-relaxation dynamics qualitatively, one has to know the important parameters, the homonuclear and heteronuclear dipolar interaction parameters. The observable parameters are the transient oscillations and the spin diffusion rate in the depolarisation experiment. The dipolar interaction parameter b can be estimated from the oscillation frequency. It is related to the oscillation frequency by $b = 2\omega_{osc}$. The time interval from maximum to maximum is about 100 μs which corresponds to a dipolar interaction parameter of 20 kHz or 20 ms^{-1}. The dipolar interaction parameter is about five times larger than the spin-diffusion rate, as illustrated in table 4.4a and 4.4b, which would lead one to expect strong transient oscillation as depicted in figure 4.22, in which simulated depolarisations with different ratios of spin diffusion rates and heterogeneous dipolar interaction parameters are shown. This figure explains by example that transient oscillations only occur if the heterogeneous dipolar interaction is larger than the homonuclear dipolar interaction. But it does not evidently explain why the same sample (e.g NBC70) shows oscillations in some experiments (figure 4.19a and 4.21) and not in others (figure 4.18 and 4.20a). At this point the influence of MAS on cross-relaxation must be discussed. Let us assume a rotor spinning frequency of 4000 Hz. This would correspond to 250 μs for one full rotation. The rotor spinning frequency is one quarter of the heterogeneous dipolar interaction parameter; consequently MAS will influence the heterogeneous dipolar interaction. This influence is

Nylon-6					
Carbon	C1	C2	C3	C4,5	C6
M_0	0.309 ± 0.002	0.61 ± 0.01	0.70±0.01	1.08±0.02	0.318±0.007
R / ms^{-1}	3.06 ± 0.06	3.3 ± 0.2	3.2±0.2	3.5±0.2	3.9±0.3
T2 / ms	-	0.0169± 0.0006	0.0173±0.0006	0.0165±0.0005	0.0164±0.0007
NBC10					
M_0	0.382±0.003	0.63±0.01	0.66±0.02	1.10±0.03	0.283±0.008
R / ms^{-1}	3.01±0.09	3.2*	3.2*	3.4*	3.2*
T2 / ms	-	0.0154±0.0007	0.0171±0.0009	0.0156±0.0007	0.0154±0.0008
NBC20					
M_0	0.355±0.003	0.61±0.01	0.65±0.01	1.09±0.02	0.289±0.005
R / ms^{-1}	2.86±0.09	3.3±0.2	3.3*	3.7±0.2	3.7±0.3
T2 / ms	-	0.0154±0.0005	0.0171±0.0006	0.0155±0.0005	0.0136±0.0005
			NBC20(2)	(RIM)	(quenched)
M_0	0.408±0.002	0.78±0.02	0.84±0.03	1.28±0.04	0.35±0.01
R / ms^{-1}	3.12±0.06	3.3±0.3	3.1±0.4	3.5±0.4	3.4±0.4
T2 / ms	-	0.0148±0.0007	0.017±0.001	0.0155±0.0009	0.0136±0.0007
Carbon	C1(am)	C2(am)	C3(am)	C4,5(am)	C6(am)
M_0	-		-	-	0.292±0.009
R / ms^{-1}	-		-	-	3.3±0.3
T2 / ms	-		-	-	0.0156±0.0008
			NBC20(3)	(RIM)	(quenched)
M_0	0.396±0.004	0.62±0.01	0.65±0.01	1.04±0.02	-
R / ms^{-1}	2.53±0.07	3.3*	2.8*	3.5*	-
T2 / ms	-	0.0179±0.0007	0.0209±0.0008	0.0195±0.0008	-
Carbon	C1(am)	C2(am)	C3(am)	C4,5(am)	C6(am)
M_0	-	-	-	-	0.330±0.007
R / ms^{-1}	-	-	-	-	2.8*
T2 / ms	-	-	-	-	0.0191±0.0009
NBC25					
M_0	0.340±0.002	0.60±0.01	0.63±0.01	1.08±0.02	0.282±0.004
R / ms^{-1}	2.91±0.06	3.4±0.2	3.1±0.3	3.5±0.2	3.5±0.2
T2 / ms	-	0.0147±0.0005	0.0196±0.0007	0.0157±0.0005	0.0147±0.0004
NBC30					
M_0	0.347±0.002	0.62±0.01*	0.67±0.01*	1.09±0.02*	0.323±0.005*
R / ms^{-1}	3.57±0.09	4.2±0.3*	4.2±0.3*	4.2±0.2*	4.2±0.4*
T2 / ms	-	0.0147±0.0005*	0.0156±0.006*	0.0156±0.0006*	0.0159±0.0006*

Table 4.4a Optimised parameter for the spin-depolarisation experiment from a non-linear least-squares analysis using equation 4.11 for nylon-6 and various NYRIM-materials. Only the methylene carbons from nylon-6 block are considered

*** These values were fitted separately by using a Gaussian or Exponential function (for more details, see text)**

NBC40(1)					
Carbon	C1	C2	C3	C4,5	C6
M_0	0.37±0.03*	0.64±0.01*	0.68±0.01*	1.08±0.02*	0.30±0.01*
R / ms^{-1}	1.9±0.2*	3.3±0.3*	3.3±0.2*	3.1±0.2*	3.1±0.3*
T2 / ms	0.066±0.007*	0.0141±0.0008*	0.0136±0.0007*	0.0139±0.0008*	0.0142±0.007*
NBC40(2)					
M_0	0.386±0.002	0.63±0.02	0.66±0.02	1.10±0.03	0.345±.009
R / ms^{-1}	3.52±0.06	3.7±0.5*	4.0±0.2*	3.9±0.4*	3.8±0.3*
T2 / ms	-	0.0158±0.0008	0.017±0.001	0.0159±0.0009	0.0153±0.0008
NBC70(1)					
M_0	0.392±0.001	0.595±0.009	0.65±0.01	1.09±0.01	0.359±0.005
R / ms^{-1}	3.02±0.06	3.2±0.2	3..3±0.2	3.5±0.2	3.4±0.2
T2 / ms	-	0.0151±0.0005	0.0153±0.0005	0.0150±0.0004	0.0147±0.004
NBC70(2)					
M_0	0.33±0.03*	0.57±0.01*	0.64±0.02*	1.08±0.02*	0.33±0.01*
R / ms^{-1}	3.3±0.2*	3.5±0.3*	3.9±0.4*	3.8±0.3*	3.5±0.4*
T2 / ms	-	0.0151±0.0005*	0.0153±0.0007*	0.0148±0.0007*	0.0152±0.0009*
NBC70(3)					
M_0	0.418±0.002	0.59±0.01*	0.64±0.01*	1.09±0.02*	0.371±0.006*
R / ms^{-1}	3.56±0.06	3.6±0.5*	3.6±0.4*	4.1±0.3*	4.1±0.4*
T2 / ms	-	0.0150±0.0005*	0.0148±0.0005*	0.0151±0.0005*	0.0138±0.0004*
NBC70(4)					
M_0	0.345±0.001	0.57±0.02*	0.60±0.02*	1.07±0.03*	0.33±0.01*
R / ms^{-1}	3.8±0.2	4.4±*	4.4±*	4.4±*	4.4±*
T2 / ms	-	0.0152±0.0009	0.016±0.001	0.0150±0.0007	0.015±0.001
NBC70(5)					
M_0	0.296±0.003	0.58±0.01*	0.63±0.02*	1.11±0.03*	0.323±0.007
R / ms^{-1}	4.1±0.1	4.3±0.3*	4.3±0.2*	4.3±0.3*	4.3±0.4
T2 / ms	-	0.0149±0.0006*	0.0152±0.0007*	0.0149±0.0007*	0.0151±0.0006

Table 4.4b Optimised parameter for the spin-depolarisation experiment from a non-linear least-squares analysis using equation 4.11 for various NYRIM-materials. Only the methylene carbons from nylon-6 blocks are considered

*** These values were fitted separately by using a Gaussian or Exponential function (for more details, see text)**

illustrated in the different "amounts" of transient oscillation in the depolarisation curves of the various NYRIM samples. There are no observable oscillations if the spinning frequency is 4000 Hz, but damped oscillation if

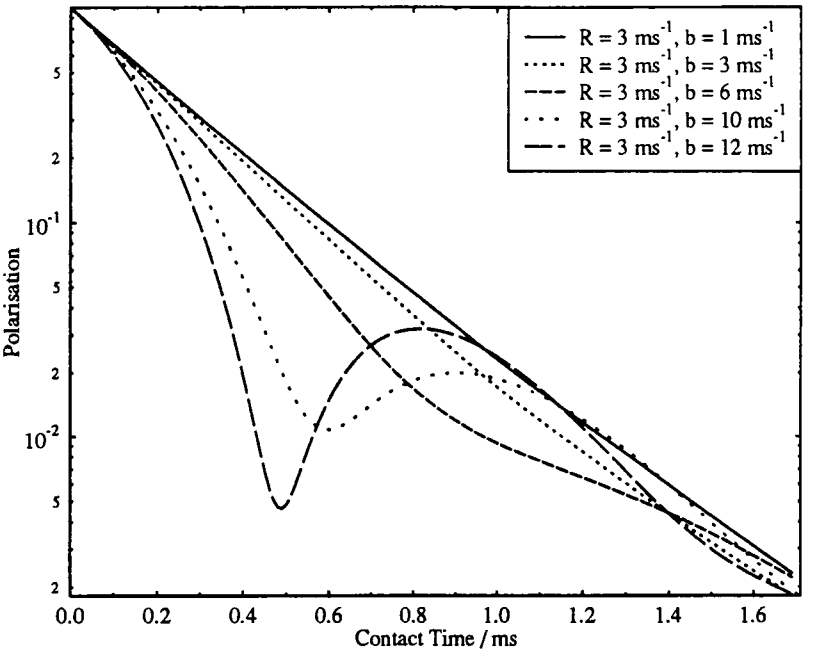

Figure 4.22 Simulated depolarisation behaviour of a CH_2-carbon using equation 4.12. The magnetisation intensity is plotted as a function of contact time. Different ratios of spin-diffusion rates and heterogeneous dipolar interaction parameters are illustrated

the spinning frequency is 3000 Hz and less. Wu et al. have found that oscillations which occur in static powder samples of ferrocene and glycine [26] completely vanish if rapid MAS is applied. (Note that the authors did not make any comments on how fast they spun the rotor. It is assumed that they used "standard" spinning frequencies of about 3000 to 5000 Hz). In the case of the methylene carbons in NYRIM, the heterogeneous dipolar interactions are twice as strong as the dipolar interactions in glycine or ferrocene investigated by Wu. This may explain why at moderate spinning frequencies the methylene carbons show transient oscillations in nylon-6. All depolarisation experiments showing no transient oscillations were spun at 4000 Hz. In all the other depolarisation experiments, the rotor was spun at 3000 Hz or less, and the depolarisation

NBC30				
Carbon	CH (PPO)	CH_2 (PPO)	CH_3(PPO)	CH_2 (PEO)
M_0	0.134±0.003	0.164±0.002	0.121±0.003	0.055±0.002
R / ms^{-1}	0.14±0.04	0.2±0.1	0.2±0.1	0.2±0.1
NBC40(2)				
M_0	0.146±0.003	0.165±0.007	0.150±0.005	0.065±0.002
R / ms^{-1}	0.98±0.06	0.9±0.1	0.9±0.1	0.9±0.2
NBC70(1)				
M_0	0.135±0.002	0.154±0.002	0.117±0.001	0.036±0.001
R / ms^{-1}	0.32±0.06	0.36±0.05	0.29±0.09	0.8±0.2
NBC70(2)				
M_0	0.299±0.004	0.359±0.006	0.219±0.002	0.158±0.002
R / ms^{-1}	0.84±0.05	0.77±0.06	0.75±0.05	0.85±0.05
NBC70(3)				
M_0	0.169±0.003	0.182±0.003	0.151±0.004	0.097±0.002
R / ms^{-1}	0.49±0.07	0.54±0.05	0.56±0.09	0.56±0.09
NBC70(4)				
M_0	0.279±0.004	0.326±0.005	0.253±0.002	0.140±0.002
R / ms^{-1}	1.2±0.1	1.4±0.1	1.2±0.1	1.2±0.1
NBC70(5)				
M_0	0.413±0.007	0.532±0.005	0.398±0.006	0.195±0.004
R / ms^{-1}	0.13±0.05	0.14±0.03	0.19±0.06	0.23±0.06

Table 4.5 Optimised parameter for the spin-depolarisation experiment from a non-linear least-squares analysis using an exponential model for various NYRIM-materials. Only the polyether prepolymer carbons from nylon-6 block copolymer are considered

exhibits damped oscillations. Spinning at 2500 Hz (figure 4.21) reveals the most pronounced transient oscillations, which supports the assumption of the MAS influence on cross-relaxation.

Tekely et al. [40] have investigated transient oscillations of powdered ferrocene samples at low (248 Hz) rotor spinning frequency. At that spinning frequency they could not detect any, in contrast to the case of the

static sample. However, as discussed earlier in this section, no dipolar oscillations should be observed in rapidly rotating samples as a result of the destructive interference of oscillations from crystallites with different orientations. Instead of damped oscillation a two-stage decay of carbon magnetisation may be observed as derived in eqn. 4.11. As shown by the experiments these results must be handled with great care, because MAS is not entirely removing the transient oscillations, and quantitative description of the coherent and spin-diffusion magnetisation transfer is not easily accessible.

Secondly, the cross-relaxation behaviour of the carbonyl carbon will be discussed. In all samples the carbonyl carbon exhibits an exponential cross-relaxation behaviour. This is readily understandable, bearing in mind that the carbonyl carbon has no hydrogen attached. The only way a carbonyl carbon may cross-relax is via spatial magnetisation transfer to the neighbouring protons. A coherent magnetisation transfer is not possible. The time constant for the transfer is in excellent agreement with the spin-diffusion time constant of the methylene carbons, which can be considered as evidence that we are dealing with the same transfer mechanism (see tables 4.4a and 4.4b). The fact that the cross-relaxation time of the carbonyl carbon is a little bit smaller than that of the methylene carbons cannot be explained easily. A possible reason is that in the case of carbonyl groups we are dealing only with spin-diffusion mechanism for magnetisation transport. Methylene carbons additionally are able to undergo a coherent magnetisation transfer

which may "pump" magnetisation with a larger velocity from the attached protons to the remote protons. Of course, the spin diffusion process is the rate-limiting step and consequently the "pumping" effect is small.

At this point it must be mentioned that the ^{13}C-resonances of the α-crystalline modification of nylon-6 overlap with the ^{13}C-resonances of the amorphous form except for carbon-6. Any deviations of the amorphous phase with respect to the crystalline phase should be detectable in carbon-6. As illustrated in table 4.4a, neither coherent nor spin-diffusion magnetisation transfer values of carbon-6 differ from the other carbons. This result is also supported by an investigation of quenched nylon-6 block copolymer (NBC20(2) and NBC20(3) in table 4.4a), where the depolarisation behaviour of carbon-6 is in accord for both modifications. This result becomes readily understandable, bearing in mind that all measurements were taken at room temperature, which is much below the glass transition temperature of nylon-6 (T_g = 67 °C). The glass transition is dealt with in the next chapter in more detail. So far it is only relevant to know that below the glass-transition temperature, the amorphous phase of a polymer is in a glassy, rigid form, similar to the crystalline state. This is important to know because the dipolar interactions are strongly dependent on intramolecular mobility.

This leads to the final part of the discussion, the cross-relaxation behaviour of the prepolymer carbons. In nearly all measurements in which the Hartmann-Hahn match was set correctly on adamantane, no oscillation of

coherent polarisation transfer is observable. One exception is depicted in figure 4.19b. This experiment definitly exhibits transient oscillations in the first 100 μs. It was not possible to explain why just oscillations occur in this one experiment.

The spin-diffusion rate is about a factor of 10-15 smaller with respect to the spin diffusion rate for the methylene carbons in the nylon-6 phase. The intensity ratio prepolymer carbons/nylon-6 carbons also indicates the smaller cross-polarisation efficiency of the prepolymer carbons. This has its origin in the higher mobility of the prepolymer. The homonuclear dipolar interactions strongly depend on the correlation time τ_c. Roughly speaking, the more mobile a material is, the smaller the dipolar interaction and the smaller is the cross-relaxation rate. Another point is the so-called match width. This is the half width of the magnetisation intensity expressed in kHz in which the magnetisation intensity is plotted as a function of mismatch parameter $\Delta = (\omega_{II} - \omega_{IS}) / 2\pi$ [41]. In rigid solids the match width has a gaussian shape and can be as wide as 50 kHz. For mobile materials or liquids the width is usually smaller than 1 kHz. Achieving an exact Hartmann-Hahn match deserves an accurate fulfilment of the match setting which is often not possible. Evidently the spin-diffusion rates of the prepolymer show how sensitive the measurements are with respect to the Hartmann-Hahn mismatch. The values for the spin diffusion-rate vary between 0.14 and 0.98 ms^{-1} for the different compositions without following any trend. An expected modulation of dipolar interaction

between the protons by macroscopic rotation could not be detected. One would expect the faster the rotation, the smaller the effective dipolar interaction, because of partial averaging of the interactions. A direct comparison of spin diffusion-rates of the NBC70 sample rotating at 2500 Hz, 3000 Hz and 4000 Hz yields that, contrary to expectation the experiment in which the sample is rotating at 2500 Hz has the smallest rate rather than the one rotating at 4000 Hz. The spin-diffusion rate of the sample rotating at 3000 Hz is in between the other two values. A reason for this could be a Hartmann-Hahn mismatch of the experiment, that would change the polarisation transfer rate. Now the question arises, how such mismatch can be possible providing the match was carefully set on adamantane. In principle there are three answers:

1. The match width of the prepolymer carbons is smaller than the match width of adamantane, which would make an accurate setting of the match impossible. A simple experiment to prove this would be to compare the match width of adamantane with the prepolymer carbons.
2. The Hartmann-Hahn match was not stable on the instrument. This problem occurred occasionally on the CXP200 to such an extent that quantitative CP/MAS measurements were not possible.
3. Polarisation transfer with MAS does not neccessarily work optimally on the matched condition as Wu et al. discussed in their work [41]. When the MAS speed is larger than or comparable to the ^{1}H-^{1}H dipolar couplings, the Hartmann-Hahn spectrum breaks up into a series of sidebands. Maximal polarisation transfer

occurs when the mismatch parameter Δ is a multiple of the MAS rate. The optimum transfer-rate is not neccessarily at matched condition but often happens at the first maximum $\Delta=\omega_{II}-\omega_{IS}$. Figures 4.25b and 4.26b illustrate the result of polarisation transfer of the prepolymer carbons at their first maximum. Two things are important to note here. Firstly, the magnetisation transferred in the non-matched condition is larger than in the matched experiment. Secondly, the depolarisation occurs with a two feature-behaviour. This illustrates that, especially for mobile samples with relatively strong heterogeneous dipolar interactions, the optimum polarisation transfer is not happening at the Hartmann-Hahn condition but when the mismatch parameter is set to a multiple of the MAS frequency.

4.3.5 The Cross-Polarisation Experiment

The second type of experiment is known as the *variable contact time* experiment. It is the simplest amongst the CP-experiments and consists basically of 3 pulses as depicted in figure 4.23. After the 90° pulse on the protons the ^{1}H-magnetisation is locked along B_{1H} during t_{CP}. The carbons are now polarised along B_{1C}. By varying t_{CP} the dynamics of the polarisation transfer is monitored. The theory behind this experiment is basically the same as in the depolarisation experiment. The only important parameter that has additionally to be considered is the proton spin-lattice relaxation time in the rotating frame, $T_{1\rho}^{H}$. In contrast to the depolarisation experiment,

where during the depolarisation time the carbon spins relax with $T_{1\rho}^{C}$ (which is usually much longer than T_{CH} and the spin-diffusion rate), $T_{1\rho}^{H}$ may be of the same length as the spin-diffusion time constant. Therefore an additional term considering the rotating-frame spin relaxation has to be included in the expression that describes the cross-polarisation dynamics. In section 4.3.2 an expression for CP-dynamics has been given for a system with a single spin-temperature in which the proton spin-lattice relaxation time is involved (eqn. 4.5).

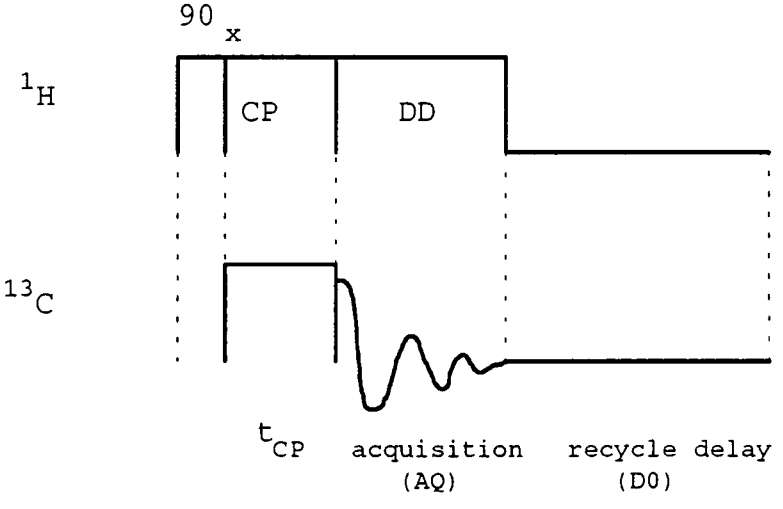

Figure 4.23 Pulse sequence for a variable contact-time experiment, where t_{CP} is the time for the S spins to be polarised

This expression, although still frequently used for organic solids [42], does not adequately describe the cross-polarisation dynamics with strong heteronuclear dipolar interactions, as discussed in the last section.

For analytical purposes, I have basically used the model developed by Müller et al. [16]. However, to account for the proton rotating-frame spin relaxation $T_{1\rho}^{H}$, an effective

single $T_{1\rho}^{H}$ behaviour was assumed. Although this is a restrictive assumption and does not satisfy the reality, as will be seen in chapter 5 by direct measurement of $T_{1\rho}^{H}$, the cross-polarisation data are described quite well. Originally expression 4.13 was used with a relaxation term added, so it becomes:

$$M_S(\tau) = M_{S0}\left(1 - \frac{1}{3}e^{-R\tau} - \frac{2}{3}e^{-3R\tau/2}e^{-\tau^2/2T_2^2}\right)\cdot \exp\left(-\frac{\tau}{T_{1\rho}^{H}}\right) \quad (4.14)$$

Before the discussion of the cross-polarisation dynamics results starts, an alternative CP/MAS experiment will be introduced, namely the inversion-recovery cross-polarisation experiment (IRCP).

4.3.6 The Inversion-recovery Cross-polarisation Experiment

Wu and co-workers [43] developed a cross-polarisation technique which enhances the sensitivity of the ordinary CP/MAS experiment by applying an additional pulse during the contact time. The pulse-sequence is outlined in figure 4.24. The difference from the normal CP-pulse sequence is a 180° pulse on the carbon channel after an ample contact time τ_1, which results in an inversion of the spin-populations of the carbons, producing a situation in which the spins of the carbons are antiparallel to the rotating-frame magnetic field. The upper energy level is now more populated than the lower level. Because the ^{13}C-system is now at a negative spin-temperature, thermal equilibrium between the ^{1}H and the ^{13}C is broken, and energy transfer will occur again until a new common spin-temperature is reached. This process, however, proceeds at quite

different rates for different components of ^{13}C-magnetisation, depending on their associated polarisation transfer rates. This magnetisation transfer is monitored as a function of the contact time τ_2.

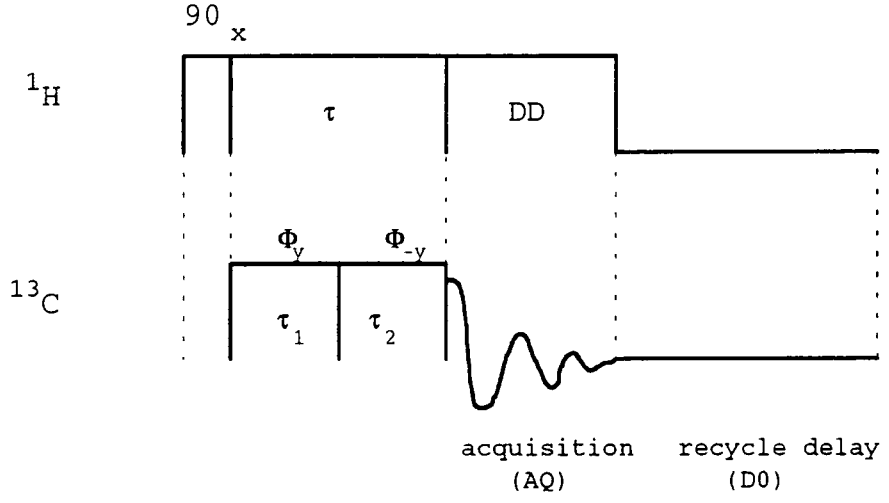

Figure 4.24 Pulse sequence for the Inversion-Recovery Cross-Polarisation experiment

The main advantage of this experiment is that the effective signal intensity is doubled by the spin inversion, because the magnetisation goes from $M_0 = -M_\infty$ (for τ_2=0, and no spin relaxation) to $+M_\infty$. The physical properties of the polarisation transfer are the same as in the depolarisation or polarisation experiment. It is easy to modify expression 4.14 of the variable contact-time experiment to satisfy the purposes of the inversion-recovery cross-polarisation experiment.

$$M_S(\tau) = \left(-M_{S0} + 2M_{S0}\left(1 - \frac{1}{3} e^{-R\tau} - \frac{2}{3} e^{-3R\tau/2} e^{-\tau^2/2T_2^2} \right) \right) \cdot \exp\left(-\frac{\tau}{T_{1\rho}^H} \right) \qquad (4.15)$$

4.3.7 Results and discussion

Expression 4.14 has been used to analyse the polarisation dynamics of the methylene carbons from the variable contact-time cross-polarisation experiment. The polarisation dynamics of the carbonyl carbon was determined by using the Mehring equation 4.5. This is a sensible model for the carbonyl carbon because the proton system can be described by a single spin-temperature. The numerical results are summarised in table 4.6 for various NYRIM materials.

The simulated and experimental data are depicted in figures 4.25 to 4.27. The analytical fit using 4.14 was only possible for the nylon-6 carbons because the prepolymer carbons exhibit a too long cross-relaxation time to be meaningfully analysed. This is simply because the polyether phase is so mobile that polarisation transfer from the protons to the carbons becomes very inefficient. The cross-polarisatiopn dynamics of the polyether carbons are graphically represented in figure 4.28. The lower efficiency of cross-polarisation for the polyether carbons is obvious. After a relatively fast signal increase in the first two milliseconds, which is due to the heteronuclear dipolar interactions, the signal levels off. At this stage spin-diffusion is less important and only long-time $T_{1\rho}^{H}$ relaxation is effective. The results of the numerical analysis for the inversion-recovery cross-polarisation experiment are summarised in table 4.7 and are graphically illustrated in figures 4.29 to 4.32. The classical variable contact time CP/MAS experiment shows that the cross-polarisation dynamics are

Nylon-6 (1)					
Carbon	C1	C2	C3	C4,5	C6
M_0	0.369±0.007	0.62±0.02	0.70±0.02	1.09±0.03	0.293±0.009
R / ms^{-1}	2.94±0.08	4±1	4±1	4±1	4±1
T2 / ms	-	0.025±0.002	0.026±0.002	0.025±0.002	0.023±0.002
$T_{1\rho}^H$ / ms	7.1±0.3	8.1±0.5	8.3±0.5	8.4±0.6	7.2±0.4
Nylon-6 (2)					
M_0	0.370±0.008	0.62±0.02	0.71±0.02	1.08±0.03	0.291±0.009
R / ms^{-1}	2.9±0.2	4±1	5±1	5±1	4±1
T2 / ms	-	0.025±0.002	0.026±0.002	0.025±0.002	0.023±0.002
$T_{1\rho}^H$ / ms	7.1±0.4	8.1±0.6	8.4±0.6	8.5±0.7	7.5±0.6
NBC20					
M_0	0.313±0.009	0.61±0.01	0.69±0.01	1.05±0.02	0.275±0.005
R / ms^{-1}	4.0±0.3	11±2	11±3	10±2	14±4
T2 / ms	-	0.019±0.002	0.022±0.004	0.020±0.002	0.022±0.006
$T_{1\rho}^H$ / ms	5.7±0.4	6.5±0.3	6.2±0.3	6.9±0.3	7.0±0.4
NBC20 (quenched)					
M_0	0.35±0.01	0.65±0.03	0.67±0.04	1.07±0.05	0.38±0.02
R / ms^{-1}	3.4±0.3	6±3	6±4	5±3	8±4
T2 / ms	-	0.020±0.003	0.023±0.004	0.020±0.003	0.017±0.003
$T_{1\rho}^H$ / ms	5.3±0.5	5.2±0.5	4.7±0.5	5.8±0.6	4.6±0.4
NBC40 (1)					
M_0	0.310±0.006	0.61±0.01	0.67±0.02	1.06±0.04	0.288±0.006
R / ms^{-1}	3.4±0.2	5±1	5±1	5±2	5±1
T2 / ms	-	0.0097±0.0005	0.0102±0.0005	0.0099±0.0008	0.0068±0.0008
$T_{1\rho}^H$ / ms	6.0±0.2	6.8±0.4	6.6±0.4	7.5±0.7	6.7±0.3
NBC40 (2)					
M_0	0.331±0.005	0.62±0.07	0.66±0.02	1.09±0.02	0.332±0.005
R / ms^{-1}	3.1±0.1	4.8±0.5	4±1	4.2±0.6	6±1
T2 / ms	-	0.020±0.001	0.027±0.002	0.023±0.001	0.04±0.01
$T_{1\rho}^H$ / ms	7.7±0.3	7.6±0.2	7.5±0.4	8.2±0.3	7.7±0.3

Table 4.6 Parameters of the variable contact-time cross-polarisation experiment for various NYRIM materials, obtained from eqn. 4.14 (only the nylon-6 carbons are presented)

governed by two general processes.

The first one is the polarisation transfer from the protons to the carbons, which is responsible for the signal increase. The second one is the loss of magnetisation by spin-relaxation to the lattice. Therefore

CP/MAS experiments in rigid organic solids generally have an optimum contact time where the signal of the carbons is maximised. While the methylene carbons exhibit a fast signal growth in the first 500 μs, the carbonyl carbon reaches its maximum at 1000 μs. The reason was already given in section 4.3.3. It is simply because magnetisation transfer for carbonyl carbons only works by transport of polarisation from the protons to the relatively-distant carbons. Methylene carbons may be polarised additionally by coherent polarisation transfer which is generally a magnitude faster. Therefore methylene carbons reach 2/3 of their magnetisation in a fraction of 100 μs, a timescale where coherent polarisation is active. A measure of the quality of the numerical analysis may be obtained by comparison of the three different techniques. Starting with the two parameters responsible for the polarisation transfer, R and T_2, probably not enough experimental data have been recorded in the IRCP experiment for a completely stable numerical fit. Especially for Nylon-6 and NBC40(1) (see table 4.7) the cross-polarisation time was so short that considerable $T_{1\rho}^H$-relaxation could take place. In the second experiment on NBC40, the cross-polarisation time was 4 ms, consequently only the short-time $T_{1\rho}^H$-value was detected. However, the T_2-values are between 0.009 and 0.027 ms, which is in good agreement with those obtained from the depolarisation measurements. Also the spin-diffusion rates are in good agreement with those obtained by depolarisation measurements. The only exception concerns annealed NBC20, where the spin-diffusion rates are calculated to be between 10 and 14 ms^{-1} for the

different methylene carbons. Figure 4.27 represents the polarisation curve of annealed NBC40. It shows noisy data especially in the first millisecond of contact. The reason for the large spin-diffusion rates is not to be found in certain properties of the material but in the low data quality which results in a relatively poor fit.

Another reason for the difficulty of the numerical analysis of the variable contact-time experiment is $T_{1\rho}^{H}$ relaxation. The data points now have to be described by four instead three parameters, which demands a more data points to achieve the same accuracy as in the depolarisation experiment. Here time-limiting boundaries are set by solid-state NMR, because each single data point requires up to one hour in acquisition time. The alternative way to obtain the polarisation parameter is

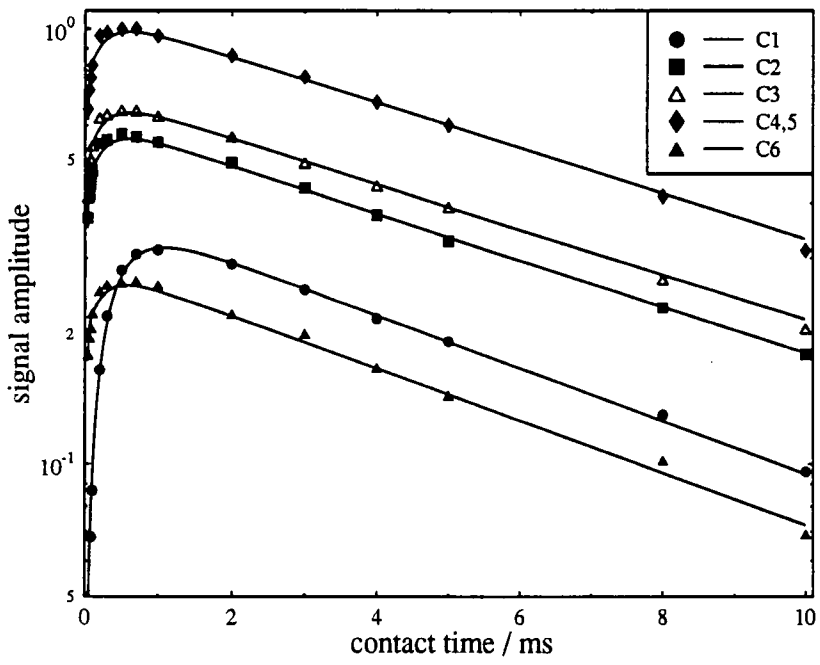

Figure 4.25 Time-dependence for the intensity of C-13 signals in a powder sample of nylon-6 (1) in the variable-contact time cross-polarisation experiment (D0=2 s, AQ=51.2 ms, TD=2048, NT=2048, rotor spinning frequency: 4000 Hz) markers represent experimental data, solid lines represent data from eqn. 4.14 (CH_2) and eqn. 4.5 (carbonyl)

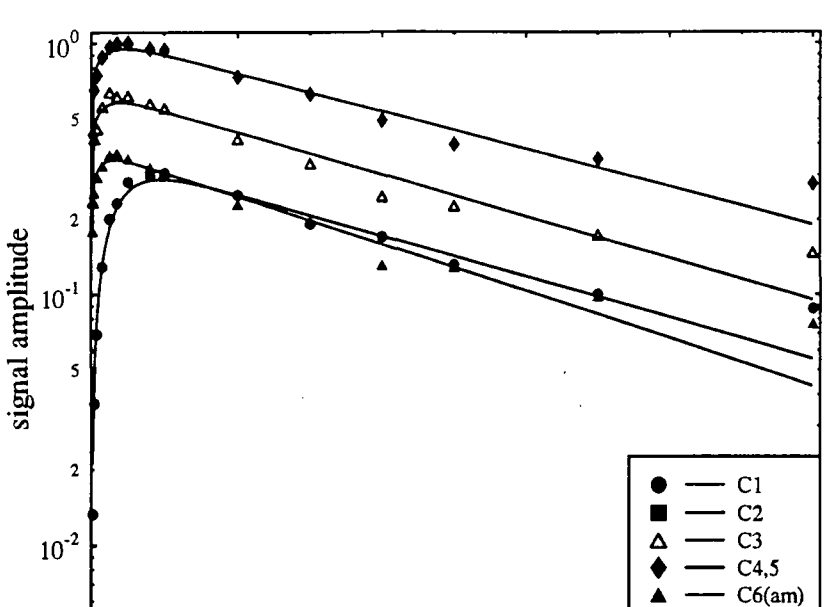

Figure 4.26 Time-dependence for the intensity of C-13 signals in a quenched powder sample of nylon-6 + 20% prepolymer in the variable contact-time cross-polarisation experiment (D0=4 s, AQ=51.2 ms, TD=2048, NT=1000, rotor spinning frequency: 3000 Hz) markers represent experimental data, solid lines represent data from eqn. 4.14 (CH_2) and 4.5 (carbonyl)

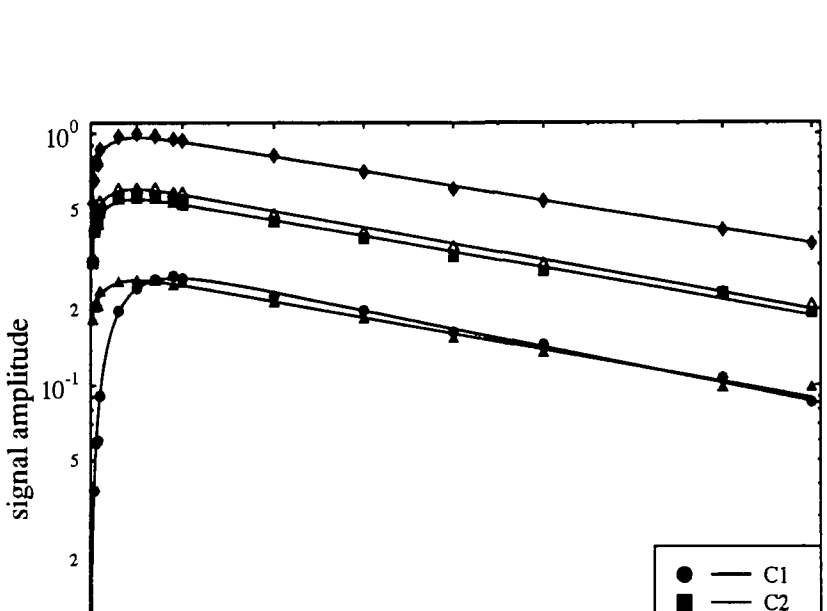

Figure 4.27 Time-dependence for the intensity of C-13 signals in a powder sample of nylon-6 + 40% prepolymer (1) in the variable contact-time cross-polarisation experiment (D0=4 s, AQ=51.2 ms, TD=2048, NT=1000, rotor spinning frequency: 3000 Hz) markers represent experimental data, solid lines represent data from eqn. 4.14 (CH_2) and eqn. 4.5 (carbonyl)

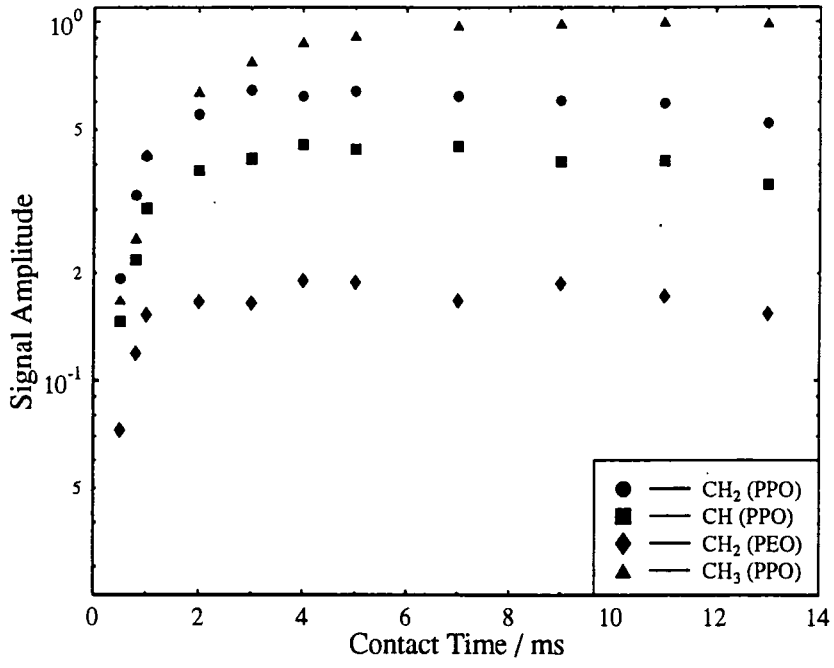

Figure 4.28 Time-dependence for the intensity of C-13 signals in a powder sample of nylon-6 + 40% prepolymer in the variable contact-time cross-polarisation experiment (D0=1 s, AQ=51.2 ms, TD=2048, NT=2048, rotor spinning frequency: 4000 Hz)

the IRCP-experiment. The inversion of the spin-temperature gives emphasis to the sensivity of the polarisation part. If the contact time τ_2 is chosen small enough such that $T_{1\rho}^H$ relaxation is negligible small, the T_2-value and spin-diffusion rate can be measured with a reasonable accuracy. The T_2-value and spin-diffusion rates are in very good agreement with those obtained from the depolarisation measurements.

However, for the experiments NBC40(2) and NBC70 (see also figures 4.31 and 4.32) the numerical analysis of the spin-diffusion rate yields values which are smaller than those obtained from the depolarisation measurements. The numerical fit is, however, in good agreement with the experimental data points as illustrated in figures 4.31 and 4.32. Two points have to be made to understand the problem. The first point is that, in contradiction to the

depolarisation experiment, the IRCP shows damped oscillations, although the sample was spun at 4000 Hz. This observation could not be explained. The resulting distorted curve might give an inaccurate fit by using equation 4.15. The curious thing is that nylon-6 and NBC40(1) (see figure 4.29 and 4.30) yield a spin-diffusion rate very similar to those measured by the depolarisation technique. For this reason it is doubtful that the oscillatory behaviour is responsible for the small values. It must be noted that in these two experiments only contact times τ_2 up to 0.3 ms have been used, and $T_{1\rho}^H$ relaxation probably could be neglected.

Nylon-6					
Carbon	C1	C2	C3	C4,5	C6
M_0	0.297±0.002	0.31±0.01	0.52±0.03	0.99±0.05	0.60±0.02
R / ms^{-1}	3.46±0.04	4.3±.7	4.2±0.4	4.4±0.8	4.3±0.8
T2 / ms	-	0.0174±0.0008	0.025±0.002	0.019±0.001	0.019±0.001
$T_{1\rho}^H$	-	-	-	-	-
NBC40(1)					
M_0	0.306±0.004	0.287±0.01	0.56±0.02	1.02±0.04	0.62±.002
R / ms^{-1}	3.73±0.05	4.3±0.6	4.7±06	4.9±0.7	4.7±0.6
T2 / ms	-	0.0180±0.0008	0.0186±0.0007	0.0188±0.0008	0.0195±0.0009
$T_{1\rho}^H$	-	-	-	-	-
			NBC40(2)		
M_0	0.488±0.004	0.273±0.008	0.56±0.02	0.98±0.03	0.59±.002
R / ms^{-1}	2.40±0.04	2.3±0.3	2.2±0.4	2.5±0.4	2.3±0.4
T2 / ms	-	0.0203±0.0007	0.0184±0.0003	0.0195±0.0008	0.0213±0.0004
$T_{1\rho}^H$	2.3±0.1	2.5±0.3	3.3±0.5	3.6±0.5	3.5±0.5
			NBC70		
M_0	0.326±0.003	0.268±0.005	0.50±0.01	1.03±0.02	0.62±.001
R / ms^{-1}	2.58±0.05	2.7±0.3	2.6±0.3	2.8±0.3	2.6±0.3
T2 / ms	-	0.0172±0.004	0.0182±0.0003	0.0179±0.0005	0.0189±0.0005
$T_{1\rho}^H$	6.8±0.3	7.7±0.4	8.4±0.5	8.9±0.5	8.6±0.5

Table 4.7 Parameters of the Inversion-recovery cross-polarisation experiment for various NYRIM materials, obtained from eqn. 4.15 for methylene carbons of the nylon-6 and exponential function for carbonyl carbon

An indirect experimental proof gives the direct measurement of $T_{1\rho}^{H}$ (see chapter 5), which yields $T_{1\rho}^{H}$-values that would not affect the polarisation curve in such a short time-interval.

The model used to fit the polarisation dynamics assumes a single $T_{1\rho}^{H}$ behaviour. The direct measurement, however, yields multi-component $T_{1\rho}^{H}$ behaviour. The time constants of those components are in the range of the spin-diffusion rate and therefore not necessarily negligible. These $T_{1\rho}^{H}$ components are difficult to detect indirectly by using carbon-13 CP/MAS, because they relax during the CP-period, with the result that only the long-time components are detectable. A schematic representation (figure 4.33) of the pulse sequence for indirect $T_{1\rho}^{H}$ measurement makes the

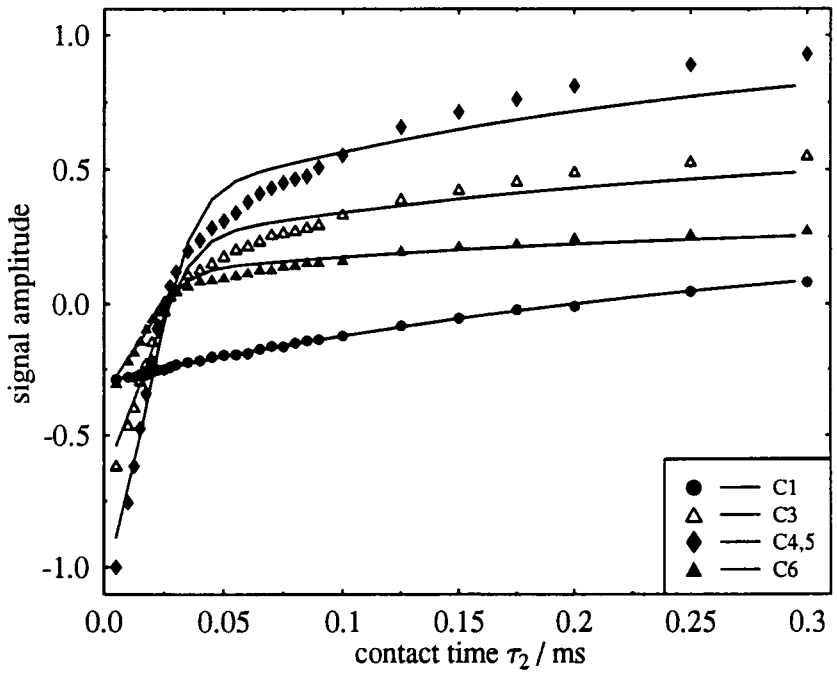

Figure 4.29 Time-dependence for the intensity of C-13 signals in a powder sample of nylon-6 in the inversion-recovery cross-polarisation experiment (D0=1 s, τ_1=1 ms, AQ=51.2 ms, TD=2048, NT=2048, rotor spinning frequency: 4000 Hz) markers represent experimental data, solid lines represent data from eqn. 4.15 (CH_2)

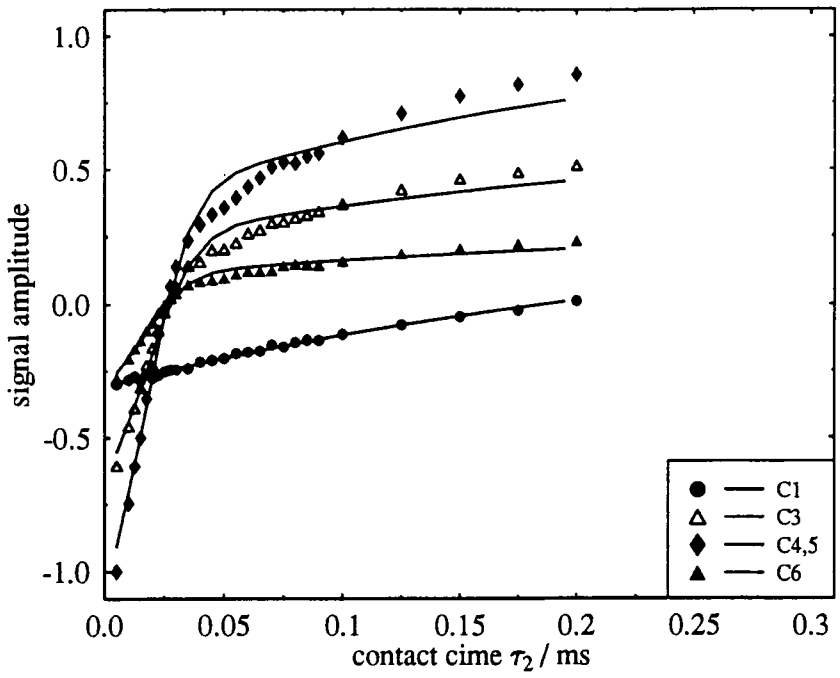

Figure 4.30 Time-dependence for the intensity of C-13 signals in a powder sample of nylon-6 + 40% prepolymer in the inversion-recovery cross-polarisation experiment (D0=1 s, τ_1=1 ms, AQ=51.2 ms, TD=2048, NT=2048, rotor spinning frequency: 4000 Hz) markers represent experimental data, solid lines represent data from eqn. 4.15 (CH_2)

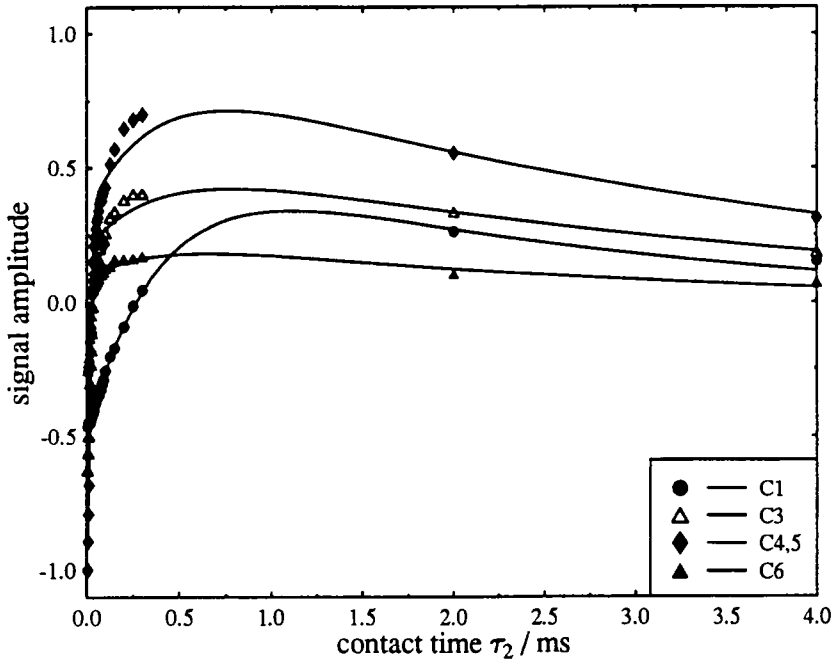

Figure 4.31 Time-dependence for the intensity of C-13 signals in a powder sample of nylon-6 + 40% prepolymer (NBC40(2)) in the inversion-recovery cross-polarisation experiment (D0=2 s, τ_1=1 ms, AQ=25.6 ms, TD=512, NT=2048, rotor spinning frequency: 4000 Hz) markers represent experimental data, solid lines represent data from eqn. 4.15 (CH_2)

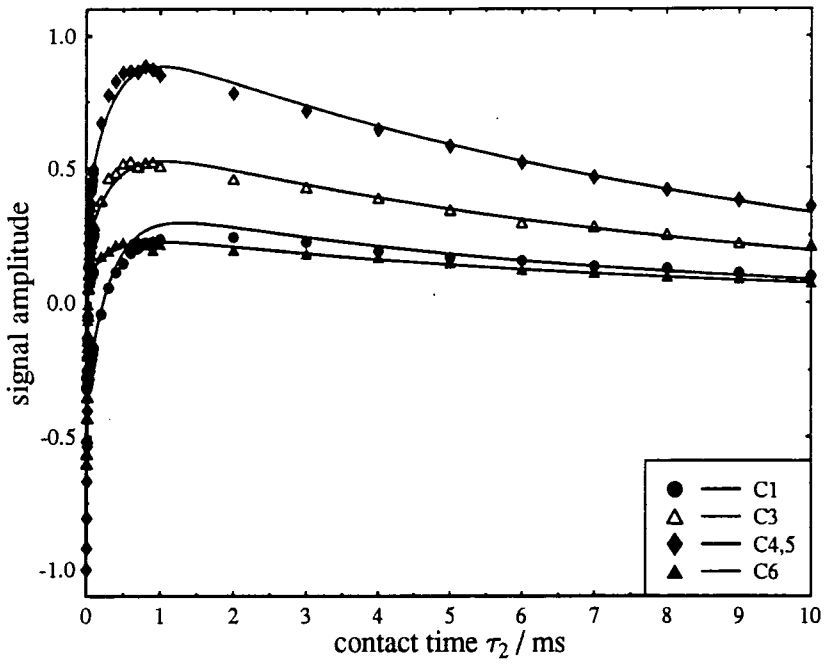

Figure 4.32 Time-dependence for the intensity of C-13 signals in a powder sample of nylon-6 + 70% prepolymer in the inversion-recovery cross-polarisation experiment (D0=2 s, τ_1=1 ms, AQ=51.2 ms, TD=1024, NT=1024, rotor spinning frequency: 4000 Hz) markers represent experimental data, solid lines represent data from eqn. 4.15 (CH_2)

problem clear. The minimum spin-lock time in this experiment is the cross-polarisation time t_{cp}, which allows magnetisation transfer from the protons to the carbons. This time is typically 1 ms for the polymer under investigation in order to achieve a reasonable signal-to-noise ratio. Consequently, $T_{1\rho}^H$ values of the order of one millisecond or less are not measurable by this technique. A $T_{1\rho}^H$ value of the order of 1 ms would affect the value of the spin diffusion rate in the IRCP (and normal CP) in the way it was determined. The consequence therefore is that the numerical value is smaller than the real value.

In order to check if a multi-component $T_{1\rho}^H$ is present, a selective measurement of $T_{1\rho}^H$ has been carried out using the pulse sequence depicted in figure 4.33. The results are summarised in table 4.8. A graphical representation is

given in figures 4.34 for nylon-6 and 4.35 for NBC40(1). The experimental data in figure 4.34 and 4.35 do not show any sign of a multi-component $T_{1\rho}^{H}$ relaxation behaviour. However, an indication that NBC40 has not a single $T_{1\rho}^{H}$, yields two separate measurements with two different t_{cp} values. The t_{cp} values of 0.2 ms gives emphasis to short $T_{1\rho}^{H}$ values, while the larger t_{cp} (8 ms) gives emphasis to longer $T_{1\rho}^{H}$ values because the short components have already relaxed in that time before the acquisition starts.

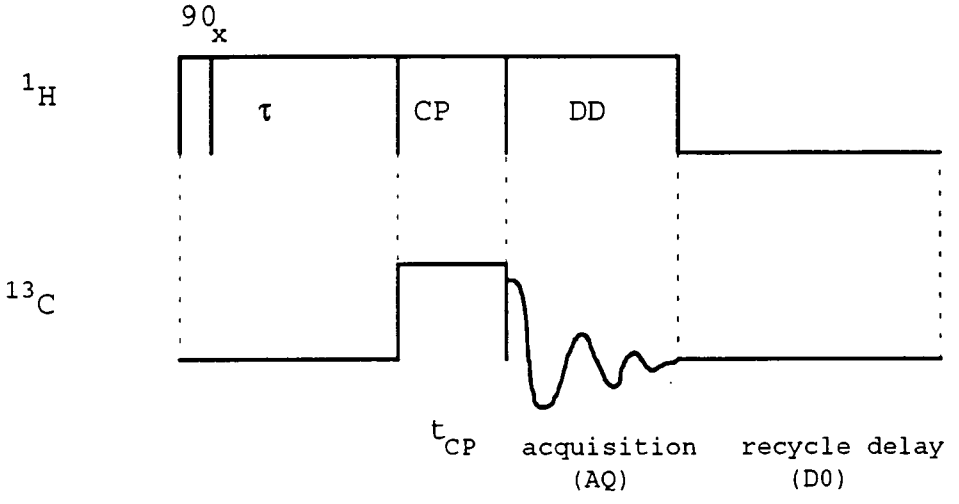

Figure 4.33 Pulse sequence of a CP/MAS variable-delay experiment for a selective $T_{1\rho}^{H}$ measurement via the carbons.

	C1	C2	C3	C4,5	C6
Nylon-6					
$T_{1\rho}^{H}$ / ms	10.6±0.4	11.3±0.4	10.8±0.4	11.8±0.4	11.7±0.3
NBC40(1)					
$T_{1\rho}^{H}$ / ms	3.9±0.6	4.1±0.3	3.5±0.2	5.1±0.3	5.0±0.9
NBC40(2)					
$T_{1\rho}^{H}$ / ms	9.4±0.8	8.9±0.4	8.3±0.4	8.3±0.3	7.4±0.4

Table 4.8 Selective $T_{1\rho}^{H}$ measurement for nylon-6 carbons and methylene carbons of NBC40. For experiments NBC40(1) and NBC40(2) a t_{cp} of 200 μs and 8 ms has been used respectively

The $T_{1\rho}^{H}$ values obtained by using these two t_{cp}-values are different by a factor of about two, where the short-time value (about 4 ms) would indeed interfere with the spin diffusion rate. This point makes it clear, although it has not been proved for every sample, that the assumption of a single $T_{1\rho}^{H}$ could disturb the numerical analysis of CP-dynamics. Using short contact times is certainly not an insurance to justify neglecting relaxation phenomena, but it could be the only way to overcome the relaxation problem if one uses this relatively simple model to analyse the cross-polarisation dynamics. For analytical purposes concerning the cp-dynamics the depolarisation technique is certainly preferable because of the generally longer $T_{1\rho}^{C}$. However, techniques like IRCP were not designed to investigate cp-dynamics but for applications, e.g., in spectral editing (using the different polarisation

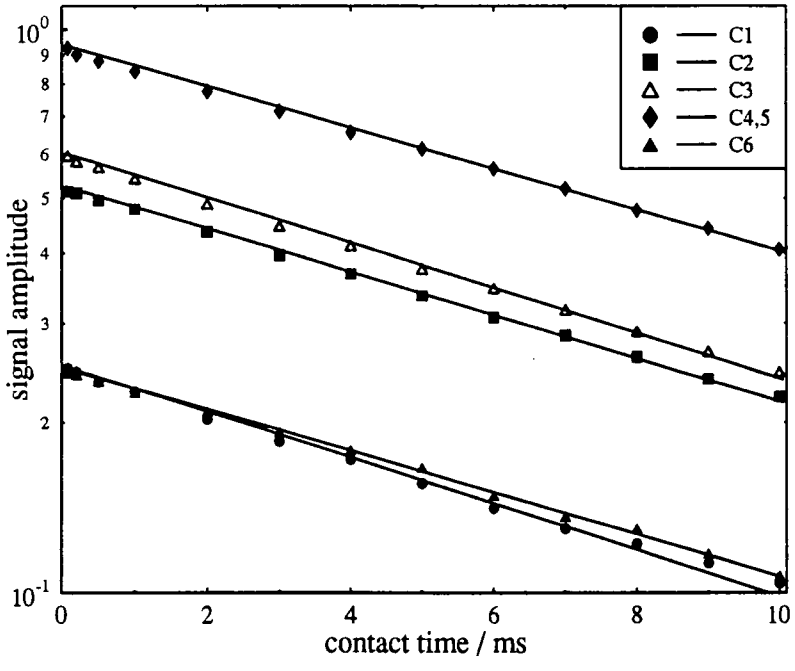

Figure 4.34 Selective $T^{H}_{1\rho}$ for nylon-6 using the pulse sequence of figure 4.33 (D0=2 s, AQ=25.6 ms, CT=0.8 ms, TD=1024, NT=2048 markers represent experimental data, solid lines represent fitted data

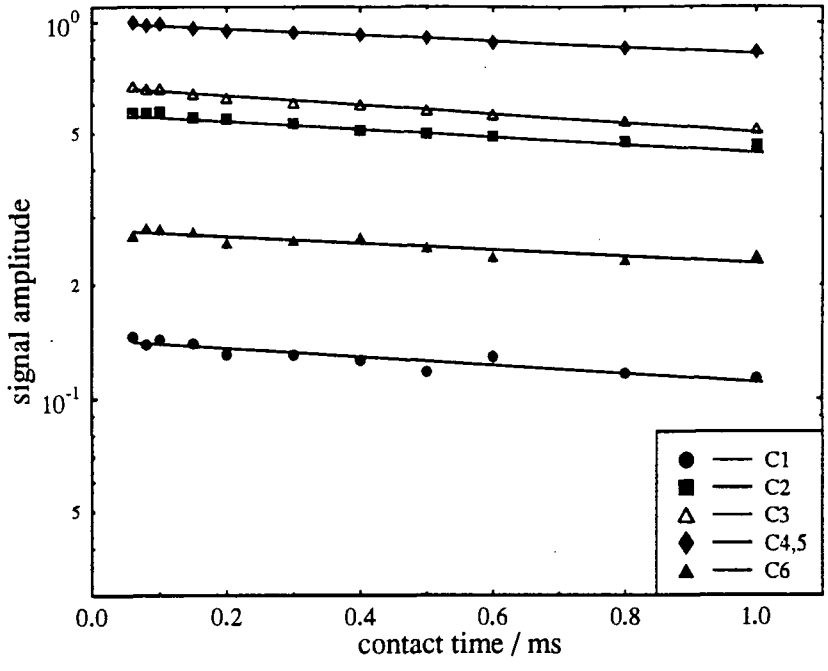

Figure 4.35 Selective $T^{H}_{1\rho}$ for nylon-6 + 40% prepolymer using the pulse sequence of figure 4.33 (D0=2 s, AQ=25.6 ms, CT: 0.2 ms, TD=1024, NT=2048) markers represent experimental data, solid lines represent fitted data

properties of the different carbons in a molecule or moiety to assign solid-state spectral.

A last example will point out that the advanced model of describing cp-dynamics in organic solids is, however, an improvement with respect to the classical Mehring technique. As a model material, nylon-6 + 40% prepolymer has been chosen. The results of the numerical fit using eqn. 4.5 are summarised in table 4.9 and graphically illustrated in figure 4.36.

The deviation of the numerical fit and the experimental data make it obvious that this model using a single spin-temperature does not hold with the reality. It does not account for the two mechanisms responsible for polarisation transfer, resulting in a bad description of the signal increase. However, some authors still use the model by Mehring using a parameter set of two different

NBC40				
	C2	C3	C4,5	C6
M_0	0.268±0.005	0.50±0.01	1.03±0.02	0.62±.001
R / ms^{-1}	2.7±0.3	2.6±0.3	2.8±0.3	2.6±0.3
$T_{1\rho}^{H}$	7.7±0.4	8.4±0.5	8.9±0.5	8.6±0.5

Table 4.9 Parameters of the variable contact-time cross-polarisation experiment for NBC40, obtained from eqn. 4.5 (only the carbons of the nylon-6 are presented)

polarisation time constants and assigning these to two distinct moieties in the polymer [44, 45], which is definitely wrong.

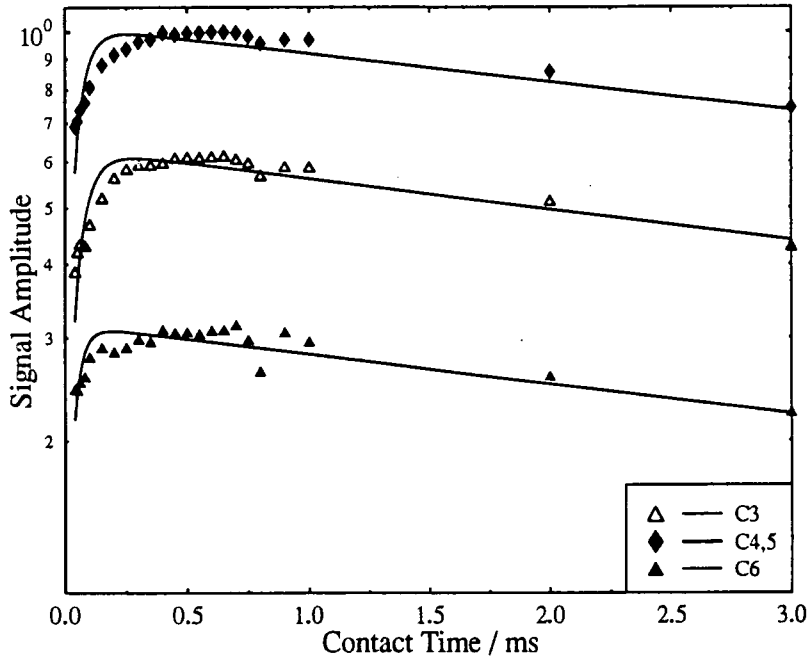

Figure 4.36 Time-dependence for the intensity of C-13 signals in a powder sample of nylon-6 + 40% prepolymer (2) in the variable contact-time cross-polarisation experiment (D0=1 s, AQ=51.2 ms, TD=2048, NT=2048, rotor spinning frequency: 4000 Hz) markers represent experimental data, solid lines represent data from eqn. 4.5

4.4 Spin-lattice Relaxation T_1^C and Solid-state High-resolution Single-pulse MAS spectra of NYRIM and the Prepolymer

In some cases CP/MAS is less preferable than a single pulse experiment. Especially if the material under investigation is very mobile, cross-polarisation becomes very inefficient. The additional effect which gives the single-pulse experiment an advantage for mobile materials with respect to rigid materials, is the relatively short spin-lattice relaxation time of the rare nucleus. Quantification of the resonances is possible and yields further information of the different sites in the molecules, a technique usually used in liquid-state NMR. For determination of the T_1^C values in the polyether, the inversion-recovery technique has been applied, which is shown in figure 4.37.

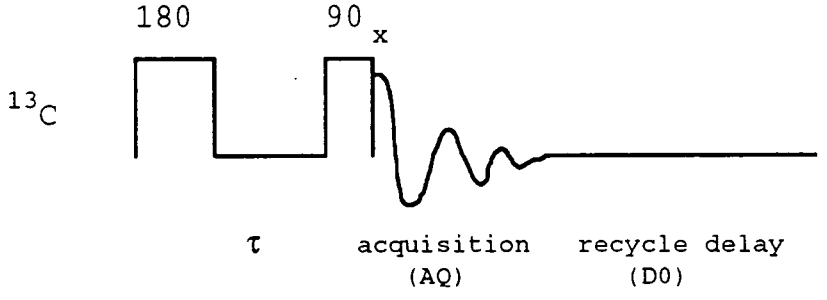

Figure 4.37 Inversion-recovery pulse sequence for measurement of the carbon-13 spin-lattice relaxation time

4.4.1 Measurement of T_1^C: Results and Discussion

Measurements of T_1^C have been carried out for the prepolymer, quenched nylon-6 + 20% prepolymer and nylon-6 + 40% prepolymer. These results have already been

presented by the author for his German Diploma degree. However, they are summarised in table 4.10.

	PPO, T_1^C / s			PEO, T_1^C / s
Sample	CH	CH_2	CH_3	CH_2
Prepolymer	0.16	0.11	0.36	0.17
quenched NBC20	0.17	0.10	0.37	-
annealed NBC40	0.17	0.11	0.37	0.17

Table 4.10 T_1^C / s values obtained by the inversion-recovery technique (single-pulse MAS)

The acquisition conditions were: 1 s recycle delay, 4 μs 90° pulse-duration, acquisition time 102 ms, number of transients 512, τ values between 1 ms and 2 s have been used.

Relaxation in solids and highly viscous liquids is normally dominated by the dipolar relaxation mechanism. The relaxation depends on the number of directly bonded hydrogens and the mobility of the carbon under investigation. The relaxation time of the methine carbon is nearly twice as long as that from the methylene carbon because the methylene carbon has two hydrogens attached rather than one. The fact that the methylene carbon is actually not relaxing twice as fast, indicates that the relaxation mechanism is not entirely dipolar. The methyl carbon relaxes relatively slowly in view of the number of hydrogens attached to it. This relaxation is controlled by its fast rotation. The dipolar interaction is also a function of the correlation time τ_c. Generally speaking, the more mobile the carbon, the shorter its correlation time and the longer the relaxation time assuming we are

looking at the short τ_c side of minimum. The relation of the relaxation rate, the correlation time and the dipolar interaction is shown for a simple process in equation 4.16:

$$\frac{1}{T_{1dd}} = \gamma_C^2\gamma_H^2\left(\frac{\mu_0}{4\pi}\right)^2\hbar^2\frac{\tau_c}{1+\omega^2\tau_c^2}\sum\frac{1}{r_{CH}^{-6}} \qquad (4.16)$$

where T_{1dd} is the dipolar relaxation time

r_{CH} is the distance between the carbon and the hydrogen

the other symbols have their usual meaning. By knowing the relaxation time, it is possible to study the composition of the prepolymer quantitatively as will be described in the next section.

4.4.2 Quantitative Solid-state NMR of the Prepolymer

It was of particular interest to know the proportion of PPO and PEO in the prepolymer. The prepolymer is a commercial product for which only a little information was available. The knowledge of its composition allows conclusions to be made of the molecular weight of the polyether because PEO is used to end-functionalise PPO, as mentioned in chapter 3. The ^{13}C-MAS single-pulse spectrum of the prepolymer is shown in figure 4.39. A recycle delay of 2 s was found to be sufficient long. The methyl-carbon, as the carbon with the longest T_1^C, did not gain any signal intensity by applying a longer recycle delay. The integration facility of the CXP 200 spectrometer has been used to quantify the areas of the carbon resonances. The result is an average of three independent measurements.

The ratio PEO:PPO was determined to be 1 : 6.9±0.4. As mentioned in chapter 3 the high amount of PEO is necessary to increase the reactivity for the preparation of the prepolymer. With this value, the molar mass of the polyether can be estimated. Assuming a polyether-structure as illustrated in figure 4.38, for a PEO:PPO-ratio 1:7, it follows that n = 14 and the molecular weight is concluded to be 936 g/mol. This is about half of the molecular weight according the information of the manufacturers, but, however, a molecular weight, that is commercially used [46].

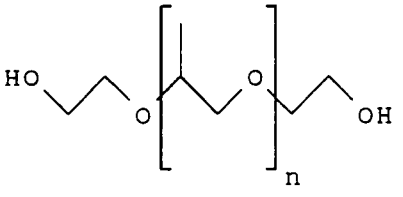

polyether

Figure 4.38 Assumed structure of PEO end-functionalised PPO

4.5 Variable Temperature Measurements of NYRIM

4.5.1 Introduction

Solid-state high-resolution NMR spectroscopy is a very interesting topic for studying the kinetics of a polymer [47-53]. NYRIM has been investigated on a temperature scale from -100 °C to +100 °C. The high-resolution spectra were compared with direct T_1^H and $T_{1\rho}^H$ using the WRAC spectrometer. The high-resolution spectra were acquired on the VXR 300 using a variable-temperature probe head.

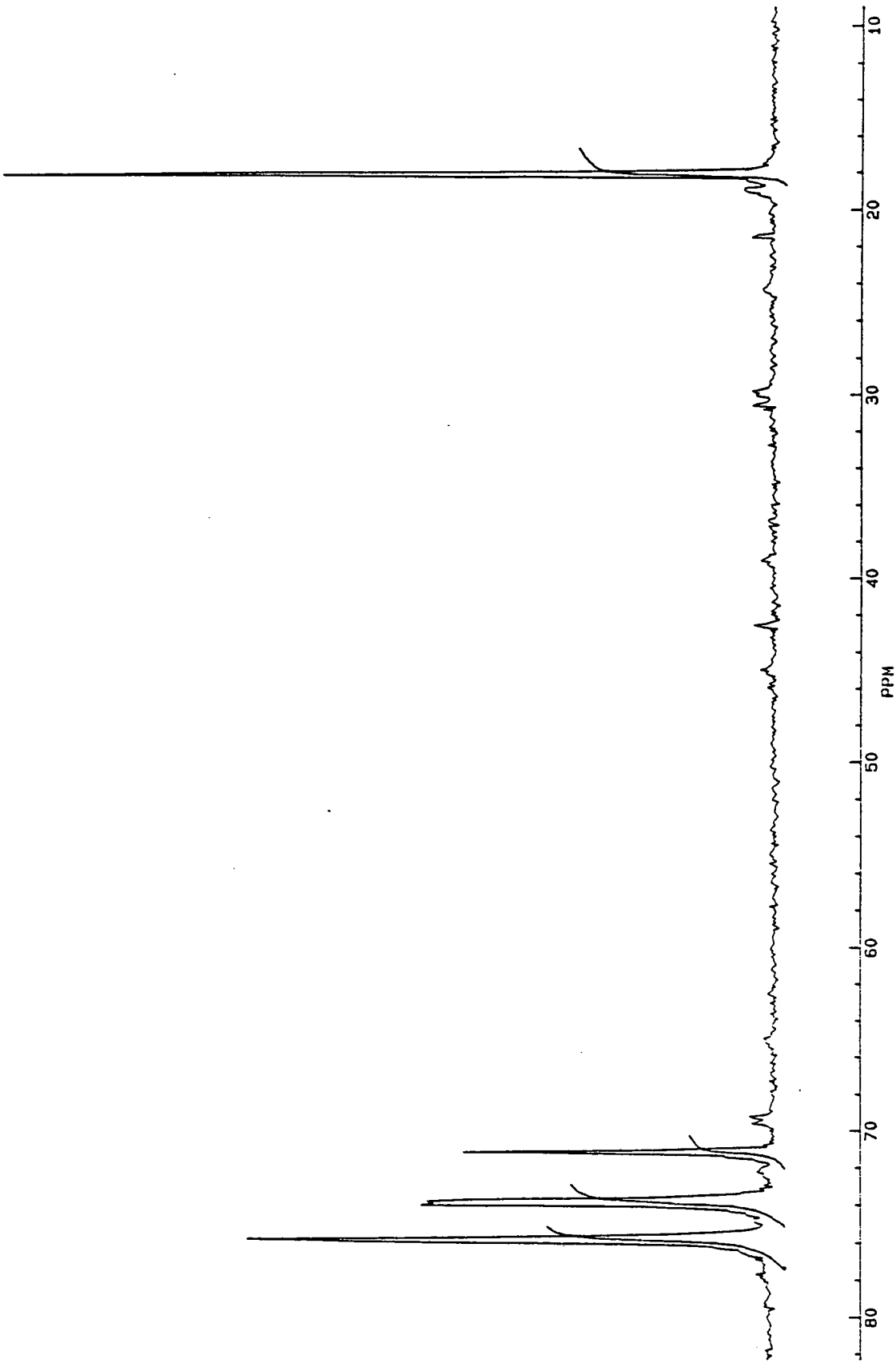

Figure 4.39 Carbon-13 single-pulse MAS spectrum of the prepolymer. The carbon resonances were integrated (see text for more details)

4.5.2 Measurements from Room Temperature up to 100 °C.

In this section the temperature-dependence of the high-resolution carbon-13 CP/MAS spectrum and the single-pulse MAS spectrum of nylon-6 + 50% prepolymer will be investigated. The CP/MAS spectrum detects the crystalline and amorphous phase of nylon-6 at the same time. The single-pulse experiment gives emphasis to the amorphous part of nylon-6 if the recycle delay is set to an appropriate time, which is no problem because, as seen in an earlier section, the amorphous carbons have a shorter spin-lattice relaxation time than the carbons of the crystalline phase.

4.5.3 Results and Discussion

The temperature-dependence of the CP/MAS spectrum is investigated first. For this purpose, two spectra of NBC50 have been acquired, at room temperature and at 80 °C, respectively. Figure 4.40 presents the two spectra plotted on the same graph. The two spectra are almost identical. The different chemical shifts of the spinning sidebands (indicated as SSB) are simply because the sample was spinning at two different frequencies in the two experiments. In the spectrum acquired at 80 °C, the nylon carbon resonances are slightly narrower than in the room temperature spectrum. The reason for this is that thermal energy is put into the polymer by heating it up to 80 °C. This induces thermal motion, which is responsible for the line-narrowing. It is interesting to note that the glass

transition temperature of nylon-6 is 50 °C. The spectrum was recorded at 80 °C. One would expect that the amorphous part of the nylon-6 would appear substantially narrowed, which it is not. This is because T_g appears to be at higher temperatures with higher frequency measurements in NMR.

The experiment was repeated with the same sample by using the single-pulse technique. A series of spectra with successively increasing temperatures have been acquired, which are shown in figures 4.41a to 4.41d. These experiments reveal two new properties of NYRIM and nylon-6. Now the temperature dependence of the single-pulse spectrum will be investigated. Only the nylon-6 resonances will be discussed, because the polyether resonances do not change significantly at higher temperatures. The spectrum at 303 K (fig. 4.41a) shows very broad signals, indicating the unordered structure of the amorphous region. The resonance at 43 ppm (C6 of the crystalline region) is only very weak, testifying that the spectrum of the crystalline region is quasi-saturated, so that visible resonances arise mainly from the amorphous region. At 323 K the spectrum is already starting to narrow. The resonance of C4 (28.3 ppm) is now clearly resolved (see figure 4.41b). At 343 K the resonances become appreciably narrower. An interesting fact is that the resonance at 28 ppm seems to decrease in intensity and at the same time the signal at 26.3 ppm (C3) is splitting up (see figure 4.41c). This trend continues, when the temperature is increased further to 373 K (see figure 4.50d). Now the resonance at 26.3 is well-resolved into two signals (26.0 ppm and 27 ppm). The

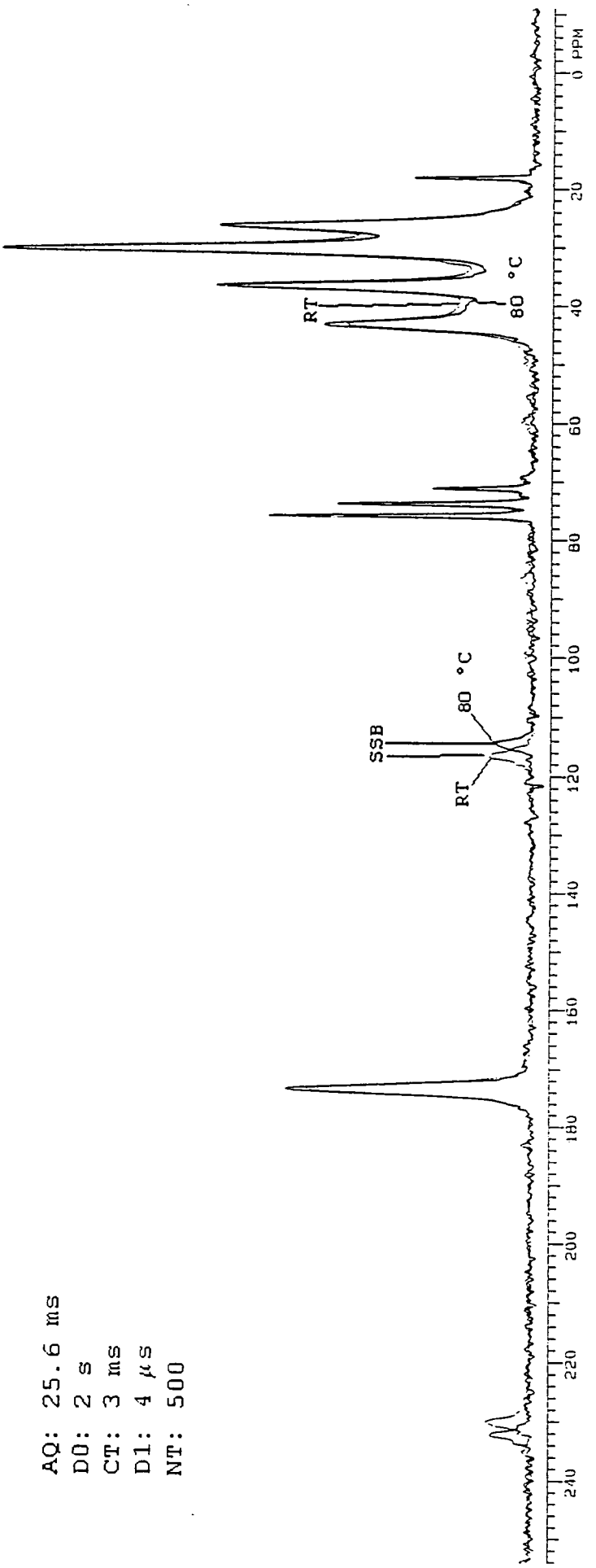

Figure 4.40 Carbon-13 CP/MAS spectrum of NBC50 at room temperature and 80°C

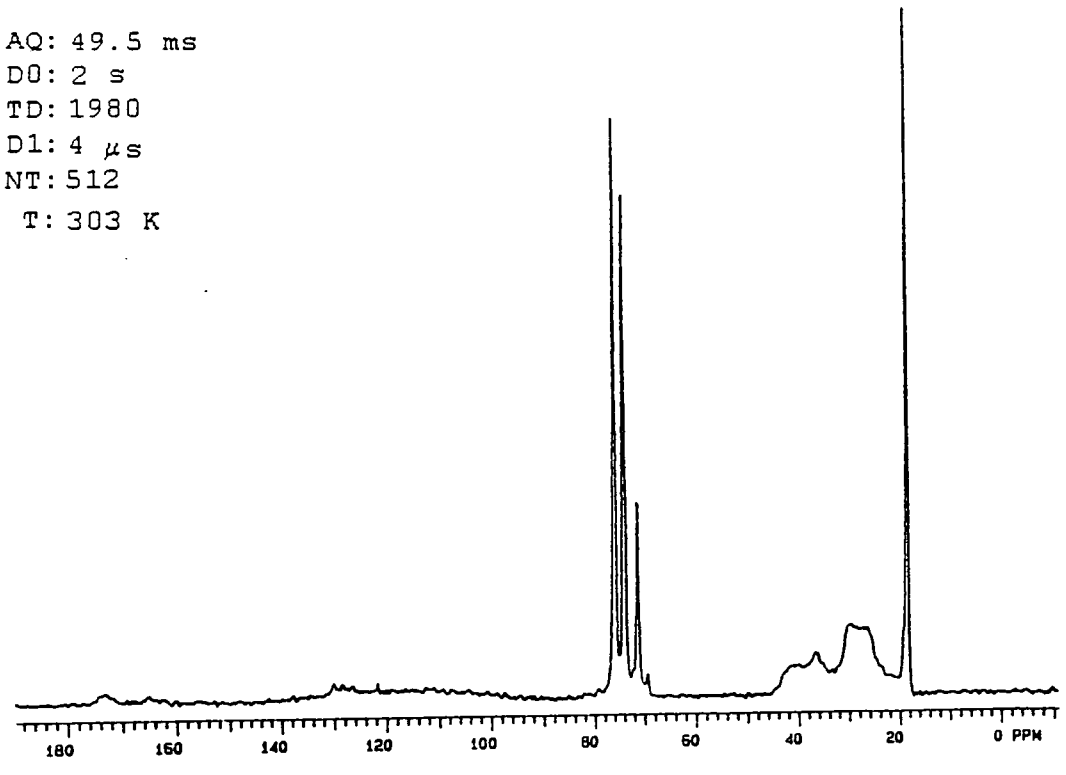

Figure 4.41a 75.43 MHz carbon-13 single-pulse spectrum of NBC50 at 303 K

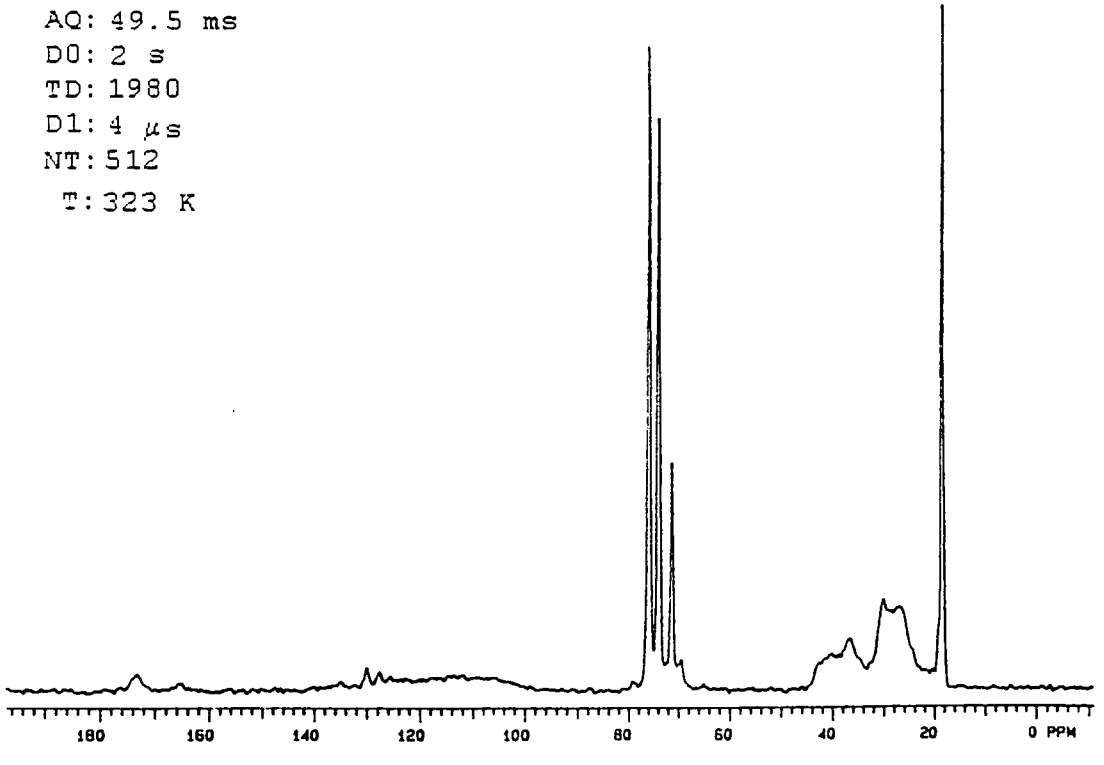

Figure 4.41b 75.43 MHz carbon-13 single-pulse spectrum of NBC50 at 323 K

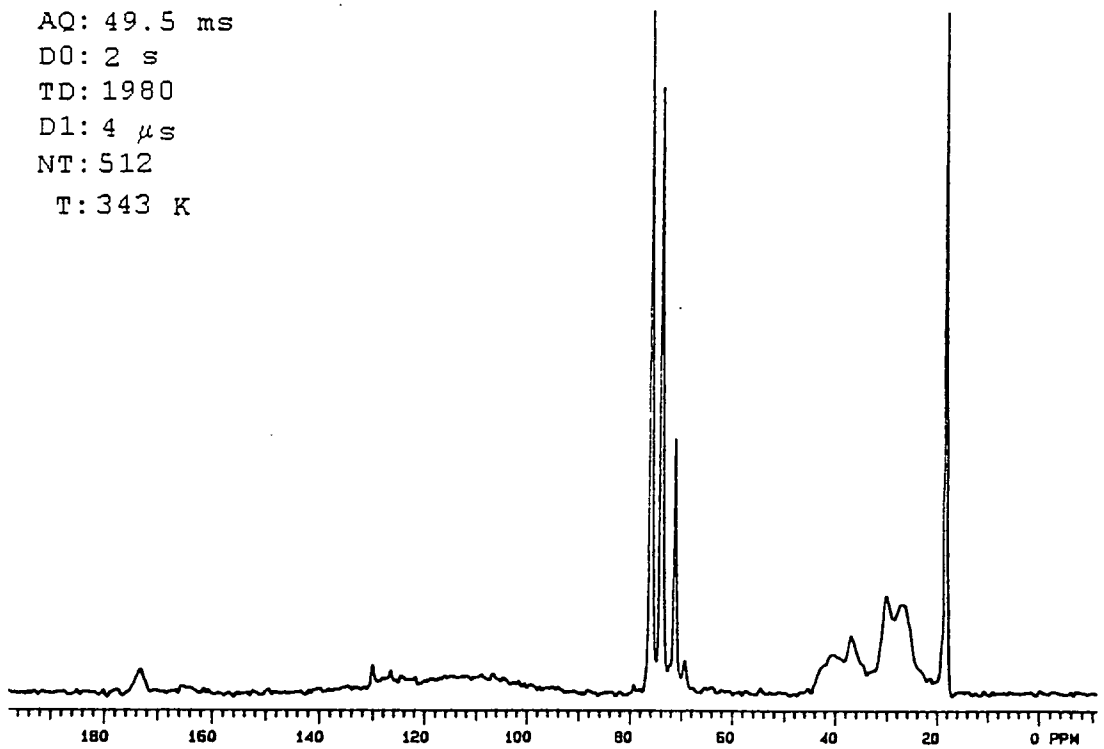

Figure 4.41c 75.43 MHz carbon-13 single-pulse spectrum of NBC50 at 343 K

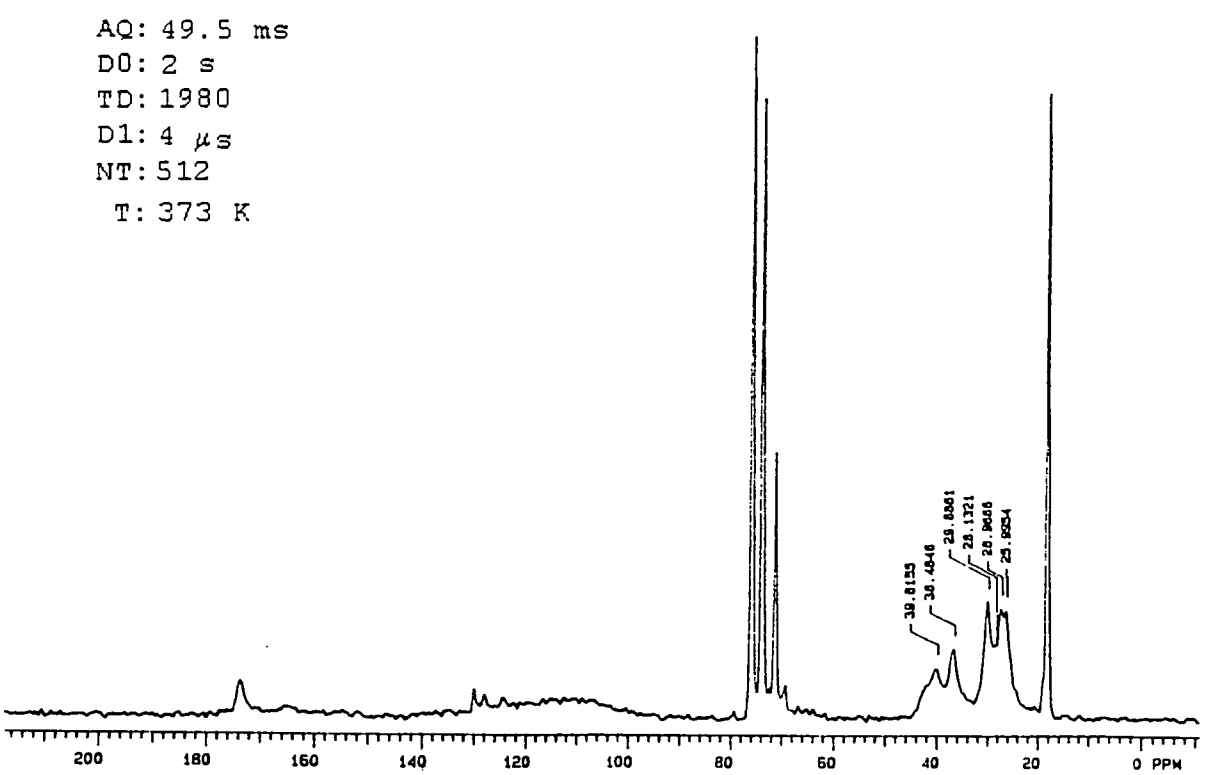

Figure 4.41d 75.43 MHz carbon-13 single-pulse spectrum of NBC50 at 373 K

signal of C4 at 28.3 ppm is still there but with reduced intensity. Unfortunately the temperature could not be increased further, because of instrumental limiting factors. An explanation for the chemical shifts, in particular the decreasing signal of C4 and the "splitting" of the signal at 26.3 ppm is not straightforward. Comparing the chemical shifts obtained at 373 K with those from solution-state NMR (see table 4.1a), a remarkable agreement is found. Solution-state ^{13}C-NMR unveils an almost exact agreement for the carbons C3 (26.0 ppm, solid-state; 26.4 ppm, solution) and C4 (27.0 ppm, solid-state; 27.1 ppm, solution), suggesting the amorphous phase forms an extended chain. These resonances could lead to the conclusion that raising the temperature would cause entanglement of the polymer chain and form a conformation similar to that in solution. However, it remains unsolved why the two signals at 26.0 ppm and 27.0 ppm have the same intensity. If one of those resonances is coming from C4, than it would be expected that as the signal at 28.3 ppm decreases the other signal would increase. Another possibility to explain the chemical shifts is the presence of two different non-crystalline phases. Measurements of the specific-volume by Illers and Haberkorn [54] indicated that there were two types of amorphous regions in nylon-6, which depended upon the crystalline polymorph present in greatest abundance. An indication that the splitting is due to a structural regime and not due to a change in the arrangement of the carbons by increasing the temperature is the relatively broad signal at 26.3 ppm. The splitting of that signal is believed to emanate from two different

amorphous structures. High-temperature NMR enables one to observe the two signals arising from those regions because of line-narrowing. Other explanations, such as the γ-gauche effect, fail because these would include a chemical shift change on other carbons as well, which could not be observed. However, the lack of information about the amorphous region does not allow an absolutely sure conclusion about it.

4.5.4 Measurements from Room Temperature down to -100 °C

In this section the temperature dependence of the ^{13}C-CP/MAS spectra of NBC50 at low temperatures will be investigated. As for nylon-6 at high-temperature, the polyether runs through its glass-transition temperature (−50 °C; see figure 5.4 in chapter 5) where interesting structural and mobility changes take place.

4.5.5 Results and Discussion

The high-resolution spectra were acquired on a VXR 300 using a variable temperature probehead and liquid nitrogen to cool down the bearing gas stream. Temperatures down to 173 K (-100 °C) were possible over the period which the experiments last, without freezing the rotor into the probe. Rotor spinning frequencies between 3000 and 4000 Hz were achieved without problems.

The temperature dependence of the ^{13}C CP/MAS spectra for NBC50 at various temperatures is graphically illustrated in figures 4.42a to 4.42i. The discussion this time is

limited to the polyether part of the block copolymer because the spectrum of the nylon fraction is independent of the temperatures used in this part of the study. The ^{13}C-CP/MAS spectrum of NBC50 (figure 4.42a) shows nicely resolved sharp signals of the polyether carbons. If the temperature is lowered to 263 K the intensities of the resonances start to decrease (figure 4.42b). This trend continues with decreasing temperature (figures 4.42c to 4.42e). At 223 K (-50 °C) the methylene resonances of PPO have apparently vanished (figure 4.42f). The resonance of the methyl group is still visible but with reduced intensity. Further lowering of the temperature to 213 K (-60 °C) lets the signals of the polyether reappear as seen in figure 4.42g. The resonances of the methylene and methine carbons are now completely unresolved. If the temperature is reduced down to 193 K (figure 4.42h) the polyether signals gain in intensity. The methyl carbon is now further broadened than at higher temperatures. At 173 K (figure 4.42i) the methyl carbon is again losing intensity but without broadening. The top of its signal appears to be flattened.

The polyether signals at room temperature are very sharp, from the solid-state point of view, because they are highly mobile. This is because the glass-transition temperature, T_g, is -50 °C and the polyether therefore exists in a highly mobile amorphous form. By decreasing the temperature the mobility is reduced and the resonance line is broadened. The answer why the signal vanishes at 223 K is not trivial. In principle several mechanisms could be responsible for the signal loss:

1. T_1^H has a maximum at that temperature therefore the recycle delay in insufficient long and the signal is saturated
2. The cross-polarisation time constant has a maximum, and so the magnetisation transfer from the protons to the carbons is reduced such that no carbon signal is observable
3. The rotating frame spin relaxation $T_{1\rho}^H$ has a minimum, so that the proton magnetisation is relaxing faster than it can be transferred to the carbons

All three points have been checked by varying the appropriate parameters. The first two points are not the reason for the signal loss, so there will be no deeper discussion for those. In order to check the influence of the rotating frame spin-relaxation a direct measurement of $T_{1\rho}^H$ at variable temperature has been carried out using the WRAC instrument. The temperature has been calibrated by placing a thermocouple into the probe and taking the actual temperature before each single measurement. The results of such measurements are summarised in table 4.11. The relaxation time behaviour of solids will be discussed in more detail in chapter 6 (spin-lattice relaxation and spin-diffusion). The only important information about spin-relaxation in heterogeneous systems influenced by spin-diffusion which needs to be known here is that spin-diffusion may greatly modify the overall observed relaxation behaviour from that expected from the intrinsic relaxation properties of the various sites. This is the

case for nylon block copolymers and the reason why only a single spin-lattice relaxation is found although NYRIM is built up from at least three components, the polyether, the amorphous and the crystalline nylon, with three distinct intrinsic relaxation times. The $T_{1\rho}^{H}$ relaxation is distorted in proportion and values, so the three relaxation components found are not necessarily in quantitative relation to the real components as demonstrated in table 4.11 (see also chapter 5). Figure 4.43 illustrates the weighted-averaged relaxation rate versus the inverse temperature. The reason why the weighted-average relaxation rate has been used to visualise the $T_{1\rho}^{H}$-minimum needs some more discussion.

The results of a $T_{1\rho}^{H}$ measurement of the prepolymer at room temperature obtained from the WRAC instrument are summarised in table 4.12.

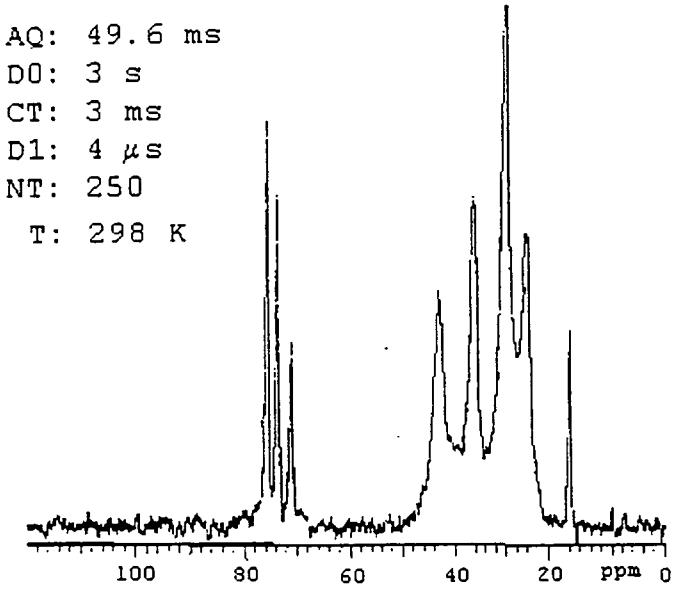

Figure 4.42a Carbon-13 CP/MAS spectrum of NBC50 at 298 K

T / K	T^{-1} / K^{-1} *10^{-3}	ϑ / °C	T_1^H / s	T_1^{-1} / s^{-1}	$T_{1\rho}^H$ / s	$T_{1\rho,av}^{-1}$ / s^{-1}
298.2	3.35	25	0.185	5.41	0.0204 (47.3%)	
					0.0076 (37.9%)	165.4
					0.0016 (14.8%)	
273.1	3.60	-0.1	0.255	3.94	0.0114 (30.9%)	
					0.0029 (41.8%)	584.9
					0.0007 (27.3%)	
261.6	3.82	-11.6	0.347	2.88	0.0118 (27.2%)	
					0.0024 (29.0%)	1075.8
					0.0005 (43.8%)	
250.1	4.00	-23.1	0.437	2.29	0.0102 (34.8%)	
					0.0018 (28.9%)	1263.3
					0.0003 (36.3%)	
235.7	4.24	-37.5	0.463	2.16	0.0140 (29.2%)	
					0.0036 (48.8%)	429.3
					0.0009 (25.1%)	
224.7	4.45	-48.5	0.471	2.12	0.0123 (41.6%)	
					0.0034 (47.6%)	344.5
					0.0006 (10.8%)	

Table 4.11 Static 60 MHz proton spin-relaxation times (T_1^H, $T_{1\rho}^H$) at variable temperatures for nylon-6 + 50% polyether prepolymer. Column 5 presents the $T_{1\rho}^H$´s and their proportion (in brackets). Column 6 shows the weighted-average relaxation rates

Time / s	%
0.044	73.9
0.017	26.1

Table 4.12 $T_{1\rho}^H$ data of the prepolymer at room temperature

Kenwright [55] has proved that in a heterogeneous system which is spin-diffusion influenced, the observed relaxation times are not the same as the intrinsic relaxation times of the components. However, he showed that the fastest relaxation component may be closely associated with the intrinsic relaxation process of the faster relaxing region.

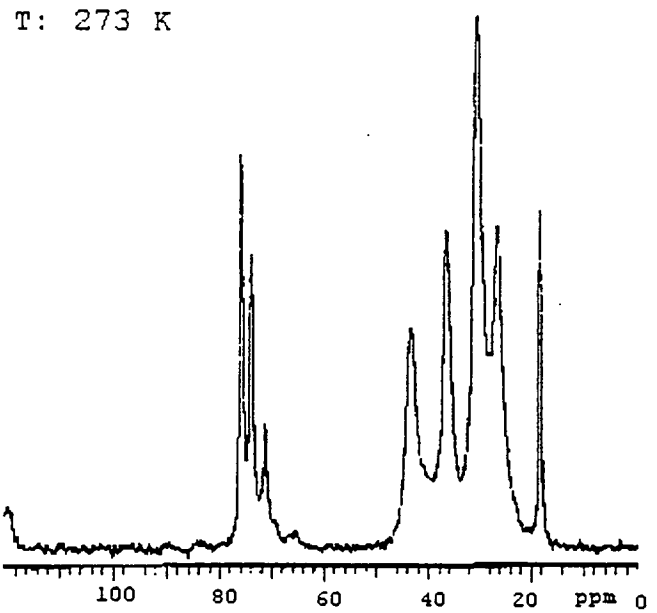

Figure 4.42b Carbon-13 CP/MAS spectrum of NBC50 at 273 K

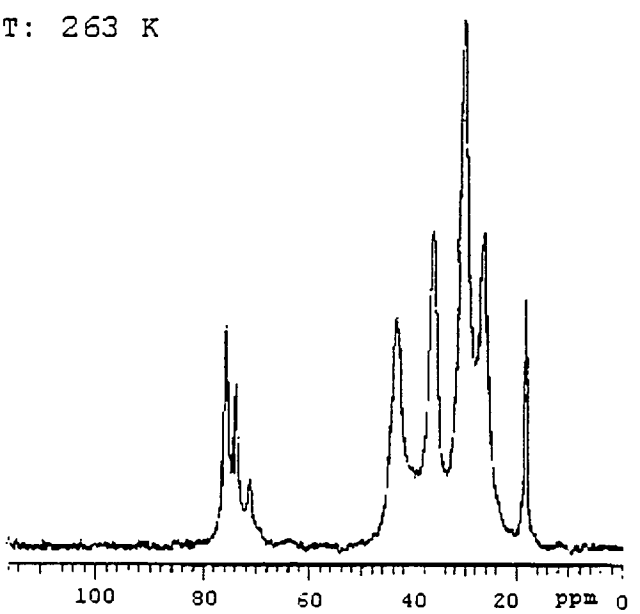

Figure 4.42c Carbon-13 CP/MAS spectrum of NBC50 at 263 K

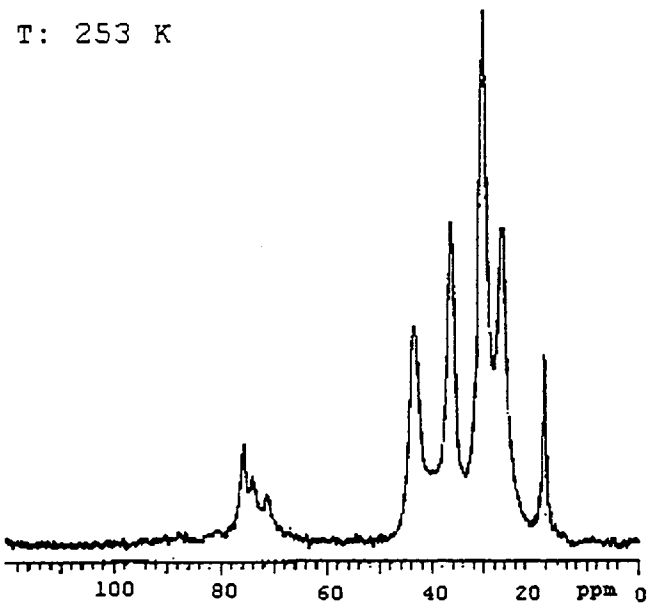

Figure 4.42d Carbon-13 CP/MAS spectrum of NBC50 at 253 K

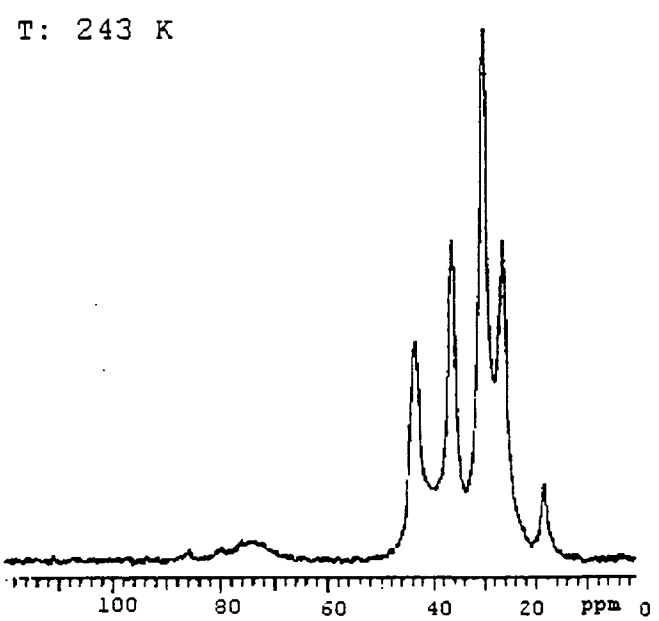

Figure 4.42e Carbon-13 CP/MAS spectrum of NBC50 at 243 K

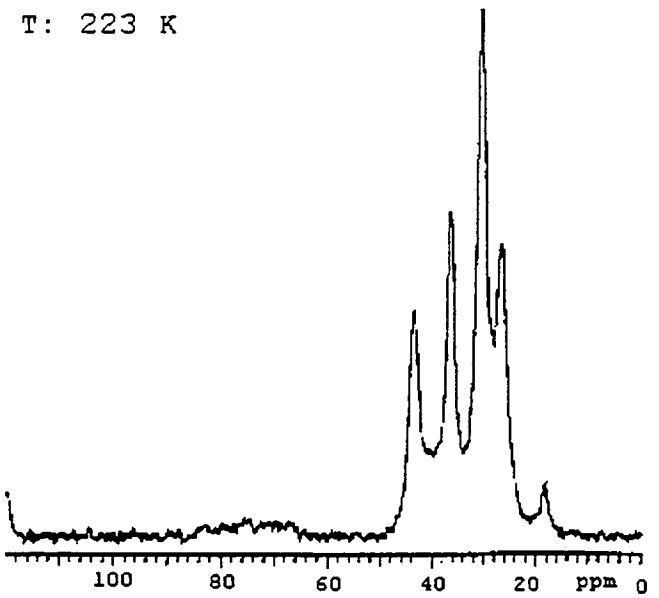

Figure 4.42f Carbon-13 CP/MAS spectrum of NBC50 at 223 K

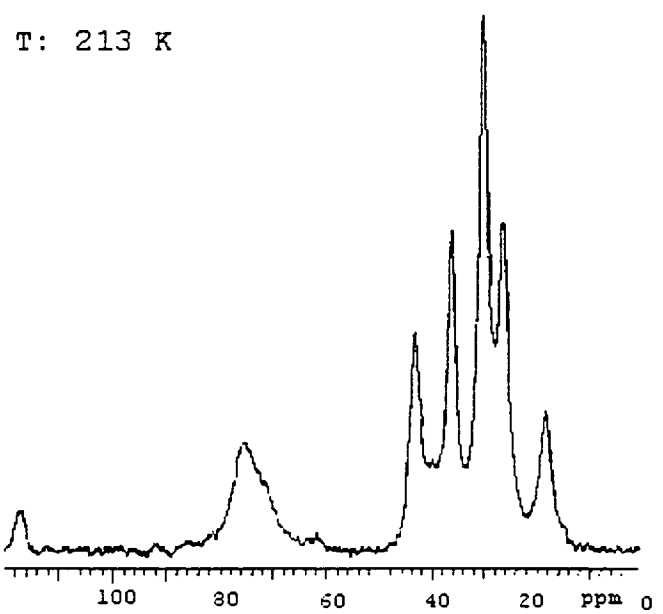

Figure 4.42g Carbon-13 CP/MAS spectrum of NBC50 at 213 K

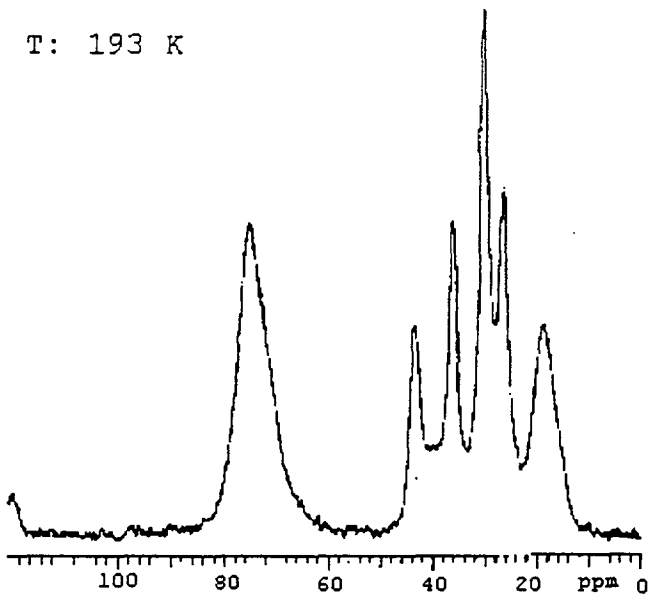

Figure 4.42h Carbon-13 CP/MAS spectrum of NBC50 at 193 K

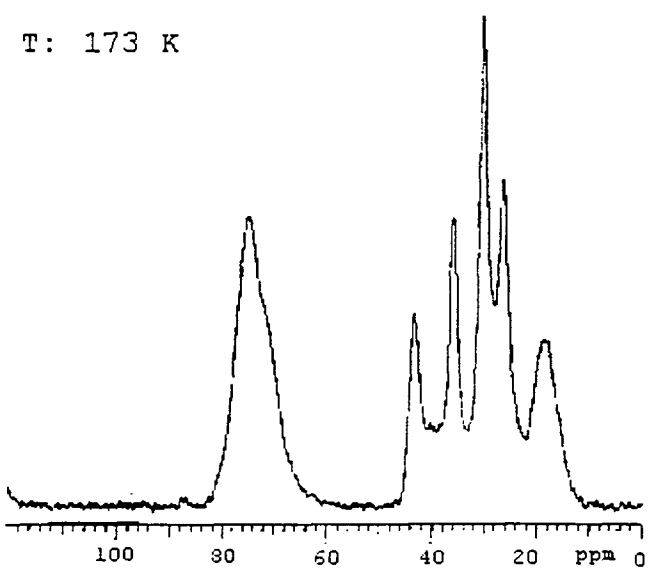

Figure 4.42i Carbon-13 CP/MAS spectrum of NBC50 at 173 K

The next fastest relaxation component may be associated with the rate of establishment of a diffusion profile. The slowest relaxation component may be associated with the rate of relaxation of the magnetisation followed by the establishment of a steady state diffusion profile across the entire sample. Since, by this stage in the relaxation process, only a very small amount of magnetisation remains in the faster relaxing region, it is reasonable to associate the slowest relaxation time to the slower relaxing region. The rotating-frame relaxation time of the prepolymer is reasonable long, hence its relaxation rate is small, contributing only a little to the weighted-average relaxation rate in figure 4.43. The observed $T_{1\rho}^{H}$-minimum at 250.1 K therefore is most likely not the reason of the signal loss in the C-13 CP/MAS high-resolution spectra. Additionally one has to bear in mind, providing the intrinsic $T_{1\rho}^{H}$ of the polyether would have such a minimum that the prepolymer resonances completely disappears, then one would also expect that the magnetisation in the polyamide region diffuses to the polyether region resulting in smaller intensities of the polyamide resonances.

Another point is that the temperature of the $T_{1\rho}^{H}$-minimum obtained from the WRAC instrument does not match with the signal minimum obtained by the high-resolution measurement. However, it has to be borne in mind that the rotating-frame relaxation times obtained by the WRAC-spectrometer were measured at a spin-lock field of 40 kHz while the VXR300-spectrometer has a spin-lock field of 60 kHz. $T_{1\rho}^{H}$ depends on the dipolar interaction and is

therefore B_1-dependent. The rotating-frame relaxation can be described by a similar function to the spin-lattice relaxation in equation 2.27. The relaxation rate has the following relation (4.17) to the correlation time τ_c (see also eqn. 4.16):

$$\frac{1}{T_{1\rho}} \propto \frac{\tau_c}{1 + \omega_1^2 \tau_c^2} \qquad (4.17)$$

This proportionality predicts a relaxation rate maximum i.e. a relaxation time minimum. The $T_{1\rho}$ minimum occurs when $d\,T_{1\rho}/d\tau_c = 0$. This means when $\tau_c = \omega_1^{-1}$. The correlation time is a function of temperature and defined as the time which a molecule needs to rotate through one radian. A qualitative consideration would lead one to expect the $T_{1\rho}$ minimum at 60 kHz spin-lock field to occur at higher temperature in comparison to a 40 kHz spin-lock field because τ_c at the minimum relaxation time is smaller at

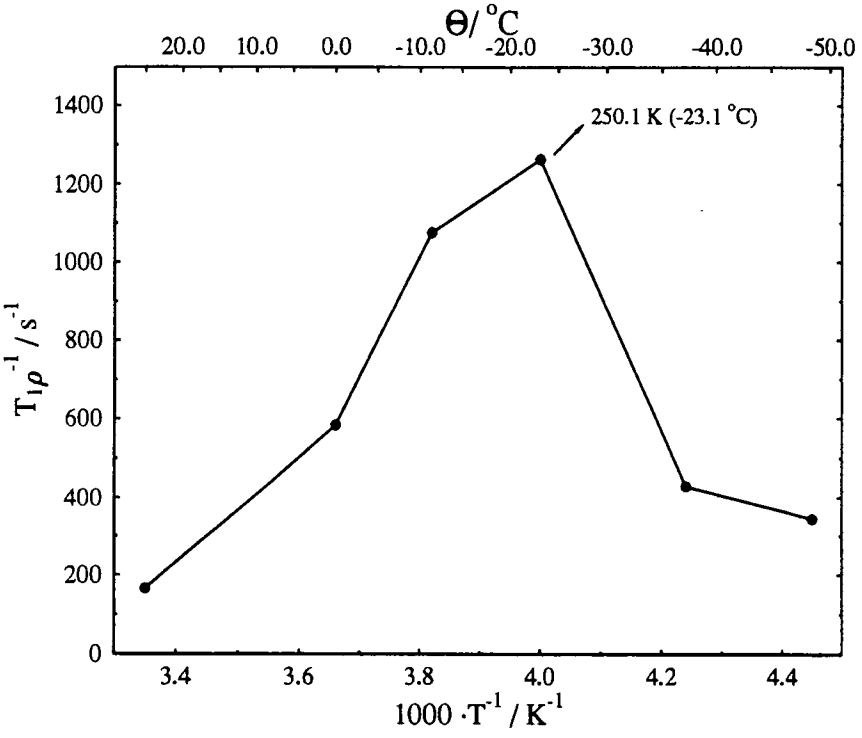

Figure 4.43 Temperature dependence of the weighted-average rotating-frame proton relaxation rate of nylon-6 + 50% prepolymer
D0: 4 s, pulse duration: 2 μs, echo-delay: 10 μs, 40 points with time spacing 70 μs 40 points with time spacing 0.7 ms, 40 points with time spacing 3 ms
The line has no significance other than joining the points

larger spin-lock frequency. This is just the opposite drift as found in the experiment, leaving the attempt to make a $T_{1\rho}$ minimum responsible for the signal loss in the CP/MAS high-resolution CP/MAS spectrum at 223 K doubtful.

Additional parameters can be responsible for the loss of the polyether resonances at 223 K. The contact time has been changed to check its influence. Contact times of 0.2 ms and 1.5 ms have been chosen and the spectra were acquired at 223 K, with otherwise the same parameters as used in the variable temperature experiment. The results are shown in figure 4.44. The spectrum using 0.2 ms contact-time reveals a significant signal on the polyether site, while with 1.5 ms contact time hardly any of the polyether resonances are visible. Although this experiment does not prove the effect of the cross-polarisation time quantitatively, it gives a qualitative impression of its temperature dependence. Theoretically two reasons are possible for the fact that a short contact time is preferable to a longer one. Firstly, the $T_{1\rho}^{H}$ time is in the range of the cross-polarisation time constant, i.e. for longer contact times most of the magnetisation has already relaxed to the lattice. Secondly, the cross-polarisation time constant exhibits a temperature dependence. However, in the case here, the cross-polarisation time constant cannot be made responsible for the observed behaviour. For a given contact time and a temperature independent $T_{1\rho}^{H}$, the cross-polarisation time constant must have a maximum at 223 K. It has to be long compared to the 3 ms contact time so that no significant magnetisation transfer could have

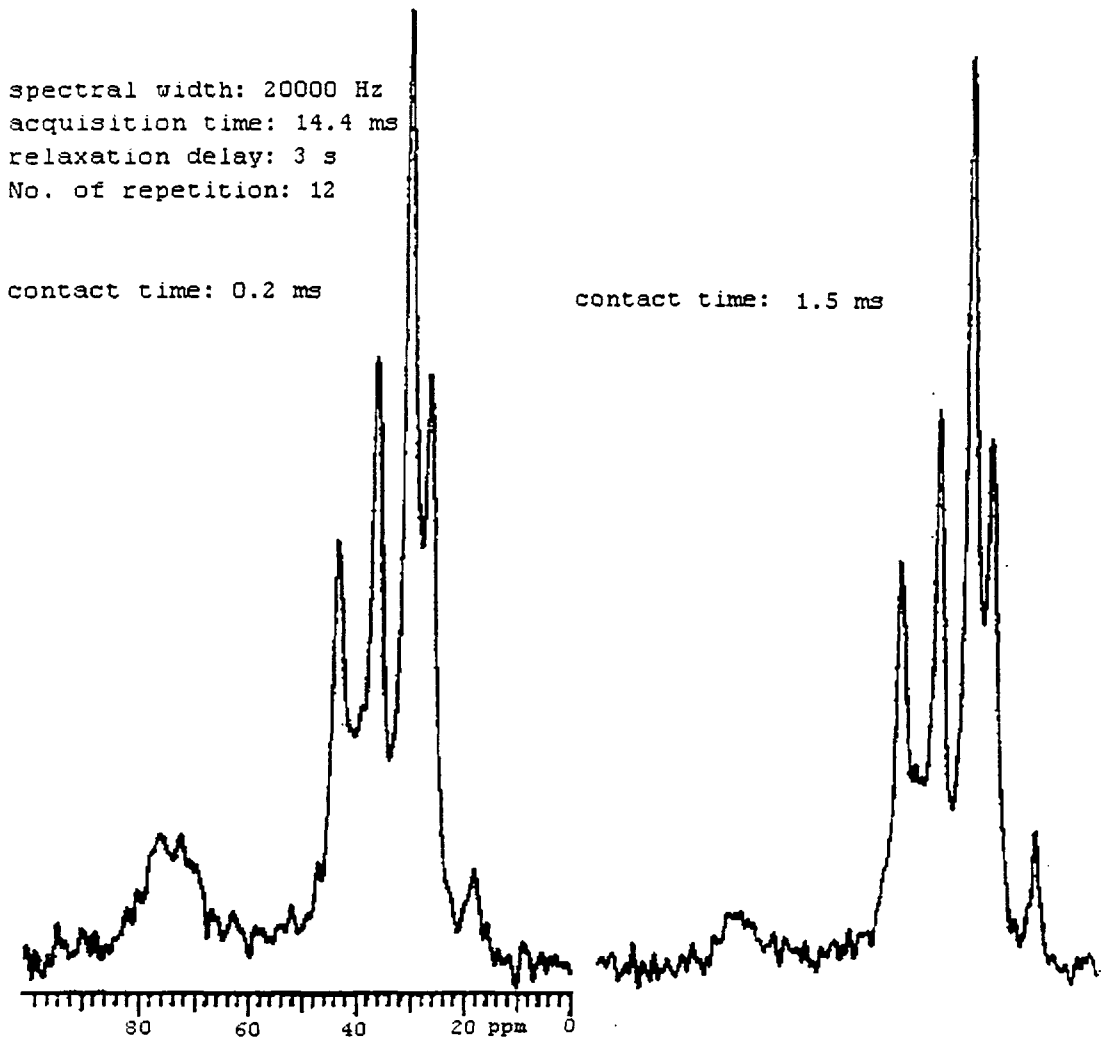

Figure 4.44: C-13 CP/MAS spectrum at 75.4 MHz and 223 K for NBC50 at two different contact times

taken place. However, the result above shows that this is not the case. This indicates that $T_{1\rho}^{H}$ has a minimum at that temperature. Figure 4.44 exhibits a polyether signal, which is possibly only the consequence of the short contact times used, i.e. within 0.2 ms contact-time, the cross relaxation is more efficient than the rotating-frame relaxation. However, it cannot be excluded that the cross-polarisation time is changing with temperature. A quantitative measurement of the cross-relaxation time could not be carried out for experimental reasons (time

consuming and therefore the possibility of icing the probe). The discussion showed that the diminishing signal of the polyether at 223 K could not be explained for sure but is more likely due to a $T_{1\rho}$-minimum.

Now the question arises what mechanism is causing the line-broadening of the spectra when the temperature is reduced. In principle there are two different kinds of mechanism which could cause line-broadening in solid-state spectroscopy:

1. a relaxation mechanism, i.e. motional modulation of the dipolar carbon-proton coupling [56], motional modulation of the shielding anisotropy [57].
2. a static mechanism, i.e. bulk susceptibility of the sample, "freezing in" chemical shift dispersions due to packing effects, bond distortions, conformational inequivalence

The first mechanism is more important. For carbons having shielding anisotropy the motional modulation induces a line broadening denoted $(\pi T_{2\sigma})^{-1}$, that is a maximum when the rate of molecular motion is equal to the sample spinning frequency. The main cause of motional line broadening is found when a carbon has strong carbon-proton coupling under suitable conditions of decoupling. This mechanism gives maximum line broadening, $1/\pi T_{2m}$, when the rate of molecular motion is equal to proton decoupling radio-frequency field strength expressed in angular frequency units, because the suppression of dipolar coupling becomes inefficient.

The second one is expected to induce only a very small effect, $(\pi T_{2res})^{-1}$, generally on the order of 2-6 ppm.

However, the overall line-broadening is the sum over all mechanisms and may be written as:

$$\frac{1}{\pi T_2} = \frac{1}{\pi T_{2m}} + \frac{1}{\pi T_{2\sigma}} + \frac{1}{\pi T_{2res}} \qquad (4.18)$$

$1/\pi T_2$ is the observed full linewidth at half-height. It is difficult to prove the influence of the static mechanism in a polymer system like this, because of the range of possibilities which could cause line-broadening. The relaxation mechanisms are easier to determine. Different conformations in solids can result in differing isotropic chemical shifts for a given carbon position. At higher temperatures or in liquids, this kind of inequivalence resulting from frozen conformations is not often seen in the motionally averaged NMR spectra. From 213 K (figure 4.42g) the linewidth of the methyl-carbon resonance begins to broaden dramatically. The full linewidth at half-height increases from 245 Hz at 213 K to 425 Hz at 173 K figure 4.42i), with basically no difference between 193 K and 173 K. This line-broadening mechanism is not believed to be due to chemical shift dispersion alone but is also caused by motional modulation of the dipolar CH-coupling. Molecular motion must be at the frequency, ω_{1H}, corresponding to the decoupling field strength, B_{1H}, where $\omega_{1H} = 2\pi\nu_{1H} = \gamma_H B_{1H}$ which equals $\gamma_C B_{1C}$ under the Hartmann-Hahn condition. $T_{1\rho}^C$ relaxation results from the modulation of internuclear dipolar interactions at the precession rate round B_1 and thus relates to the same motions which cause the motional ^{13}C line broadening. It is maximum when the rate of molecular motion is equal to the carbon spin-locking field strength ω_{1C} expressed in angular frequency

units. Under the Hartmann-Hahn matching condition $T_{1\rho}^{C}$ is equal to T_2^C [58]. A $T_{1\rho}^{C}$-minimum would consequently result in a maximum line-broadening. A direct proof that the line-broadening at temperatures less than 213 K is caused by dipolar modulation would be a $T_{1\rho}^{C}$-minimum at that temperature. $T_{1\rho}^{C}$ has not been measured at variable temperature, because of the prohibitively time consuming reason. Another proof whether motions in the mid-kilohertz are present, which may interfere with the dipolar decoupling frequency and thus re-introduce line-broadening is to investigate the C-13 CP/MAS spectrum as a function of the decoupling power.

A simple experiment which changes the decoupler power (frequency) has been carried out. Starting from 60 kHz, using a contact time of 0.2 ms and a temperature of 223 K, the decoupling frequency has been changed to a lower value. It is expressed in decoupling units, where 60 kHz is equivalent to 21 units. Figures 4.45a to 4.45d illustrate the effect of changing the decoupling field. The spectra show no significant effect. For the very low decoupling frequency (15 decoupling units, figure 4.45d), the nylon-6 resonances start to broaden, because the decoupling field is not strong enough for sufficient decoupling of the carbons from the protons.

Finally the interplay of motion and MAS-rates has been studied. The results are depicted in figures 4.46a and 4.46b, where the spinning speed of the rotor was varied from 3100 Hz to 1700 Hz. The two spectra do not indicate any substantial difference in line-broadening (seen via the methyl carbon of PPO). These two experiments show that

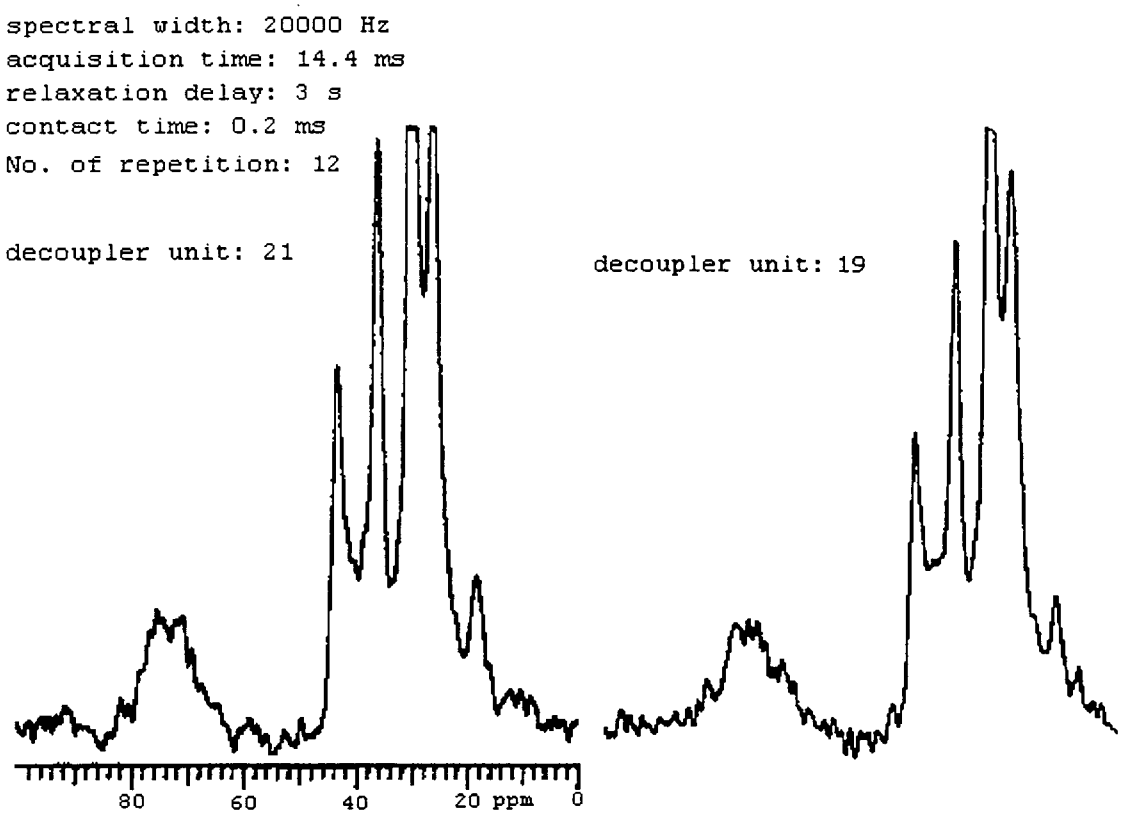

Figure 4.45 a+b: C-13 CP/MAS spectrum at 75.4 MHz of NBC50 at two different decoupling frequencies

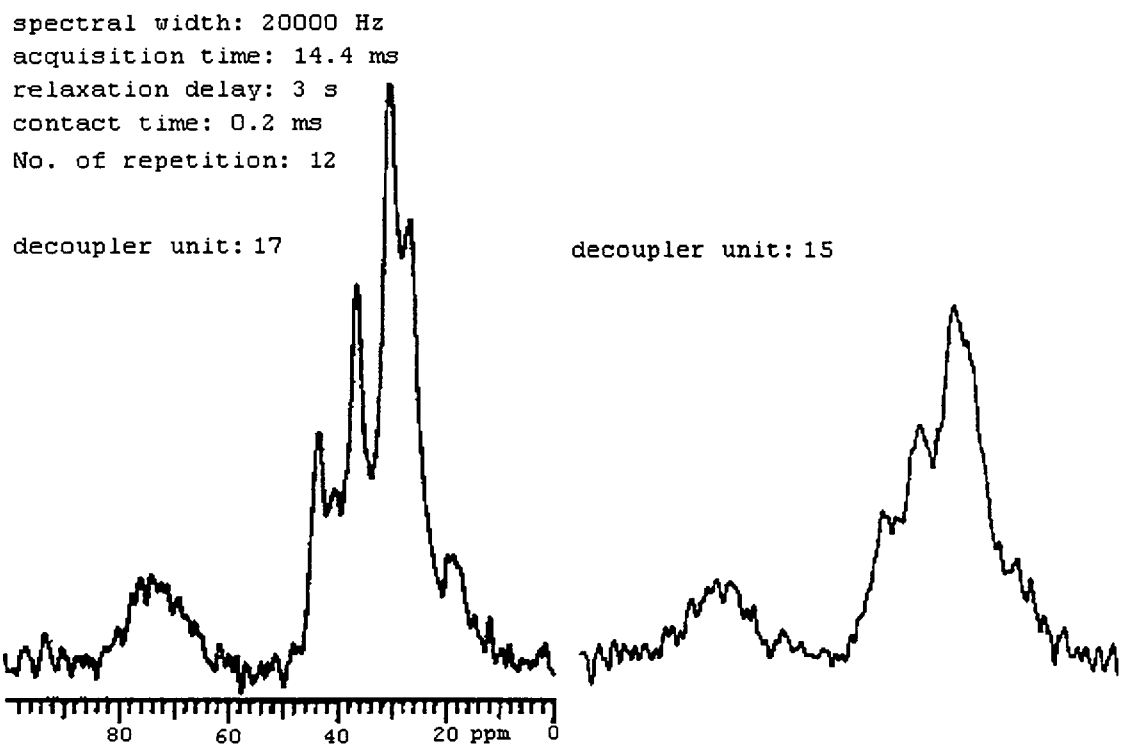

Figure 4.45 c+d: C-13 CP/MAS spectrum at 75.4 MHz of NBC50 at two different decoupling frequencies

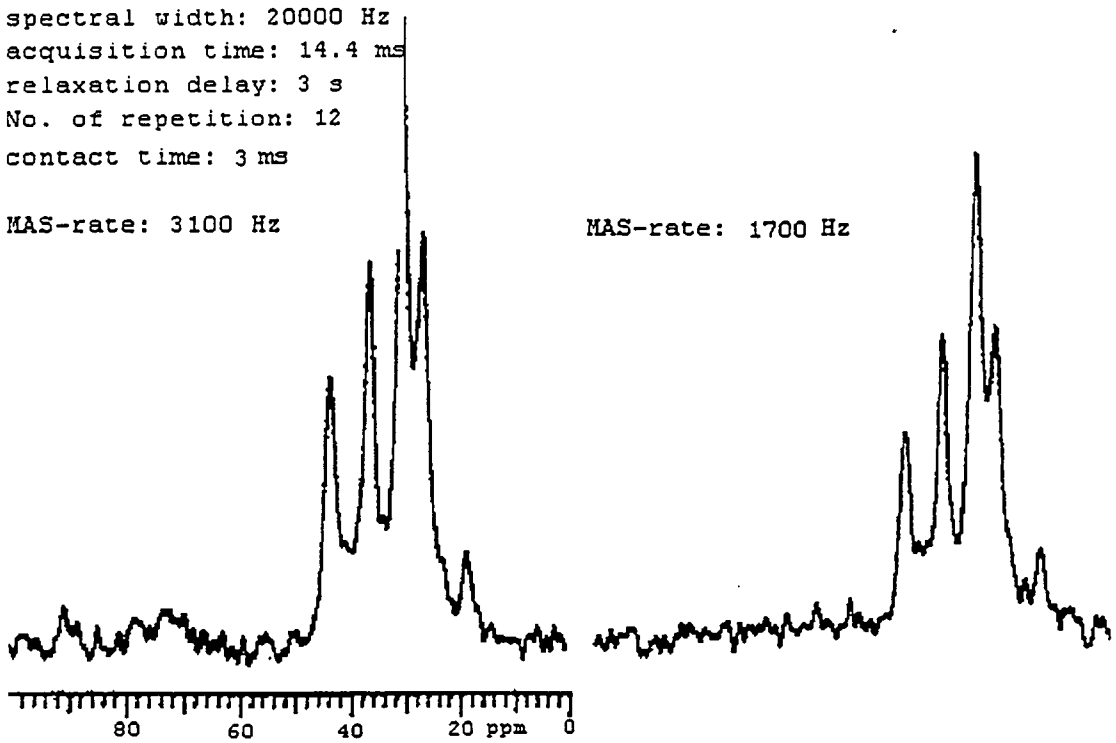

Figure 4.46: C-13 CP/MAS spectrum at 75.4 MHz of NBC50 at two different MAS-rates

the line-broadening is presumably not caused by motions in the kilohertz- and mid-kilohertz region.

The last point which needs to be considered is the glass transition temperature, T_g. For the polyether in NBC50 this has been determined to be -50 °C (see figure 5.4 in chapter 5). It is believed that there is a direct connection between the line-broadening in the C-13 CP/MAS spectrum and the T_g of the polyether. Below the glass transition temperature, the very mobile amorphous polyether becomes immobile. All possible conformations of the polymer chain are now "frozen in" and no substantial motional averaging occurs. Hence, these different conformations with their various magnetic shieldings cause

the broadening in the high-resolution C-13 CP/MAS spectrum.

The T_g may also account for the $T_{1\rho}^H$ minimum at 250 K. Spiess [59] showed that the T_g obtained from mechanical relaxation measurement is different from that determined by NMR. $T_{1\rho}^H$ is influenced by rapid fluctuations of the C-H bond directions around the mean orientation. Therefore their correlation times, τ_c, are smaller than the ones which are due to chain motions. Consequently the T_g measured by spin-lattice relaxation is at a substantially higher temperature compared to the one determined by mechanical measurements. However, this does not explain the diminishing resonances at 223 K in the C-13 CP/MAS spectrum.

The discussion shows that the main cause of the line-broadening of the polyether resonances below 223 K arises from the passage through the relevant T_g. It has been shown that there is probably no re-introduction of line broadening caused by interference of dipolar coupling and motion or shielding anisotropy and motion.

References to Chapter 4

[1] F.C. Schilling, A.E. Tonelli, Macromolecules 19 (1986) 1337

[2] H. Arimoto, M. Ishibashi, M. Hirai, Y. Chantani, J. Polym. Sci., A3 (1965) 317

[3] D.R. Holmes, C.W. Bunn, D.J. Smith, J. Polym. Sci., 17 (1955) 159

[4] G.R. Hatfield, J.H. Glans, W.B. Hammond, Macromolecules, 23 (1990) 1654

[5] T.L. Weeding, W.S. Veeman, Macromolecules, 21 (1988) 2028

[6] T.L. Weeding, W.S. Veeman, Macromolecules, 22 (1989) 706

[7] N.S. Murthy, M. Stamm, J.P. Sibilia, S. Krimm, Macromolecules, 22 (1989) 1261

[8] A. Okada, M. Kawasumi, I. Tajima, T. Kurauchi, O. Kamigaito, J. Appl. Polym. Sci. 37 (1989) 1369

[9] K. Kubo, T. Yamanobe, T. Komoto, I. Ando, J. Polym. Sci, Polym. Phys. Ed., 27 (1989) 929.

[10] A.E. Tonelli, F.C. Schilling, Acc. Chem. Res., 14 (1981) 233

[11] D.G. Powell, L.J. Mathias, J. Am. Chem. Soc., 112 (1990) 669

[12] C.A. Fyfe, *Solid State NMR for Chemists*, C.F.C. Press, Ontario (1983)

[13] F.M. Lurie, C.P. Slichter, Phys. Rev., **133A** (1964) 1108

[14] M. Mehring, *Principles in High-Resolution NMR in Solids*, Springer Verlag, Berlin (1983)

[15] D.A. McArthur, E.L. Hahn, R.E. Walstedt, Phys. Rev., **188** (1969) 609

[16] L. Müller, A. Kumar, R.R. Ernst, Phys. Rev. Lett., **32** (1974) 1902

[17] A. Abragam, *The Principles of Nuclear Magnetism*, Clarenden Press: Oxford (1961)

[18] A. Abragam, W.G. Proctor, Phys. Rev., **109** (1958) 1441

[19] A.G. Redfield, Phys. Rev., **98** (1955) 1787

[20] M. Goldman, "*Spin Temperature and Nuclear Magn. Res. in Solids*", London: Oxford Univ. Press 1970

[21] S.R. Hartmann and E.L. Hahn, Phys. Rev., **128** (1962) 2042

[22] L.B. Alemany, D.M. Grant, T.D. Alger, R.J. Pugmire, J. Am. Chem. Soc., **105** (1983) 6697

[23] X. Wu, Z. Shanmin, X. Wu, Phys. Rev., **37B** (1988) 9827

[24] D.A. McArthur, E.L. Hahn, R.E. Walstedt, Phys. Rev., **188** (1969) 609

[25] J.H. Van Vleck, Phys. Rev., **74** (1948) 1168

[26] X. Wu, S. Zhang, Chem. Phys. Lett., **156** (1989) 79

[27] X. Wu, X. Xie, X. Wu, Chem. Phys. Lett., **162** (1989) 325

[28] P. Résibois, M. DeLenner, Phys. Rev., **167** (1966) 305

[29] M. DeLenner, P. Résibois, Phys. Rev., **167** (1966) 318

[30] G.F. Reiter, Phys. Rev., **B5** (1972) 222

[31] G.F. Reiter, Phys. Rev., **B7** (1973) 3325

[32] H. Mori, K. Kawasaki, Prog. Theor. Phys., **27** (1962) 529

[33] H.S. Bennet, P.C. Martin, Phys. Rev., **A138** (1965) 608

[34] P. Mansfield, Phys. Rev., **151** (1966) 199

[35] G.W. Parker, Phys. Rev., **B2** (1970) 2453

[36] B.T. Gravely, J.D. Memory, Phys. Rev., **B3** (1971) 3426

[37] G.W. Parker, F. Lado, Phys. Rev., **B8** (1973) 3081

[38] G.W. Parker, F. Lado, Phys. Rev., **B9** (1974) 22

[39] D.E. Demco, J. Tegenfeldt, J.S. Waugh, Phys. Rev., **B11** (1975) 4133

[40] P. Palmas, P. Tekely, D. Canet, J. Magn. Reson., **104** (1993) 26

[41] X. Wu, K.W. Zilm, J. Magn. Reson., **A104** (1993) 154

[42] T.P. Huijgen, H.A. Gaur, T.L. Weeding, L.H. Jenneskens,H.E.C. Schuurs, H.G.B. Huysmans, H.S. Veeman, Macromolecules**23** (1990) 3063.

[43] X. Wu, S. Zhang X. Wu, J. Magn. Reson., **77** (1988) 343

[44] D.G. Cory, W.M. Ritchey, Macromolecules, **22** (1989) 1611

[45] A.A. Parker, J.J. Marcinko, Y.T. Shieh, C. Shields, D.P. Hedrick, W.M. Ritchey, Polym. Bull., **21** (1989) 229

[46] K.M. Hedrick, J.D. Gabbert, "A New RIM System From Nylon 6 Block Copolymers Chemistry" AIChE **14** (1981) 1

[47] I. Ando, T. Yamanobe, S. Akiyama, T. Komoto, Solid State Communications, **62** (1987) 785

[48] I. Ando, T. Yamanobe, S. Akiyama, T. Komoto, H. Sato, T. Fujito, K. Degushi, M. Imanari, Macromolecules, **62** (1987) 785

[49] P.M. Henrichs, M. Linder, J.M. Hewitt, D. Massa, H.V. Isaacson, Macromolecules, **17** (1984) 2412

[50] L.H. Jelinski, F.C. Schilling, F.A. Bovey, Marcomolecules, **14** (1981) 581

[51] V.J. McBrierty, D.C. Douglass, T.K. Kwei, Macromolecules, **11** (1978) 1265

[52] S. Ni, L. Shen, F. Yu, B. Qian, Polym. Comm., **27** (1984) 318

[53] R.D. De la Batie, F. Laupretre, L. Monnerie, Macromolecules, **21** (1988) 2052

[54] K.-H. Illers, H. Haberkorn, Makromol. Chem., **142** (1971) 31

[55] A.M. Kenwright, K.J. Packer, B.J. Say, J. Magn. Reson., **69** (1986) 426

[56] W.P. Rothwell, J.S. Waugh, J.Chem. Phys., **74** (1981) 2721

[57] D. Suwelack, W.P. Rothwell, J.S. Waugh, J.Chem. Phys., **73** (1980) 2559

[58] D.L. VanderHart, W.E. Earl, A.N. Garroway, J. Magn. Reson., **44** (1981) 361

[59] H.W. Spiess, Ann. Rev. Mater. Sci., **21** (1991) 131

Chapter 5

5 Morphological Investigations of NYRIM 2000

5.1 Dynamic Mechanical Thermal Analysis (DMTA)

5.1.1 Introduction

Dynamic mechanical thermal analysis has proved to be a sensitive technique to investigate slow motions in macroscopic materials, typically of 1 Hz [1]. Therefore it is predestined to detect transitions such as the glass-rubber transition in amorphous or semicrystalline polymers. The glass-transition emphasises the onset of the associated molecular motions. In fact, upon polymer synthesis, the glass-transition temperature is among the first parameters measured and is perhaps the most important single parameter which one needs to know before one can decide on the applications of the non-crystalline polymers.

5.1.2 Theory

In DTMA a small sinusoidial stress is imparted to the sample in the form of a torque, push-pull, or a flexing mode, of angular frequency ω. If the polymer is treated as a classical damped harmonic oscillator, both the elastic modulus and the damping constant can be obtained. If a sinusoidal strain is applied to a viscoelastic material, the resulting stress will also be sinusoidal, but will be out of phase when there is energy dissipation or damping

in the polymer. The resulting strain can be described in terms of its angular frequency ω and the maximum amplitude ε_0 using complex notation, by

$$\varepsilon^* = \varepsilon_0 \exp(i\omega t) \tag{5.1}$$

where $\omega = 2\pi\nu$, the frequency is ν and $i = -1^{1/2}$. The relation between the alternating stress and strain is written as

$$\sigma^* = \varepsilon^* E^*(\omega) \tag{5.2}$$

where $E^*(\omega)$ is the frequency-dependent complex dynamic modulus defined by

$$E^*(\omega) = E'(\omega) + iE''(\omega) \tag{5.3}$$

Expression 5.3 shows that $E^*(\omega)$ is composed of two frequency-dependant components. $E'(\omega)$ is the real part in phase with the strain called the storage modulus, and $E''(\omega)$ is the loss modulus defined as the ratio of the components out of phase with the strain amplitude. Hence $E'(\omega)$ measures the amount of stored energy and $E''(\omega)$, sometimes called the imaginary part, is actually a real quantity measuring the amount of energy dissipated by the material. Figure 5.1 illustrates the parameter discussed for the Maxwell model. The damping of the system or the energy loss per cycle can be measured from the loss tangent $\tan\delta$. This is a measure of the internal friction and is related to the complex moduli by

$$\tan\delta = (\omega\tau)^{-1} = E''(\omega) / E'(\omega) \tag{5.4}$$

Below the glass transition temperature, T_g, of the material, the amorphous polymer-chain conformations are frozen into a rigid network, yielding a high value for the elastic modulus, E', and a low value for the loss tangent, $\tan\delta$. The onset of molecular motion in a polymer sample

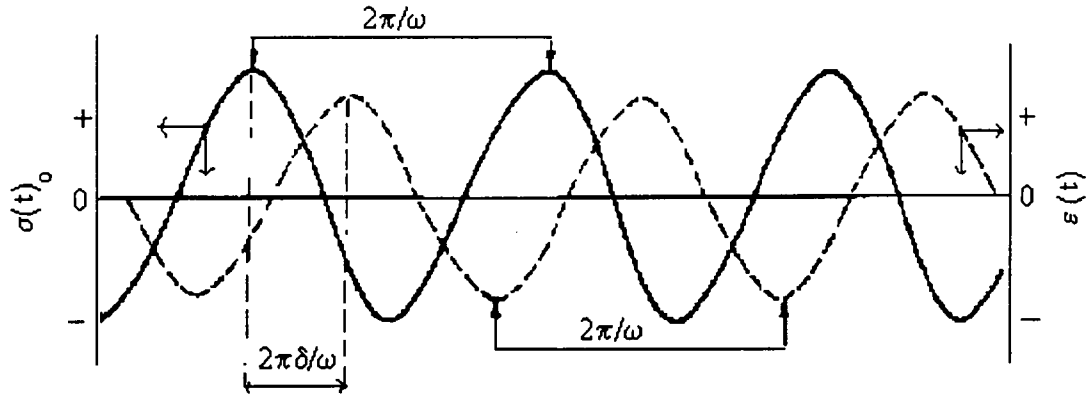

Figure 5.1 Harmonic oscillation of a Maxwell model with the solid line representing the stress and the broken line the strain curve

is reflected in the behaviour of the complex moduli. It has been shown that the variation of $E'(\omega)$ and $E''(\omega)$ has a maximum at the loss angle where $\omega = 1/\tau$. This usually represents a transition point such as T_g, T_m or some other region where significant molecular motion occurs in the polymer sample

5.1.3 Experimental

The temperature-dependent viscoelastic properties of the NBC-system were studied using a PL Thermal Sciences Dynamic Mechanical Thermal Analyser. The DMTA measurements were carried out by Dr. S.W.-Tsui at the University of Bradford. Samples were prepared approximately 8 mm wide, 30 mm long and 3 mm thick. The sample testing was carried out by using the dual-cantilever bending mode. The operating temperature range was from over -90°C to 100 °C with a heating rate of 2 $^{\circ}C\,min^{-1}$, and operating frequency of 1 Hz. The storage modulus, loss modulus and mechanical damping factor for the sample were recorded into a computer throughout the test.

Two sets of samples have been investigated: Firstly the block copolymers as they were prepared and secondly annealed samples. The latter were heated to 190 °C for 30 minutes in a nitrogen atmosphere, and then quenched in liquid nitrogen. Finally they were annealed at 135 °C for 17 hours in a nitrogen atmosphere. This temperature was adopted because nylon-6 homopolymer exhibits the maximum rate of crystallisation at 135 °C [2,3].

5.1.4 Results and Discussion

The results for the elastic modulus as a function of temperature are summarised in figures 5.2 and 5.3. These data illustrate that there are two transitions in the 10% to 50% materials. The ones at lower temperatures (-58 to -50 °C) are assigned to the T_g's of the polyether soft blocks, whilst the ones with higher temperatures (13 to 32 °C) correspond to the T_g's of the polyamide-6 hard blocks. Two transition temperatures are very common in block copolymers, indicating the incompatibility of the polyamide and polyether components and their two-phase behaviour. The transition of the polyether soft block in the 5 % material is not obvious, probably because of the low concentration of the polyether in the composition. Therefore the 5 % material will not be considered in the following. More interesting are the $\tan\delta$ values as a function of temperature. Figures 5.4 and 5.5 illustrate that the $\tan\delta$ for the soft block is much more pronounced for the 40 % and 50 % materials than for the 10 to 30 % materials. The results are closely similar for the

original and the annealed samples, suggesting that the polyether phase becomes the continuous phase in the systems. The net result would be that less nylon can contribute to the dynamic elastic modulus. This would result in a sharp drop in the modulus as seen in figure 5.2 and 5.3. Another interesting observation is that the glass transition temperatures in the original sample continuously approach each other as the polyether concentration increases, indicating a consecutive mixing of the domains. However, the two clearly-distinct T_g's illustrate that although there is partial domain mixing, the two phases are mainly separated. If we look at the tan δ traces for the annealed samples (fig. 5.5) three main different features can be observed. The T_g's for the soft block are very similar to those of the corresponding original materials, but those for the nylon-6 blocks have broadened and shifted to higher temperatures, showing that there is a change in morphology after annealing. The most interesting feature is that now the T_g's for the 10 and 20 % materials are the same. Although for the annealed materials the same trend of decreasing T_g's is valid as for the original materials, the T_g's of the 40 and 50 % materials only differ by 6 K, whilst the T_g's for the 20 % and 30 % materials differ by 10 K and for the 30 % and 40% materials by 12 K. This result indicates a morphological change between 20 % and 40 % polyether concentration and is indirectly supporting the continuous/disperse phase inversion proposed by Hedrick and Gabbert [4]. The principle of the continuous/disperse phase inversion should be understood to be that in a two-phase system the

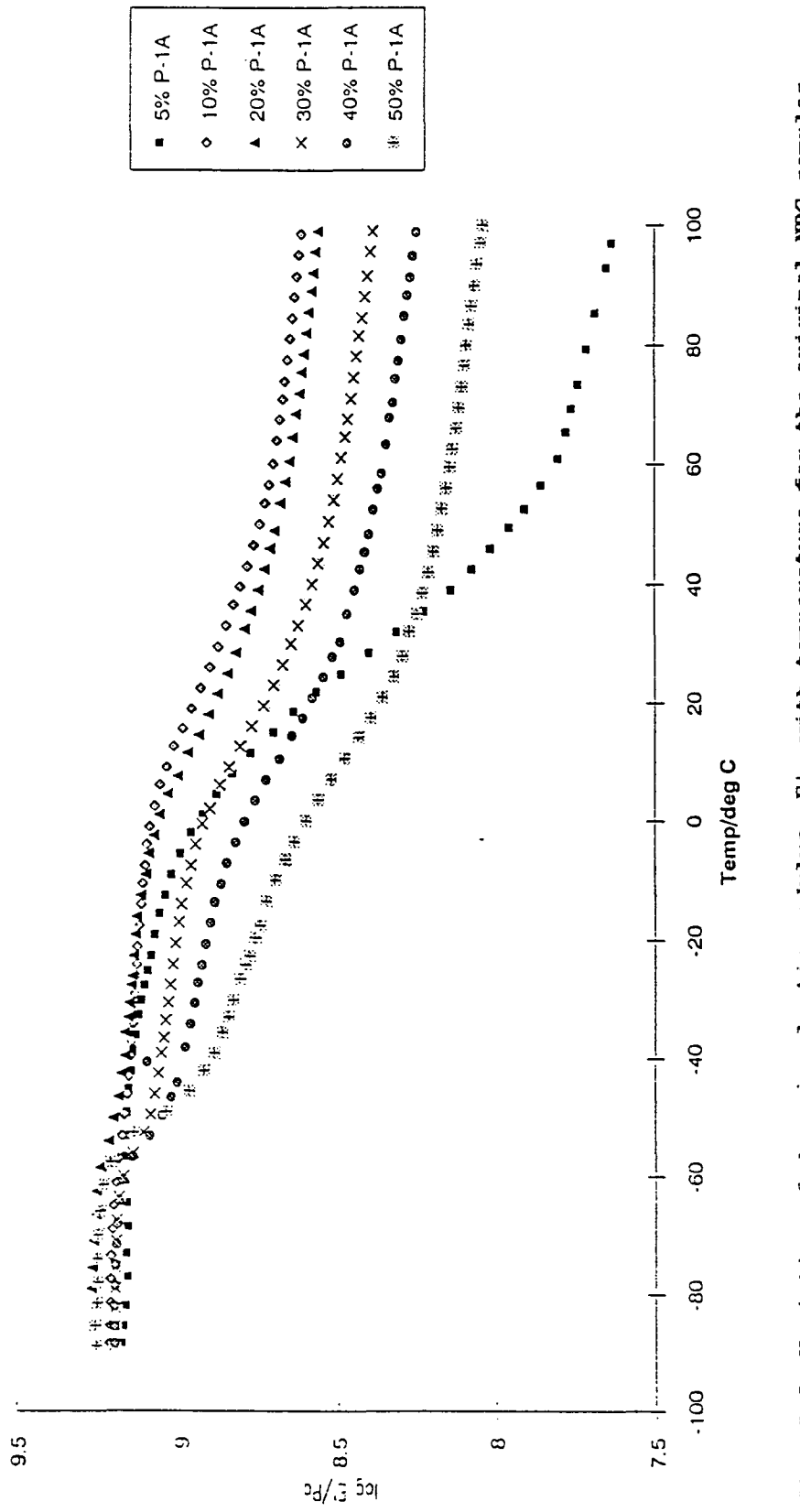

Fig. 5.2 Variation of dynamic elastic modulus, E', with temperature for the original NBC samples

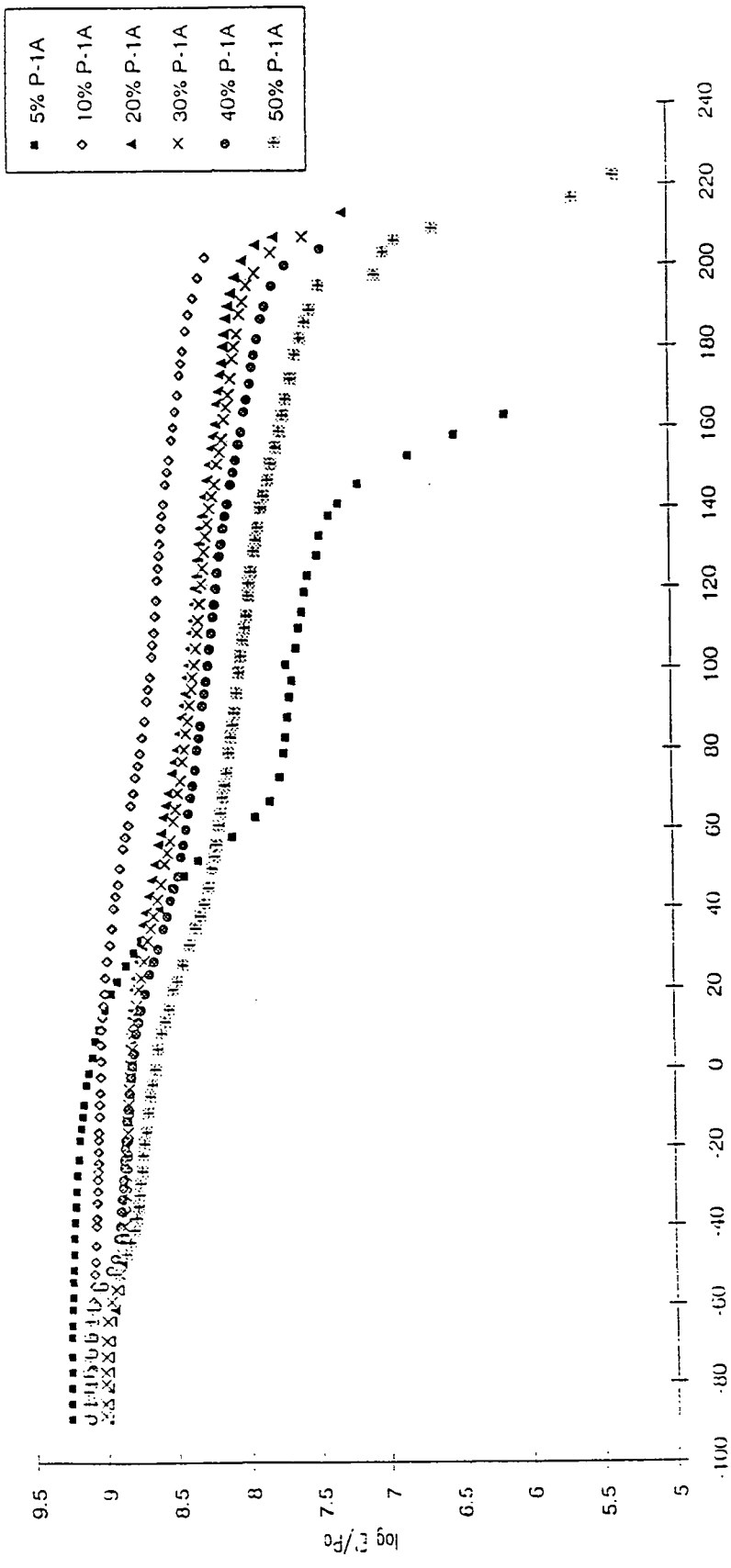

Fig. 5.3 Variation of dynamic elastic modulus, E', with temperature for the annealed HBC samples

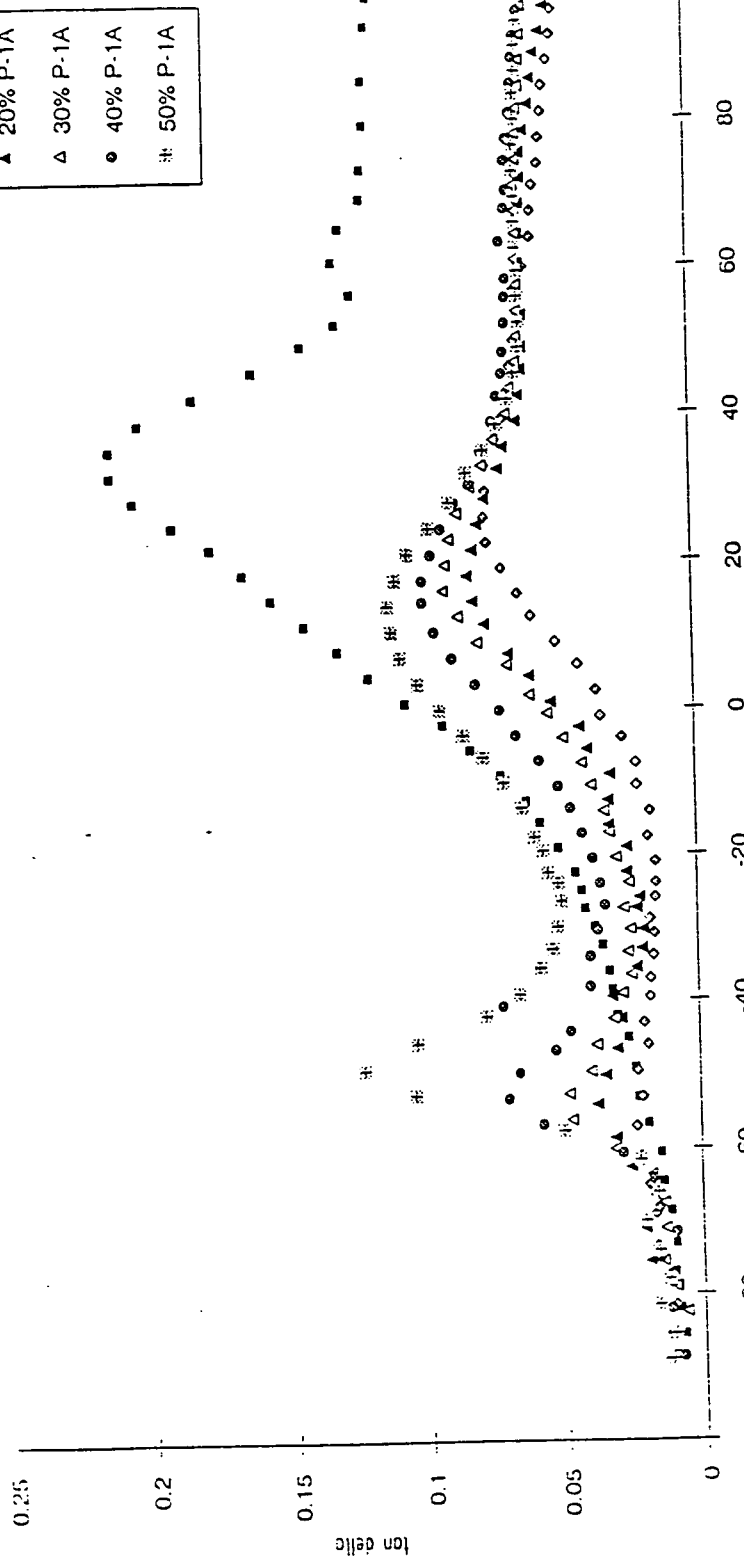

Fig. 5.4 Variation of loss factor, tan δ, with temperature for the original NBC samples

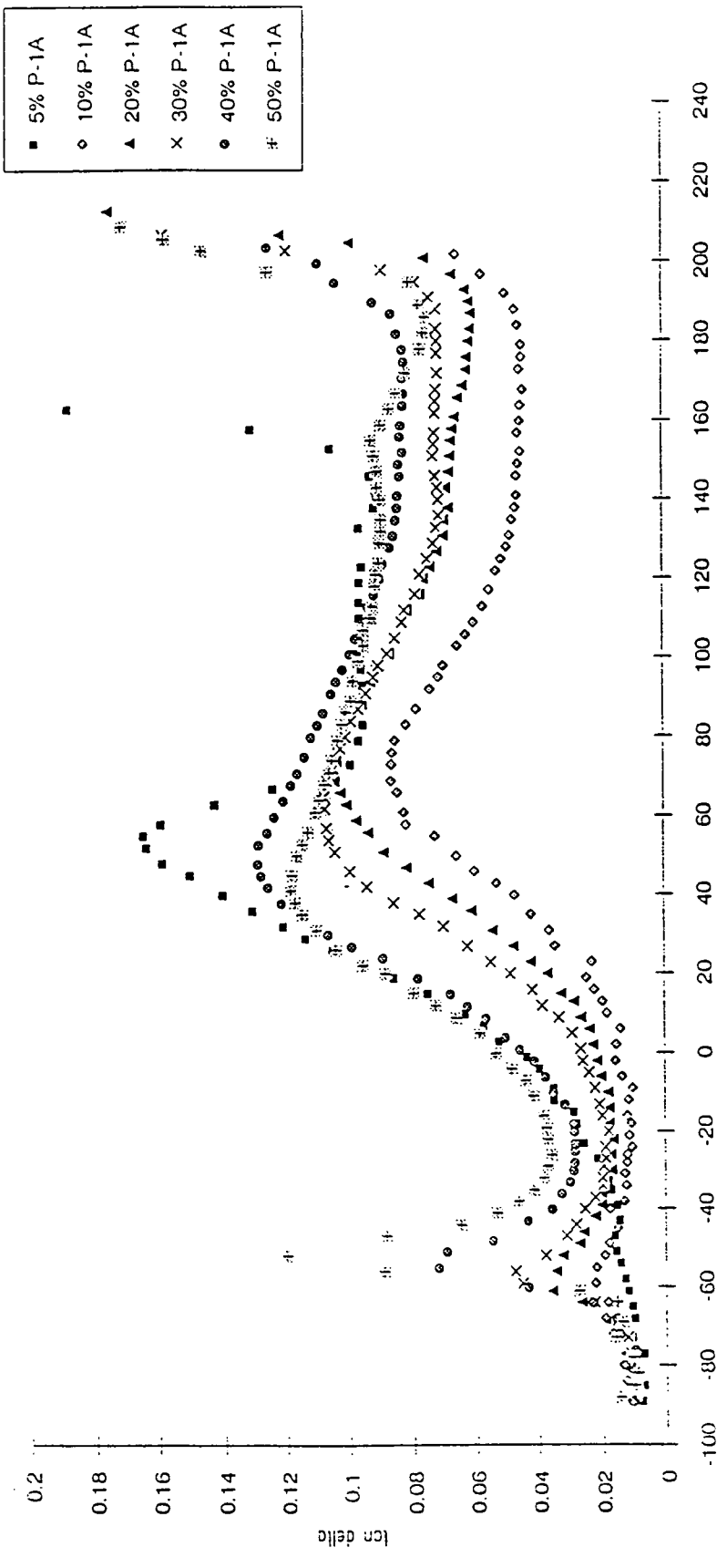

Fig. 5.5 Variation of loss factor, tan δ, with temperature for the annealed MBC samples

component with the higher concentration forms a continuous phase with the other component dispersed in it.
By increasing the concentration of the less concentrated component the situation may invert, so that now this component forms the continuous phase. The concept of the morphological transition will be further investigated by means of Differential Scanning Calorimetry, small-angle X-ray scattering and 1H-spin diffusion measurements.

5.2 Differential Scanning Calorimetry (DSC)

5.2.1 Introduction

Whenever a material reacts chemically, or undergoes a change in physical state such as e.g. melting, heat is either absorbed or evolved. The DSC technique maintains a constant mean heat input during a change. Therefore a servo-system immediately increases the energy input to either sample or reference to maintain both at the same temperature. The thermogram obtained represents the amount of electrical energy supplied to the system, and so the areas under the peaks will be proportional to the change in enthalpy, ΔH, which occurred. An actual reference sample can be dispensed with in practice and an empty sample pan used instead. Calibration of the instrument will allow the heat capacity of a sample to be calculated in a quantitative manner. This information is additional to that gained on crystallisation, melting, glass transitions, and decompositions. The most important parameters which can be obtained from DSC-traces are

illustrated in figure 5.6. One is the glass transition temperature, denoted by ΔC_p. Another is the crystallisation peak, ΔH_c, which illustrates the exothermic process of crystallisation in the system. Finally there is the fusion peak, ΔH_f, which shows the endothermic melting process.

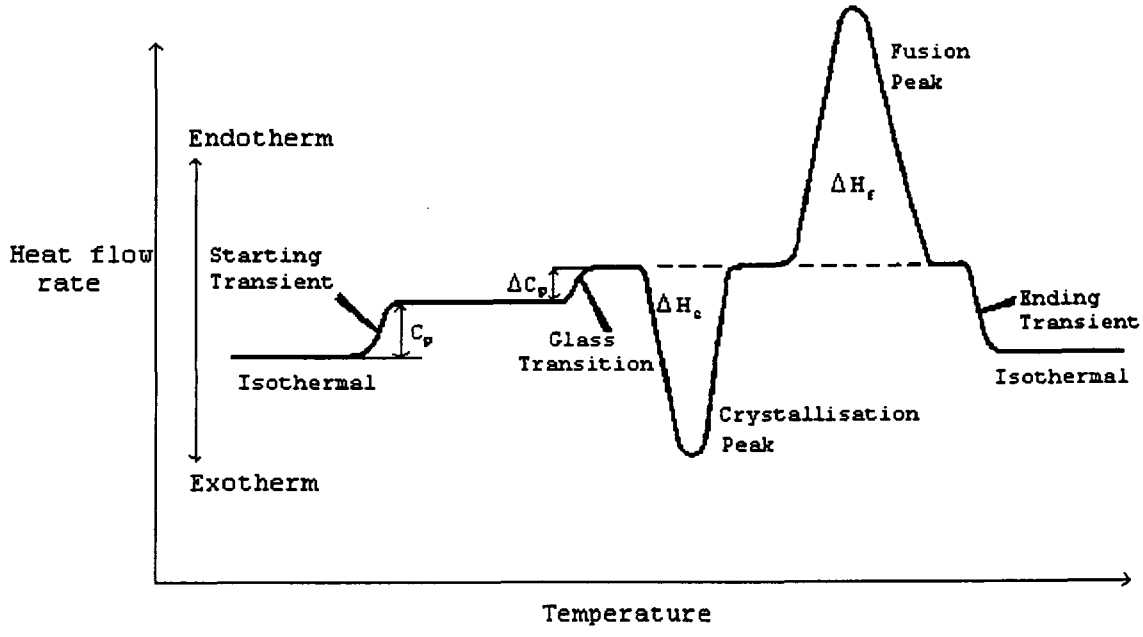

Fig. 5.6 Typical DSC thermogram

5.2.2 Experimental

The morphologies of the NBC samples were examined by means of a Perkin-Elmer DSC-7 differential scanning calorimeter in Bradford. The machine was calibrated using an indium standard. Each sample was cut into small pieces and sealed in a metal foil packet and then weighed. A similar empty packet was used as the reference. These metal foil packets were then heated in the sample and reference pans in the calorimeter respectively, in accordance with the preset heating programme. Power changes due to the change in state of the sample during

heating were recorded into a computer. Each as prepared sample was heated from 0 °C to 237 °C at a rate of 20 $^{\circ}C\,min^{-1}$. The sample was then kept at 237 °C for 5 min before quenching to 0 °C at a nominal rate of 200 $^{\circ}C\,min^{-1}$. The sample was then kept at 0 °C for 5 min. Finally the sample was reheated to 237 °C at a rate of 20 $^{\circ}C\,min^{-1}$. The cooling-reheating processes were eliminated for the annealed samples. They were heated from 0 °C to 237 °C directly.

A second set of DSC measurements was carried out in Durham on a Perkin-Elmer DSC-7 differential scanning calorimeter. The experiments were performed on the same samples which were used for the NMR and SAXS-experiments for better comparison of the results. The samples were dried under vacuum at 70 °C overnight and finally powdered in liquid nitrogen. They were heated from -80 °C to 240 °C at a rate of 10 $^{\circ}C\,min^{-1}$, then cooled down to −80 °C and finally reheated to 240 °C at a rate of 10 $^{\circ}C\,min^{-1}$.

5.2.3 Results and Discussion

When analysing a thermoplastic polymer by DSC, the thermal history effect makes it extremely difficult to come to any definite conclusion about the material from a single thermogram. This becomes even more difficult when comparing different materials. When a polymer-melt is allowed to cool slowly, the polymer chains may have enough time to orientate themselves and form crystals. However, in reality, they almost always build partial amorphous domains. The ratio of amorphous and crystalline domains

depends on the cooling conditions, i.e. the thermal history of the polymer. In this section of the thesis the crystallinities of the various NYRIM compositions have been measured by DSC. The results of the two experiments with an applied artificial thermal history are compared with the DSC-results obtained in Durham, which had conditions closer to the ones in the NMR and SAXS-experiments. A value of ΔH_{f0} = 167.2 Jg^{-1} [5] has been used as a reference for 100 % nylon-6 crystallinity. The results are summarised in tables 5.1a-c and illustrated in figures 5.7 to 5.11 for the NMR/SAXS samples, for the as prepared samples (fig. 5.12) and for the annealed samples (fig. 5.13). It can be seen that the melting points of the block copolymers are all in the range of about 207 to 218 °C. The large exothermic peaks seen in figure 5.12 for the 30%, 40% and 50% materials at temperatures of about 69 to 86 °C are due to cold-crystallisation of the nylon-6. These peaks are not observable for lower polyether concentrations. The absence of these peaks suggests high rates of crystallisation from the melt for the hard blocks. The annealed samples do not show any exothermic peaks in their thermograms, as seen in figure 5.13, demonstrating that the crystallisation has been completed by annealing. The DSC thermograms (figures 5.7 to 5.11) obtained in Durham also do not reveal any exothermic peak, indicating that crystallisation is in an advanced state by leaving the polymers under vacuum at 70 °C. The crystallinities of the samples are higher than the ones with the heating-cooling and reheating procedure, but less than the crystallinity of the annealed samples. Note that

the extent of crystallinity related to nylon-6 is increasing from 10% to 25% polyether concentration.

prepolymer / %	ΔH_f / Jg^{-1}	crystal. total / %	crystal. nylon / %
0	66.03	39.5	39.5
10	63.34	37.9	42.1
25	60.45	36.2	48.3
30	38.70	23.1	33.0
40	36.17	21.6	36.0

Table 5.1a Heat of fusion for various compositions of NYRIM from DSC measurements of the NMR/SAXS samples dried at 70 °C

prepolymer / %	ΔH_f / Jg^{-1}	ΔH_c / Jg^{-1}	crystal. total / %	crystal. nylon / %
10	50.56	0	30.2	33.6
20	52.32	0	31.3	39.0
30	46.93	-19.24	16.6	23.7
40	33.40	-14.99	11.0	18.3
50	34.63	-14.4	12.1	24.2

Table 5.1b Heat of fusion for various compositions of NYRIM from DSC measurements for the as prepared samples with preset heating procedure

prepolymer / %	ΔH_f / Jg^{-1}	crystal. total / %	crystal. nylon / %
10	80.38	48.1	53.4
20	69.77	41.7	52.1
30	60.20	36.0	51.4
40	48.13	28.8	48.0
50	32.47	19.4	38.8

Table 5.1c Heat of fusion for various compositions of NYRIM from DSC measurements of the annealed samples

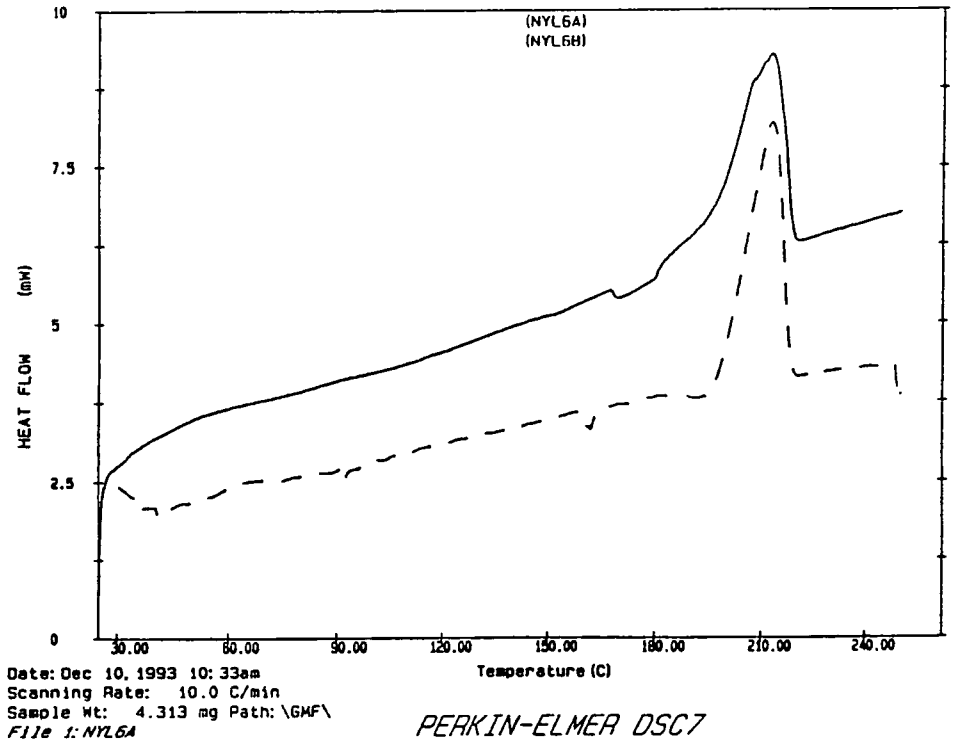

Fig. 5.7 DSC results for nylon-6 (NMR/SAXS samples)

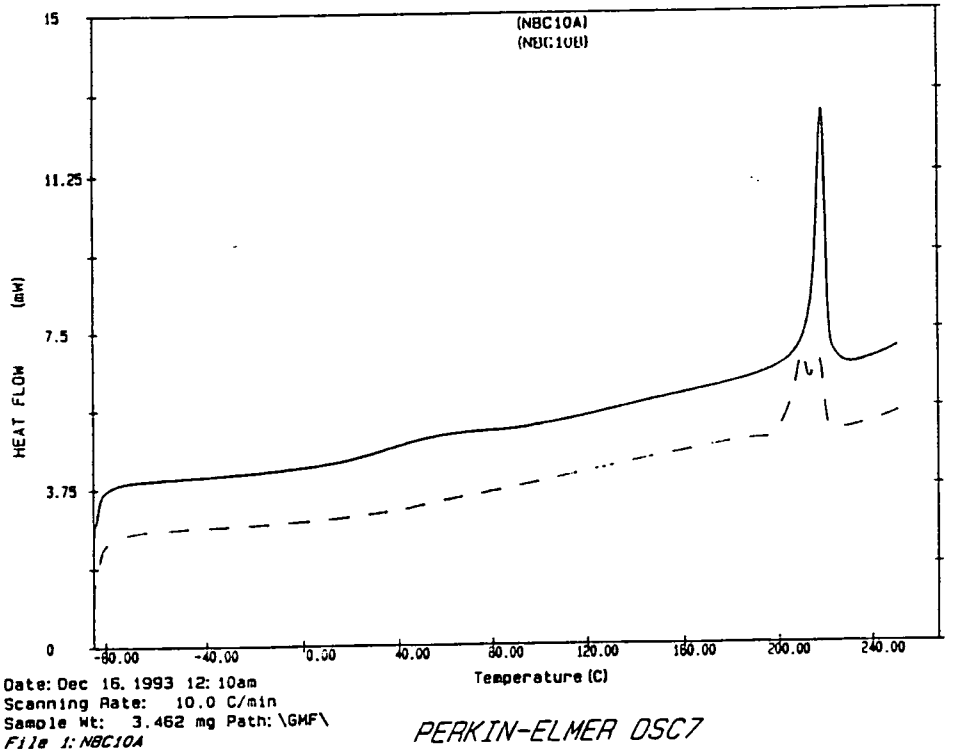

Fig. 5.8 DSC results for NBC10 (NMR/SAXS samples)

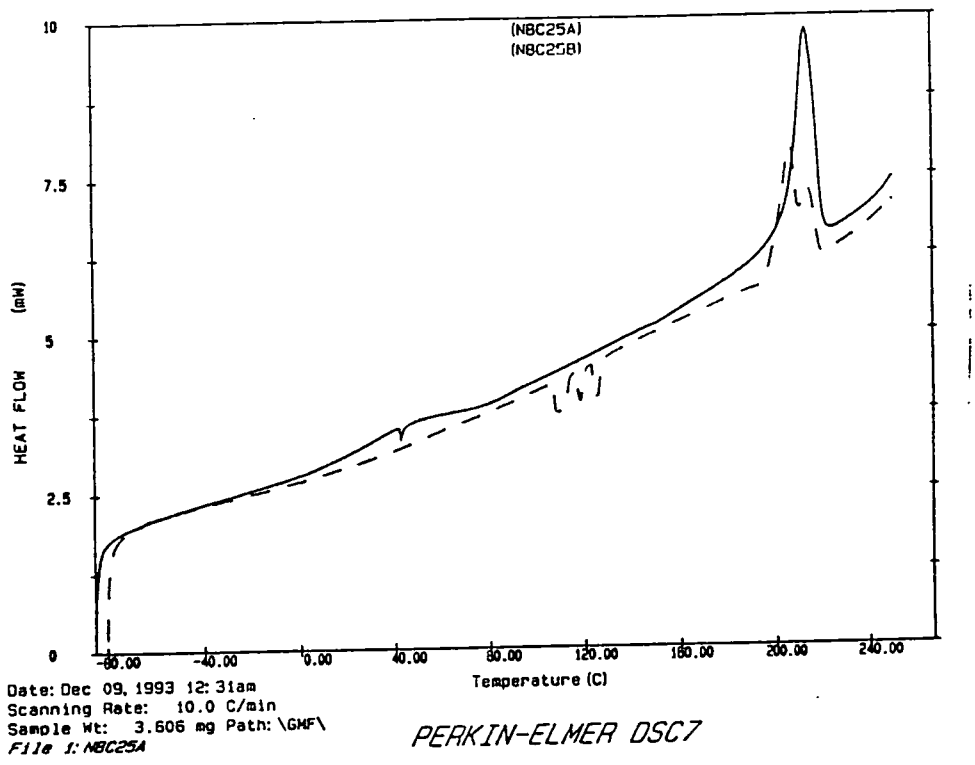

Fig. 5.9 DSC results for NBC25 (NMR/SAXS samples)

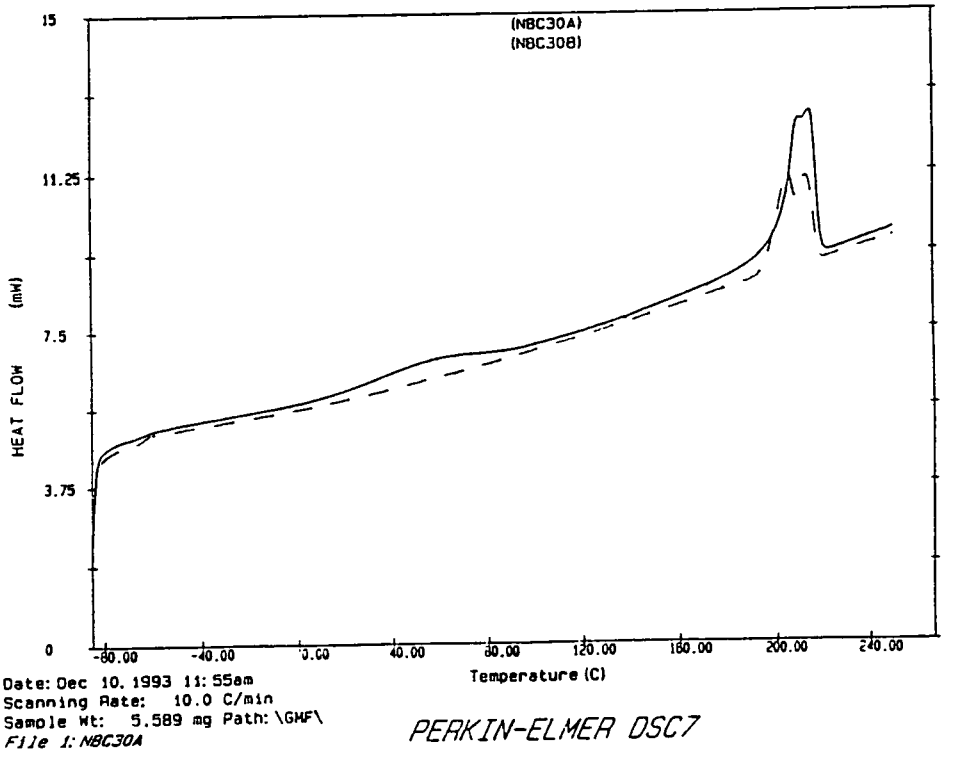

Fig. 5.10 DSC results for NBC30 (NMR/SAXS samples)

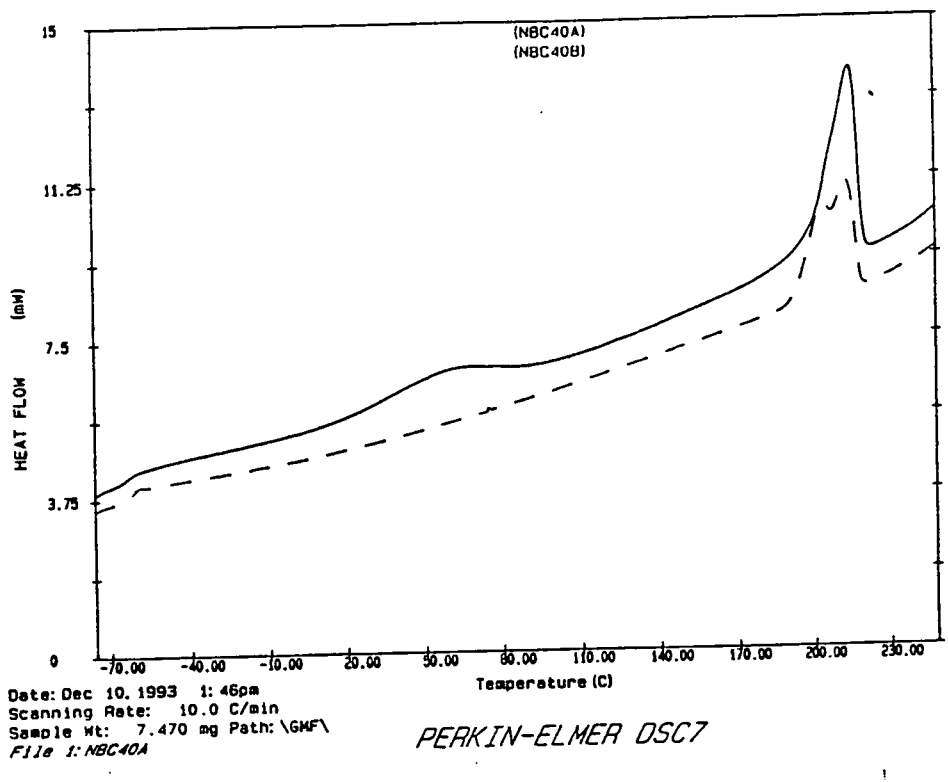

Fig. 5.11 DSC results for NBC40 (NMR/SAXS samples)

A further addition of polyether results in a drop of crystallinity.

Another interesting aspect is that the DCS trace of the second run of the nylon-6 block copolymer NMR/SAXS samples which have dried at 70 °C and the annealed 40 and 50% materials have two heat fusion peaks, one at about 206 °C and the other at about 212 to 218 °C. Nylon-6 only shows one heat fusion peak at 213 °C, both in the first and in the second run. Note the small maximum at 50 °C in the first run of the NMR/SAXS samples which is due to the glass transition temperature, T_g, of Nylon-6. It does not appear in the second run but instead a second fusion peak is present, indicating the importance of thermal history in these experiments. All the observations suggest that there must be more than one crystal type and different

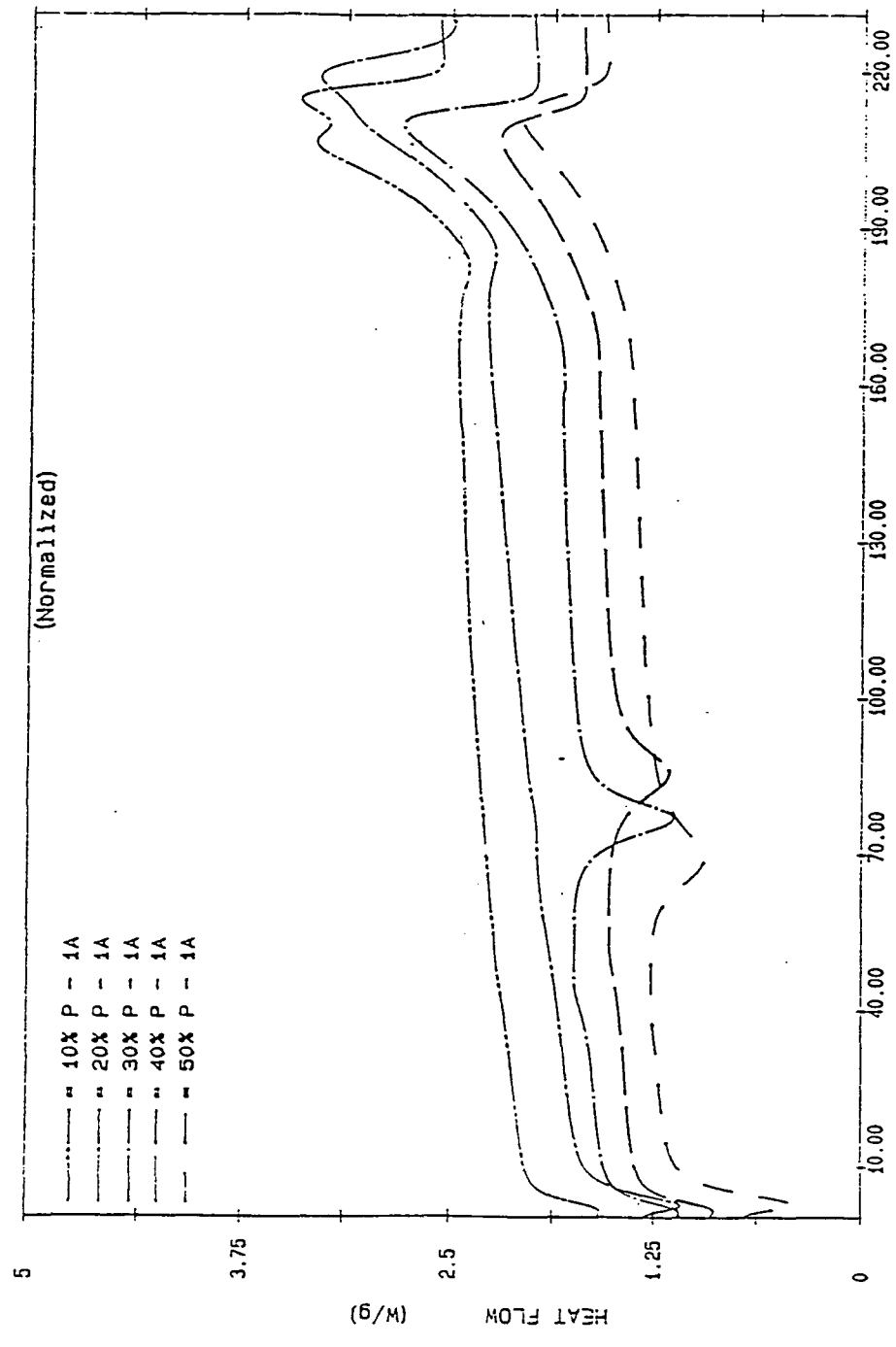

Fig. 5.12 DSC results of as prepared NBC samples with preset heating procedure

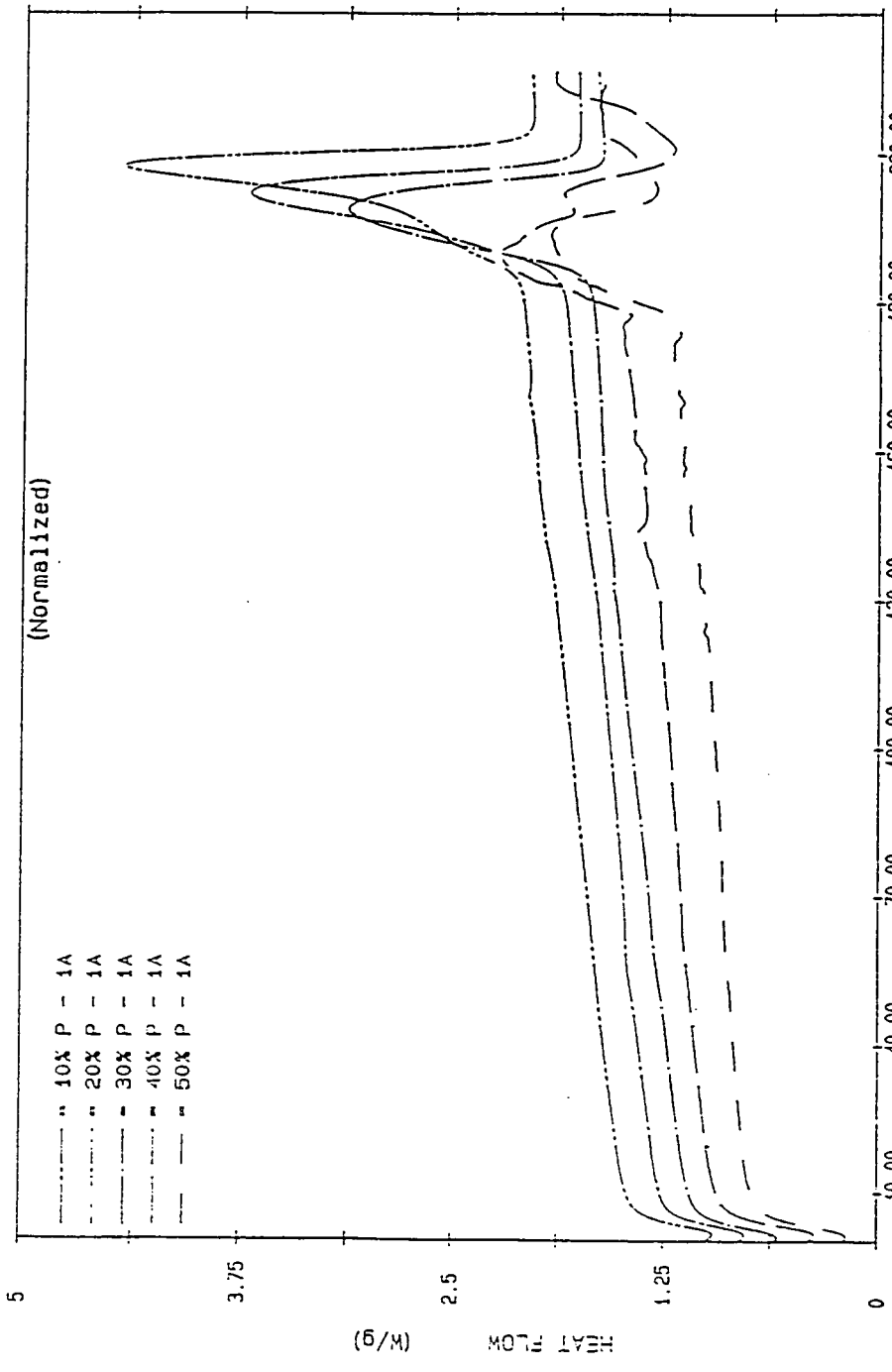

Fig. 5.13 DSC results of annealed NBC samples

crystallisation kinetics for the 10 to 20% materials and the ones with 30 to 50% polyether concentration. As far as the relationship between the two peaks in the DSC thermograms and crystals forms is concerned, one would expect distinct crystal forms to have distinct melting points. However, it is not possible uniquely make such a deduction from the DSC thermograms because it is also possible that the same crystal form might show two peaks if the degree of perfection of the crystal is not uniform. The higher melting point is related to the more ordered domain with a greater thermal stability.

A subsequent discussion will be presented after the results from SAXS and solid-state NMR have been given.

5.3 Small-angle X-ray Scattering, SAXS

5.3.1 Theory

Small-angle X-ray scattering is a powerful tool for the determination of structural parameters of semi-crystalline polymers. As in any scattering process, an inverse relationship between particle size and scattering angle is present. The crystallites present in a powdered polymer sample diffract X-ray beams from parallel planes for incident angles Θ which are determined by the Bragg equation:

$$n\lambda = 2d \sin\Theta \qquad (5.5)$$

Where λ is the wavelength of the radiation, d is the distance between the parallel planes in the crystallites,

called the Bragg spacing, and n is an integer. Small-angle X-ray scattering has provided useful information on macromolecules with dimensions in the range 1 to 100 nm. For the work presented in this chapter, the results from the X-ray measurements were used as reference values to the ones obtained by the spin-diffusion technique. The dimensions in the block copolymer were accomplished by using a technique presented by Zachmann et al. [6]. They employed the 1-dimensional correlation function to determine the structural parameters. Figure 5.14 displays a typical 1-dimensional correlation function and the parameters that can be extracted from this function. The position of the first maximum, L_c^M, indicates the most probable distance between the centres of two adjacent crystals or lamellar stacks. The position of the first minimum, $L_c^m/2$, represents half the most probable distance between the centres of adjacent amorphous regions. If the lamellae form a one-dimensional ideal lattice, both values coincide. However, if this superlattice is not ideal, the position of the maximum, L_c^M, and the minimum, $L_c^m / 2$, in the correlation function may be slightly shifted. Another important parameter is the degree of crystallinity within the lamellar stacks, the so-called linear crystallinity, x_{CL}. The correlation function cannot distinguish between the amorphous fraction $1 - x_{CL}$ and the crystalline fraction x_{CL}. The assignment that the polyether phase is entirely amorphous is intuitive. Nylon-6 is known to exist with both amorphous and crystalline domains, as has been discussed in chapter 4. However, the composition of the block copolymer is known and conclusions about the

structural parameters of the amorphous and crystalline nylon phase and the polyether phase can be accomplished. In the following the larger fraction will be denoted by x_1 and the smaller one by x_2. Two methods are given to determine x_1, x_1^0 and x_2 [6]

1. $$\frac{1 - x_1}{x_1} = cy \qquad (5.6)$$

where y is the value of the correlation function at its first maximum and c is a factor determined in such a way that $c\gamma_1(0) = 1$, depending on the normalisation used for the correlation function. In this work the correlation function is normalized in such a way that $\gamma_1(0) = 1$, so that the constant $c = 1$

2. $$x_1^0(1 - x_1^0)L_c^M = A \qquad (5.7)$$

where A is the intercept of the correlation function with the abscissa. The values determined in this way will be

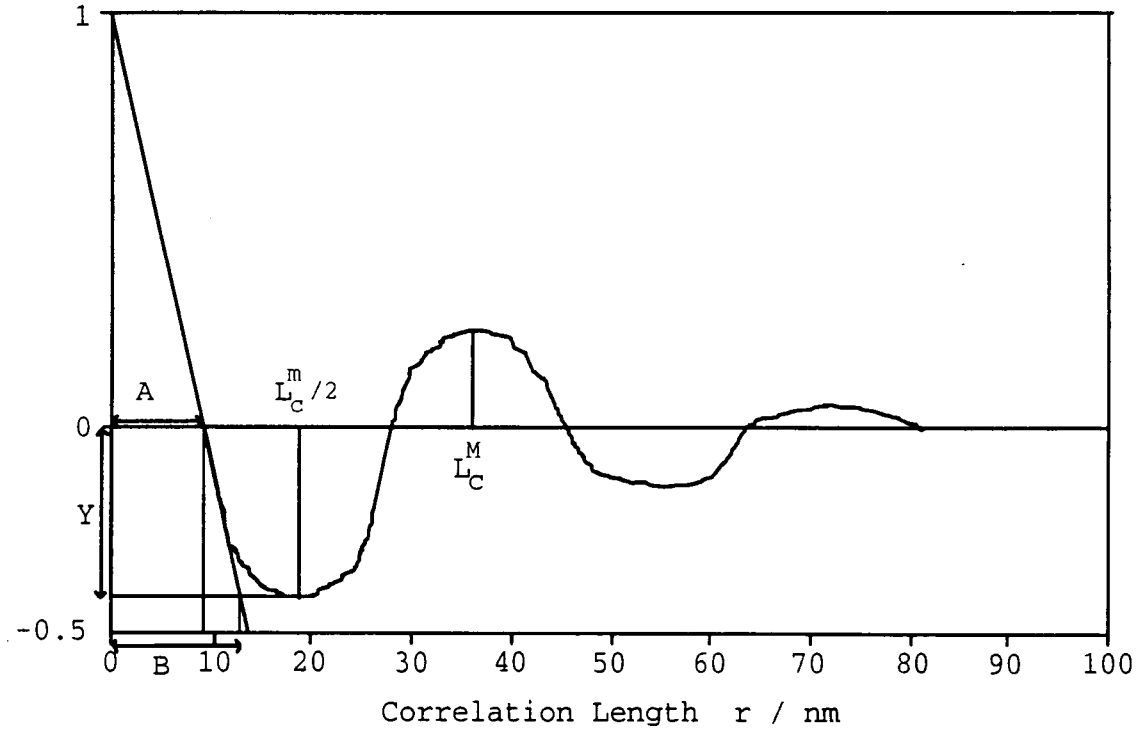

Figure 5.14 Typical 1D-correlation function showing the main parameters to be used

denoted as x_1^0. With $L = \left(L_C^m + L_C^M\right)/2$ the thickness of the crystals, l_c, and that of the amorphous region, l_a, may be determined using equations (5.8) and (5.9). As a consequence of the fact that this technique cannot assign x_1 and $1 - x_1$ to a certain phase, l_1 and l_2 cannot be assigned to the amorphous and crystalline region, hence the larger thickness is designated l_1 and the smaller l_2.

$$l_1 = x_1 L \tag{5.8}$$

$$l_2 = (1 - x_1)L \tag{5.9}$$

Furthermore, l_2 can also be derived by means of the equation (5.10) [7]

$$l_2 = B \tag{5.10}$$

where B is defined in figure 5.9. If l_2 is determined by equation 5.10, there arises a new possibility to obtain $1 - x_1$ by using eq. 5.9 [8]. The value determined in this way will be designated x_{1L}.

5.3.2 Apparatus

Small angle x-ray scattering experiments were carried out using a Kratky Compact Small Angle System (Anton Paar K.G.A-8054 GRAZ Austria). The camera is held in a cast brass housing and the whole system can be evacuated to 0.5 mbar using the integrated vacuum system connected to a vacuum pump. An XRG 3000 Generator (INEL, Z.A. de Courtaboeuf Av.de.Scandinavie - 91953 LES ULIS) run at 20 mA/20 kV generated electrons which are fired off a copper target creating a source of x-rays of wavelength 1.54 Å. The linear, gas tight (argon/methane 90/10 %) detector is

a LPS50 model as supplied by INEL, with a beryllium window. A fast analog-to-digital converter (model 8077, Canberra Industries, Inc., One State Street, Meriden CT 06450) converts the detected signal and displays the scattering profile on the screen of an interfaced PC. A temperature controllable sample holder (Anton Paar) enables samples to be heated from room temperature up to 523 K. To obtain sufficient scattering intensity, the Kratky camera is fitted with a slit collimation system. The resultant desmeared intensity was corrected to eliminate such collimation effects during the analysis procedure. A moving slit device driven by a synchronous motor attached to the slit holder facility, supplied by Anton Paar, allowed the measurement of both the absolute scattering intensity and the sample absorption. Figure 5.15 illustrates a cross section of the geometrical set-up for the collimated system.

The bridge and the middle slit are precisely coplanar, thus minimising the level of parasitic scattering [9]. For the SAXS runs decribed in this work, the middle slit was placed in position b and the system orientated with a projection angle of 6°. This position of the middle slit optimises the set-up in terms of the medium to high resolution, medium incident x-ray intensity and an accesssible set-up alignment. The width and intensity of the primary beam are determined by the position of the entrance slit.

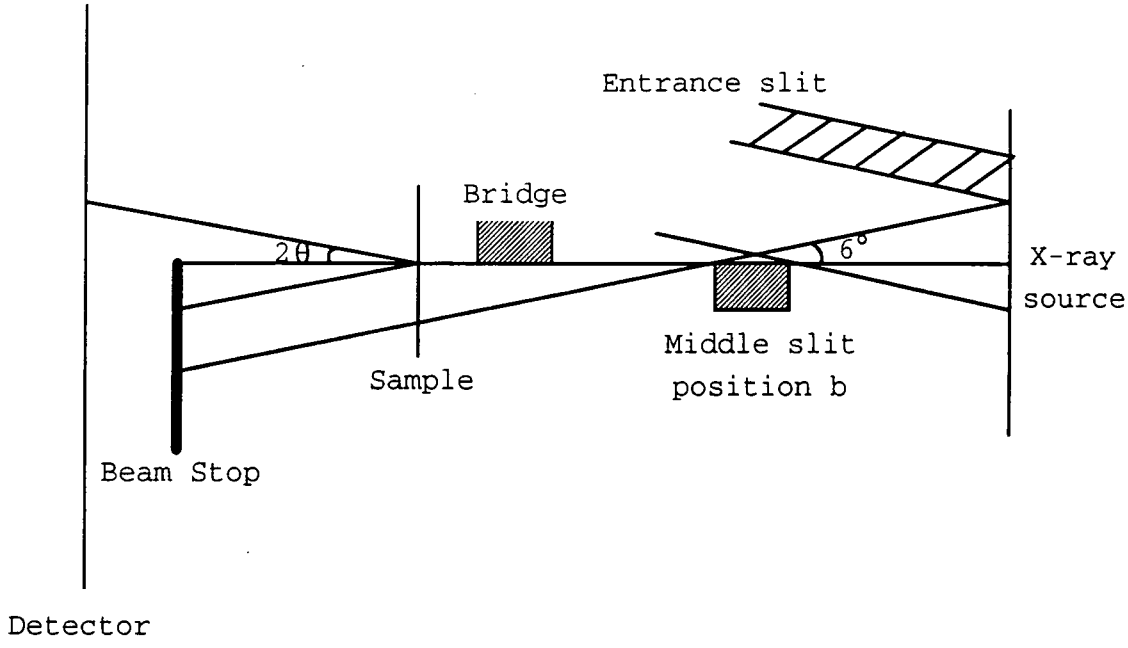

Figure 5.15 Geometrical Set-up of the Collimated Kratky Camera

5.3.3 Experimental

The samples were moulded in a retangular 26 mm x 15 mm x 1 mm brass holder. A polymer sample slice was placed in a rectangular hole (approx. 5x6 mm) which was cut in the brass holder and wrapped in aluminium foil. The polymer samples were dried at 60 °C under vacuum before the SAXS runs. A number of SAXS runs were performed at room temperature with different amounts of polyether and pure nylon-6. The raw data need a mathematical massage before they can be used in an advantageous manner. Therefore the intensity of the parasitic instrumental background needs to be substracted from the sample data. The sample background, sometimes called liquid scattering, was also substracted from the sample data. The resulting smeared background-corrected data were desmeared according to Vonk

[10]. The one-dimensional correlation function was calculated by means of a Fourier transformation [11]. The structural parameters were determined by Zachman's method using the one-dimensional correlation function.

5.3.4 Results and Discussion

The analysis of the SAXS experiments are based upon a lamellar two-phase model with sharp interphase boundaries. The normalised, corrected raw data result in a desmeared x-ray scattering intensity distribution as a function of s, where $s = 2\pi / \lambda \sin(\theta / 2)$. Figure 5.16 displays the desmeared intensity distribution for NBC40. The shape of the intensity profile was found to be very typical for all SAXS runs. The sharp peak at s=0.00125 $Å^{-1}$ is due to the contribution from the main beam spilling over the beam stop, whereas the peaks of lower intensity at larger s are due to sample scattering. To facilitate in the evaluation of the scattering peak position, logarithmic intensity vs. s was used as shown in figure 5.17. No Bragg peaks are observable. This indicates that the standard deviation of the domain radii is large. The imperfect structure is also manifested in the correlation functions. In the case of an ideal ordered structure, L_c^M must be twice as large as $L_c^m / 2$. The experimental ratios of $L_c^M : L_c^m / 2$ are between 2.4 and 2.6 instead (see table 5.2). The structural parameters were obtained from the 1D-correlation functions by Zachmann's method. The correlation functions are presented in figures 5.18 to 5.23.

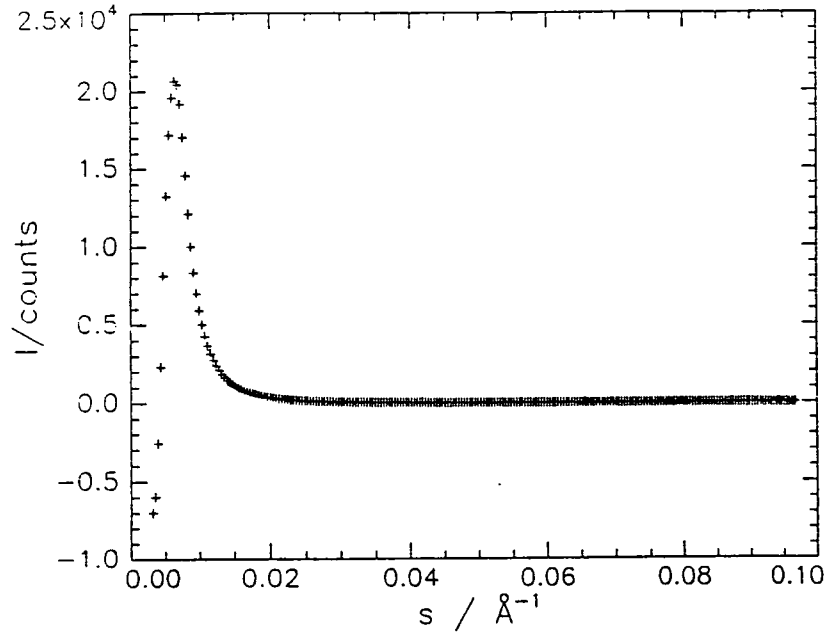

Figure 5.16 Desmeared Scattered Intensity as a function of s

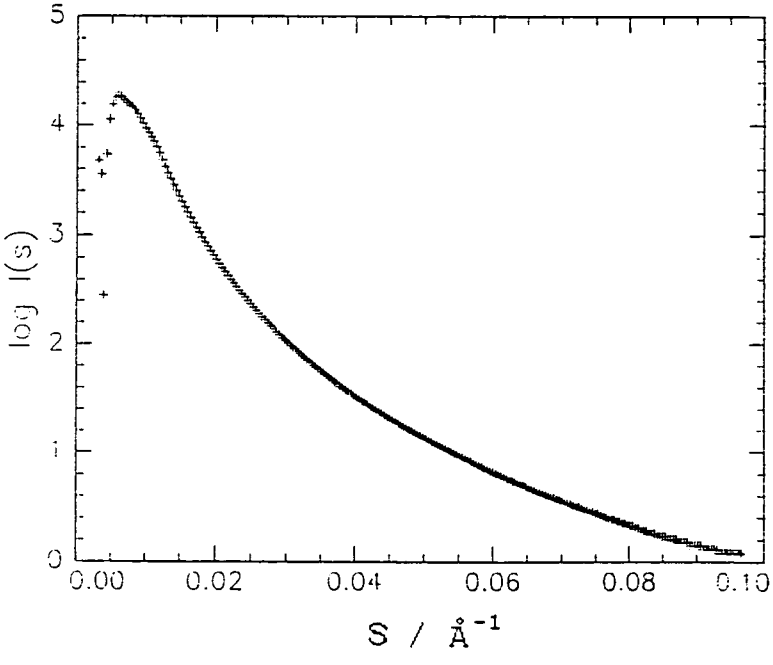

Figure 5.17 log I(s) as a function of s for NBC40

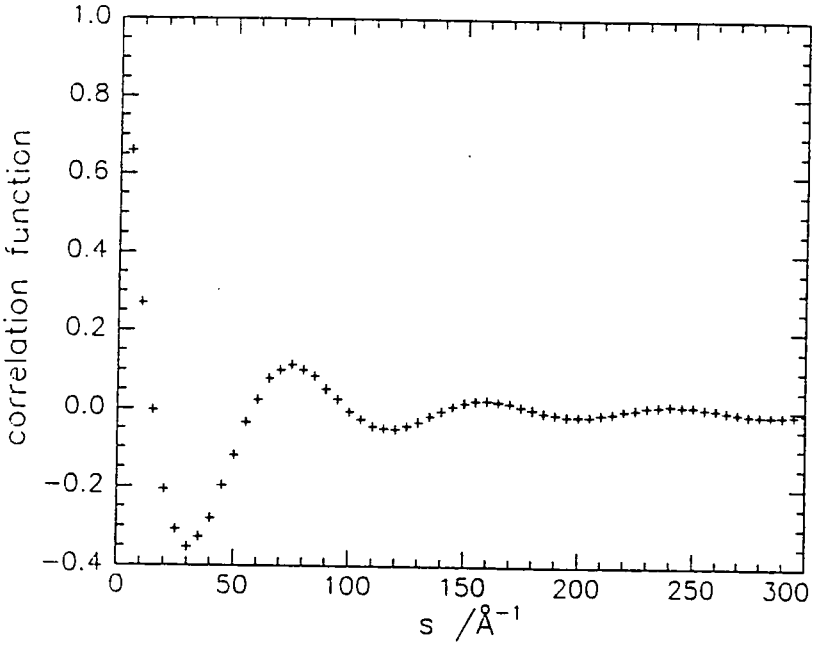

Figure 5.18 Correlation function for nylon-6

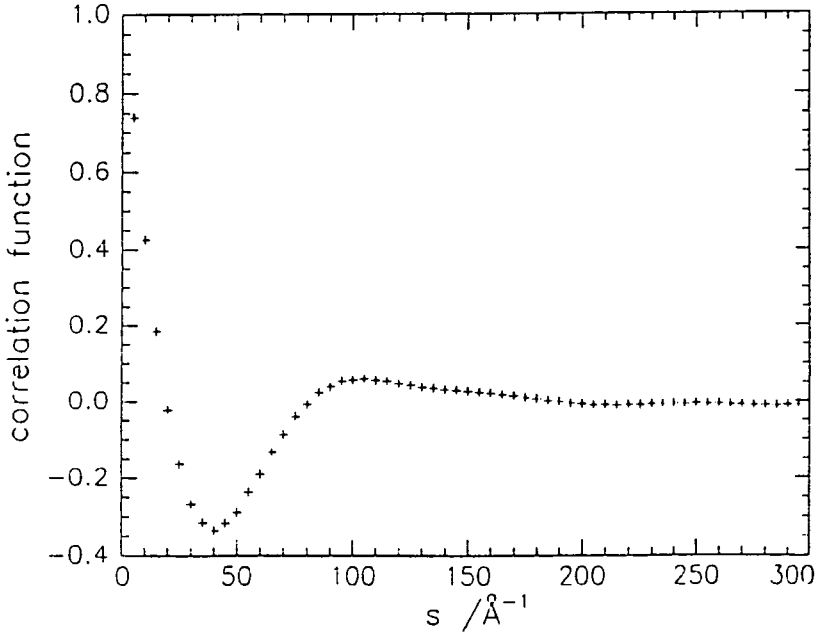

Figure 5.19 Correlation function for NBC15

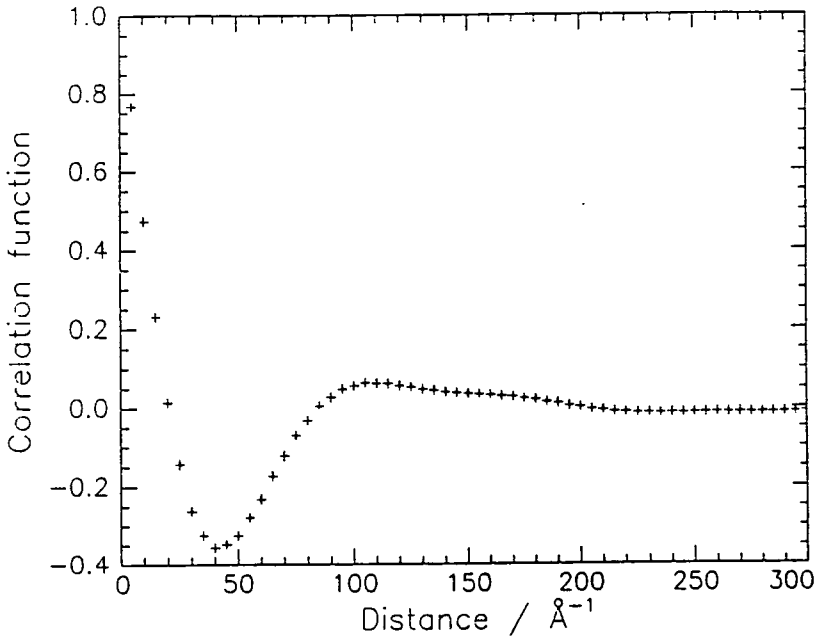

Figure 5.20 Correlation function for NBC20

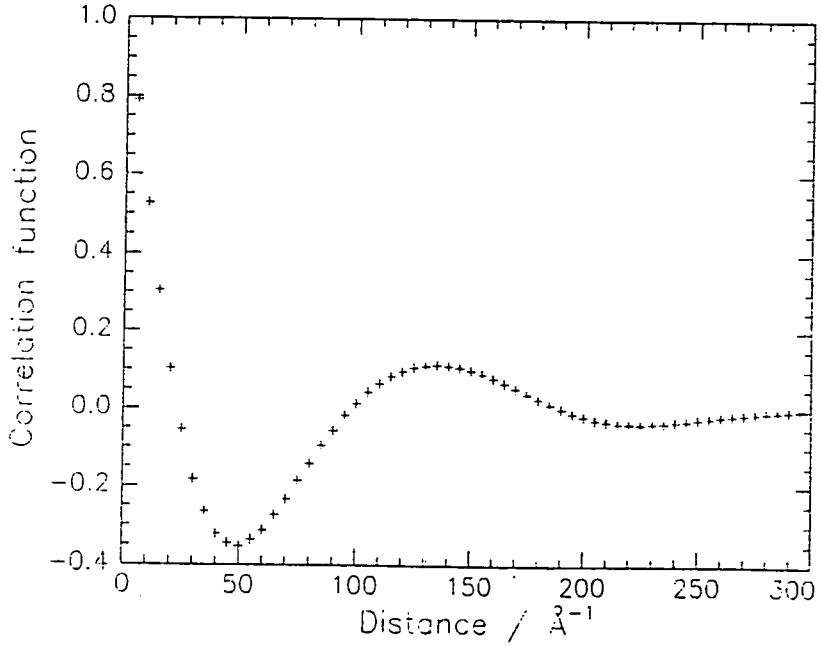

Figure 5.21 Correlation function for NBC30

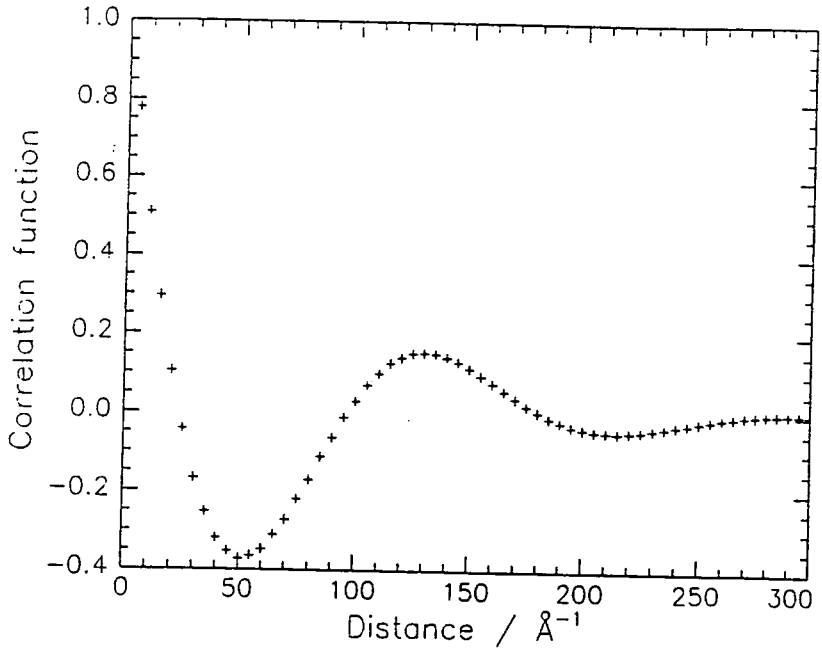

Figure 5.22 Correlation function from NBC40

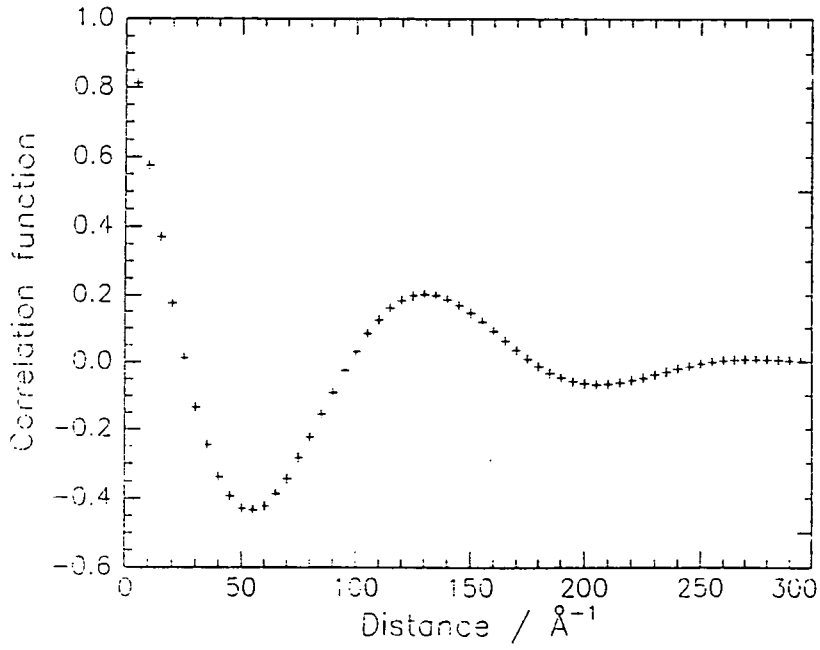

Figure 5.23 Correlation function from NBC50

The 1D-correlation functions reveal some very interesting structural characteristics of the block copolymers with varying polyether concentration.

	A	B=l_2	Y	$L_c^m/2$	L_c^M	L	x_1	l_1	l_2	$x_1°$	$l_1°$	$l_2°$	x_{1I}	l_{1I}
nylon-6	14	19	0.42	30	70	70	0.70	49	21	0.77	54	16	0.73	51
NBC15	20	22	0.37	40	100	90	0.73	66	24	0.72	65	25	0.76	68
NBC20	21	29	0.37	42	105	95	0.73	69	26	0.72	68	27	0.69	66
NBC30	22	31	0.35	50	135	118	0.74	87	31	0.80	94	24	0.74	87
NBC40	22	32	0.37	51	130	116	0.73	85	31	0.78	90	26	0.72	84
NBC50	25	36	0.44	55	130	120	0.69	83	37	0.74	89	31	0.70	84

Table 5.2 Structural parameters of various nylon-6 block copolymers obtained from SAXS. Y, x_1 and $x_1°$ are dimensionless. A, B, l_1, $l_1°$, $L_c^m/2$, L_c^M and L are in Å units. L is the average of L_c^m and L_c^M

If we disregard nylon-6, because of its different preparation mode, the most probable distance between the centre of two adjacent crystal regions evinces a transition between 20% and 30% polyether concentration. That means a structural change in the block copolymer may occur between 20% and 30% polyether concentration. A reasonable assumption for the parameters l_1 and l_2 is that l_1 can be denoted as the amorphous phase, whereas l_2 describes the crystalline region. This assumption has been made because of the fact that the amorphous region, i.e. the amorphous nylon-6 phase and the polyether phase, must be larger than the crystalline nylon phase. A closer look at the amorphous and the crystalline region illustrates that the structural change is entirely associated with an increase of the amorphous region, l_1, as seen in table 5.2 and figure 5.24, whereas l_2 remains constant. However,

from the SAXS experiment alone it cannot be distinguised whether the structural change occurs in the polyether region, in the amorphous nylon-6 region, or in both regions. The fact that x_1 is approximately 0.73 for all concentrations of polyether is surprising and makes the applicability of this technique doubtful. The 1-D correlation functions show damped oscillations for the 15 and 20% materials, whereas the oscillations of the correlation functions of the 30, 40 and 50% materials are more pronounced, indicating a higher ordered structure for the 30, 40 and 50% materials. This is at the first glance a contradictory result, bearing in mind that DSC measurements (see section 5.2.3, table 5.1a-c) indicate that the crystallinity is lower for the 30% to 50% materials than for the 10% and 20% samples. The crystallisation dynamics to build up the crystallites are definitely faster for the low-concentration polyether block copolymers. Nevertheless, although the DSC results indicate lower crystallinity for the more highly concentrated materials, ^{13}C high-resolution solid-state NMR shows no indication of a larger amorphous polyamide proportion and a different order of crystallinity (see section 4.2, figures 4.1 to 4.4).

At the end of this chapter investigations of the morphology by means of spin-diffusion will be discussed. Finally all results will be collated and a model of the structural and morphological properties will be presented.

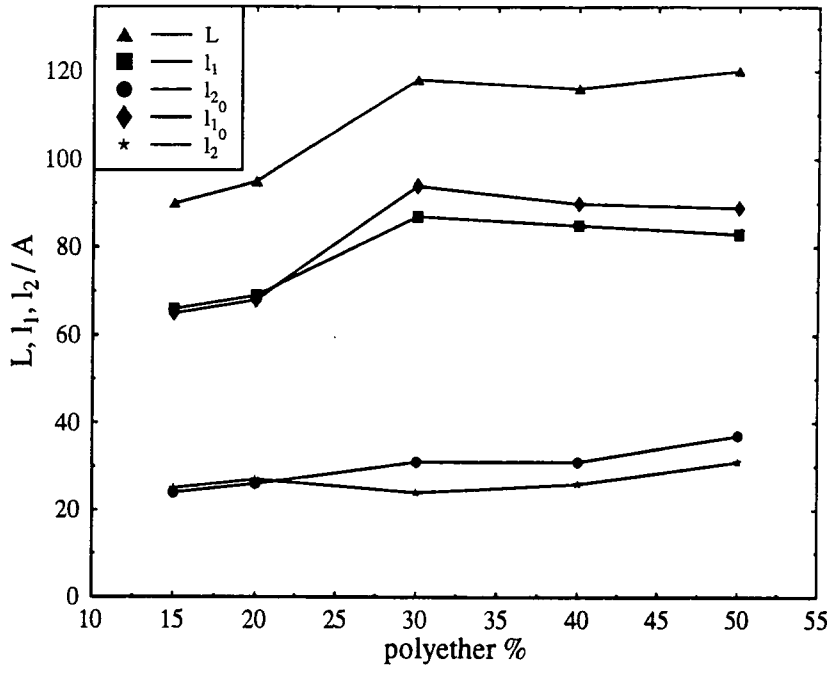

Figure 5.24 Dimensions of the amorphous and crystalline domains in powder samples of nylon-6 block copolymers from SAXS experiment

5.4 Computer Simulations of the Goldman-Shen Experiment

5.4.1 Introduction

This chapter will explain the usefulness of proton spin-diffusion measurements in terms of the determination of domain sizes in heterogeneous systems.

A computer program has been developed and implemented on a Sun 4 and HP 700 series Workstation to allow the modelling of spin-diffusion data obtained by a Goldman-Shen-type experiment (see listing in appendix II). The central computer program is based on a program originally written by Pope [12] to simulate spin-lattice relaxation in the rotating frame for a one-dimensional lamellar model. This chapter basically deals with two points:

1. The quality of different analytical techniques, involving the T_1-effect minimisation in the Goldman-Shen experiment, will be judged.
2. A new advanced analytical technique will be presented to obtain domain sizes in heterogeneous systems using computer modelling of the Goldman-Shen experiment.

In the following section the computer model being used is explained.

5.4.2 The Model

The model has been developed by Kenwright et al. [13] for regular intrusions of one type of material, jacketed by an interfacial layer, in a matrix of another type of material. The intrusions may be lamellar, cylindrical (each cylinder having six equidistant neighbours), or spherical (the spheres taking up hexagonal close-packed lattice sites in the matrix).

The program has been developed now to model experimental data of the Goldman-Shen experiment with the intrinsic spin-lattice relaxation times and the domain sizes of the different regions as the crucial parameters. The program is written in FORTRAN 77 and calls, as its core, the Numerical Algorithms Group (NAG) routine D03PBF. Basically a two-region model has been used, i.e. an intrusion in a matrix. This is a justified simplification because firstly the interface can often be considered as negligibly small (*narrow interface approximation*: $d_{interface}/d_{region} \ll 1$, where d is the length of the interface or region) and secondly in terms of proton solid-state NMR only two distinguishable

regions could be detected. However, a three-region model, involving regular intrusions of one type of material, jacketed by another type of material, in a matrix of a third type is also available which may be converted to a two-region model by considering two regions to be identical. In the cylindrical and spherical models there is a small degree of approximation because of the problem of describing a totally space-filling matrix in the model. A schematic representation of the models used is given in figure 5.25. In the case of lamellar morphology the distance $\overline{AB}$ is simply half the distance between the centres of neighbouring intrusions $\overline{AA}$. The models in the case of cylindrical and spherical morphologies face the problem of having "empty spaces" (see the gray shadowd areas in figure 5.25). In order for region 2 to be a continuous matrix, it is necessary to model a hexagonal unit-cell as illustrated in figure 5.25. This cannot be done simply using the model described. However, the thickness of region 2 may be increased such that the volume considered in the model is the same as that in the hexagonal unit cell. This has the effect of smearing the missing volume evenly around the outside of the cylinder. The approximation involved in this is believed to be negligible if region 2 is the major component. It can be shown by simple trigonometry that the "additional distance" in the space-filling model r_c is related to r by:

$$r_c = r \times \sqrt{\frac{6 \tan \pi/6}{\pi}} \cong r \times 1.05008$$

Similarly, for the spherical case:

$$r_c = r \times \sqrt[3]{\frac{3\sqrt{2}}{\pi}} \cong r \times 1.10534$$

Note that the change in dimension is taken up entirely in region 2. The inherent symmetry of the model allows the calculation of the behaviour of the system along a line from the centre of one intrusion to a point in the matrix halfway between the first intrusion and a neighbour. A full characterisation in NMR terms is given through the spin-diffusion coefficients, the region sizes and the intrinsic spin-lattice relaxation times. Spin-diffusion is spatial transport of magnetisation, normally without material transport. It is mediated by homonuclear dipolar couplings [14]. Their strength is proportional to the square of the gyromagnetic ratio and inversely proportional to the cube of the relevant internuclear distance. Consequently, in organic materials spin-diffusion is most efficient among protons. They possess a

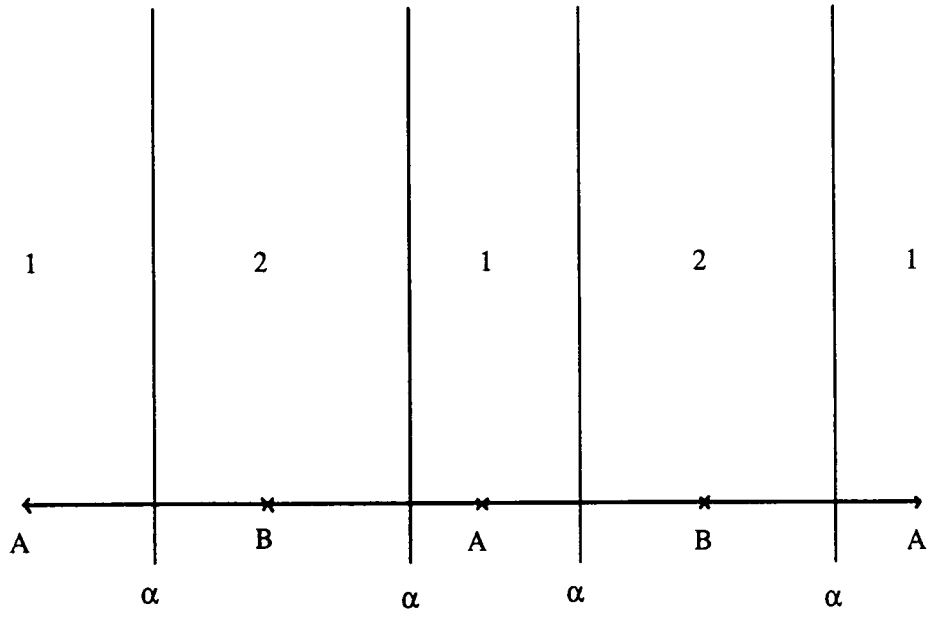

a) lamellar morphology

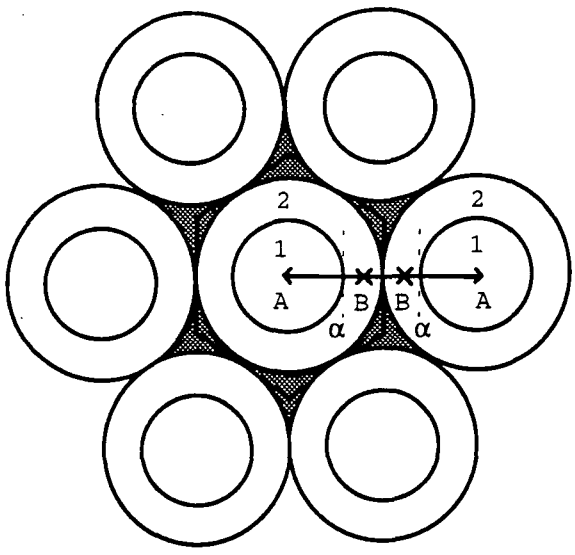

b) cylindrical morphology

Fig. 5.25 Morphology models used in the computer simulation (two-region model only)

large gyromagnetic ratio and small average separations because of their high abundance. These features allow the description of proton spin-diffusion by a quasi-continuous theory of diffusion [15].

The general behaviour of magnetisation M(x,t), at point x, at time t is described by equation 5.11:

$$\rho_i\left(\frac{dM(x,t)}{dt}\right) = x^{-m}\frac{d}{dx}\left[x^m D_i \frac{dM(x,t)}{dx}\right] + \frac{\left(M_\infty - M(x,t)\right)}{T_{1,i}^H}\rho_i \qquad (5.11)$$

Where ρ_i is the relative proton density in region i

D_i is the effective spin-diffusion coefficient

M_∞ is the equilibrium value of the magnetisation

$T_{1,i}^H$ is the relaxation time in region i

m determines the morphology of the model (m=0: lamellar, m=1: hexagonally packed cylinders, m=2:

spheres on a hexagonally packed lattice)

This equation must be solved for each x and for the required values of t, subject to suitable boundary conditions, which may be defined as follows: The space coordinate x runs from the centre A of the intrusion *1* to a point B in the matrix halfway between the intrusion *1* and the next intrusion thereby passing the boundary α. The boundary conditions may be expressed as:

1. at x=A and x=B, by symmetry there is no net diffusion across the centres of region 1 and 2

$$\left[\frac{dM(x,t)}{dx}\right]_{x=A,B} = 0 \quad \text{(for all t)}$$

2. at the boundary, α

a) $M_1(\alpha,t) = M_2(\alpha,t)$

i.e. the magnetisation must be continuous across the boundary

b) $D_1 \frac{dM_1(\alpha,t)}{dx} = D_2 \frac{dM_2(\alpha,t)}{dx}$

i.e. the magnetisation cannot accumulate at the boundary

A homogeneous proton density for the two regions has been assumed. The magnetisation of each region is defined by 30 mesh-points plus one mesh-point at the contact of two regions. Integration over these mesh-points gives the observed magnetisation.

The data-modelling has been carried out by the well-known *Simplex*-algorithm [16]. The *Simplex* algorithm has

been used because the response-surface [17], defined as the sum of the squared residuals

$$\sum_i (y_i - y_i')^2 \qquad (5.12)$$

where y_i is the ith value of the experiment

y_i' is the ith value of the calculation

is found to be very flat and to consist of many local minima. The least-squares criterion is to minimise the sum of the squared residuals. The advantage of the Simplex-algorithm is that it does not need any derivation of the function as, e.g., the Marquardt-algorithm does, which would present a problem for this special case. How the data-modelling was carried out will be discussed in more detail in section 5.5.

5.4.3 The Goldman-Shen Experiment and the T_1-Problem

Goldman and Shen developed a neat experiment which yields information about domain sizes in heterogeneous systems by means of spin-diffusion [18]. The experiment consists basically of three pulses as demonstrated in figure 5.26:

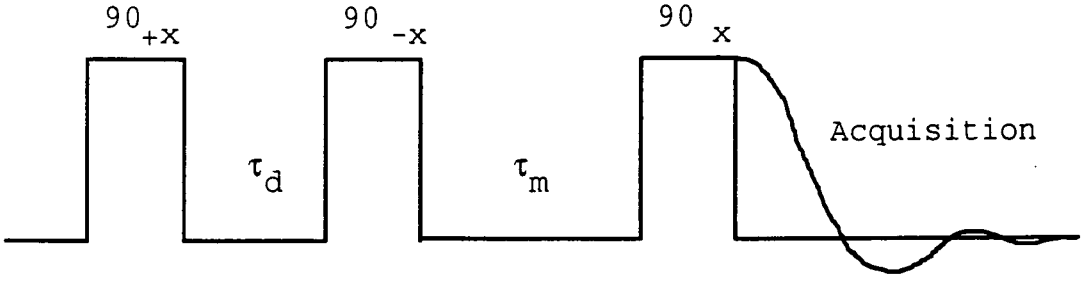

Fig. 5.26 Goldman-Shen pulse sequence

The main idea of this experiment is that it makes use of the fact that different types of domains, in terms of mobile and rigid, have different spin-spin relaxation times T_2 ($T_{2,rigid} << T_{2,mobile}$) [19]. Magnetisation in a rigid type of domain can be selectively removed by applying NMR pulses while there is still sufficient magnetisation remaining in the mobile domain system. The first 90 degree pulse flips the magnetisation into the xy-plane. During an adequate time τ_d, $T_{2,rigid} << \tau_d << T_{2,mobile}$, the magnetisation of the rigid region will be dephased, while the magnetisation in the mobile region is hardly affected. A second 90 degree pulse is applied after time τ_d, bringing the remaining magnetisation of the mobile region back to the +z-direction, followed by a mixing time τ_m, where the magnetisation is allowed to diffuse back into the rigid region. The final 90 degree pulse flips the magnetisation from the z-direction back to the xy-plane for acquisition. However, the technique only works exactly if during the mixing time spin-lattice relaxation has only a negligible effect, in other words, the mixing time must be much smaller than the spin-lattice relaxation time ($\tau_m << T_1$). This special case was dealt with by Cheung and Gerstein [30]. They discussed an analytical solution of the spin-diffusion equation where T_1 was significantly larger than the time regime they examined. In practice this case finds relevance only in very special examples. The normal case is where $\tau_m \cong T_1$ and therefore the Goldman-Shen experiment is flawed by the fact that it is not possible to be sure that the effects observed are due solely to spin-diffusion

without any contribution due to T_1 relaxation during the evolution period τ_m. Hence, in principle it should be possible to apply the analytical function by Cheung and Gerstein when one can remove the T_1-influence from the spin-diffusion.

It has been suggested that the effects due to spin-lattice relaxation could be reduced by alternating the phases of the second 90° pulse in the sequence [12,20]. This experiment will be named the *modified Goldman-Shen experiment*. The effects of this experiment are visualised in Figure 5.27. The main idea of the phase alternation is that the spin-lattice relaxation affects both response-curves in the Goldman-Shen experiment in the same direction, i.e. the magnetisation is relaxing parallel to the applied $\vec{B}_0$-field towards its thermal equilibrium. But spin-diffusion affects the magnetisation in opposite directions by alternating the phases during the preparation period (see figures 5.27 A+B). By adding both values of the magnetisation and dividing by two, $\left(m(\tau_m) - m'(\tau_m)\right) / 2$, the T_1-effect will therefore be reduced in size, though not cancelled. This is due to the T_1-profile, which is shown in Figure 5.28. In an inversion-recovery experiment, the difference of the magnetisation for a given time-interval Δt is decreasing with increasing t, i.e. in a certain time interval a larger amount of magnetisation relaxes in the negative of the phase of the modified Goldman-Shen experiment than in the normal experiment because its initial magnetisation after the preparation time is further away from its equilibrium value. The magnetisation value obtained by

alternating the phases is consequently smaller than the magnetisation would be due only to spin-diffusion. This inaccuracy will occur in all T_1-minimisation techniques using the phase-alternation. An experimentally more advanced technique was carried out by Kenwright and Packer [21]. It introduced an additional 180°-pulse into the evolution period. The time spacings were chosen to make the T_1-effects in the two periods (before and after the 180°-pulse) absolutely equal but opposite in sign, thereby cancelling out the T_1-effect from the finally observed spectrum. Although the cancellation works perfectly for a system where the different regions have the same intrinsic T_1-value, it fails for a system with non-uniform intrinsic T_1, which is generally the case. Two other techniques will be explained in more detail, because they are the basis for the next section.

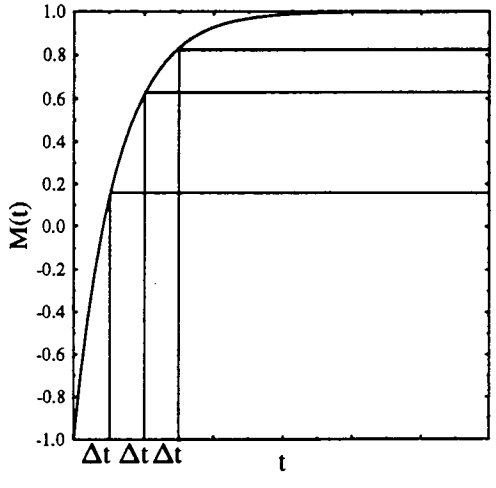

Figure 5.28 Typical T_1-profile

The first technique is intuitive. If the Goldman-Shen experiment is governed by spin-lattice relaxation, one is

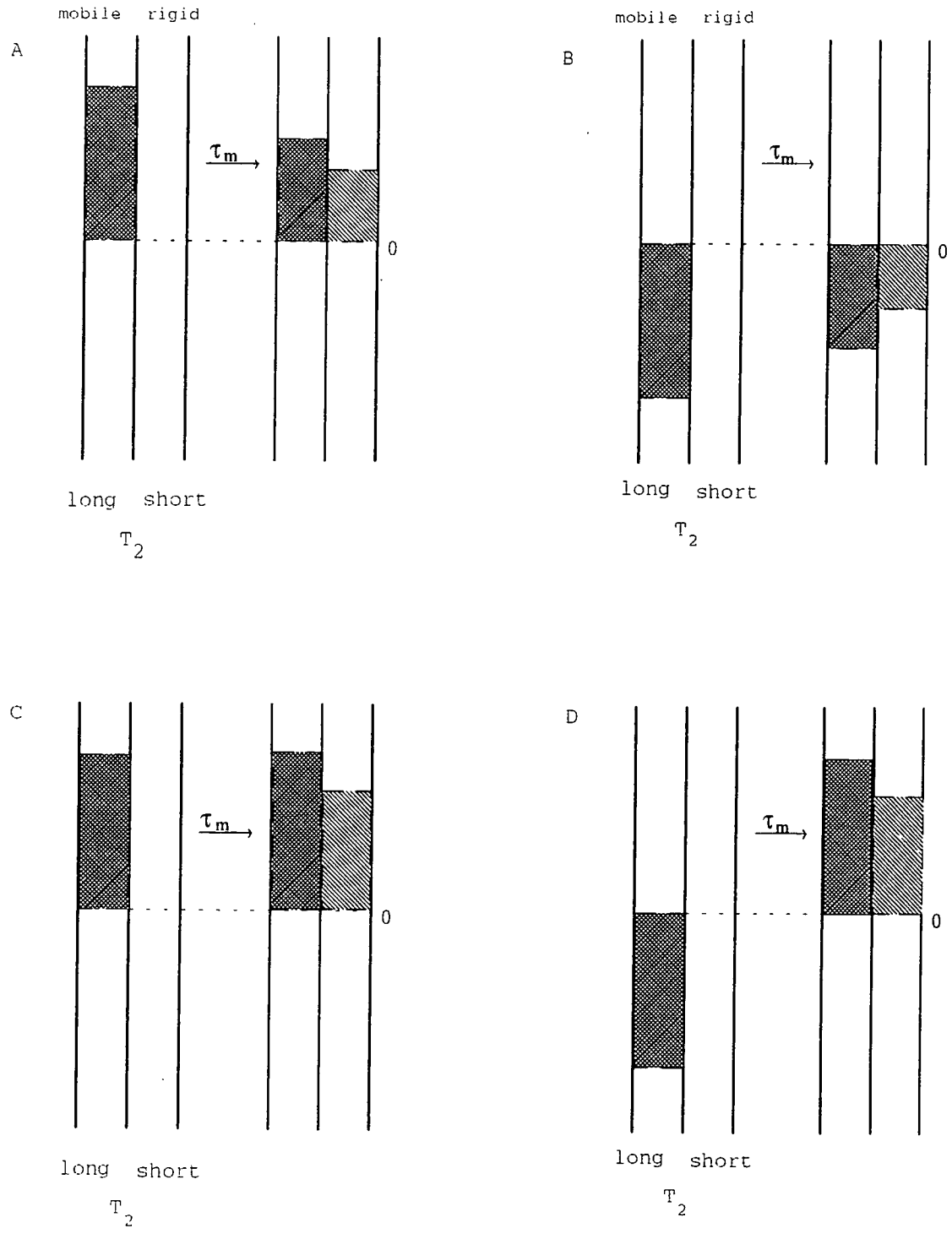

Fig. 5.27 The figure shows schematically the development of the magnetisation during the mixing time, starting after the second 90°-pulse. The two figures at the top with the pulse sequences 90_{+x}-90_{-x}-90_{+x} for A and 90_{+x}-90_{+x}-90_{+x} for B represent spin-diffusion without T_1-relaxation. The two figures at the bottom (C+D) using the same pulse-sequences as A+B respectively represent spin-diffusion with efficient T_1-relaxation.

tempted to correct this perturbation by back-multiplying the data with a factor $\exp(\tau_m/T_1)$. This is basically an expression used to describe spin-lattice relaxation, but with an opposite sign in the exponential. It is expected that this back-multiplication should cancel out all the contribution of the spin-lattice relaxation. In the next section, simulation of the Goldman-Shen experiment will prove when this technique is working correctly.

The second technique was suggested by Newman [22]. The experimental technique is the same as discussed above and suggested originally by Packer et al. [12]. The only difference lies in the presentation of the data-points. Instead of plotting $\left(m(\tau_m) - m'(\tau_m)\right) / 2$, Newman uses a presentation of the data-points that places more emphasis on spin-diffusion. The difference $m(\tau_m) - m'(\tau_m)$ is divided by a function that is dominated by spin-lattice relaxation $m(\infty) + m'(\infty) - m(\tau_m) - m'(\tau_m)$. In the absence of spin-diffusion the value of T_1 affects the two functions to precisely the same extent. Therefore the ratio of the two functions becomes independent of τ_m. A proof of the independence of τ_m has been carried out:

The magnetisation in the mobile phase, e.g., calculated by Newman's technique is:

$$M(\tau_m) = \frac{m(\tau_m) - m'(\tau_m)}{m(\infty) + m'(\infty) - m(\tau_m) - m'(\tau_m)} \qquad (5.13)$$

with

$$m'(\tau_m) = -c$$

$$m(\infty) = m'(\infty) = c$$

$$m'(\tau_m) = c - 2c\exp\left(-\frac{\tau_m}{T_1}\right)$$

$$m(\tau_m) = c$$

$$M(\tau_m) = \frac{c - c + 2c\exp\left(-\frac{\tau_m}{T_1}\right)}{c + c - c - c + 2c\exp\left(-\frac{\tau_m}{T_1}\right)}$$

$$\therefore M(\tau_m) = \frac{\exp\left(-\frac{\tau_m}{T_1}\right)}{\exp\left(-\frac{\tau_m}{T_1}\right)} = 1$$

(5.14)

The independence of τ_m in the ratio of these two equations has been proved. This technique will also be examined in terms of accuracy by simulating the magnetisation behaviour in the Goldman-Shen experiment.

5.4.4 Comparison of the Different Analytical Techniques used in the Goldman-Shen Experiment

Several simulations of the Goldman-Shen experiment have been carried out to prove the accuracy of the different analytical techniques described in the last section. A heterogeneous two-region system with cylindrical morphology, i.e. cylinders of a mobile phase incorporated into a rigid matrix, has been chosen. The composition of the heterogeneous system consists of 80% rigid material and 20% of mobile material. The interface between the two

region is considered as negligibly small for simplicity (*narrow-interface approximation*). The transverse relaxation time for the mobile and the rigid regions were set to 367 μs and 12 μs respectively. A dephasing time of 50 μs has been chosen to select the ^1H-magnetisation of the mobile region sufficiently. The magnetisation behaviour during the mixing time is represented by 60 data-points ranging from 0 s to 0.5 s. The parameters used for the simulations are summarised in tables 5.3 to 5.6. In addition simulations have been carried out with the same parameter sets as described above, but where the spin-lattice relaxation time is set to 10^6 s, which can be considered as infinitely long. The response curve from this experiment is used as a reference for all the three T_1-minimisation techniques because it has no contribution due to spin-lattice relaxation. Comparison of the response curves from the T_1-minimisation techniques and the reference curve gives information about the quality of the analytical technique. The remaining spin-lattice relaxation contribution in the Goldman-Shen experiment is taken as a measure of how accurately the minimisation techniques are working.

Graphical presentations of the simulations carried out for the simple Goldman-Shen experiment (i.e. without T_1 minimisation techniques) are shown in figures 5.29a to 5.29d. The graphs show the time-dependence of the magnetisation in the Goldman-Shen experiment of the mobile (bottom) and rigid (top) regions as a function of the mixing time. The graphs show two different simulations for the corresponding parameters. The filled circles represent

	Region 1	Region 2
thickness of region / m	$5.0000 \cdot 10^{-9}$	$5.6472 \cdot 10^{-9}$
spin-diffusion coeff. / $m^2 s^{-1}$	$6.1000 \cdot 10^{-17}$	$4.1000 \cdot 10^{-16}$
intrinsic T_1 / s	0.3000	0.3000
intrinsic T_2 / s	$3.6700 \cdot 10^{-4}$	$1.2000 \cdot 10^{-5}$
T_2-relaxation type	exponential	gaussian
proportion of the components (vol%)	20	80
dimension in repeat unit / m	$2.5000 \cdot 10^{-9}$	$3.0902 \cdot 10^{-9}$
periodicity / m	$1.0647 \cdot 10^{-8}$	
$l_i^2 / D_i T_{1,i}$	1.37	0.26

Table 5.3 Goldman-Shen Experiment for cylindrical morphology with uniform T_1. (For the definition of the parameters see text.)

	Region 1	Region 2
thickness of region / m	$5.0000 \cdot 10^{-9}$	$5.6472 \cdot 10^{-9}$
spin-diffusion coeff. / $m^2 s^{-1}$	$6.1000 \cdot 10^{-17}$	$4.1000 \cdot 10^{-16}$
intrinsic T_1 / s	0.5000	5.0000
intrinsic T_2 / s	$3.6700 \cdot 10^{-4}$	$1.2000 \cdot 10^{-5}$
T_2-relaxation type	exponential	gaussian
proportion of the components (vol%)	20	80
dimension in repeat unit / m	$2.5000 \cdot 10^{-9}$	$3.0902 \cdot 10^{-9}$
periodicity / m	$1.0647 \cdot 10^{-8}$	
$l_i^2 / D_i T_{1,i}$	0.82	0.02

Table 5.4 Goldman-Shen Experiment for cylindrical morphology with non-uniform T_1

	Region 1	Region 2
thickness of region / m	$5.0000 \cdot 10^{-9}$	$5.6472 \cdot 10^{-9}$
spin-diffusion coeff. / $m^2 s^{-1}$	$6.1000 \cdot 10^{-17}$	$4.1000 \cdot 10^{-16}$
intrinsic T_1 / s	0.0500	0.3000
intrinsic T_2 / s	$3.6700 \cdot 10^{-4}$	$1.2000 \cdot 10^{-5}$
T_2 -relaxation type	exponential	gaussian
proportion of the components (vol%)	20	80
dimension in repeat unit / m	$2.5000 \cdot 10^{-9}$	$3.0902 \cdot 10^{-9}$
periodicity / m	$1.0647 \cdot 10^{-8}$	
$l_i^2 / D_i T_{1,i}$	8.20	0.26

Table 5.5 Goldman-Shen Experiment for cylindrical morphology with non-uniform T_1

	Region 1	Region 2
thickness of region / m	$5.0000 \cdot 10^{-9}$	$5.6472 \cdot 10^{-9}$
spin-diffusion coeff. / $m^2 s^{-1}$	$2.1000 \cdot 10^{-17}$	$4.1000 \cdot 10^{-16}$
intrinsic T_1 / s	0.0500	0.3000
intrinsic T_2 / s	$3.6700 \cdot 10^{-4}$	$1.2000 \cdot 10^{-5}$
T_2 -relaxation type	exponential	gaussian
proportion of the components (vol%)	20	80
dimension in repeat unit / m	$2.5000 \cdot 10^{-9}$	$3.0902 \cdot 10^{-9}$
periodicity / m	$1.0647 \cdot 10^{-8}$	
$l_i^2 / D_i T_{1,i}$	23.81	0.26

Table 5.6 Goldman-Shen Experiment for cylindrical morphology with non-uniform T_1

the normal Goldman-Shen experiment and the filled squares represent the simulation of the phase alternated Goldman Shen modification. In the mobile region, the magnetisation starts with approximately 18% of the whole magnetisation,

rather than 20% as its initial amount of material would suggest. This is simply due to T_2-relaxation in the preparation period. If we assume no spin-lattice relaxation, i.e. magnetisation only transported from the mobile to the rigid region via spin-diffusion, the equilibrium value is expected to be ≈3.5% of the total magnetisation. The simulation with an infinity long spin-lattice relaxation time gives this value correctly as seen in figures 5.29a to 5.29d (bottom). However, if the T_1 is set to a finite value, the magnetisation relaxes back to its thermal equilibrium value of 20% in the case of the mobile region and 80% in the case of the rigid region. The initial loss of signal in the rigid region (see e.g. figure 5.29b (top), magnetisation stored in the -z-direction), gives direct evidence that spin-diffusion is effective, i.e. magnetisation diffuses from the mobile to the rigid region. The strong polarisation-gradient is the driving force of the diffusion process. But at about 40 ms a turning point is reached and the signal subsequently increases, due to spin-lattice relaxation, to its thermal equilibrium value of 20% of the total magnetisation. A similar situation is found for the rigid region. If the magnetisation is stored in the -z-direction in the preparation period, the rigid region loses further magnetisation in the mixing period, so its initially zero signal becomes negative before spin-lattice relaxation brings the magnetisation back to its thermal equilibrium value of 80% of the total magnetisation (see e.g. figure 5.29c (top)). This visualises that the gradient of diffusion in the modified Goldman-Shen experiment has an

opposite sign. In order to minimise the contribution of the spin-relaxation, three different techniques have been applied, as explained in the last section. The quality of these techniques will be discussed in the following.

In order to address this question, one needs to understand spin-lattice relaxation in the presence of spin-diffusion. A more detailed discussion on this matter will be given in chapter 6. At this stage it will be pointed out that the time taken for magnetisation to diffuse out of a region is directly proportional to l_i^2/D_i [23,24], where l_i is half the thickness of region i and D_i is the spin-diffusion coefficient in region i. If that region i is coupled to an external relaxation sink, the question whether the observed relaxation in region i will be dominated by the intrinsic relaxation time in the region, $T_{1,i}$, or by diffusion to the external relaxation sink must depend on the ratio $l_i^2/D_i\,T_{1,i}$, with the intrinsic relaxation dominating when $l_i^2/D_i\,T_{1,i} >> 1$. If we consider a two-region system *1,2*, as used for the Goldman-Shen experiment simulation above, it is important to know how $l_1^2/D_1\,T_{1,i}$ and $l_2^2/D_2\,T_{1,i}$ are related to each other. Tables 5.3-5.6 show the ratios of $l_i^2/D_i\,T_{1,i}$. The systems simulated with the parameter sets given in tables 5.3 and 5.5 to 5.6 are in a regime $l_1^2/D_1\,T_{1,1} >> 1 > l_2^2/D_2\,T_{1,2}$ (which means that spin-diffusion does not effectively couple the two regions, because $l_1^2/D_1\,T_{1,1} >> 1$), but it is also not dominated by its intrinsic spin-lattice relaxation behaviour because $l_2^2/D_2\,T_{1,2} < 1$). The system simulated with the parameter set given in table 5.4, however is in a

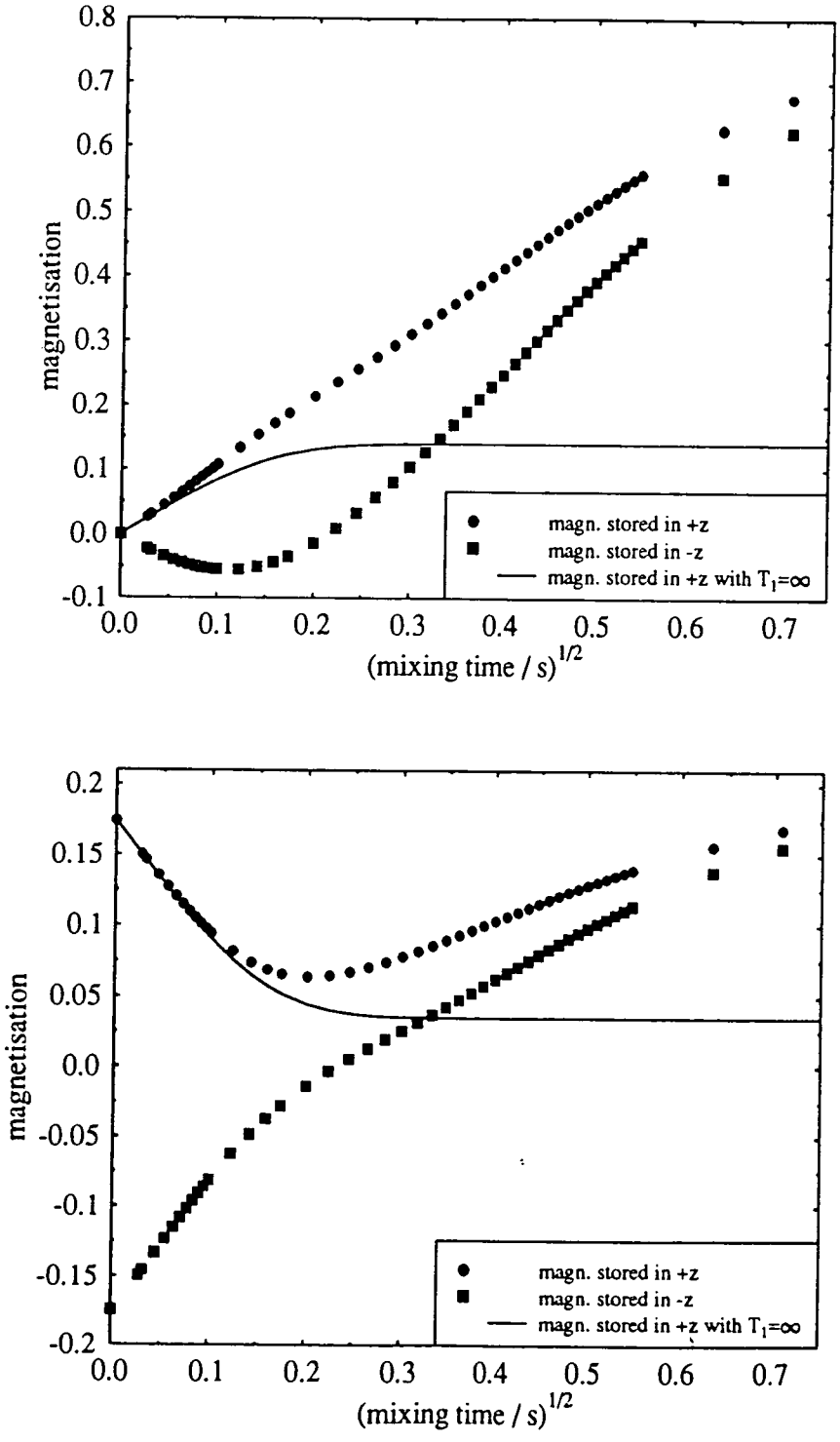

Fig. 5.29a Spin-diffusion simulation of a heterogeneous system (20% mobile, 80% rigid)
intrinsic T_1's: T_1(mobile): 0.3 s, T_1(rigid): 0.3 s, D(mobile): $6.1 \cdot 10^{-17}$ $m^2 s^{-1}$
top: rigid region, bottom: mobile region

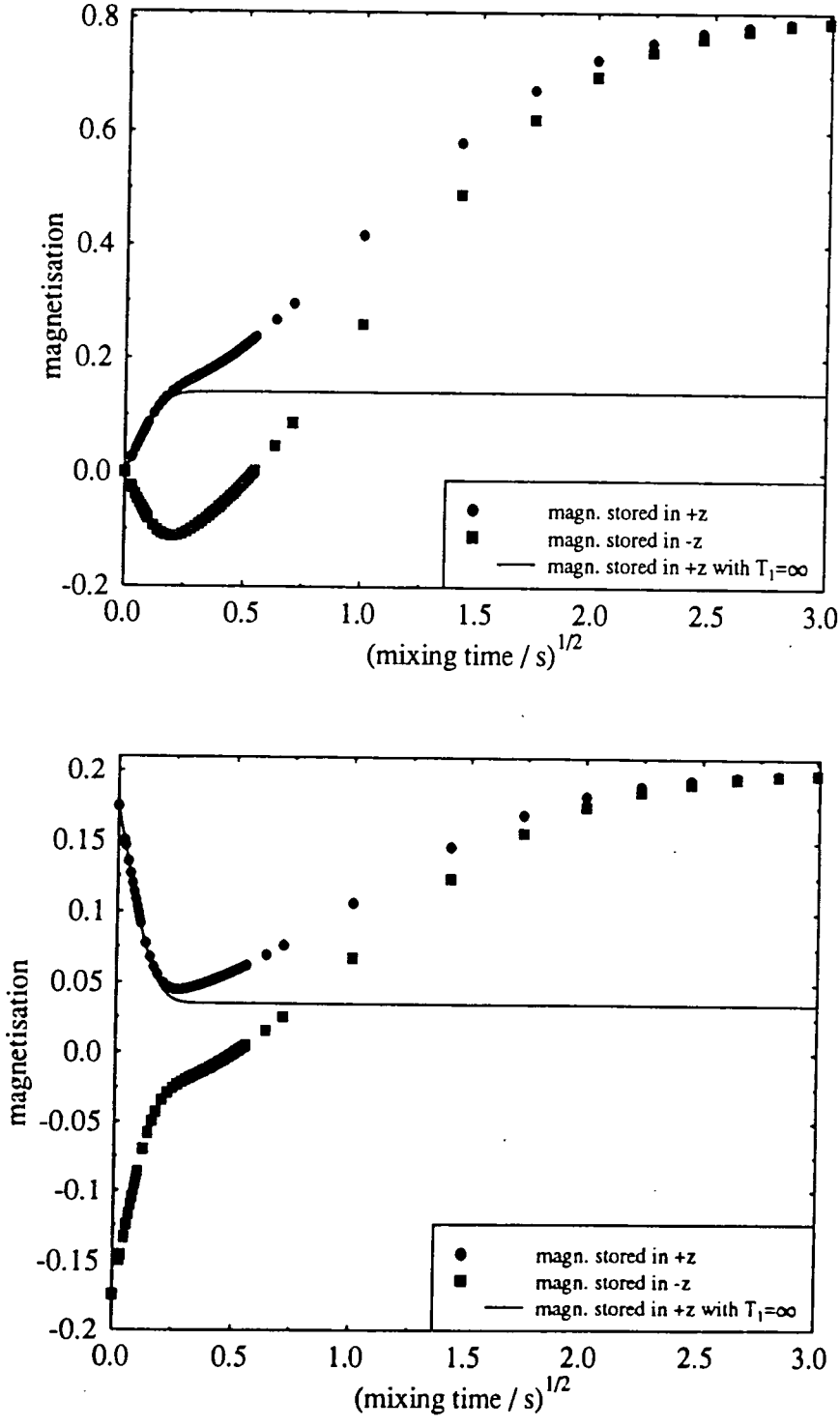

Fig. 5.29b Spin-diffusion simulation of a heterogeneous system (20% mobile 80% rigid)
intrinsic T_1's: T_1(mobile): 0.5 s, T_1(rigid): 5.0 s, D: $6.1 \cdot 10^{-17}$ $m^2 s^{-1}$
top: rigid region, bottom: mobile region

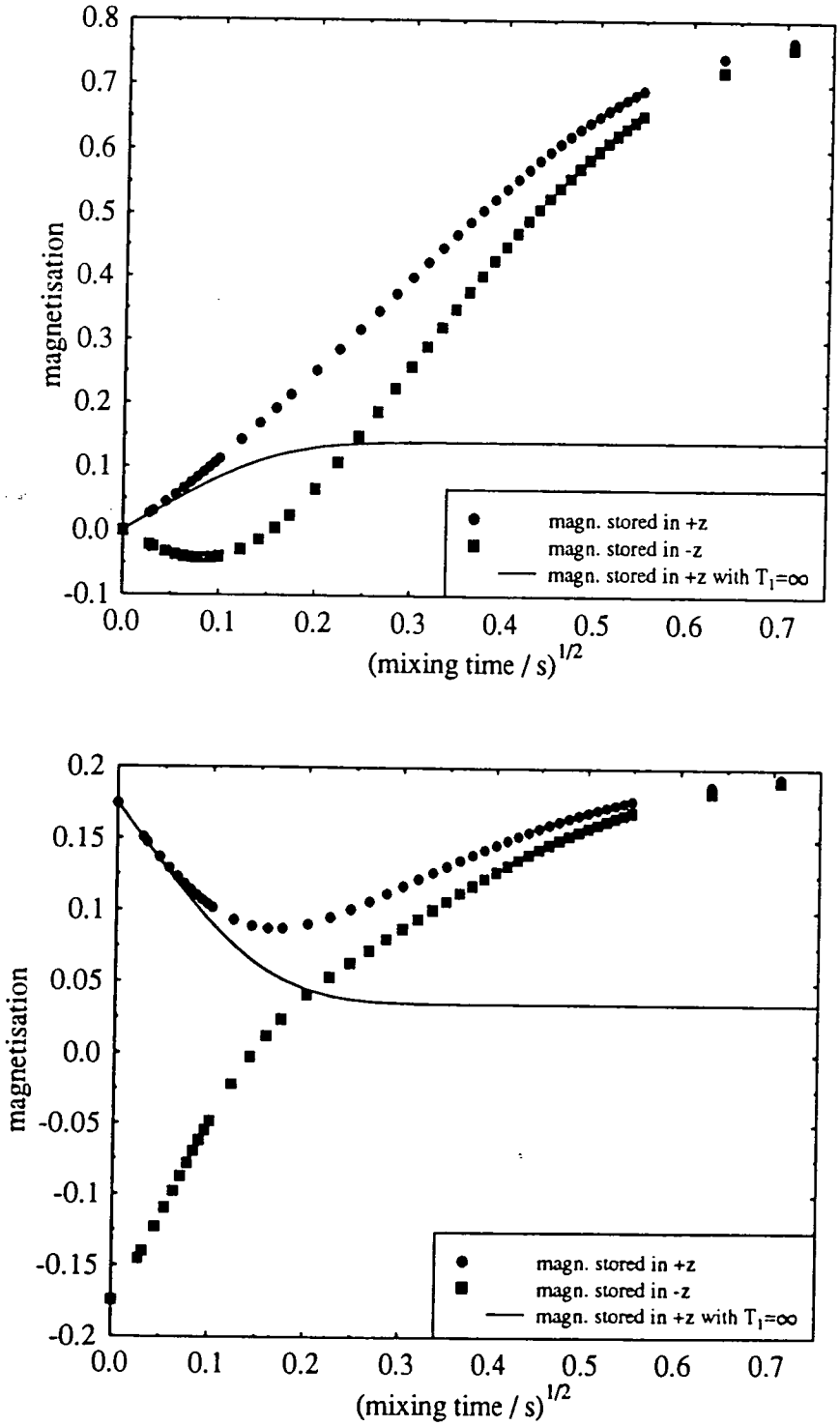

Fig. 5.29c Spin-diffusion simulation of a heterogeneous system (20% mobile, 80% rigid) intrinsic T_1's: T_1(mobile): 0.05 s, T_1(rigid): 0.3 s, D(mobile): $6.1 \cdot 10^{-17}$ $m^2 s^{-1}$
top: rigid region, bottom: mobile region

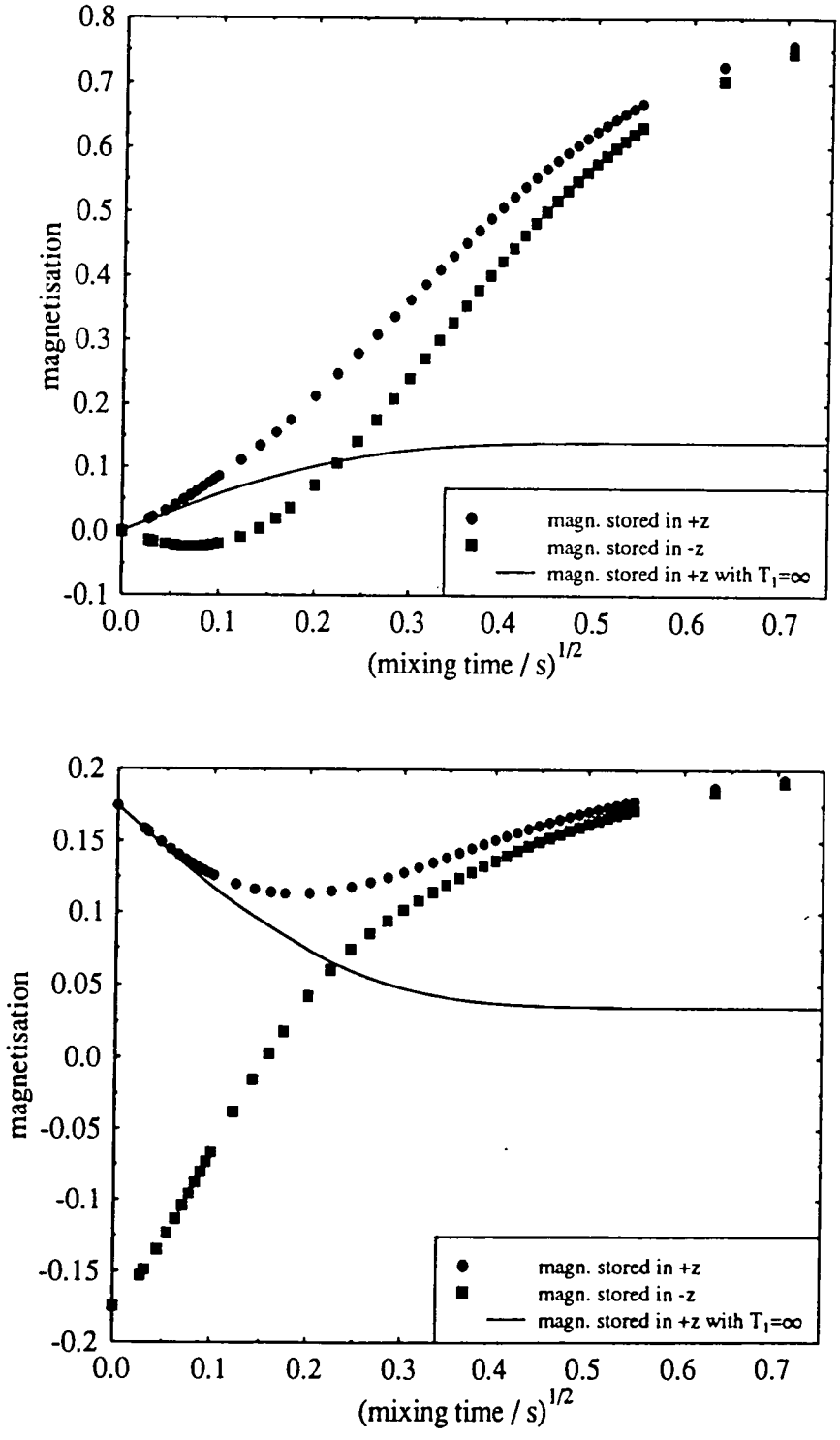

Fig. 5.29d Spin-diffusion simulation of a heterogeneous system (20% mobile, 80% rigid)
intrinsic T_1's: T_1(mobile): 0.05 s, T_1(rigid): 0.3 s, D(mobile): $2.1 \cdot 10^{-11}$ $m^2 s^{-1}$
top: rigid region, bottom: mobile region

regime where $l_2^2/D_2\,T_{1,2} << l_1^2/D_1\,T_{1,1} < 1$, which suggests that the two regions are effectively coupled by spin-diffusion.

As discussed in the last section, the simple phase-alternation cannot work because of the exponential (or in general non-linear) nature of the spin-lattice relaxation process. The graphical representation of the T_1-minimisation in figure 5.30a and 5.30c+d shows that after 20 ms mixing time the phase-alternation technique considerably deviates from the reference-curve without any spin-lattice relaxation contribution (even in the case of uniform T_1). Figure 5.30b illustrates that this effect becomes more dramatic with decreasing spin-lattice relaxation times. Here the population-weighted average spin-lattice relaxation has to be considered, because each intrinsic relaxation time is influenced by the spin-diffusion process. With a shorter spin-lattice relaxation time, the T_1-profile becomes steeper and consequently there is more magnetisation relaxing in a given time interval if it is stored in the -z-direction after the second 90°-pulse than if it is stored in the +z-direction. This explains the increasing deviation of the data from the reference curve with a decreasing T_1.

The situation becomes less obvious for the other two minimisation techniques. In order to understand why these techniques cancel out the spin-lattice contribution in the case of a uniform T_1-relaxation time in the heterogeneous system (figure 5.30a), but only reduce it if the different regions have different intrinsic T_1-relaxation times (figures 5.30b to 5.30d) one has to consider the traces of

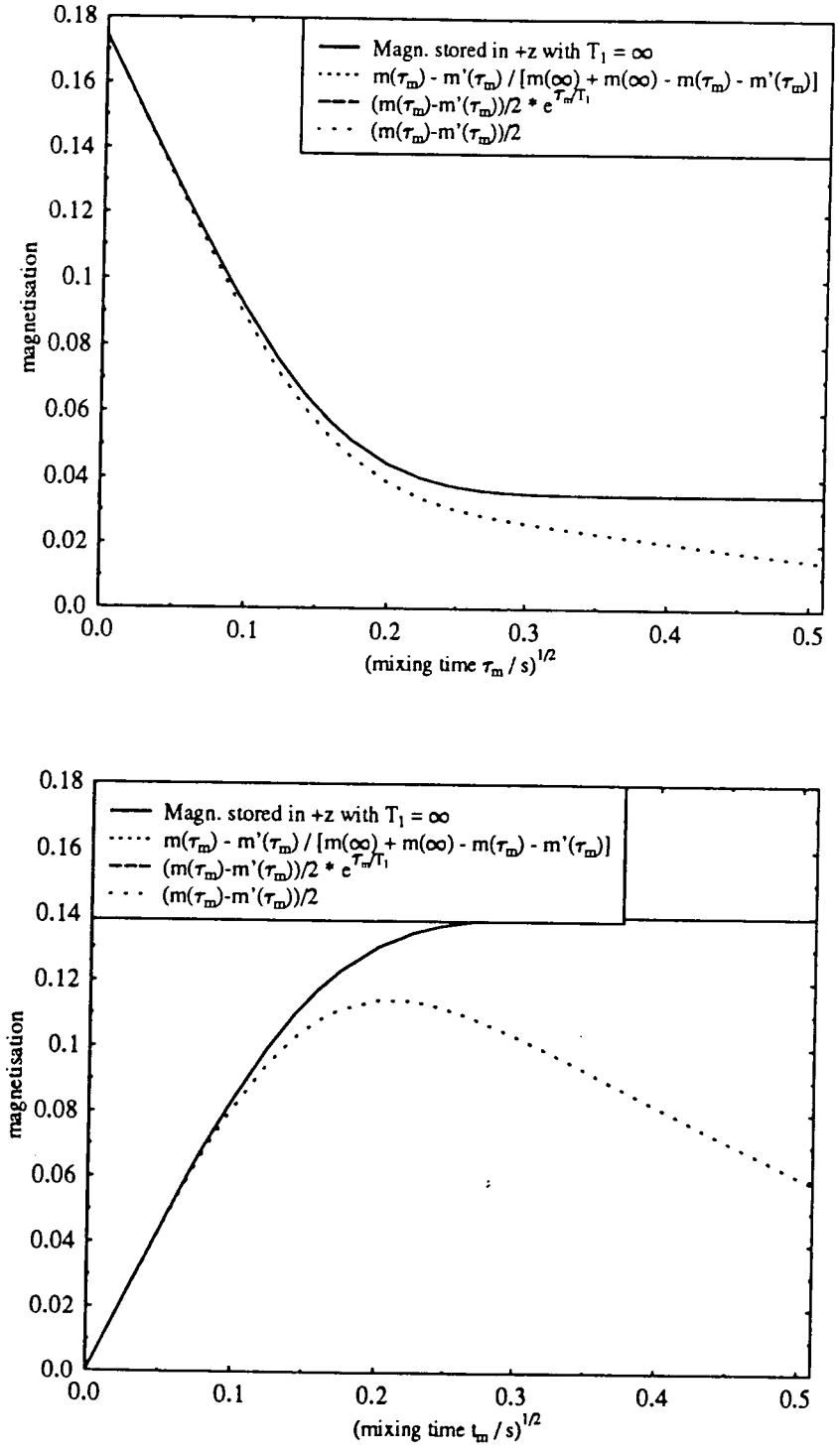

Fig. 5.30a Spin-diffusion simulation of a heterogeneous system (20% mobile, 80% rigid) intrinsic T_1's: T_1(mobile): 0.3 s, T_1(rigid): 0.3 s, D(mobile): $6.1 \cdot 10^{-17}$ $m^2 s^{-1}$
top: mobile region, bottom: rigid region (note that two of the minimisation traces are indistinguishable from the reference curve)

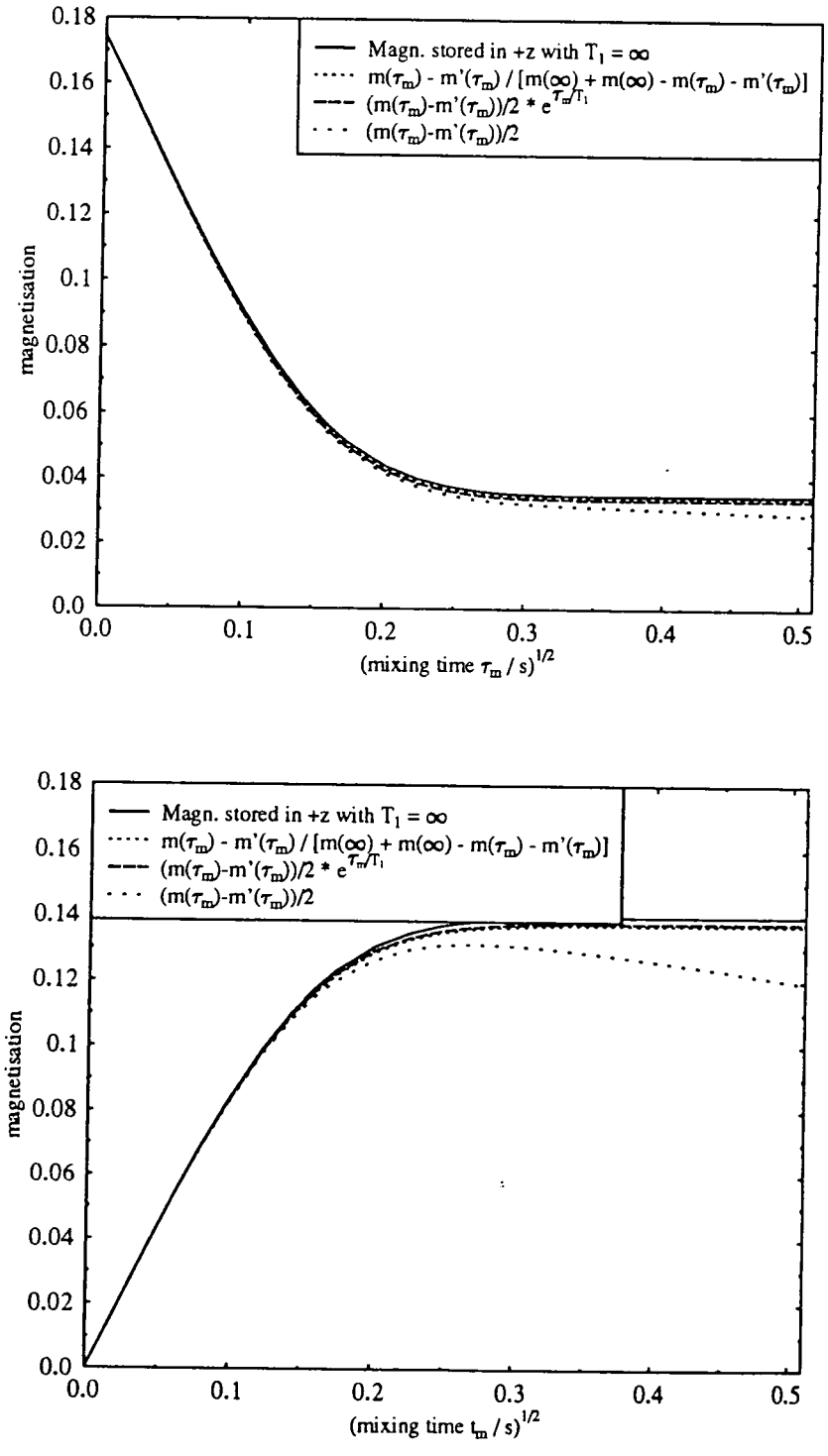

Fig. 5.30b Spin-diffusion simulation of a heterogeneous system (20% mobile, 80% rigid)
intrinsic T_1's: T_1(mobile): 0.5 s, T_1(rigid): 5.0 s, D(mobile): $6.1 \cdot 10^{-17}$ $m^2 s^{-1}$
top: mobile region, bottom: rigid region

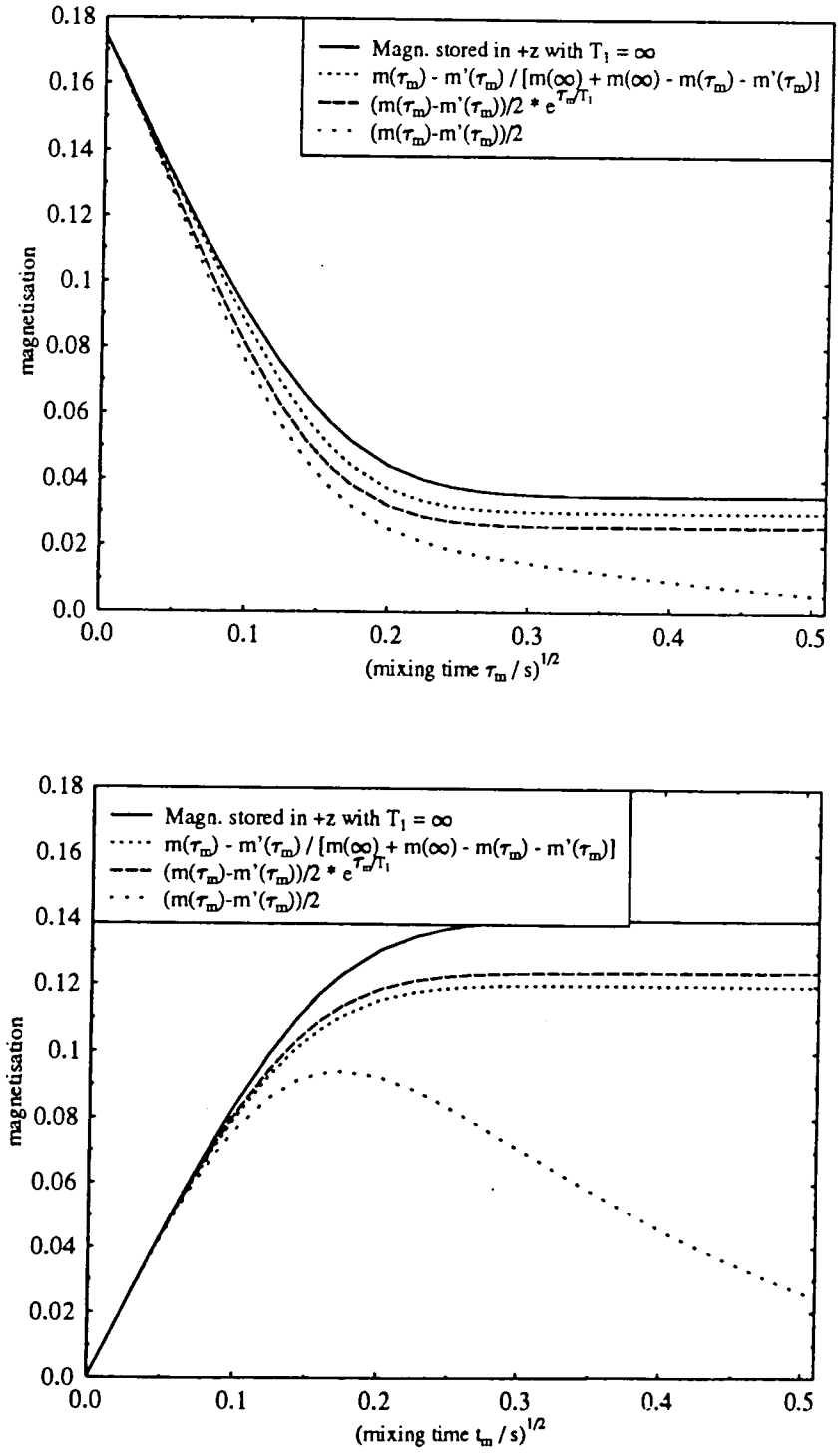

Fig. 5.30c Spin-diffusion simulation of a heterogeneous system (20% mobile, 80% rigid)
intrinsic T_1's: T_1(mobile): 0.05 s, T_1(rigid): 0.3 s, D(mobile): $6.1 \cdot 10^{-17}$ m^{2}s^{-1}
top: mobile region, bottom: rigid region

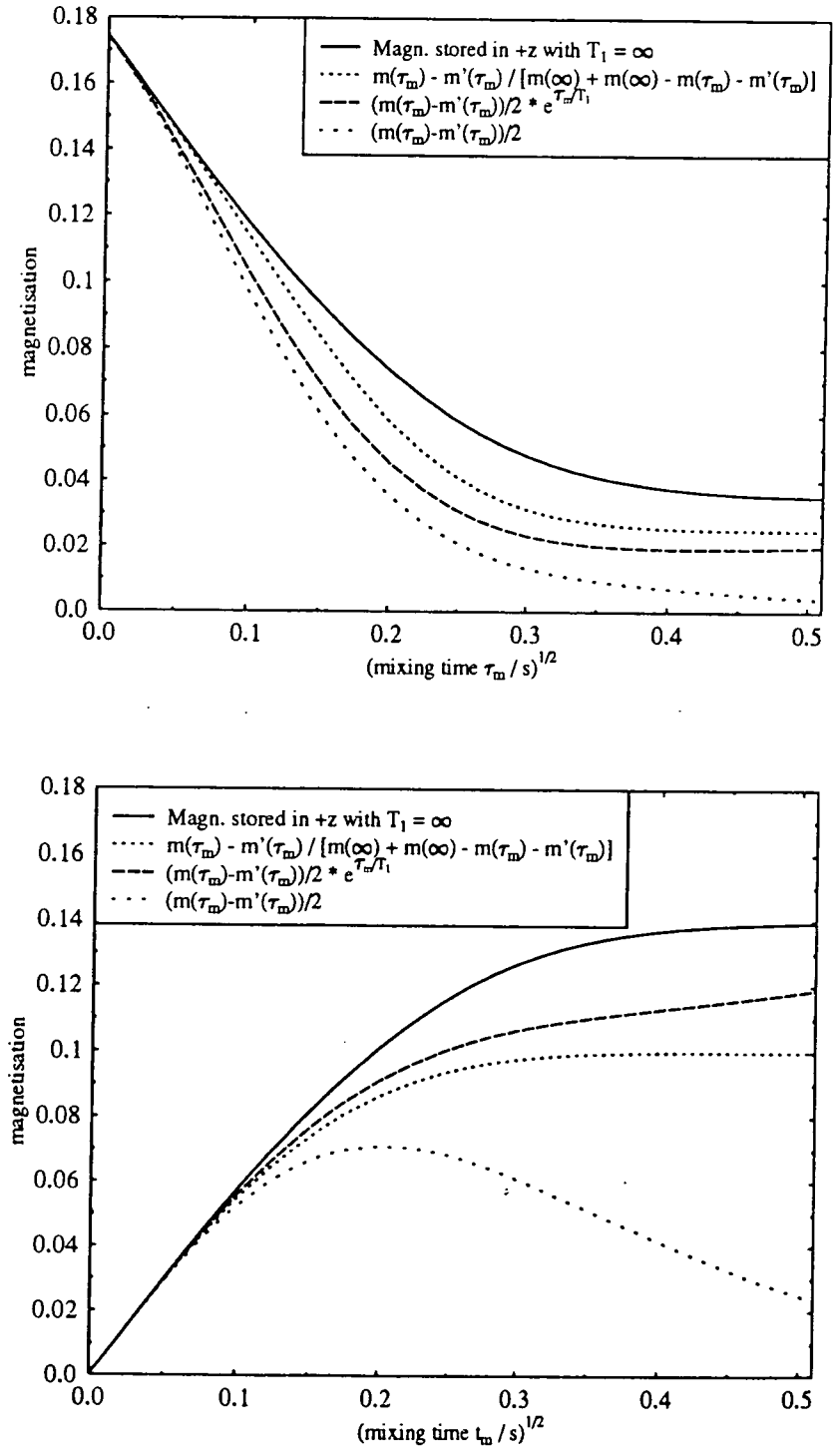

Fig. 5.30d Spin-diffusion simulation of a heterogeneous system (20% mobile, 80% rigid) intrinsic T_1's: T_1(mobile): 0.05 s, T_1(rigid): 0.3 s, D(mobile): $2.1 \cdot 10^{-11}$ $m^2 s^{-1}$
top: mobile region, bottom: rigid region

the Goldman-Shen experiment with and without spin-lattice influence (figures 5.29a to 5.29d) and the equation which describes the magnetisation time-dependence. In figures 5.29a and 5.29c+d the systems are in the regime $l_1^2/D_1\,T_{1,1} > 1 > l_2^2/D_2\,T_{1,2}$, which means that the spin-diffusion properties are influenced by spin-relaxation. The data which represents the time dependence of these systems deviate after a couple of milliseconds from the reference curve, long before they reach the spin-diffusional equilibrium. The spin-relaxation-influenced data in the system represented in figure 5.29b, however, reveal a good agreement with the reference curve in the time regime until the spin-diffusional equilibrium is established. As the experiment proceeds, spin-lattice relaxation brings the heterogeneous system to its thermodynamical equilibrium. Note that this system is in a regime $l_2^2/D_2\,T_{1,2} << l_1^2/D_1\,T_{1,1} < 1$, which means that T_1 is longer than it takes to reach the spin-diffusional equilibrium. Exactly for this system the corrections work quite accurately as figure 5.30b visualises, whereas they fail for the other two systems with a non-uniform T_1 in the two regions.

The simulations of the Goldman-Shen experiment demonstrate that data correction, based on an exponential multiplication for a heterogeneous system with a non-uniform T_1 in the two regions, only corrects the spin-lattice relaxation influence when the system is in a regime $l_2^2/D_2\,T_{1,2} \leq l_1^2/D_1\,T_{1,1} < 1$, i.e. when the two intrinsic spin-lattice relaxation times are longer than the time needed to reach the spin-diffusional equilibrium. This

signifies that data correction of this type cannot separate spin-diffusion and spin-lattice relaxation if the system is in a regime $l_2^2/D_2\ T_{1,2} < 1 << l_1^2/D_1\ T_{1,1}$, i.e. these two processes are coupled.

The case of a uniform T_1 within the two-region system is only interesting for academic reasons. However, as figure 5.30a demonstrates, another crucial point where the corrections fail is for the presence of two different intrinsic spin-lattice relaxation times in the two regions. It is interesting to note that although the system depicted in figure 5.30a is in a regime $l_2^2/D_2\ T_{1,2} < 1 < l_1^2/D_1\ T_{1,1}$, the correction modes work absolutely perfectly, i.e. T_1 and spin-diffusion are non-coupled processes if the two regions consist of a uniform spin-lattice relaxation. This point is readily understandable considering equation 5.11 which describes the time behaviour of the magnetisation in the two regions. For the case of a uniform T_1 the diffusional term and the relaxation term remain as a sum of the two processes. Hence, there are two separate processes which may be treated as such.

This consideration sets a milestone for any T_1 minimisation techniques, because it demonstrates that when spin-lattice relaxation is in a time-regime where the spin-diffusional equilibrium has not been reached, the correction cannot separate the two processes, leaving always a point of uncertainty in the data.

However, when the intrinsic spin-lattice relaxation is longer than it takes to reach the spin-diffusional equilibrium, data correction is nonessential, because the

experimental "raw-data" from the Goldman-Shen experiment may be used to examine the domain-sizes as originally described by Cheung and Gerstein [30].

In the next section a simple solid-state NMR technique will be presented which overcomes the spin-lattice relaxation problem in the Goldman-Shen experiment. It will determine the intrinsic T_1 and the domain sizes of a heterogeneous system directly from the experimental data obtained by the Goldman-Shen experiment.

5.5 Determination of the Intrinsic Spin-Lattice Relaxation Times, the Domain-Sizes and the Morphology of the NYRIM System

5.5.1 Introduction

The domain size in polymer-blends and block-copolymers is an important parameter in polymer science. The intimacy of mixing and the phase structure are important factors which may determine many mechanical properties of polymers [25,26]. Electron microscopy in its various forms is well suited for the investigation of morphological structures in polymer blends and block-copolymers with domain sizes above 20 nm, but cannot reliably resolve structures smaller that 10 nm [27]. X-ray scattering demands ordered structures in order to obtain well-resolved patterns. In solids NMR yields information on composition, molecular mobility and molecular order [28,29]. In addition, diffusion of proton magnetisation through the network of homonuclear dipolar couplings can be exploited to

investigate structures in the range of tens of nanometers [12,14,18,30-34].

In section 5.4 the problem of spin-lattice relaxation during spin-diffusion measurements was explained. In the following sections a solution will be presented to overcome the spin-lattice relaxation problem. The original Goldman-Shen experiment has been carried out using a custom-build static 60 MHz single-channel proton-spectrometer (WRAC). The domain parameters derived from this technique will be compared with those obtained by small-angle X-ray scattering (SAXS).

5.5.2 Theory of the Morphology in Semicrystalline Polymers

A number of distinct morphological units have been identified during the crystallisation of polymers from the melt.

Crystallites: In an X-ray pattern produced by a semicrystalline polymer, the discrete maxima arise from scattering by small regions of three-dimensional order, which are called crystallites. They are formed in the melt by diffusion of molecules, or sections of molecules, into packed ordered arrays which then crystallise. The sizes of the crystallites are small compared to the size of a fully-extended polymer chain, but they are also found to be independent of the molar mass and rarely exceed 1 to 100 nm. As a result, various portions of one chain may become incorporated in more than one crystallite during growth, thereby imposing a strain on the polymer which retards the process of crystallite formation. This will

introduce imperfections in the crystallites, which continue growing until the strains imposed by surrounding crystallites eventually stop further enlargement. Thus a matrix of ordered regions with disordered interfacial areas is formed. The crystallisation from the melt is described reasonably well by the *solidification model* proposed by Dettenmaier, Fischer and Stamm [35]. The crystallisation is believed to take place by the straightening of sections of the polymer coils followed by alignment of these sequences in regular arrays to form the lamellar structure. This precludes the need for the extensive, long-range, diffusion of the chain through a highly viscous medium that would be necessary if a regular chain-folded structure was to be constructed. The solidification model shows that the chains can be incorporated into the basic lamellar form with the minimum amount of movement and that there will be extensive meandering of chains between the lamellae, thus forming the interfacial amorphous regions. Examination of thin sections of semicrystalline polymers reveals that the crystallites themselves are not arranged randomly, but form regular birefringent structures with circular symmetry. These structures, which exhibit a characteristic Maltese-cross optical extinction pattern, are called *spherulites*. A study of the fine structure of a spherulite shows that it is built up of fibrous sub-units. Growth takes place by formation of fibrils which spread outwards from the nucleus in bundles, into the surrounding amorphous phase. Although the fibrils are arranged radially, the molecular chain lies at right angles to the

fibril axis. This led to the suggestion that the fine structure is created from a series of lamellar crystals winding helically along the spherulite radius. In between the branches of the fibrils are amorphous areas and these, along with the amorphous interfacial regions between the lamellae, make up the disordered content of the semicrystalline polymer. This model is illustrated in figure 5.31.

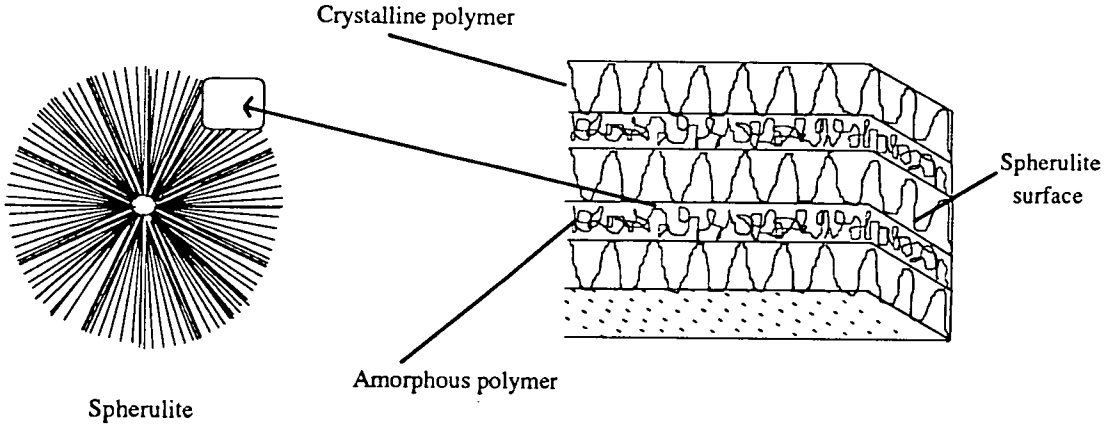

Figure 5.31 Model of a spherulite grown from the melt

5.5.3 Experimental NMR-Technique to Determine the Domain Sizes in NYRIM

In general, spin-diffusion experiments require the selection of magnetisation in one of the constituents of the system under investigation. The differences of the transversal relaxation times (T_2) [19,20,23] were therefore used for this purpose. Since these are due to differences in mobility of the components, they can be small for blends mixed on a molecular scale. This special case was dealt with by Schmidt-Rohr [36] using a chemical

shift filter. This technique needs, however, at least one separated line of one of the components for the selection of the magnetisation and one separated line of the other component for the evaluation of inter-domain spin-diffusion. However, NYRIM fortunately consists of two regions, in terms of rigid and mobile, with a significant difference in spin-spin relaxation times.

Another problem is the choice of how to record the data-points. In principle there are two possibilities:

1. direct observation of the proton magnetisation
2. indirect observation by performing a CP/MAS experiment in which the proton magnetisation is transferred to ^{13}C-spins and their signal is recorded

Both methods have their advantages and disadvantages. A direct detection of the proton signal is often difficult because of the homonuclear dipolar broadening of the spectrum. On the other hand, the proton spectrum is very quickly available, so that time-consuming CP/MAS techniques are avoided. However, using ^{13}C-spins as a probe for the proton magnetisation in a CP/MAS-variant takes advantage of the larger scale of the ^{13}C- with respect to the ^{1}H-chemical shift differences. This study will be restricted to the first technique, the direct detection of the proton magnetisation.

Instead of obtaining the time-dependence of the proton magnetisation from the spectrum, the free-induction decay (FID) is used for that purpose. NYRIM has two constituents, the rigid polyamide, built from amorphous

and crystalline polyamide which have the same T_2, and the mobile polyether. Van Vleck [37] first mentioned that the FID of crystalline material can be described by a kind of Gaussian function. Abragam [19] discussed this matter in more detail and found that the FID of a mobile material is better described by a Exponential function. For polymers especially, mobile means that the glass-transition temperature T_g must be much smaller than the temperature T at which the measurement is carried out. To prove if these models apply to the NYRIM system a simple 60 MHz ^{1}H-FID has been recorded and analysed for the block-copolymers with known composition. The data acquisition has been carried out on the WRAC. The acquisition time was 0.512 *ms* and contained 512 data-points with a dwell time of 1 μs. The recycle delay is related to the appropriate T_1 of the material under investigation. The results of these experiments are summarised in figures 5.32 to 5.37 and table 5.7. The analytical functions used to fit the FID were

$$M(t) = a \exp\left[-\left(\frac{t}{T_2}\right)^2\right] \frac{\sin bt}{bt} \qquad (5.15)$$

(referred to as an Abragamian Function)

and

$$M(t) = a \exp\left(-\frac{t}{T_2}\right) \qquad (5.16)$$

(referred to as a Exponential Function)

were a : population at time t=0

M(t) : magnetisation at time t

T_2 : time-constant of the free-induction decay

b : parameter in frequency units

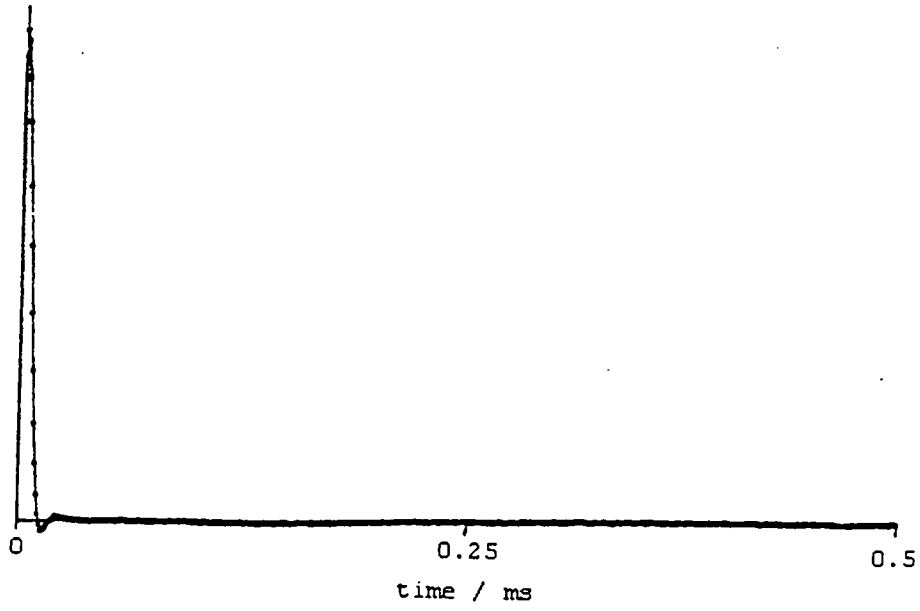

Figure 5.32 ^{1}H-FID of nylon-6 (static, 60 MHz)

Figure 5.33 ^{1}H-FID of nylon-6 + 10% prepolymer (static, 60 MHz)

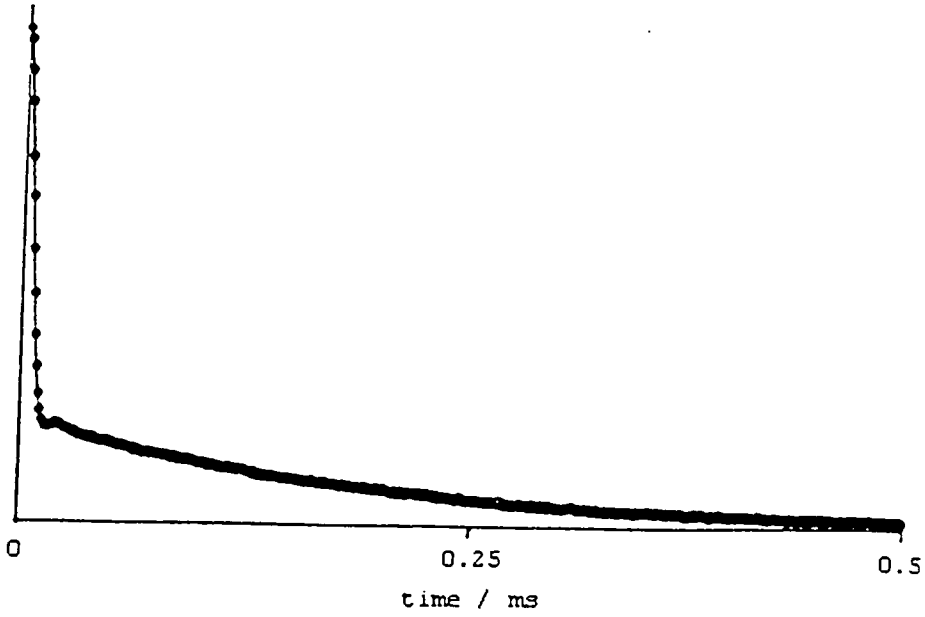

Figure 5.34 ^{1}H-FID of nylon-6 + 20% prepolymer (static, 60 MHz)

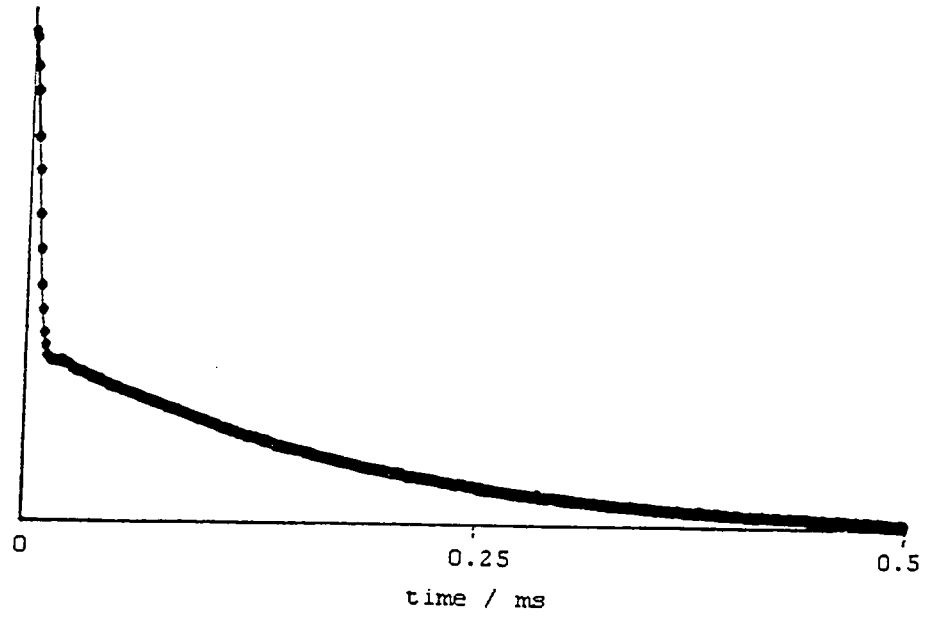

Figure 5.35 ^{1}H-FID of nylon-6 + 30% prepolymer (static, 60 MHz)

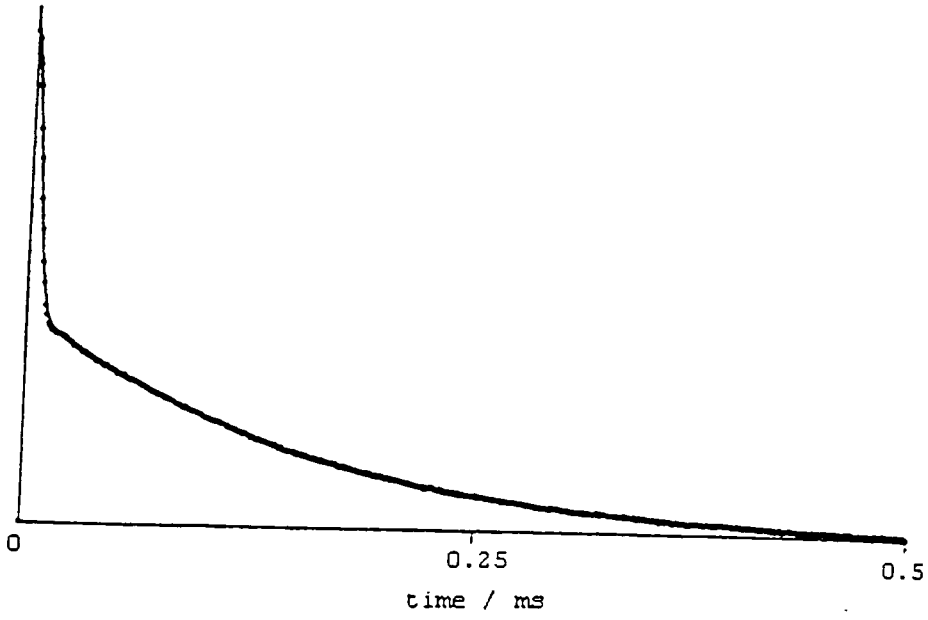

Figure 5.36 ^{1}H-FID of nylon-6 + 40% prepolymer (static, 60 MHz)

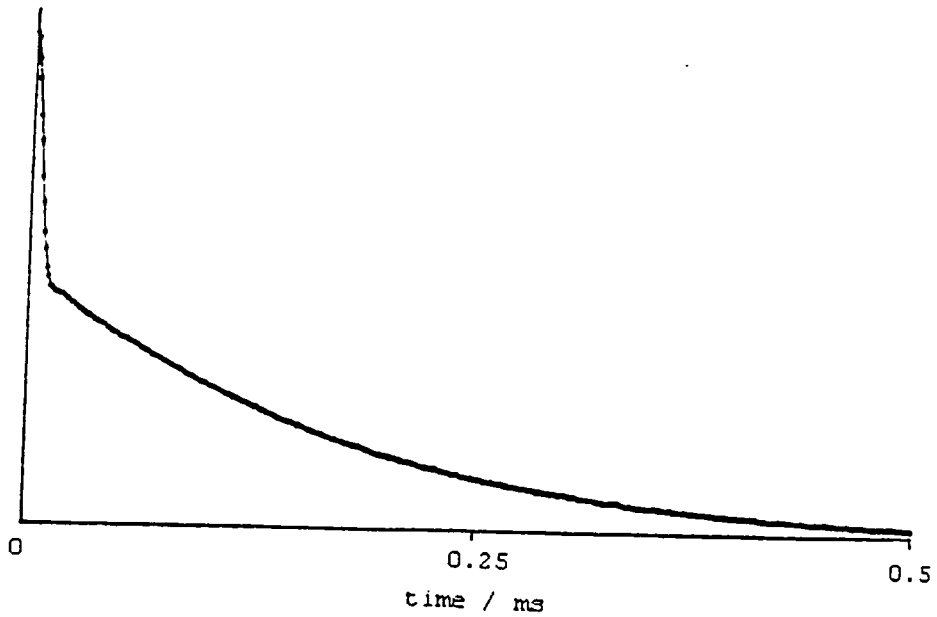

Figure 5.37 ^{1}H-FID of nylon-6 + 50% prepolymer (static, 60 MHz)

Composition	Function	POP / %	T_2 / µs	b / s^{-1}
Nylon-6	Abragamian	95.0	18.0	21000
	Exponential	5.0	66.0	
NBC10	Abragamian	90.8	18.2	20000
	Exponential	9.2	246.9	
NBC15	Abragamian	84.6	17.4	18300
	Exponential	15.4	217.0	
NBC20	Abragamian	78.4	18.1	19600
	Exponential	21.6	358.0	
NBC25	Abragamian	73.6	18.0	19600
	Exponential	26.4	340.8	
NBC30	Abragamian	62.7	19.3	21000
	Exponential	37.3	356.0	
NBC40	Abragamian	55.8	14.3	19600
	Exponential	44.2	310.9	
NBC50	Abragamian	46.5	19.4	21400
	Exponential	53.5	349.6	

Table 5.9 Determination of the composition by line-shape analysis of the ^{1}H-free-induction decay

Although the physical meaning of b (and consequently the Abragamian function) is not fully understood, it describes the line-shape of a strongly dipolar-coupled system much better then a pure gaussian function. The little bump seen in the nylon-6 FID most likely arises from strong dipolar coupling effects which are more pronounced in highly ordered systems but still visible in less ordered ones. Such kind of observations were already mentioned by Abragam [19]. The results in table 5.9 are in a remarkably good agreement with the composition of the block-copolymer. The deviations are believed to be due to

incomplete reaction and errors in balancing the adducts for the polymerisation. The time constants of the analytical fit show a fairly constant behaviour throughout the composition range. This indicates the stability of the technique, but it also confirms that within the range of composition under investigation, the system is heterogeneous and phase-separated.

Two other experiments were carried out to check if the assignment of the line-shape to the different phases is correct. Firstly a so-called CP/MAS delayed-contact experiment was implemented on the Bruker CXP200 spectrometer. It contains the normal CP pulse sequence, but after the 90°-pulse on the proton channel a variable delay time τ_d was introduced in order to dephase the proton magnetisation with the shorter relaxation time constant (see figure 5.38). The delay times were varied from 1 μs to 20 μs. After the delay-time the remaining proton magnetisation is cross-polarised to the carbon-spins and the ^{13}C-spectrum was recorded. The resulting ^{13}C-spectrum (figure 5.39 and 5.40) directly shows that the polyether part of the block-copolymer is hardly affected by the delay time and therefore has the longer relaxation time.

Hence, the assignment that was made before is considered to be correct. It also shows that the relaxation behaviour is the same for both the crystalline and the amorphous part of polyamide-6, because the signals of both parts are vanishing at the same rate. (Note that figures 5.39 and 5.40 have been presented by the author for his diploma degree).

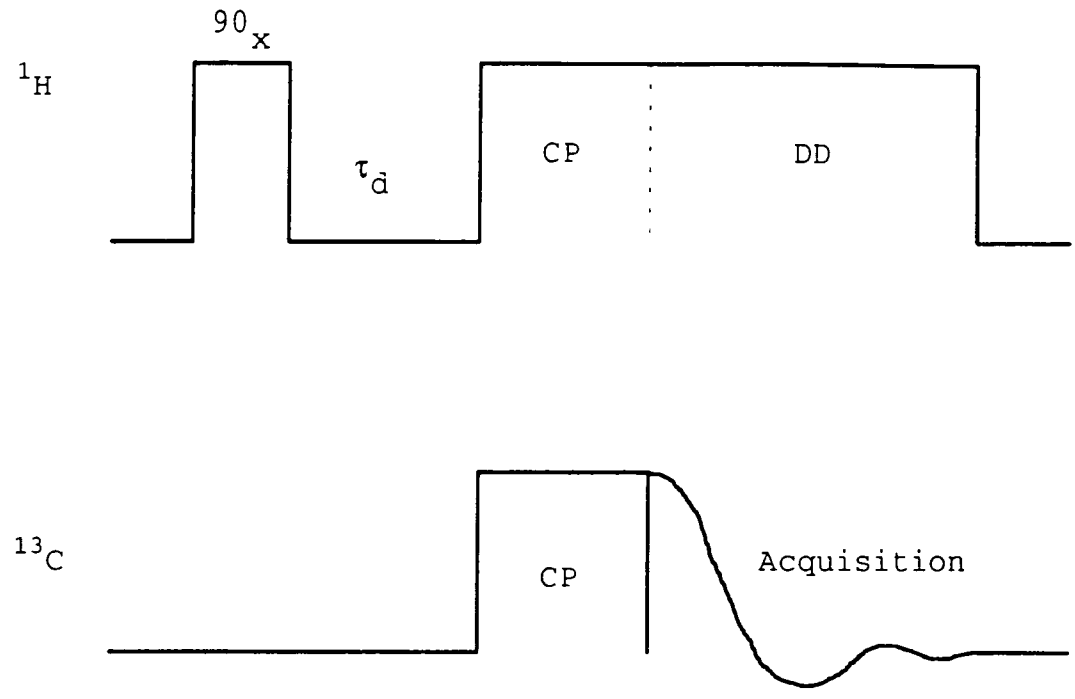

Fig. 5.38 CP/MAS variable-delay pulse sequence

Another, more-advanced technique uses a 2D-CP/MAS experiment to assign the proton line-shape to the different constituents in NYRIM. The experiment is called *WISE* (WIdeline SEparation) and was introduced by Schmidt-Rohr and Spiess [38]. It allows the correlation of mobility and structure in organic solids. Differences of molecular dynamics are probed by ^{1}H wideline shapes, which are separated in the second dimension by ^{13}C chemical shifts. The pulse sequence and principle of the WISE experiment is displayed in figure 5.41. It starts with a 90° pulse on the protons, followed by an incremented proton evolution period t_1. The remaining magnetisation of the protons after the evolution period is then transferred

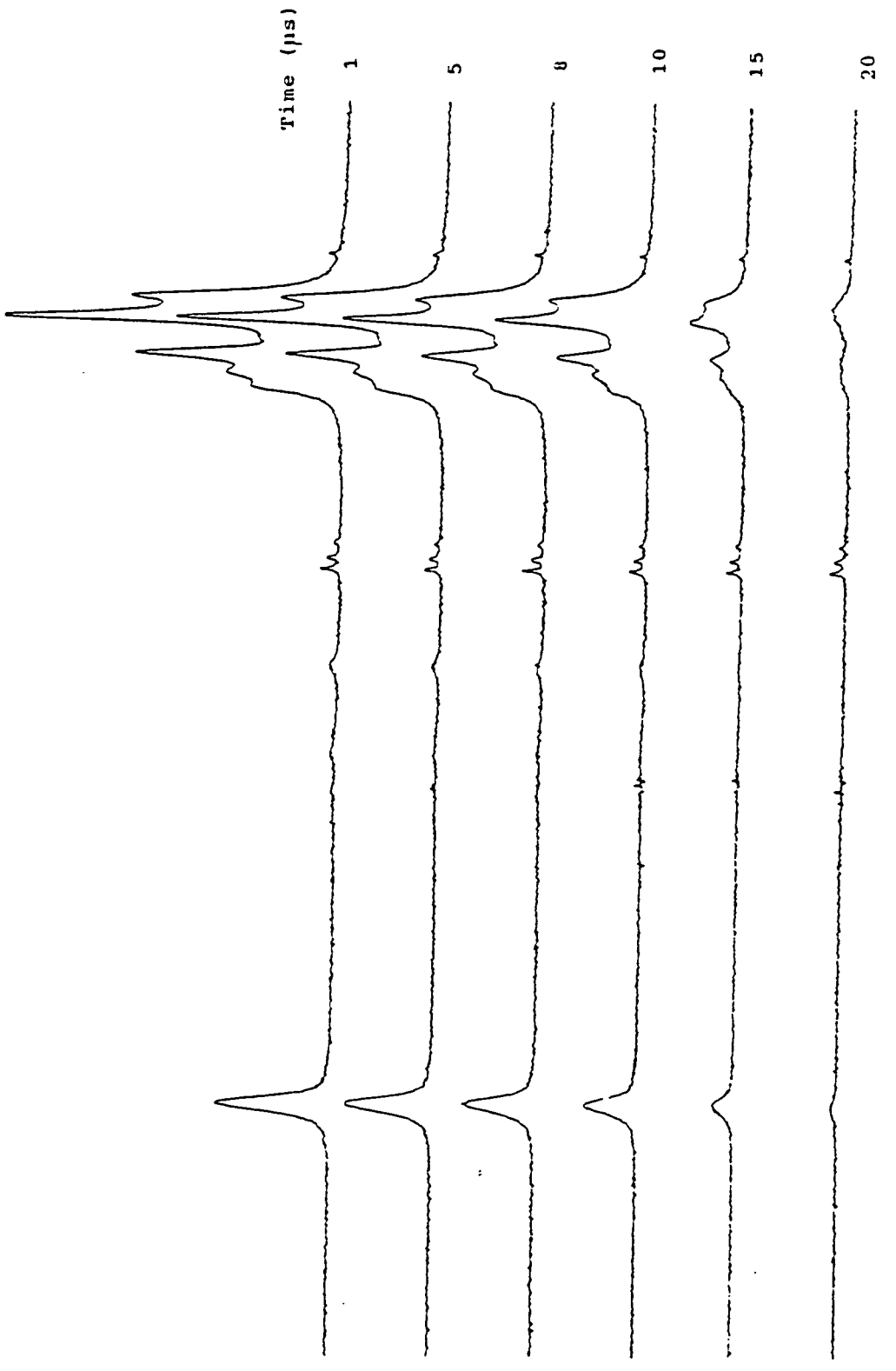

Figure 5.39 13C-CP/MAS variable-delay spectrum of quenched nylon-6 + 20% prepolymer

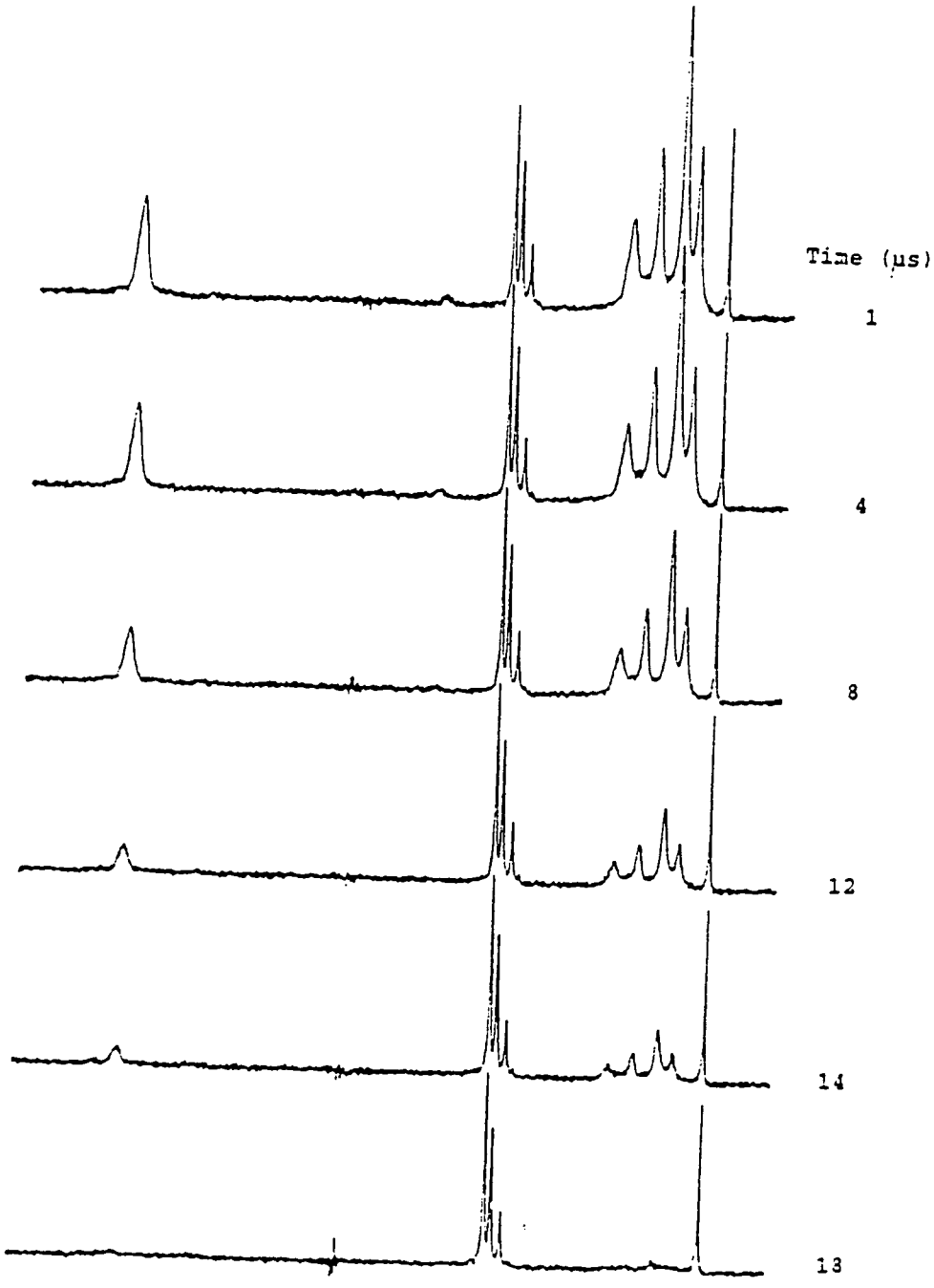

Figure 5.40 13C-CP/MAS variable delay spectrum of nylon-6 + 40% prepolymer

to the carbon spins by means of Hartmann-Hahn cross-polarisation, and is finally probed in the t_2 domain of the experiment.

For each of the resolved signals, corresponding to certain molecular moieties, the molecular mobility is characterised by the line-shape parallel to the ^1H-axis. The narrow lines indicate high segmental mobility, whereas the broad lines point to low segmental mobility. To illustrate the technique, figure 5.42 displays a WISE spectrum for NBC50. At room temperature, pure nylon-6 is below its glass-transition temperature T_g. This is reflected in the wide lines in the ^1H dimension, corresponding to a fast decay of the t_1 amplitude-modulation of the corresponding ^{13}C lines. In contrast, PPO is about 80 K above its T_g and therefore highly mobile. This is reflected in the small ^1H line width of the PPO resonances (for the ^{13}C chemical shift assignment, refer to chapter 4), which is equivalent to a slow decay of these signal-components with increasing t_1. To probe the relative spatial position of components with different mobilities, ^{1}H spin-diffusion can be introduced into the experiment. For this purpose, the ^{1}H magnetisation remaining after the evolution period is flipped to the z-axis for the subsequent mixing period of duration t_m (figure 5.43). If regions with different mobilities are sufficiently close in space they exchange ^1H-magnetisation by spin-diffusion during the mixing period. This results in a transfer of t_1 modulation between slow and fast decaying ^1H components, equivalent to a transfer of ^1H line-shape in the ω_1 frequency domain. This is best

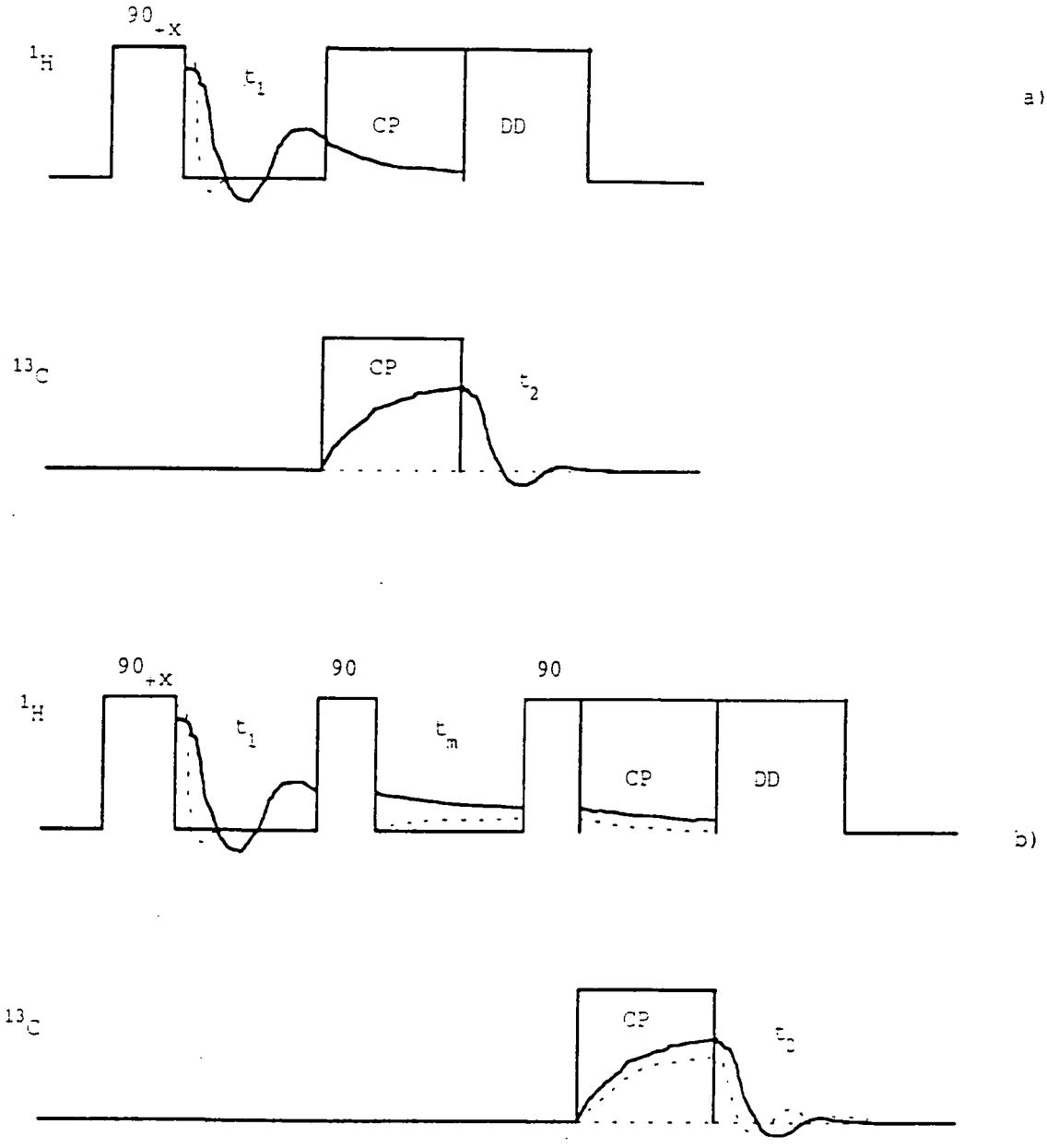

Figure 5.41 WISE pulse-sequence

a) without spin-diffusion

b) with spin-diffusion

understood in the limit of complete spatial equilibrium of ^{1}H magnetisation during very long mixing times. Then all ^{13}C signals are modulated by the same ^{1}H decay.

Hence, they exhibit the same ^1H line-shape along ω_1. Thus, the broad signals of the rigid nylon-6 in the absence of spin-diffusion (see figure 5.42) acquire, through the spin-diffusion, narrow ^1H peak contributions of the mobile PPO segments as seen in figure 5.43. Figures 5.42 and 5.43 confirm the previous result that the broad-signal (short relaxation time) correlates with the polyamide carbons, whereas the narrow signals correlate to the polyether signals.

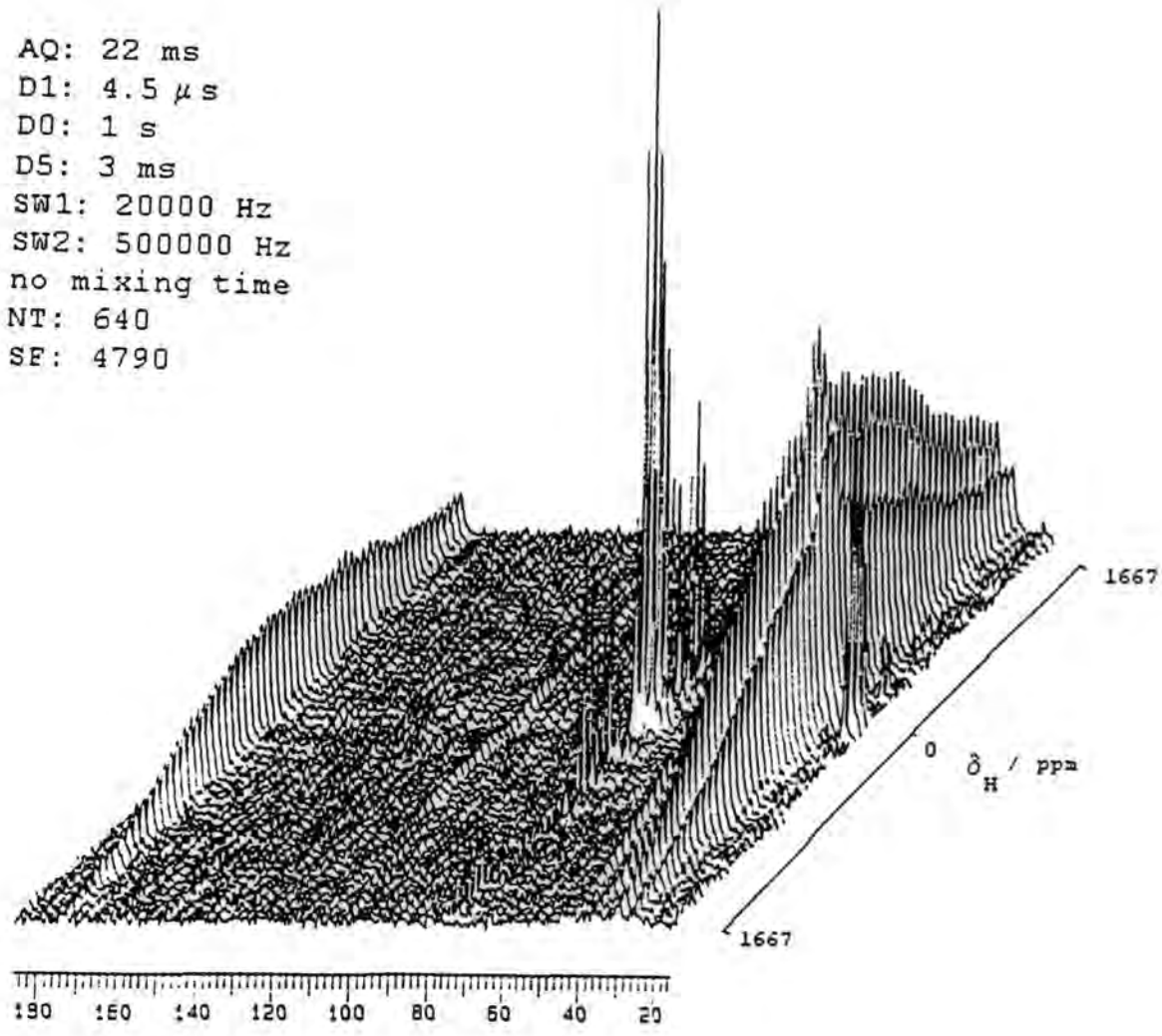

Figure 5.42 WISE-experiment of Nylon-6 + 50% Prepolymer with no mixing time (pulse sequence figure 5.41a)

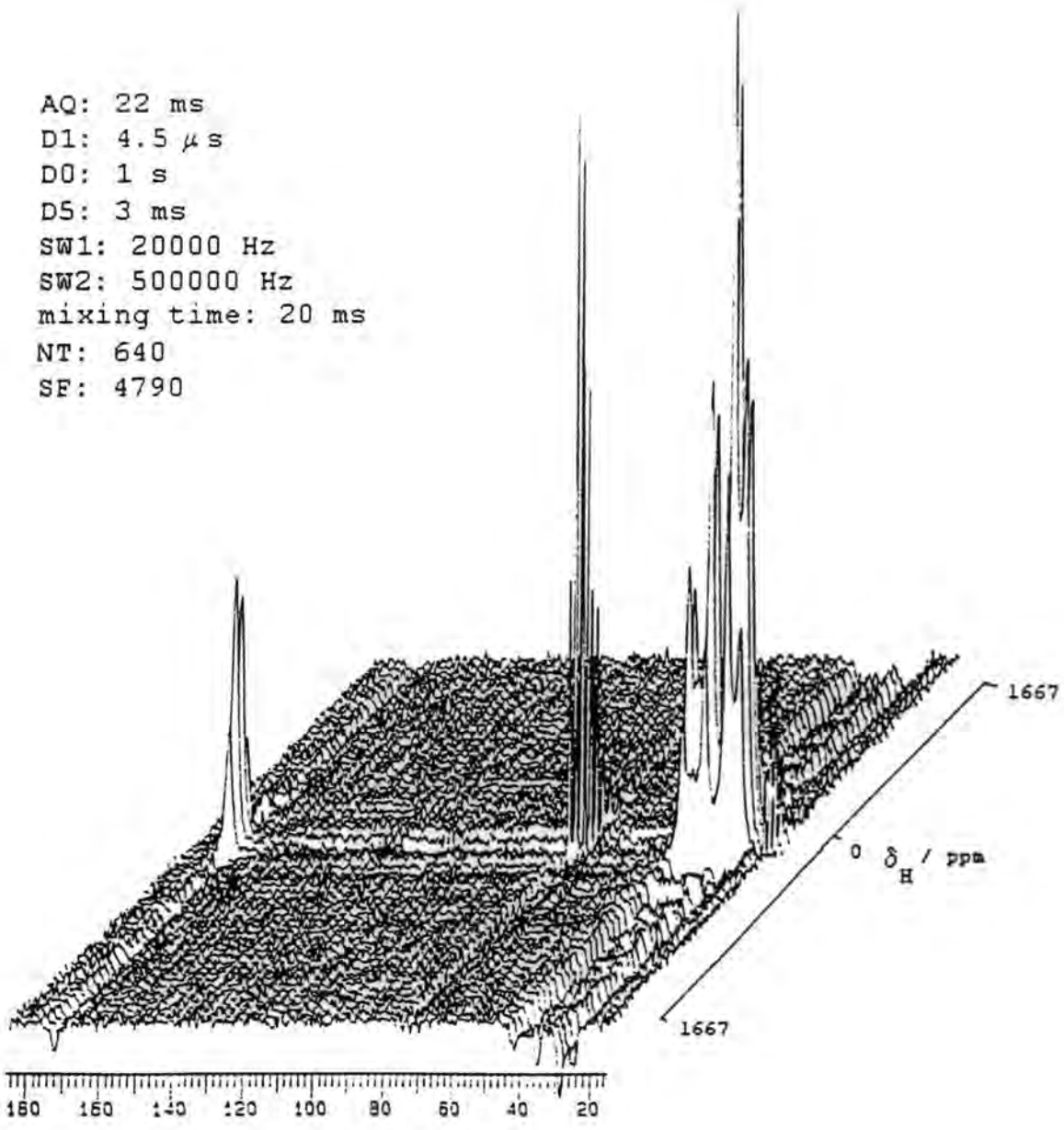

Figure 5.43 WISE-experiment of Nylon-6 + 50% Prepolymer with 20 ms mixing time (pulse sequence figure 5.41b)

The advantage of this technique is that it does not need any model to qualitatively explain the results but instead a direct interpretation of the spectrum is possible. Additionally figure 5.43 shows that spin-diffusion is effective between the polyamide and the polyether sites.

5.5.4 Data-modelling of the Goldman-Shen Experiment

A Goldman-Shen experiment has been carried out to obtain the time-dependence of the magnetisation during the mixing time. The appropriate dephasing time, which selects the magnetisation of the polyether-attached protons, was obtained from a separate experiment, in which after the 90°-pulse a dephasing time was introduced before recording the FID. This experiment showed that a 50 μs dephasing time is sufficient to dephase all the magnetisation of the polyamide protons. For the Goldman-Shen experiment, mixing times between 0 s and 0.5 s were used. In the first 100 μs more data-points were recorded because in that time-interval the experiment is governed by the spin-diffusion process, while at longer mixing times spin-relaxation determines the time-dependence of the magnetisation. The acquisition time was chosen to be 0.512 ms, represented by 512 points with a dwell time of 1 μs. The spin-diffusion coefficients were estimated by a technique introduced by Gerstein and co-workers [30,39]. It uses the fact that in a regular lattice, with lattice constant a, the spin-diffusion due to dipolar spin-flips is given by:

$$D = 0.13a^2\sqrt{M_2} \qquad (5.7)$$

where M_2 is the second moment of the NMR line-shape. For both Gaussian and Exponential decay $(M_2)^{1/2} = T_2^{-1}$. The domain-sizes obtained from the Goldman-Shen experiment will be compared with those derived from small-angle X-ray scattering. The experiment has been carried out for the 15%, 20%, 25%, 30%, 40% and 50% material. To compare the domain sizes obtained from SAXS and spin-diffusional

measurements, it is important to apply a model for both techniques which allows a comparison of the results. At this point some assumptions concerning the morphology have to be made. The NBC systems form regular birefringent structures with circular symmetry, so called spherulites, which grow radially from the nucleus, therefore they comprise of chain folded lamellae [40] (see also figure 5.31 magnified section). However, NBC consists of three different domains. For thermodynamical reasons it is sensible to assume that amorphous nylon-6 is adjoining the amorphous PPO. For the reasons discussed above a lamellar morphology has been used to model the experimental data. The morphological model is sketched in figure 5.44. It takes into account that nylon-6 exists in a crystalline and amorphous form and that amorphous PPO is neighbouring the amorphous nylon-6. The distance which SAXS measures is the most probable distance between the centres of two adjacent crystals. Note that for this model the distance measured by SAXS counts region two twice. This has to be born in mind when comparing with the distance obtained by spin-diffusion measurements. The model involves altogether 6 parameters to fit, 3 for the spin-lattice relaxation times and 3 for the domain sizes. However, the spin lattice relaxation times of amorphous and crystalline nylon-6 were considered to be the same. This could be done because their intrinsic relaxation time is considerably longer than the one of PPO, hence the influence of their spin-lattice relaxation is negligibly small in the

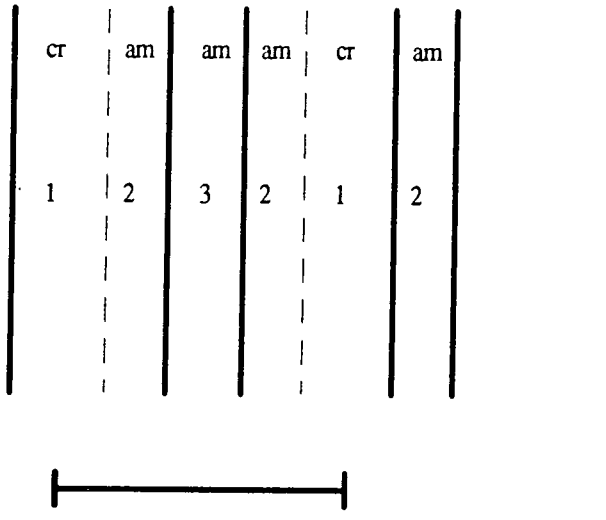

Figure 5.44 NBC three-region lamellar morphology

investigated time-interval. Another simplification is possible by using the crystallinity data obtained by DSC measurements (see section 5.2.3). By knowing the crystallinity of NBC and its composition the domain size of amorphous nylon-6 can readily be calculated from the one of crystalline nylon-6 and vice versa. Another simplification would be possible by calculating the lamellar width of the polyether phase with a given one of the nylon-6 phase. This is possible in theory because of the known composition of the block copolymer. However, it has proved to be very difficult to model the experimental data by this simplification, because the least-squares computing routine aborted in physically meaningless results. The spin-diffusional behaviour may now be described by 4 parameters (assuming the spin-diffusion coefficient is constant).

The actual data-modelling is sketched in a flow-diagram (Fig. 5.45). After the program has read in the parameters, it minimises the squared residuals between the experimental data-points and the modelled data by varying the relaxation times and the domain-sizes. The experimental and the modelled data-points for various NBC compositions are depicted in figures 5.46 to 5.51. The plots represent the magnetisation time-dependence in a simple Goldman-Shen experiment without phase alternation of the polyether protons as a function of mixing-time. In table 5.8 the results from the data modelling are summarised. For mixing times up to 0.3 s the modelled and experimental data are in good agreement, but with longer mixing times the modelled magnetisation is relaxing faster than the experimental.

prepolymer /%	L(PPO) / Å	L(nylon{am}) / Å	L(nylon{cr}) / Å	T_1(PPO) /s	T_1(nylon) /s
15	21	31	51	0.05	2.6
20	26	32	52	0.07	3.6
25	29	22	40	0.09	1.2
30	29	21	21	0.11	4.3
40	31	17	19	0.09	2.0
50	37	15	17	0.12	2.1

Table 5.8 Domain-sizes and intrinsic T1's obtained from the Goldman-Shen experiment for various compositions

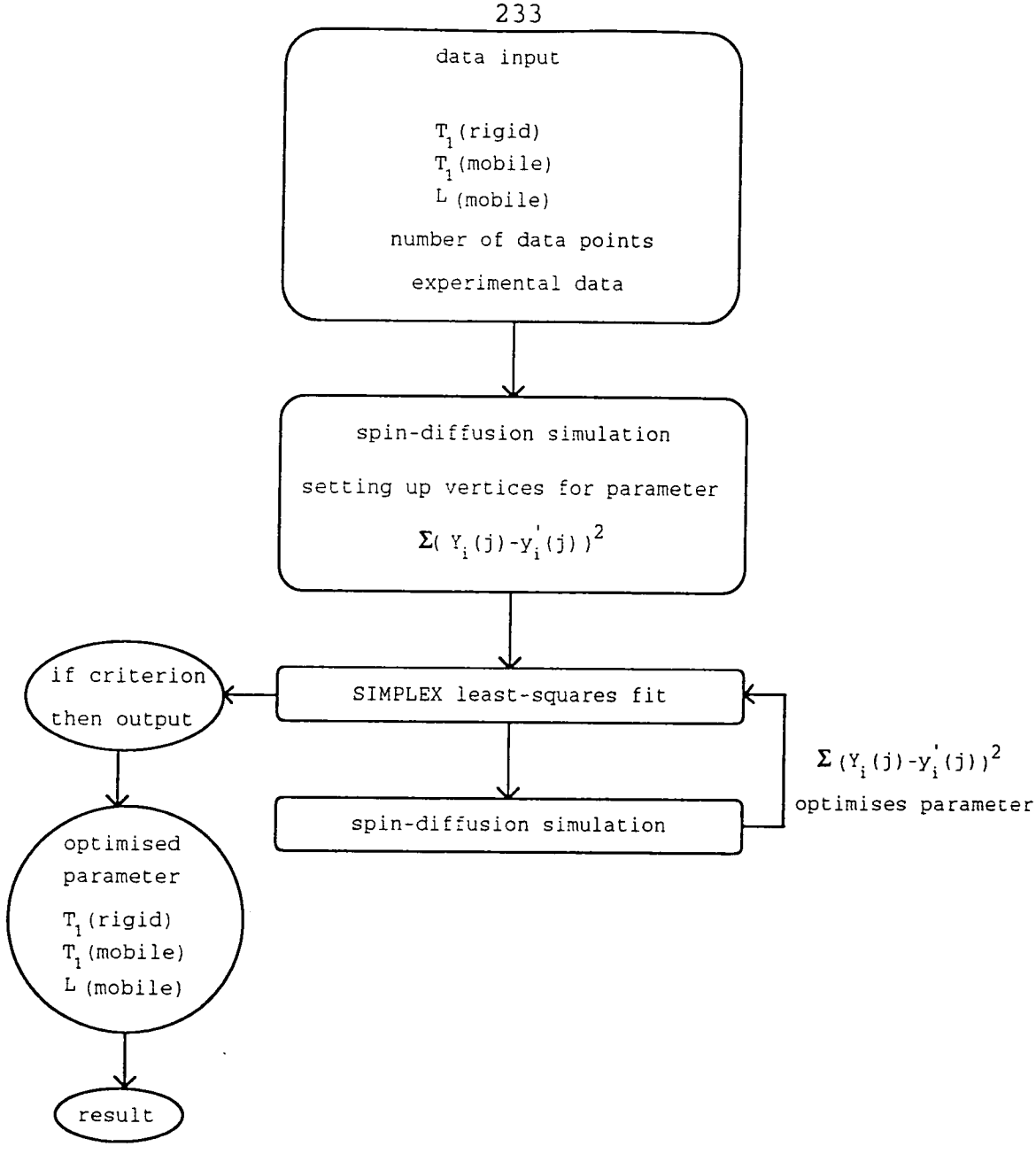

Figure 5.45 Flow diagram of the Goldman-Shen data-modelling program *GOLD.F*

This is particularly seen in figures 5.50 and 5.51 which represent the magnetisation of NBC40 and NBC50.

Another interesting observation should be pointed out. The measured spin-lattice relaxation rate of the protons is the sum of the weighted-average intrinsic relaxation rates for each domain [41]:

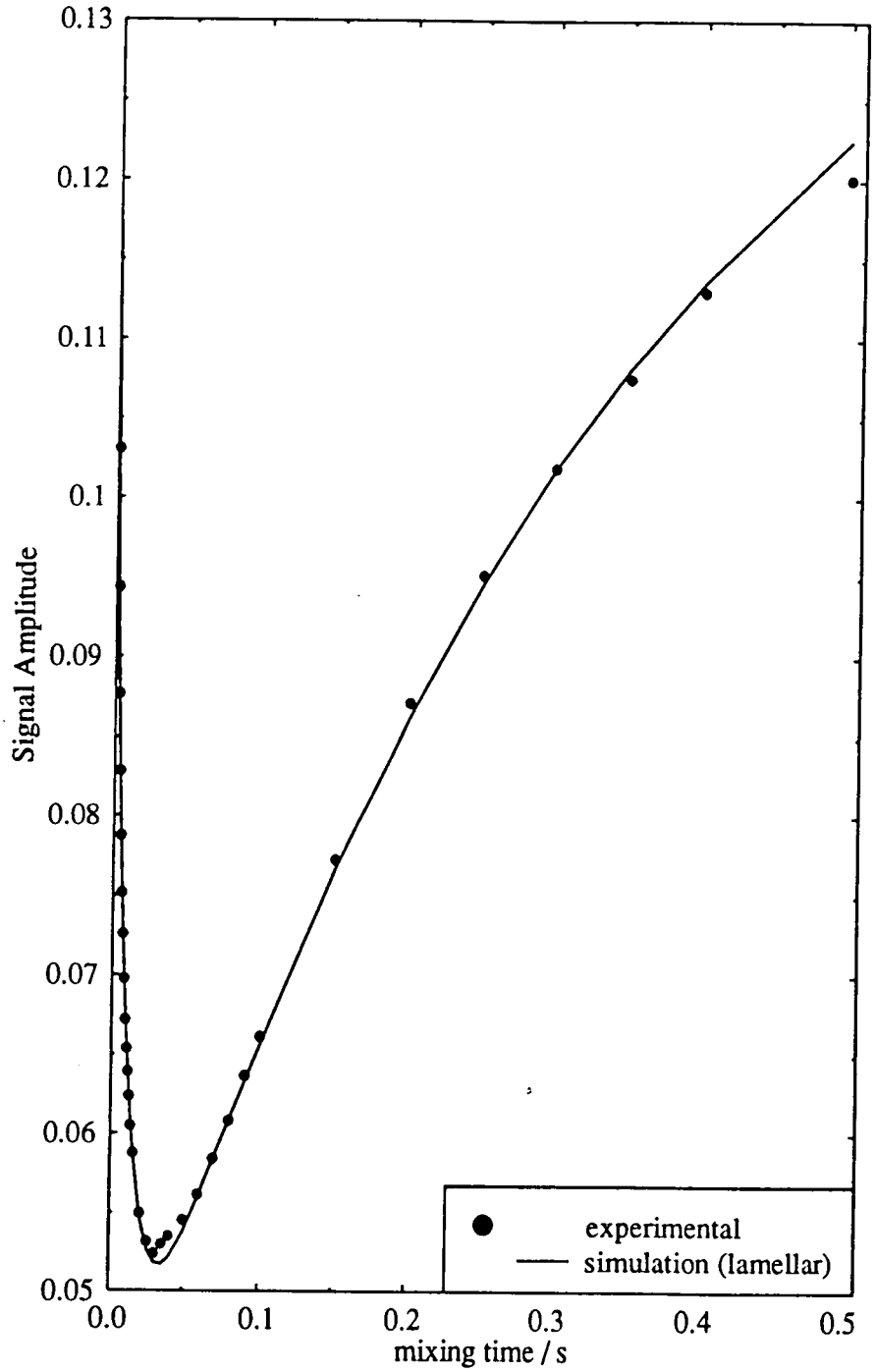

Fig. 5.46 Spin-diffusion data modelling for NBC15 (three-region model)

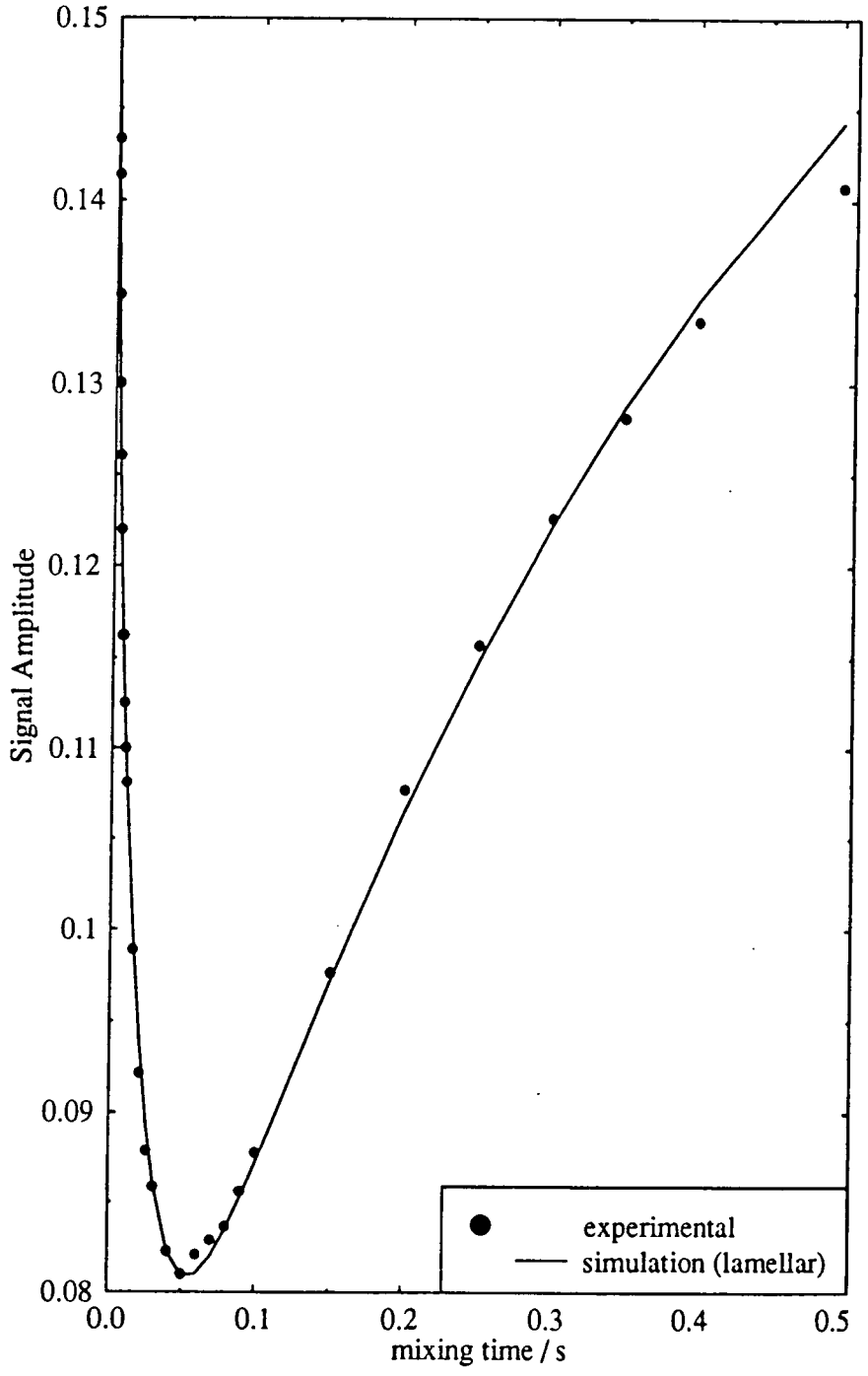

Fig. 5.47 Spin-diffusion data modelling for NBC20 (three-region model)

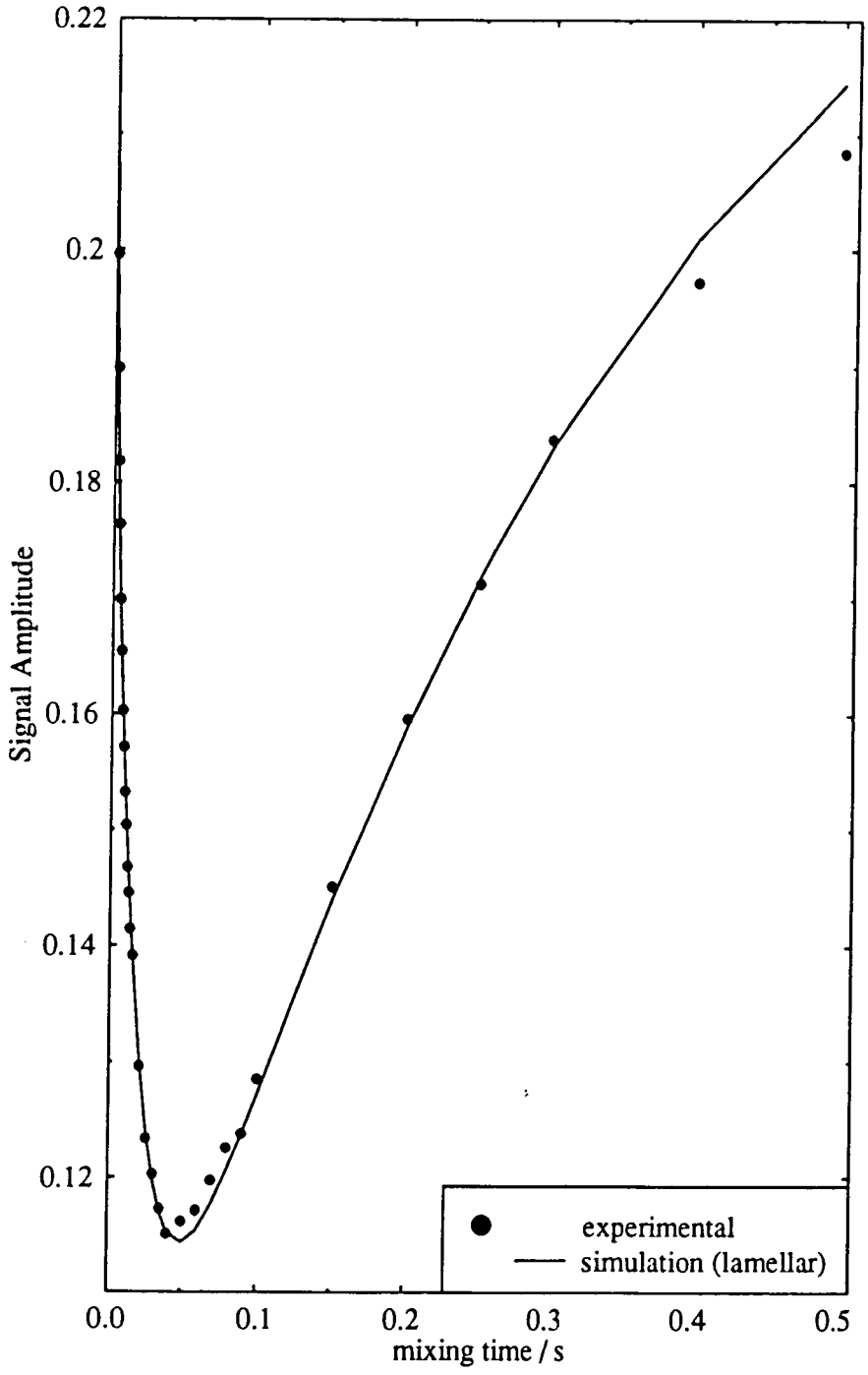

Fig. 5.48 Spin-diffusion data modelling for NBC25 (three-region model)

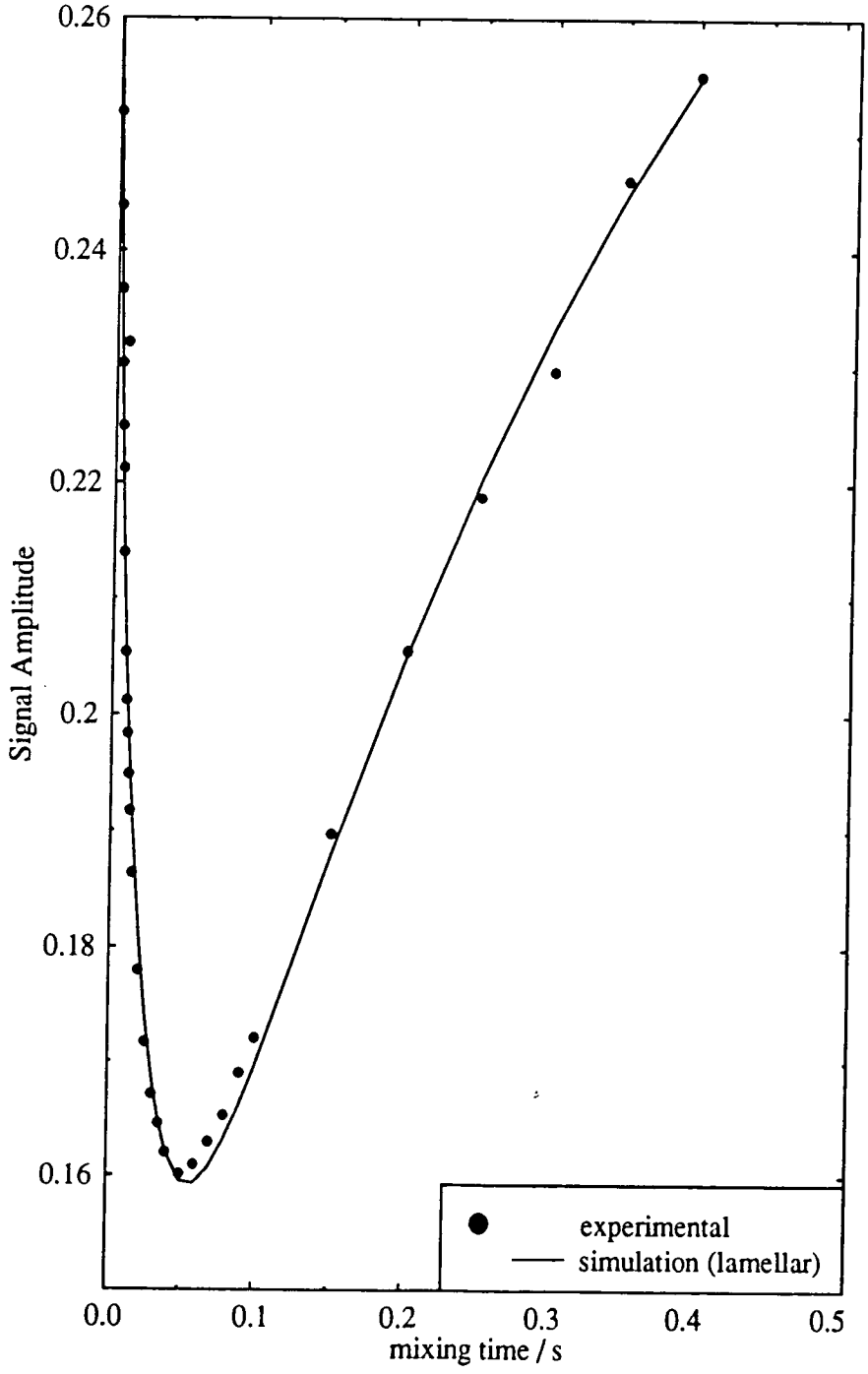

Figure 5.49 Spin-diffusion data modelling for NBC30 (three-region model)

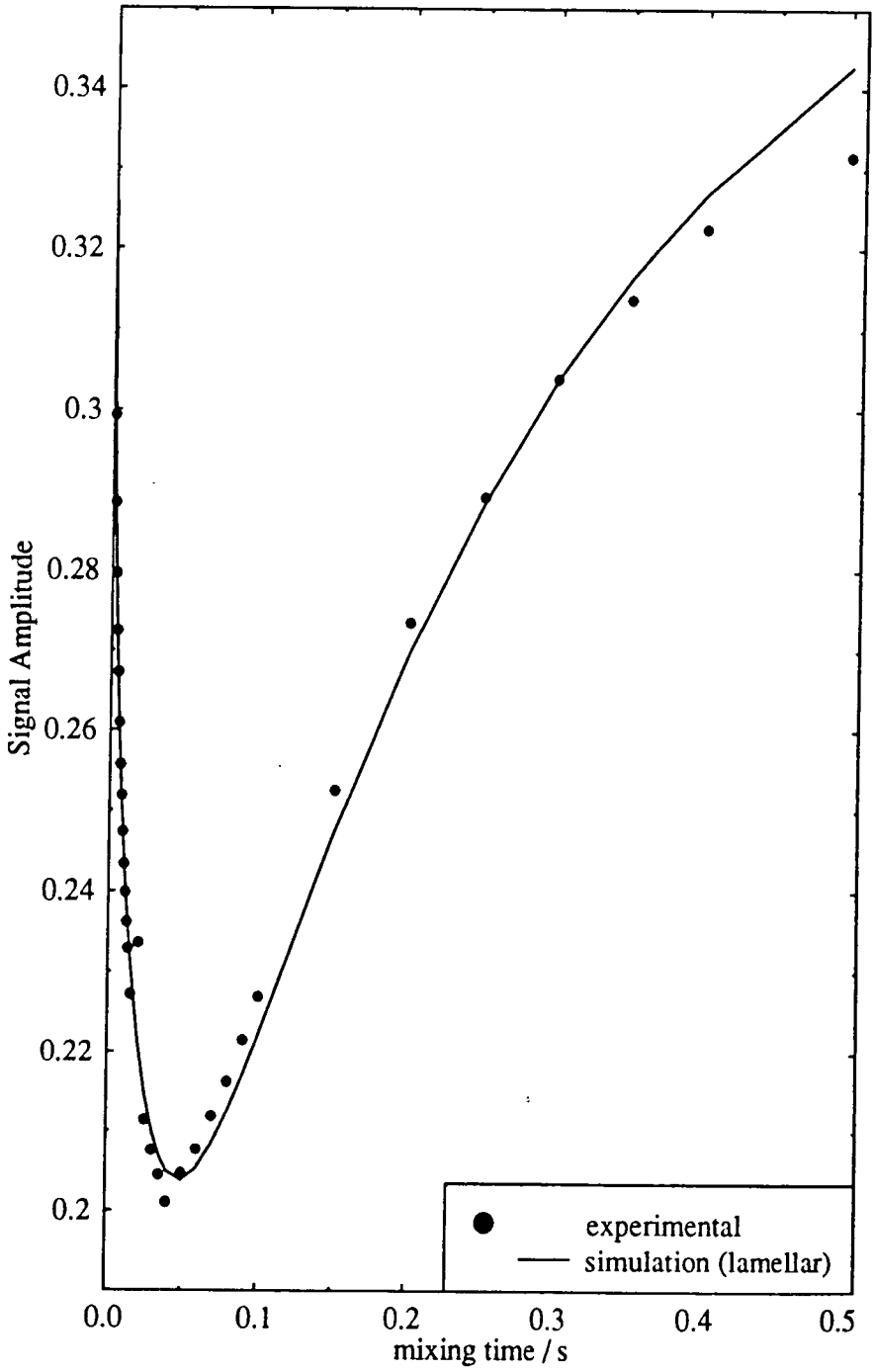

Figure 5.50 Spin-diffusion data modelling for NBC40 (three-region model)

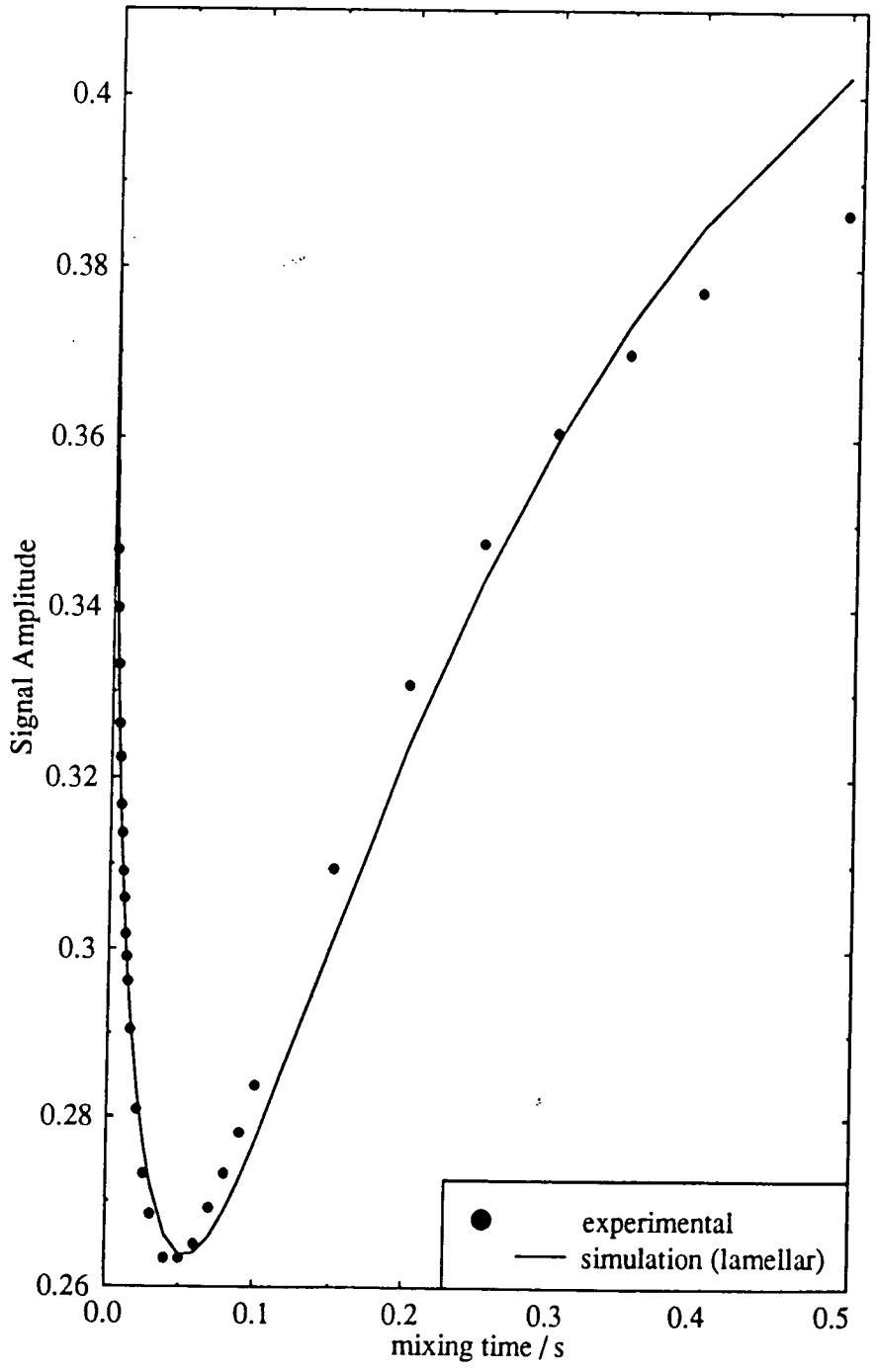

Figure 5.51 Spin-diffusion data modelling for NBC50 (three-region model)

$$\frac{1}{T_1(observed)} = \sum_i w_i \frac{1}{T_{1,i}} \qquad (5.8)$$

where w_i is the fraction of domain i

$T_{1,i}$ is the intrinsic relaxation rate in domain i

An inversion-recovery experiment (see chapter 6) has been carried out to check if the weighted-average intrinsic relaxation times obtained from the Goldman-Shen experiment are equal to those measured by the inversion-recovery method. Table 5.9 represents the experimental weighted-average T_1^{-1}-values and the weighted-average T_1^{-1} calculated from the intrinsic T_1^{-1} obtained from the spin-diffusion measurement.

prepolymer / %	T_1^{-1} / s^{-1} (experimental)	T_1^{-1} / s^{-1} (Goldman-Shen)
15	3.52	3.33
20	3.76	3.08
25	3.94	3.40
30	4.29	2.89
40	4.93	4.74
50	5.41	4.40

Table 5.9 Weighted-average experimental and intrinsic proton T_1^{-1} data, the latter from the spin-diffusion measurement (three-region lamellar model)

The analysis of the spin-diffusion experiment gives values different from the T_1-measurement. Apparently the modelled weighted-averaged relaxation rates are smaller than the experimental ones although the plots reveal a different picture. As illustrated in table 5.8 the intrinsic

relaxation time of PPO is about 2 magnitudes smaller than the one of nylon-6. As a result, the relaxation time behaviour of the block copolymer is almost entirely dominated by the relaxation properties of the PPO protons. However, before going into a detailed discussion the other parameter, the lamellar width, needs to be discussed.

5.5.5 Comparison of NMR and SAXS-Results

The most probable distance between the centres of two adjacent crystals, L_c^M, obtained by SAXS and the sum of the distance between the mobile (polyether) and the rigid (amorphous and crystalline polyamide) domains from solid-state NMR should roughly give the same answer. Note that region 2 (amorphous nylon-6) has to be counted twice because of the utilised model. In tables 5.11a and 5.11b the results of the NMR- and the X-ray data are summarised:

	NMR			SAXS	
prepolymer / %	L(PPO) / Å	L(nylon{am}) / Å	L(nylon{cr}) / Å	amorphous / Å	crystalline / Å
15	21	31	51	66	24
20	26	32	52	69	26
25	29	22	40	-	-
30	29	21	21	87	31
40	31	17	19	85	31
50	37	15	17	83	37

Table 5.11a Lamellar width from SAXS and solid-state NMR for various compositions of NYRIM (results for each region)

	NMR	SAXS		
Prepolymer/%	Distance / Å	L_c^m/Å	L_c^M/Å	L/Å
15	134	80	100	90
20	142	84	105	95
25	113	-	-	-
30	92	100	135	118
40	84	112	130	116
50	84	110	130	120

Table 5.11b Lamellar width from SAXS and solid-state NMR for various compositions of NYRIM (results represent the full width repeat distance (NMR) and the most probable distance between the centres of two adjacent crystals (SAXS)

The NMR and X-ray data are generally comparable in that they are of the same order of magnitude. However, the lamellar widths obtained by SAXS show a discrete increase between 20% and 30% polyether concentration, whereas the widths obtained by spin-diffusional measurements reveal a discrete decrease. Now the crucial question arises as to why the two techniques experiences an opposite trend in the lamellar width by varying the composition.

Firstly, it is important to note that both techniques identify a structural change between 20% and 30% polyether concentration. Considering the crystallinity drop obtained by DSC measurements it is reasonable to assume that the change in lamellar width has its origin in the different structural forms, i.e. α-crystalline and amorphous nylon-6. SAXS and DSC measurements suggest that amorphous nylon-6 is less efficiently packed in contrast to the α-crystalline form because of the increased L_c^M and the larger amorphous phase. Hence amorphous nylon-6 requires

more space in its domain than crystalline. However, spin-diffusional measurements impart a disagreeing result. As has been discussed in chapter 4, only a little is known about the amorphous phase in nylon-6, so no absolute conclusion can be drawn about space requirements of the two phases.

However, a closer look at the experimental and the simulated data gives rise to some doubt about the accuracy of the parameters obtained by modelling the experimental Goldman-Shen data. The shape of the modelled curve does not match the experimental fully. The shape of the curve with a given morphology is influenced by the region width, the spin-diffusion coefficient and the spin-lattice relaxation time. Assuming that the spin-diffusion coefficient is isotropic throughout the region, the diffusion of the magnetisation is only influenced by the domain size, the relaxation properties and the morphology of the domains. Note that the domain size and the population-weighted average relaxation rate are influenced by the relation $l_i^2/D_i\,T_{1,i}$. The shape of the time-dependent magnetisation curve is also controlled by these parameters. Especially for the 40 and 50% materials the deviations of the fitted and the experimental curves are significant in the relaxation-dominated part of the Goldman-Shen experiment. Thus, a deviation of the modelled parameter from the real data is likely. Bearing in mind that SAXS, DSC, DMTA and solid-state NMR detect a structural and morphological transition between 20 and 30% polyether concentration, one can readily understand that the block copolymer is most likely not built up by perfect

lamellae but with a much more complicated morphology which is not necessarily purely lamellar, cylindrical or spherical. Unfortunately only very little is known about the morphology in NBC systems. The morphology and structure of the amorphous nylon-6 is still mysterious [44-46]. The reason is the small domain size of the components. Electron microscopy faces its limits with such small domain sizes. Atomic-force microscopy is limited to analysis of the surface, which experiences other crystallisation properties, hence building most likely another morphology from the bulk polymer.

5.6 Conclusion

The analysis of the dynamic mechanical and the thermal properties in correlation with the domain sizes and microstructure of the polyether polyesteramide block copolymer gives some interesting prospects of the relationship between structure, morphology and mechanical properties in this block copolymer.

Summarising the results from solid-state high resolution ^{13}C NMR spectroscopy the block copolymer appears in the α-crystalline form in all compositions. Only drastic cooling processes such as quenching in liquid nitrogen built an amorphous nylon-6 structure which can be detected as such as relatively sharp resonances with high-resolution ^{13}C solid-state NMR. However, interpretation of the amorphous nylon-6 spectrum is still unsatisfactory [43-46]. A very interesting point is the fact that nylon-6 is a semicrystalline polymer with low crystallinity even when

annealed. This property is readily spotted by DSC and SAXS. The crystallinity was obtained to be 20 to 50% depending on the composition of the copolymer. CP/MAS ^{13}C solid-state NMR shows hardly any resonance of the carbons of the amorphous domains, whilst the quenched sample reveals relatively sharp peaks as seen in figure 4.3a in chapter 4. However, given the knowledge that the ^{13}C spin-lattice relaxation times of crystalline nylon-6 are about 30 to 138 s [47,48], a MAS single-pulse solid-state ^{13}C spectrum with a 2 s recycle delay should filter out all resonances which arises from the crystalline domain. However, as figure 4.41a in chapter 4 shows, a large proportion of nylon-6 resonances remain. The part of the nylon-6 in the single-pulse spectrum is now solely resolved at room temperature indicating the rigidity of the phase. However, as has been illustrated in section 4.5.2 the carbon resonances of nylon-6 in a single-pulse experiment become narrow by increasing the temperature to 100 °C and they are nearly identical to the ones of the amorphous phase in the ^{13}C CP/MAS experiment. This is a very interesting observation because it suggests two different kinds of "amorphous" domains, a rigid and mobile one. A third phase beside the crystalline and amorphous was already mentioned by Powell and Mathias [49]. Their interpretation of the second amorphous phase as an interphase is doubtful because of its large quantity in relation to the other two phases. However, the ^{13}C solid-state CP/MAS and single-pulse spectra strongly suggest the presence of two non-crystalline phases of which one is liquid-like mobile and the other rigid.

The analysis of the domain-sizes by SAXS illustrates some interesting aspects about the morphology of the NYRIM system.

The crystal-domain sizes remain constant within the composition range under investigation. Apart from the discontinuity between the 20% and 30% material, the size of the amorphous domain remains constant for the 30%, 40% and 50% material. The first maximum, L_c^M, interpreted as the most probable distance between two adjacent crystals, confirms this discontinuity in the domain size. Its value is larger than the L_c^m-value. According to Zachmann [30] this implies that there is a broad distribution in lamellar thicknesses. This result is also supported by the semi-logarithmic plot of the intensity vs. the distance of correlation function. Hardly any regular lamellar structure could be found from this plot. This is not a very surprising result because the reaction temperature was 140 °C, much below the melting point of the block-copolymer, which results in rapid unordered crystallisation of the lamellae.

The DSC results illustrate that crystallinity drops between 25% and 30% prepolymer weight-fraction, which indicates that the amorphous fraction in the block copolymer is preferably built. These observations mirror the mechanical properties of the block copolymer. The flexural modulus and tensile strength decrease quickly if the composition goes beyond 20% prepolymer. This is a very illustrative example of how the micro structure is related to the mechanical properties of a material. The drop in flexural modulus and tensile strength clearly supports the

suggestion that the mobile polyether is jacketing the stiffer spherulites, making the block copolymer more flexible.

The complex morphology of NYRIM is likely to be responsible for the fact that the spin-diffusion analysis disproves the results for the domain-sizes concerning the trend with varying proportions of polyether. The modelling program assumes regular lamellae of polyamide and polyether, but it does not consider irregularities. However, the data-modelling program proves its capability of measuring the domain-sizes for such complex block-copolymers with a discrepancy of a factor two in comparison to the SAXS results. This is the first time that such intensive investigations have been made to compare these two techniques.

The main sources of error are the non-perfect lamellae, the unknown structure and morphology of crystalline and amorphous nylon. Another point is approximate spin-diffusion coefficient, especially for the mobile polyether, in which additionally to the dipolar interaction contribution motional effects could influence the value. Finally the proton spin-lattice relaxations of the crystalline and amorphous region in nylon-6 are a source of error. The mobile fraction of amorphous nylon, has a ^{13}C spin-lattice relaxation time which is 2 orders of magnitude smaller than the one of the crystalline region. It is tempting to assume that the "mobile" amorphous nylon-6 domain has also a smaller ^{1}H spin-lattice relaxation time. However, it is not possible to determine the intrinsic spin-lattice relaxation times of the nylon-6

domains because they are completely averaged by spin-diffusional processes. The observation of only one T_2 in the proton free-induction decay in nylon-6 makes a conclusion even more problematic.

An interesting work for the future would be to investigate morphologically well-defined polymers. SAXS and NMR data could be compared without assumptions. If morphologically different specimens could be available, it could be studied whether the data-modelling of spin-diffusion measurements can distinguish between those micro-structures.

5.7 Summary of Chapter 5

In this chapter it has been shown that it is possible to simulate the behaviour of magnetisation in a Goldman-Shen experiment with spin-lattice relaxation contributions (figures 5.5 to 5.7). The time-dependence of the magnetisation can be represented in a distinct manner for each region. A careful judgement of existing spin-lattice relaxation time minimisation techniques has been carried out. Three existing techniques have been applied for this purpose.

1. phase alternation
2. back-multiplication with an exponential factor which describes T_1-relaxation
3. a new data-representation that gives emphasis to the spin-diffusion

It has been shown that, except for the special cases of uniform T_1-behaviour and mixing times much shorter than the shortest T_1, all techniques fail to do their job. The crucial factor is a multi-exponential spin-lattice relaxation behaviour of the heterogeneous system, which forbids a separation of spin-lattice relaxation and spin-diffusion. The experimental data-points of the Goldman-Shen experiment were modelled with the intrinsic T_1-values and domain-sizes as parameters and known spin-diffusion coefficients. The complex copolymer with incompletely known morphology is the main reason as to why the NMR results for the domain sizes do not agree exactly with the SAXS results. Both techniques illustrate the change in morphology between 20% and 30% prepolymer weight-fraction. It has its origin most likely in a different crystallisation dynamic. The qualitative relationships between the mechanical properties and the micro structure were illustrated by the dependence of the flexural modulus and tensile strength with the crystallinity and domain sizes.

This chapter explains by example that one technique alone is not able to describe a complex polymer-system such as NYRIM. However, using a variety of techniques enables one to classify even such complex polymers.

References to Chapter 5

[1] D.C. Allport, W.H. Jones, *Block Copolymers*, Applied Science Publishers CTB London (1973)

[2] B.B. Burnett, W.F. McDevit, J. Appl. Phys., **28** (1957) 1101

[3] J.H. Magill, Polymer, **3** (1962) 655

[4] K.M. Hedrick, J.D. Gabbert, "A New RIM System From Nylon 6 Block Copolymers Chemistry" AIChE **14** (1981) 1

[5] M. Inoue, J. Polym. Sci., Part A, **1** (1963) 2697

[6] S. Cruz, N. Stribeck, H.G. Zachmann,Macromolecules, **24** (1991) 5980

[7] C.G. Vonk, G. Kortleve, Kolloid-Z., **19** (1967) 220

[8] G.R. Strobl, M. Schneider, J.Polym.Sci., **18** (1980) 1343

[9] O. Kratky, Z. Elektrochem., 58 (1954) **49**, (1958) 62 66, ibid, O. Kratky, Z. Skala, Z. Elektrochem., **62** (1958) 73

[10] C.G. Vonk, J.Appl.Cryst., **4** (1971) 340

[11] P. Debye, N.R. Anderson, H. Brumberger, J.Appl.Phys., **28** (1957) 679

[12] K.J. Packer, J.M. Pope, R.R. Yeung, J. Polym. Sci., Polym. Phys. Ed., 22 (1984) 589.

[13] A.M. Kenwright, K.J. Packer, B.J. Say, J. Magn. Reson. 69 (1986) 426.

[14] N. Bloembergen, Physica, 15 (1949) 368

[15] T.T.P. Cheung, Phys. Rev., B23 (1981) 1404

[16] J.A. Nedler, R. Mead, Computer Journal, 7 (1965) 308

[17] M.S. Caceci, W.P. Cacheris, Byte, May 1984, 340

[18] M. Goldman, L. Shen, Phys. Rev., 144 (1966) 321.

[19] A. Abragam, *The Principles of Nuclear Magnetism*, Clarenden Press: Oxford (1961)

[20] S. Zhang, M. Mehring, Chem. Phys. Lett., 160 (1989) 644

[21] A.M. Kenwright, K.J. Packer, Chem. Phys. Lett 173 (1990) 471.

[22] R.H. Newman, Chem. Phys. Lett. 180 (1991) 301.

[23] M.E.A. Cudby, K.J. Packer, P.J. Hendra, Polym. Comm., 25 (1984) 303

[24] K.J. Packer, J.M. Pope, R.R. Yeung, M.E.A. Cudby, J. Polym. Sci. Polym. Phys. Ed, 22 (1984) 589

[25] A.D. Booth, K.J. Packer, Mol. Phys., 62 (1987) 811

[26] R.A. Dickie, in *Polymer Blends*, edited by D.R. Paul, S. Newman, Vol. 1, p353. Academic Press, New York (1978)

[27] O. Olabisi, L.M. Robeson, M.T. Shaw, Polymer-Polymer Miscibility, Academic Press, New York (1979)

[28] H.W. Spiess, *Advances in Polymer Science*, Vol. 66. Springer Verlag, Berlin (1985) and referneces cited therein.

[29] M. Mehring, *Principles in High-Resolution NMR in Solids*, Springer Verlag, Berlin (1983) and referneces cited therein.

[30] T.T.P. Cheung, B.C. Gernstein, J. Appl. Phys., 52 (1981) 5517

[31] P. Caravatti, P. Neuenschwander, R.R. Ernst, Macromolecules, 18 (1985) 119

[32] P. Caravatti, M.H. Levitt, R.R. Ernst, J. Magn. Reson., 68 (1986) 323

[33] P. Caravatti, P. Neuenschwander, R.R. Ernst, Macromolecules, 19 (1986) 1889

[34] J.R. Havens, D.L. VanderHart, Macromolecules, 18 (1985) 1663

[35] M. Dettenmaier, E.W. Fisher and M.Stamm, Colloid and Polymer Science, **228**, (1980) 343

[36] K. Schmidt-Rohr, J. Clauss, B. Blümich, H.W. Spiess, Magn. Res. Chem., **28** (1990) S3

[37] J.H. van Vleck, Phys. Rev., **74** (1948) 168

[38] K. Schmidt-Rohr, H.W. Spiess, Macromolecules, (1992)

[39] T.T.P. Cheung, B.C. Gernstein, C.M. Ryan, R.E. Taylor, C.R. Dybowski, J. Chem. Phys., **73** (1980) 6059

[40] J.M.G. Cowie, *Polymers: Chemistry & Physics of Modern Materials*, 2nd edition, Blackie, Glasgow and London (1991)

[41] A.M. Kenwright, K.J. Packer, B.J. Say, J. Magn. Reson., **69** (1986) 426

[42] C.S. Cruz, N. Stribeck, H.G. Zachmann, Macromolecules, **24** (1991) 5980

[43] G.R. Hatfield, J.H. Glans, W.B. Hammond, Macromolecules, 23 (1990) 1654

[44] A. Okada, M. Kawasumi, I. Tajima, T. Kurauchi, O. Kamigaito, J. Appl. Polym. Sci. 37 (1989) 1369

[45] K. Kubo, T. Yamanobe, T. Komoto, I. Ando, J. Polym. Sci, Polym. Phys. Ed., 27 (1989) 929.

[46] D.G. Powell, L.J. Mathias, J. Am. Chem. Soc., 112 (1990) 669

[47] H.Ketels, L. van de Ven, A. Aerdts, G. van der Velden, Polym. Commun., **30** (1989) 80

[48] T.P. Huigen, H.A. Gaur, T.L. Weeding, L.W. Jenneskens, H.E.C. Schuurs, W.G.B. Huysmans, W.S. Veeman, Macromolecules, **23** (1990) 3068

[49] D.G. Powell, L.J. Mathias, J. Am. Chem. Soc., 112 (1990) 669

Chapter 6

6. ^1H Relaxation

6.1 Introduction

Proton relaxation parameters are very important for the understanding of solid-state NMR. It has been shown in the previous chapters that proton relaxation influences high-resolution ^{13}C CP/MAS spectra and spin-diffusion measurements in heterogeneous systems. ^1H relaxation measurements contain information about the molecular mobility.

In this context solid-state NMR studies have been carried out in the past using ^1H relaxation measurements, broadline spectra [1,2] and ^{13}C CP/MAS spectra [3,4] in an attempt to characterise various materials.

However, in this chapter only the main important parameters will be discussed by examples to gain understanding of the previous chapters.

It is not the purpose of this chapter to present new techniques or a theory of spin-relaxation in solids, but it will deal with the most complicated case of spin-relaxation: spin-diffusion-coupled nuclear magnetic spin-lattice relaxation in a heterogeneous system. Some aspects will support the concept of population- weighted-average spin-relaxation rate.

All measurements where carried out on the NYRIM system with various polyether concentrations.

6.1.1 Theory

In this section a few definitions of relaxation parameters will be given. As mentioned in chapter 5, the magnetisation govered by the dynamics of the nuclear spins under the influence of relaxation in a heterogeneous system takes the form

$$\dot{\mathbf{M}}(\mathbf{r},t) = \nabla\left\{D(\mathbf{r})\nabla\mathbf{M}(\mathbf{r},t) + R_j(\mathbf{r})\Delta\mathbf{M}(\mathbf{r},t)\right\} \qquad (6.1)$$

$D(\mathbf{r})$: isotropic spin-diffusion coefficient as a function of the spatial variable $\mathbf{r}$

$R_j(\mathbf{r})$: spatially dependent isotropic relaxation rate (j=1, 1ρ, etc.)

$\Delta\mathbf{M}$: $\Delta\mathbf{M} = \mathbf{M}^{eq} - \mathbf{M}(\mathbf{r},t)$, is the instantaneous deviation of the nuclear magnetisation from its equilibrium value $\mathbf{M}^{eq}$

Booth and Packer [5] solved equation 6.1 exactly for a one-dimensional two-region model of lamellar morphology. They came to the conclusion that the relaxation behaviour in a system as such is described by an infinite sum of exponentials. This gave rise to the introduction of the expression *population-weighted average spin-lattice relaxation rate*. It is defined by

$$R_j(\mathbf{r}) = \sum_{i=1}^{\infty} w_i R_{ji}(\mathbf{r}) \qquad (6.2)$$

$R_{ji}(\mathbf{r})$: spatially dependent isotropic relaxation rate (j=1, 1ρ, etc.) of population i

w_i: fraction of population i

For the analytical prospect this means that, in such a case, where the fit is a truly adequate representation of

the data, the sum of the fitted populations must equal the initial population of the magnetisation. Subsequently, the population-weighted relaxation rate average of the fitted components must equal the initial rate of decay of the magnetisation. In a spin-lattice relaxation experiment, all regions have the same deviation from equilibrium after the perturbation of the initial pulse. At this point there is no influence of spin-diffusion between the region, since there is no population difference to drive it. From eqn. 6.1 it follows that, for a relaxation starting from a spatially uniform non-equilibrium magnetisation profile at $t = 0$, $\nabla \mathbf{M}(\mathbf{r}, t) = 0$, i.e. the term containing the diffusion coefficient drops out, and the initial magnetisation decay (immediately following the perturbation) is due solely to the intrinsic relaxation properties of the different regions. Thus, the initial rate of decay is given by the population-weighted rate average of the intrinsic relaxation processes. Hence, in a multi-component relaxation in a heterogeneous system, the population-weighted relaxation rate average of the fitted components must equal the population-weighted rate average of the intrinsic relaxation processes in the various regions.

6.2 Computer Simulation of an Inversion-recovery Experiment with Spin-diffusion Influence

To illustrate the relaxation time behaviour of a heterogeneous system influenced by spin-diffusion, an inversion-recovery experiment has been simulated. The

magnetisation behaviour after the 180° pulse is represented by 60 data-points using a sufficiently long delay time to let the magnetisation recovering. A lamellar morphology has been applied. The parameters used for the simulations are the same as in the spin-diffusion simulation, summarised in tables 5.3 to 5.6 in chapter 5. The magnetisation behaviour was analysed by a non-linear least-squares fit using the Marquart algorithm (the program is listed in Appendix III)

6.2.1 Results and Discussion

The relaxation behaviour of the chosen heterogeneous system in tables 5.3 and 5.4 can be described by a single component (see table 6.1). The one with the parameter set as listed in tables 5.5 and 5.6, however, reveals a small second component (see table 6.2). The importance of the small second component is illustrated in table 6.3, which shows the theoretical population-weighted average relaxation rate and the weighted average relaxation rate calculated from the simulated relaxation times. The former, calculated from the input data, significantly deviates from the rate obtained from a single-component fit but is in good agreement with the one calculated from the double-component fit. The relaxation times and the populations are, as expected, far away from their intrinsic values, but the data illustrate the importance of the second relaxation time and also the danger and difficulty of a quantitative relaxation time measurement when determining the usually short low-populated

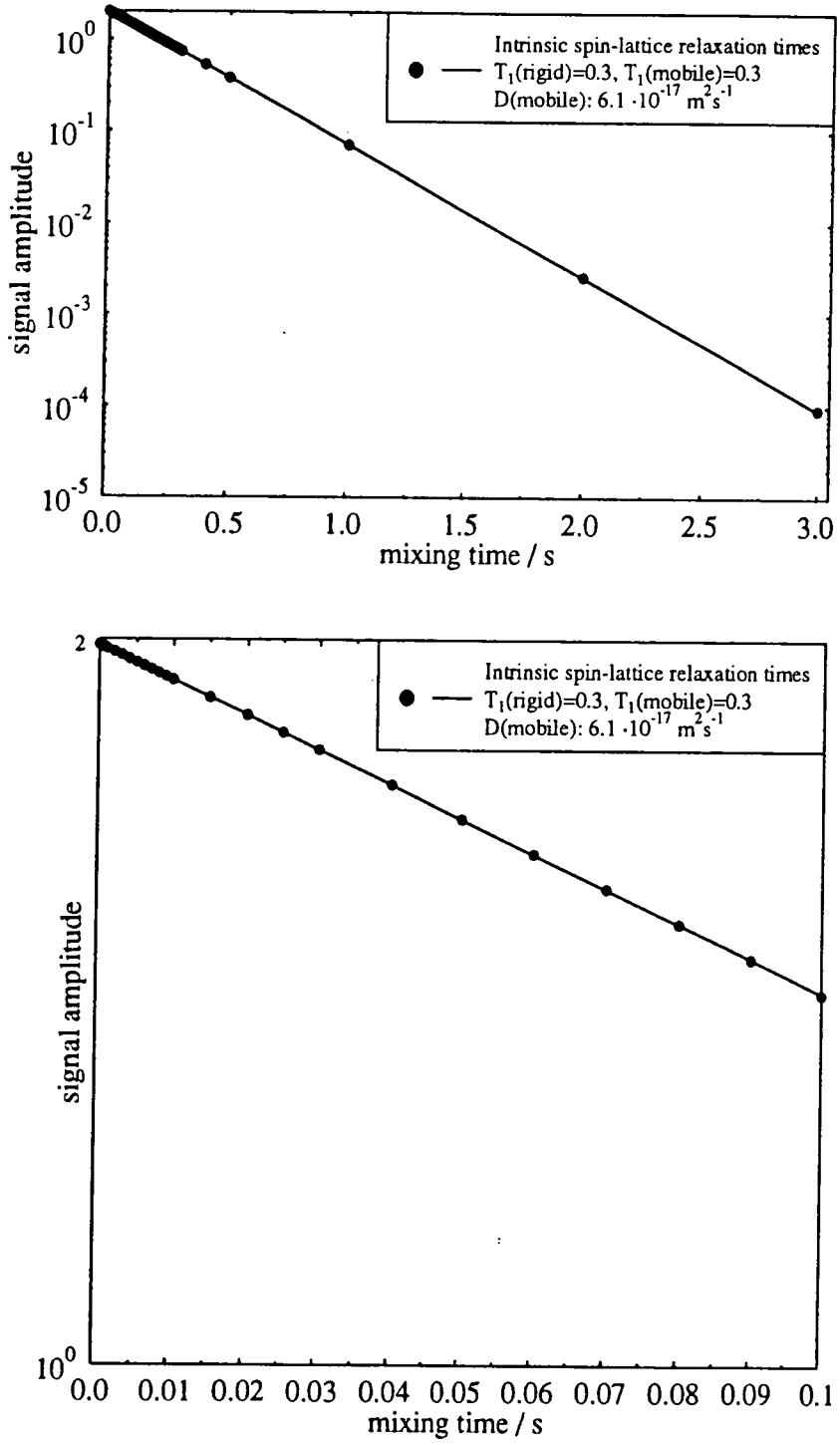

Fig. 5.31a Spin-lattice relaxation by inversion-recovery in the case of uniform T_1
experimental (marker), fitted (line)
top: whole experiment; bottom: time expansion

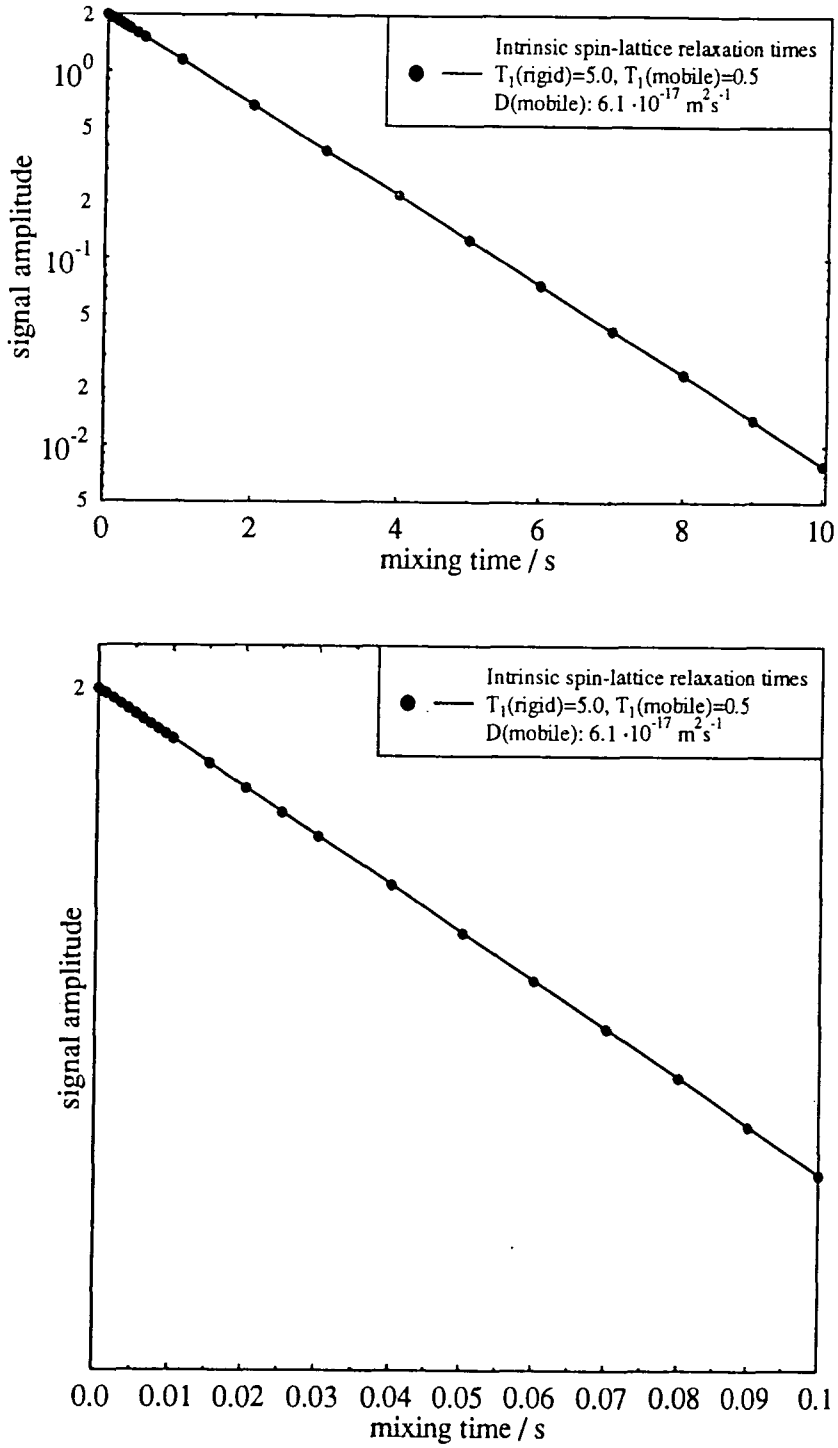

Fig. 5.31b Spin-lattice relaxation by inversion-recovery for non-uniform T1
experimental (marker), fitted (line)
top: whole experiment; bottom: time expansion

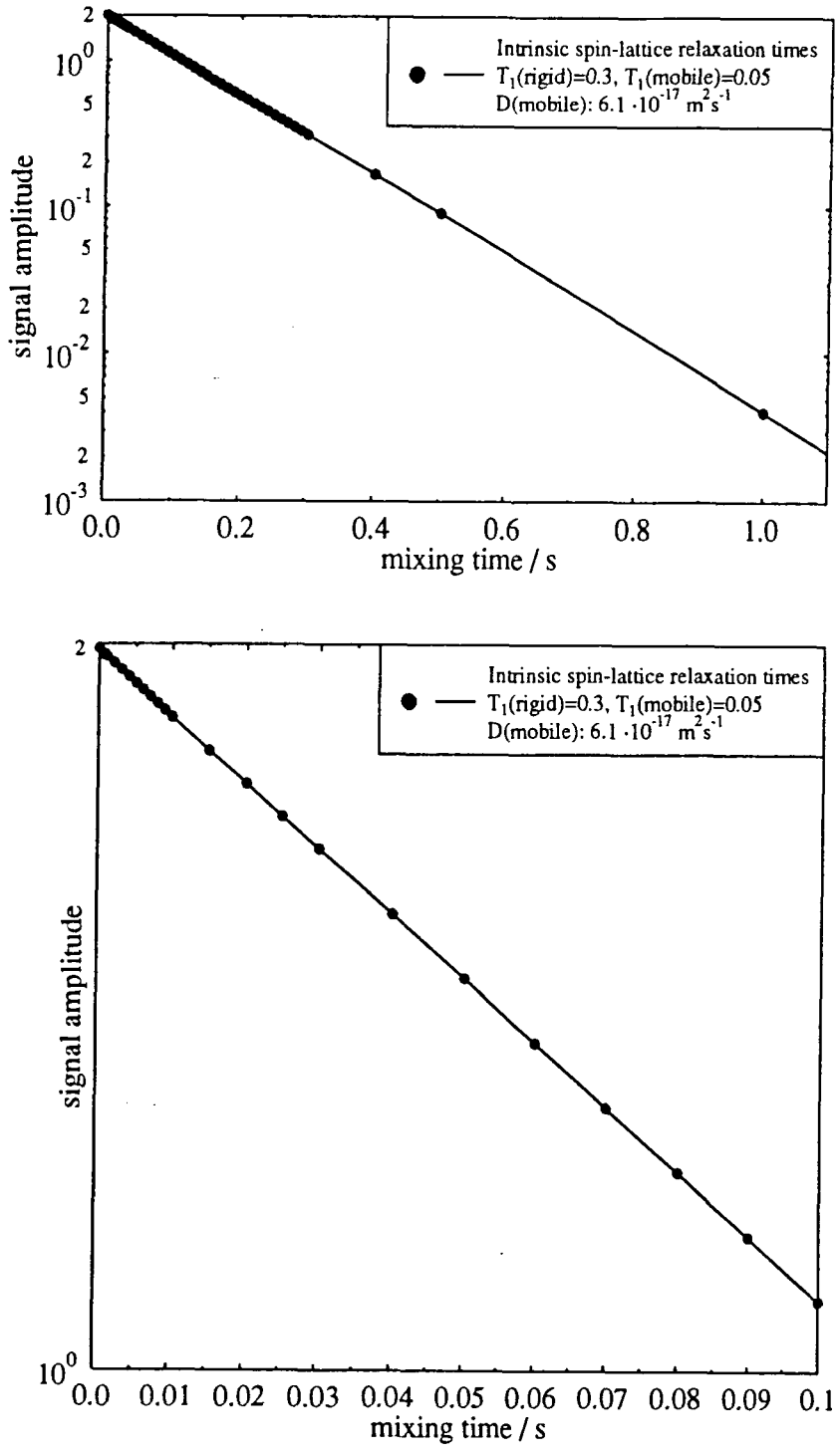

Fig. 5.31c Spin-lattice relaxation by inversion-recovery for non-uniform T_1
experimental (marker), fitted (line)
top: whole experiment; bottom: time expansion

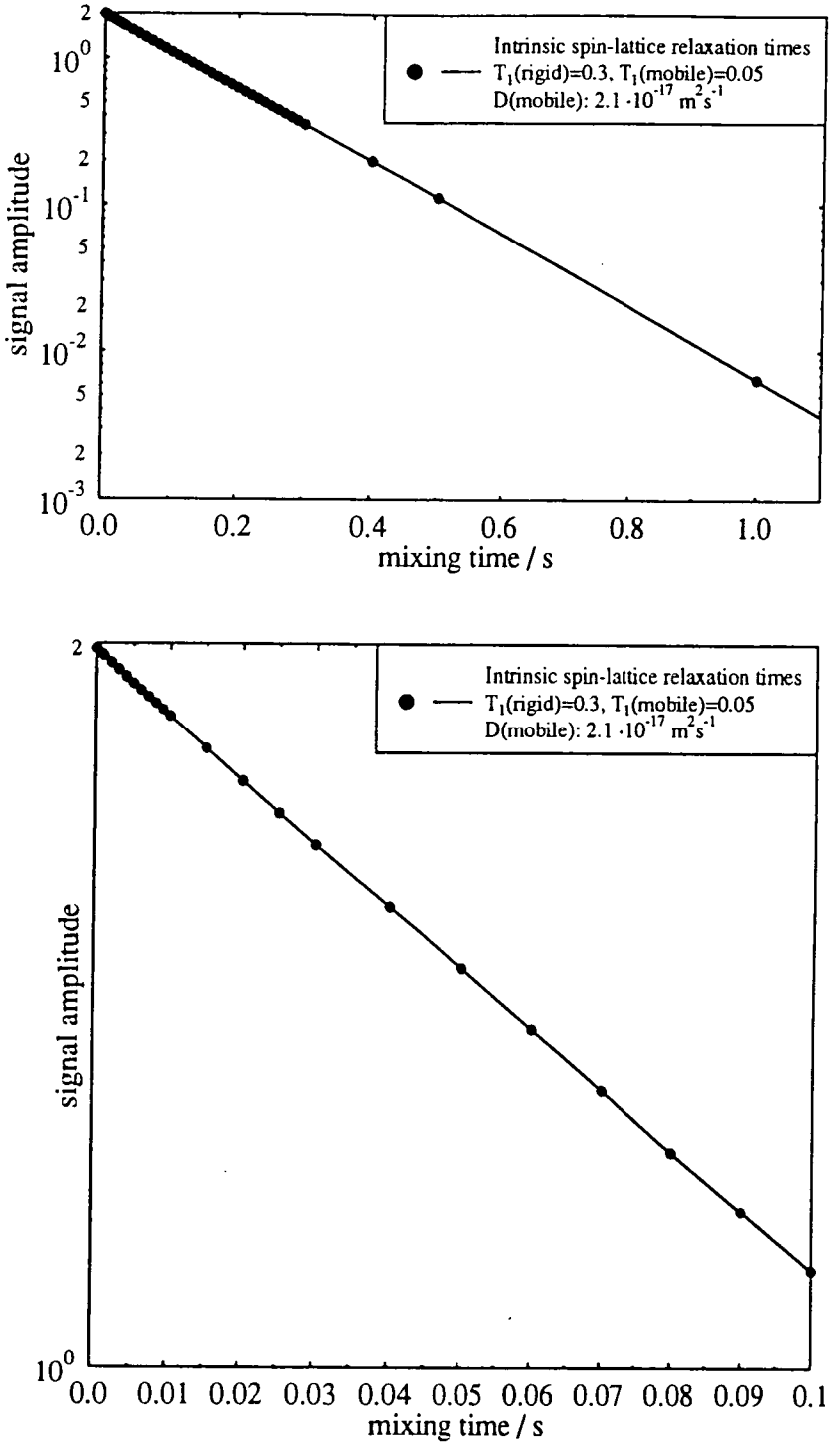

Fig. 5.31d Spin-lattice relaxation by inversion-recovery for non-uniform T_1
experimental (marker), fitted (line)
top: whole experiment; bottom: time expansion

intrinsic T_1/s (mobile/rigid)	D/m^2s^{-1} (mobile)	population	error population	T_1/s	error T_1/s
0.05 / 0.3	$2.1 \cdot 10^{-17}$	0.9939	±0.0009	0.1710	±0.0004
0.05 / 0.3	$6.1 \cdot 10^{-17}$	0.9976	±0.0003	0.1608	±0.0001
0.5 / 5.0	$6.1 \cdot 10^{-17}$	0.999932	±0.000005	1.80754	±0.00007
0.3 / 0.3	$6.1 \cdot 10^{-17}$	1.00006	±0.00006	0.29951	±0.00005

Table 6.1 Spin-lattice relaxation times of a simulated heterogeneous system (20% mobile, 80% rigid) (single exponential)

intrinsic T_1/s (mobile/rigid)	D/m^2s^{-1} (mobile)	population 1	error population 1	$T_1(1)$/s	error $T_1(1)$/s	population 2	error population 2	$T_1(2)$/s	error $T_1(2)$/s
0.05 / 0.3	$2.1 \cdot 10^{-17}$	0.02555	±0.00004	0.02415	±0.00006	0.97439	±0.00005	0.174949	±0.000008
0.05 / 0.3	$6.1 \cdot 10^{-17}$	0.006419	±0.000007	0.01285	±0.00003	0.993561	±0.000001	0.161573	±0.000001

Table 6.2 Spin-lattice relaxation times of a simulated heterogeneous system (20% mobile, 80% rigid) (double exponential)

intrinsic T_1/s (mobile/rigid)	D/m^2s^{-1} (mobile)	weighted average T_1/s (from intrinsic T_1's)	weighted average T_1/s (single exponential)	weighted average T_1/s (double exponential)
0.05 / 0.3	$2.1 \cdot 10^{-17}$	0.15	0.1710	0.1509
0.05 / 0.3	$6.1 \cdot 10^{-17}$	0.15	0.1608	0.1504
0.5 / 5.0	$6.1 \cdot 10^{-17}$	1.7857	1.8075	-
0.3 / 0.3	$6.1 \cdot 10^{-17}$	0.3	0.2996	-

Table 6.3 weighted average spin-lattice relaxation times of a simulated heterogeneous system (20% mobile, 80% rigid)

3second component in order to achieve an accurate measurement. Deviations of about 15% from the theoretical value are easily possible when neglecting the second component. It also illustrates the importance of the acquired data set which must sufficiently describe the relaxation time behaviour of the sample under investigation.

6.3 Direct Measurement of Proton T_1 and $T_{1\rho}$ Relaxation in NYRIM 2000

The spin-lattice relaxation time was measured by a modified inversion-recovery technique. The pulse sequence utilised was:

$(- 180° - \tau_d - 90° - \tau_{echo} - 90°_y - \tau_{echo}$ - acquisition - recycle delay $-)_n$

where τ_d : relaxation delay

τ_{echo}: echo delay

n : number of repetitions

The solid-echo technique was applied to detect possible short-time relaxation components which otherwise would be interfering with the electronically limited recovery time of the spectrometer. The technique was theoretically described by Mansfield [6]. 70 data points were acquired: The first 20 points with a dwell time of 2 ms, then 10 points with a dwell time of 4 ms and finally 40 data points with a dwell time between 20 and 50 ms, keeping the total relaxation delay at least 5 times longer than the

longest relaxation time. The 90° pulse was set to 2 μs, with an echo-delay of 10 μs and a recycle delay between 2 to 4 s, keeping it about 10 times longer than the longest relaxation time component. The experiments were taken at 31.5 °C in order to avoid temperature variations due to temperature changes in the air stream cooling the probe. The experiment was repeated 8 times for which the average was calculated.

Another experiment was carried out to determine the rotating frame spin-lattice relaxation time, $T_{1\rho}^{H}$. In order to obtain the short components of the relaxation properties a solid-echo pulse version was utilised:

$$(-\ 90_x^o\ -\ \text{spin-lock}_y\ -\ \tau_{echo}\ -\ 90_y^o\ -\ \tau_{echo}\ -\ \text{recycle delay}\ -)_n$$

120 data points were acquired: The first 40 points with a dwell time of 70 μs, then 40 points with a dwell time of 0.7 ms and finally 40 data points with a dwell time of 3 ms. The 90° pulse was set to 2 μs, with an echo-delay of 10 μs and a recycle delay between 3 to 4 s, keeping it about 10 times longer than the longest T_1^H component. The experiments were also taken at 31.5 °C. The experiment was repeated 8 times for which the average was calculated.

6.3.1 Results and Discussion

The results of the T_1^H and $T_{1\rho}^{H}$-measurements are summarised in table 6.4 and figure 6.5. The errors usually calculate from 4 experiments as described in the previous

section. If no error is given, then only one measurement was carried out.

fraction PPO	T_1^{H-1} / s^{-1} one component	$\pm s^{-1}$	$T_1^{H-1}(1)$ / s^{-1} two components	$\pm s^{-1}$	$T_1^{H-1}(2)$ / s^{-1} two components	$\pm s^{-1}$	$T_{1,av}^{H-1}$ / s^{-1}	$\pm s^{-1}$
0.00	2.68	0.02	38 (1%)	4	2.66 (99%)	0.02	3.0	0.2
0.10	3.09	0.03	48 (1%)	1	3.19 (99%)	0.05	3.6	0.5
0.15	3.47	0.04	34 (2%)	3	3.47 (98%)	0.09	3.9	0.3
0.20	3.87	0.01	41 (2%)	5	3.68 (98%)	0.01	4.5	0.3
0.25	4.10	0.03	44 (2%)	2	3.88 (98%)	0.01	4.7	0.1
0.30	4.52	0.03	40 (2%)	5	4.20 (98%)	0.03	5.0	0.3
0.40	5.34	0.03	41 (3%)	5	4.77 (97%)	0.03	5.9	0.3
0.50	6.16	0.04	33 (3%)	13	5.24 (97%)	0.08	6.3	0.5
0.70	7.38	0.02	-	-	-	-	-	-
1.00	10.2	-	30 (12%)	16	9.85 (88%)	0.04	12.2	2

Table 6.4 Spin-lattice relaxation rates of various NYRIM samples

Firstly the spin-lattice relaxation times will be discussed. The columns 2 and 3 represent the relaxation rate obtained from 1 exponential, such as

$$M(t)/M_0 = 1 - 2\exp\left(-t/T_1^H\right) \qquad (6.3)$$

and the corresponding maximum error. Although the relaxation behaviour could be described by this expression, the fitting of the experimental data expects a second small short-time component for nylon and the copolymers as visualised in table 6.4 in columns 4 and 6.

fraction PPO	$T_{1\rho}^{H}(1)$ / s	±s	$T_{1\rho}^{H}(2)$ / s	±s	$T_{1\rho}^{H}(3)$ / s	±s	$T_{1\rho,av}^{H-1}$ / s^{-1}	± s^{-1}
0.00	0.030 (59%)	0.005	0.010 (35%)	0.002	0.0021 (6%)	0.0006	84	5
0.10	0.025 (39%)	0.006	0.008 (44%)	0.005	0.0019 (17%)	0.0008	149	10
0.15	0.019 (52%)	0.002	0.005 (36%)	0.003	0.0013 (12%)	0.0005	188	21
0.20	0.025 (37%)	0.005	0.009 (46%)	0.002	0.0018 (17%)	0.0005	161	16
0.25	0.025 (39%)	0.006	0.008 (46%)	0.005	0.0014 (15%)	0.0010	186	27
0.30	0.025 (44%)	0.007	0.009 (41%)	0.002	0.0016 (15%)	0.0004	155	13
0.40	0.017 (55%)	0.001	0.005 (35%)	0.001	0.0009 (10%)	0.0004	223	27
0.50	0.019 (56%)	0.002	0.006 (34%)	0.003	0.0012 (10%)	0.0006	165	1
0.70	0.019 (54%)	-	0.009 (28%)	-	0.0014 (12%)	-	145	-
1.00	0.04 (55%)	0.02	0.02 (45%)	0.01	-	-	30	2

Table 6.5 Rotating-frame spin-lattice relaxation rates of various NYRIM samples

The second component makes only 1 to 3% and is about a magnitude shorter than the other one. The relaxation rates are relatively constant between 40 and 48 s^{-1}, whereas the

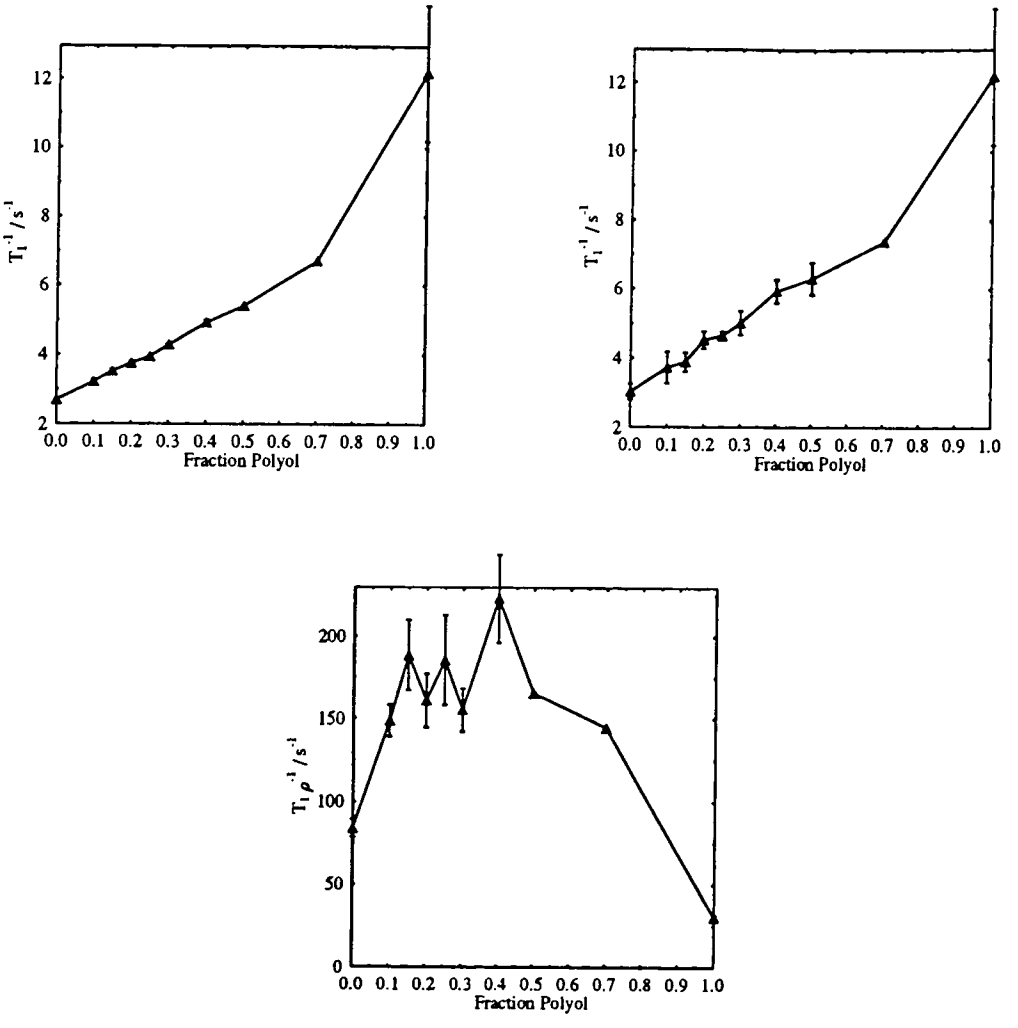

Figure 6.5 Proton spin-lattice relaxation times as a function of prepolymer concentration top left: T_1, one component fit; top right: T_1, two component fit; bottom: $T_{1\rho}$ three component fit

long-time relaxation component continuously shortens with increasing polyether concentration. This is simply due to the fact that the intrinsic relaxation time of the polyether is shorter than the one(s) of nylon-6, as the results of the pure components allow one to assume. Hence, the observed relaxation rate, which is identical with the population-weighted relaxation rate calculated from the intrinsic relaxation times of the components, becomes larger with increasing polyether concentration.

The question of the meaning of the the small component is not easily answered. Two explanations are possible:

1. End-groups of the copolymer, which show much faster motion compared to the polymer back-bone are not coupled by spin-diffusion and have a smaller relaxation time.
2. The NYRIM system is similar to the one modelled in chapter 5 concerning the NMR properties. The second component could also be due to the heterogeneous character of the copolymer and insufficient coupling due to spin-diffusion.

However, from the data obtained no explanation has any preference. The only important point to make is that the population-weighted average relaxation rates obtained from the two-component fit are larger than the ones obtained from the one-component fit. The dependence of the relaxation rate on the polyether concentration remains the same as illustrated in figure 6.5 (top). Apart from the pure PPO one finds a linear dependence, which is normal for phase-separated copolymers in which the combination of the phases does not effect the individual intrinsic relaxation rates of the components.

A more complicated situation is found in the rotating-frame relaxation behaviour. It may be described by three relaxation components whose values differ by less than one order of magnitude. As has already been discussed in chapter 4, Kenwright [7] has demonstrated that the fastest relaxation component may be closely associated with the intrinsic relaxation process of the faster relaxing region. The next fastest relaxation component may be associated with the rate of establishment of a diffusion

profile. The slowest relaxation component may be associated with the rate of relaxation of the magnetisation followed by the establishment of a steady-state diffusion profile across the entire sample. Since, by this stage in the relaxation process, only a very small amount of magnetisation remains in the faster relaxing region, it is reasonable to associate the slowest relaxation time with the slower relaxing region. This results supported by the fact that the relaxation times found are remarkably constant for all compositions. However, it is surprising that the population of the short-time component, e.g., which should be associated with the PPO, is not increasing with increasing polyether concentration. Also the fact that no linear dependency of the population-weighted average relaxation rate with the PPO concentration is found is mysterious. However, this suggests that on this timescale the combination of the phases interferes with the individual intrinsic relaxation rates, i.e. the neighbouring phases reveal interactions which influence the intrinsic relaxation properties. Another indication is the significantly different relaxation rates of the two pure polymers from the copolymers. Only when copolymerised does the population-weighted average relaxation rate establish its stable behaviour. Because of the deficiency in knowledge of the polymeric structure it is not possible to make a final conclusion of what the origin of this influence is.

However, this chapter shows that the proton relaxation behaviour is a complex topic and the results cannot be interpreted easily. Especially the quantification of the

results is problematic because spin-diffusion distorts the population and the obtained relaxation times. Hence, in solids, the measured relaxation values of the abundant spins are most likely not the intrinsic relaxation times.

References to Chapter 6

[1] V.H. McBrierty, Polymer, **15** (1974) 503

[2] V.H. McBrierty, D.C. Douglas, J.Polym.Sci, Macromol. Rev., **16** (1981) 295

[3] W.L. Earl, D.L. VanderHart, Macromol., **12** (1979) 762

[4] M.E.A. Cudby, R.K. Harris, K. Metcalfe, K.J. Packer, P.W.R. Smith, A.Bunn, Polymer, **26** (1985) 169

[5] A.D. Booth, K.J. Packer, Mol. Phys., **62** (1987) 811

[6] P. Mansfield, Progress in Nuclear Magnetic Resonance Spectroscopy, **8** (1972) 41

[7] A.M. Kenwright, K.J. Packer, B.J. Say, J. Magn. Reson., **69** (1986) 426

Summary

Nylon-6 block copolymers (NBC) are a relatively new class of Reaction Injection Moulding (RIM) systems, covering a broad range of morphologies and properties. Very rapid polymerisation occurs at temperatures between 80 °C and 180 °C, well below the temperature required for the thermal initiation (≈200 °C). In this work, NBC have been produced by anionic polymerisation of caprolactam with end-functionalised soft-block components involving polyether fragments. This gives rise to linear segmented block copolymers with alternating polyamide (hard block) and polyether-polyesteramide prepolymer (soft block) components.

Mechanical and structural parameters were measured and brought into relation. The dramatic decrease of the tensile strength from 30% PPO concentration shows its origin in a morphological change. The amorphous nylon-6 phase is enlarging if the polyether concentration exceeds 25%. A slower crystallisation dynamic is the reason. The domain sizes were obtained from spin-diffusion measurements by a theoretical model with lamellar morphology. Previous problems such as the influence of spin-lattice relaxation have been eliminated. By investigating techniques which should minimise the T_1^H influence in the Goldman-Shen type experiments it has been demonstrated that in heterogeneous systems the smallest intrinsic T_1^H must be longer than the mixing time in order to give a pure spin-diffusion profile. Otherwise the T_1^H minimisation must fail because spin-diffusion and spin-lattice relaxation are coupled processes which cannot be

separated. The domain sizes obtained from spin-diffusion measurements have been compared with the ones obtained from small-angle X-ray scattering. The data agree within an error range of a factor two. However, they reveal an opposite trend when monitoring them as a function of PPO concentration, which could not be explained, but was probably caused by a non-ideal morphology of the polymeric system. Here the incomplete information of the amorphous nylon-6 probably plays a key-role. Single-pulse ^{13}C solid-state NMR indicates a second amorphous phase in the copolymer. The reasons for that statement are the intense broad signals at room-temperature which narrow at higher temperature. The splitting of the C3 signal at 26.3 ppm is most likely due to two different amorphous regions. Another indication is that ^{13}C CP/MAS gives rise to relatively sharp and resolved signals for a quenched copolymer, whereas a single-pulse spectrum gives a broad unresolved spectrum.

The most important technique in solid-state NMR, CP/MAS, has been investigated. The cross-polarisation dynamics were of particular interest. There is a lot of confusion and misinterpretation when studying CP-dynamics with the influence of spin-diffusion. The theories which have been given in the past were summarised. Finally an attempt has been made to model CP-dynamics in non-ideal materials.

Solid-state NMR has proved its proficiency concerning the analysis of complex polymeric materials. Small-angle X-ray scattering, as a standard technique for domain-size measurements, now has a dignified competitor since static proton NMR spectrometers are as expensive as SAXS

instruments. The technique becomes particularly a matter of interest when studying heterogeneous non-crystalline materials for which SAXS is useless. However, as has been demonstrated in this thesis, one should not generally give preference to one experimental technique. The combination of many techniques enables one to gain insight into the fascinating science.

Appendix I Sample Input-File for "*MODEL.F*"

```
 0              {morphology parameter; 0:lamellar, 1:cylindrical polar; spherical polar}
1.9450E-09      {full length of region 1}
1.0000E-00      {proton density of region 1}
3.8650E-17      {spin-diffusion coefficient in m²s⁻¹ of region 1}
0.0452E-00      {proton spin-lattice relaxation time in s of region 1}
1.0000E-01      {proton T1ρ in s of region 1}
2.1700E-04      {T2 in s of region 1}
 1              {1: exponential type FID; 2:gaussian type FID}
30              {number of mesh points}
6.7710E-09      {full length of region 2}
1.0000E-00      {proton density of region 2}
4.8200E-16      {spin-diffusion coefficient in m²s⁻¹ of region 2}
9.4387E-00      {proton spin-lattice relaxation time in s of region 2}
1.0000E-01      {proton T1ρ in s of region 2}
17.400E-06      {T2 in s of region 2}
 2              {1: exponential type FID; 2:gaussian type FID}
30              {number of mesh points}
 1              {pulse in π/2 units (here 90°)}
 2              {1: T1ρ; 2: T2 relaxation}
5.0000E-06      {dwell time in s}
10              {number of points with dwell time DW}
 3              {pulse in π/2 units (here 270°)}
 1              {1: T1; 2: T2 relaxation}
2.8000E-02      {dwell time in s, not used}
29              {number of  points}
 0              {no data fit (spin-lattice relaxation)}
0.43            {fraction crystalline nylon within nylon}
 0.00075 -370.6 437.1    {data file from Goldmann-Shen experiment obtained from theWRAC
 0.001   -359.6 431.1    {spectrometer
 0.002   -329.6 411.1    {data format:
 0.003   -309.9 396.4    {time, magentisation stored in -z-direction, magentisation stored in +z-
 0.004   -287.5 384.3    {direction
 0.005   -268.3 371.9
 0.006   -253.4 354.3
 0.007   -238.3 354.3
 0.008   -223.5 343.1
 0.009   -209.5 335.4
 0.010   -197.5 329.6
 0.015   -146.2 301.5
 0.020   -104.6 280.9
 0.025    -70.9 267.9
 0.030    -59.4 261.8
 0.040     18.4 250.8
 0.050     57.2 246.9
 0.060     85.9 250.2
 0.070    109.4 252.7
 0.080    130.1 255.0
 0.090    148.7 261.0
 0.100    165.1 267.6
 0.150    228.5 297.7
 0.200    271.6 328.4
 0.250    308.7 352.8
 0.300    337.4 373.9
 0.350    361.6 390.7
 0.400    383.7 406.8
 0.500    410.6 429.1
```

Appendix II FORTRAN 77 PROGRAM "*MODEL.F*"

```
      PROGRAM MODEL

      INTEGER ITER,MPP,NDIM,NPP,NMAX,ITMAX,DATMAX,MAGCNT,FLAG,DIS,FLWR
      PARAMETER (NMAX=20,NDIM=4,DATMAX=200)
      REAL FTOL,PP(NDIM+1,NDIM),Y(NDIM+1),PTRY(NMAX),CRYST
      PARAMETER (ITMAX=5000,FTOL=3.0E-2)
      REAL FUNK,EVALUATE
      INTEGER M,RT,RT1,RT2,NP(3),GE(3),R,R1,R2,NT,NT1,NT2,N,I,DIRE
      REAL L(3),LEN(3),HD(3),D(3),TL(3),TR(3),T2(3)
      REAL S(3),SUM,SUMAG(1005),DW,DW1,DW2
      REAL XX(DATMAX),YY(DATMAX),DUM,FACT,START,SVALUE,CVALUE
      DOUBLE PRECISION U(100),AA(100)
      EXTERNAL FUNK,EVALUATE
      COMMON /ALAN/  D,TL,TR,L,HD,DIRE,FLAG,START,FLWR,CRYST
      COMMON /RES/   S,SUM,SUMAG,M,MAGCNT
      COMMON /PARAD/ U,AA,T2,XX,YY,DW,DW1,DW2,LEN
      COMMON /PARAI/ R,R1,R2,RT,RT1,RT2,NT,NT1,NT2,GE,NP,N

      MPP=NDIM+1
      NPP=NDIM

C
C     LEN(1)=WIDTH OF INTRUSION, LEN(2)=THICKNESS OF INTERFACE,
C     LEN(3)=DISTANCE THRO' MATRIX BETWEEN INTERFACIAL LAYERS
C
C     READ IN VALUE FOR M (MORPHOLOGY PARAMETER)
C     READ IN VALUES FOR LEN (SIZE IN METRES), HD (PROTON DENSITY),
C     D (SPIN DIFFUSION COEFFICIENT IN M2S-1),
C     TL AND TR (SPIN LATTICE RELAXATION TIMES IN THE LAB
C     AND ROTATING FRAMES IN SECONDS), T2 (T2! IN SECONDS),
C     GE (EXPONENTIAL(1) OR GAUSSIAN(2) T2),
C     AND NP (NUMBER OF MESH POINTS) FOR EACH REGION
C


      FLWR=0

      READ (5,*) M
      DO 10 I=1,3
       READ (5,*) LEN(I)
       READ (5,*) HD(I)
       READ (5,*) D(I)
       READ (5,*) TL(I)
       READ (5,*) TR(I)
       READ (5,*) T2(I)
       READ (5,*) GE(I)
       READ (5,*) NP(I)
       IF (GE(I).NE.1.AND.GE(I).NE.2) THEN
        WRITE(8,5999)
        STOP
       ENDIF
   10 CONTINUE
      READ (5,*) R2
      READ (5,*) RT2
      READ (5,*) DW2
      READ (5,*) NT2
      READ (5,*) R1
      READ (5,*) RT1
```

```
      READ (5,*) DW1
      READ (5,*) NT1
      READ (5,*) N
      READ (5,*) CRYST

C
C    DECISION WETHER MAGN. STORED IN + OR - Z-DIRECTION
C
      IF (R1 .EQ. 1) DIS=0
      IF (R1.EQ.3) DIS=1

      IF (DIS.EQ.0) THEN
       DO 15 I=1,NT1
         READ(5,*) XX(I), DUM, YY(I)
 15    CONTINUE
      ENDIF
      IF (DIS.EQ.1) THEN
       DO 16 I=1,NT1
         READ(5,*) XX(I), DUM, YY(I)
 16    CONTINUE
      ENDIF


C
C    INITIAL GUESSES
C
      PP(1,1) = LEN(1)
      PP(1,2) = LEN(2)
      PP(1,3) = TL(1)
      PP(1,4) = TL(2)

      PTRY(1) = PP(1,1)
      PTRY(2) = PP(1,2)
      PTRY(3) = PP(1,3)
      PTRY(4) = PP(1,4)
      SVALUE=YY(1)

      WRITE(6,*) 'INITIALIZING DATA CORRECTION FACTOR'

      DUM=EVALUATE(PTRY)
      FACT=START/YY(1)
      WRITE(6,*) START, FACT
      DO 18 I=1, NT1
       YY(I)=YY(I)*FACT
       WRITE(6,110) XX(I), YY(I)
 18 CONTINUE
      WRITE(11,*)
110 FORMAT(2F12.5)
      WRITE(11,111)
      CVALUE=YY(1)
      write(6,*) 'cvalue', cvalue

      DO 20 I=1,
      PTRY(1) = PP(1,1)
      PTRY(2) = PP(1,2)
      PTRY(3) = PP(1,3)
      PTRY(4) = PP(1,4)

      WRITE(6,*) 'INITIALIZING DATA CORRECTION FACTOR'

      DUM=EVALUATE(PTRY)
c     write(6,*) 'cvalue ',cvalue
```

```
c     IF (START.GT.CVALUE+0.03*CVALUE) START=CVALUE
c     IF (START.LT.CVALUE-0.03*CVALUE) START=CVALUE
c     FACT=START/YY(1)
c     WRITE(6,*) 'start ', START, 'fact ', FACT
c     DO 17 J=1, NT1
c       YY(J)=YY(J)*FACT
c       WRITE(11,110) XX(J), YY(J)
c  17 CONTINUE
c     WRITE(11,*)

      WRITE(6,*)'SETTING UP SIMPLEX'
      WRITE(17,*)'SETTING UP SIMPLEX'
      CALL SIMPLEX(PP,PTRY,Y,MPP,EVALUATE)
      WRITE(6,*)'FITTING'
      WRITE(17,*)'FITTING'
      CALL AMOEBA(PP,Y,MPP,NPP,NDIM,FTOL,EVALUATE,ITER)
   20 CONTINUE

      WRITE(11,111)
      DO 25 I=1,NT1
       WRITE(11,110) XX(I),YY(I)
   25 CONTINUE
      WRITE(11,*)
      WRITE(11,*)
      FACT=SVALUE/YY(I)
      WRITE(11,112)
      WRITE(11,113) 1./FACT
      FACT=SVALUE/YY(1)
      DO 30 I=1,NT1
       WRITE(11,114) XX(I),YY(I)*FACT
   30 CONTINUE
      write(8,*) iter,' iteration needed '
      write(8,*) pp(1,1), pp(1,2), pp(1,3), pp(1,4)


C     ***************** Output of the final results ******************


      FLWR=1

      DUM=EVALUATE(PTRY)
      FACT=START/YY(1)

      CVALUE=YY(1)

      PTRY(1) = PP(1,1)
      PTRY(2) = PP(1,2)
      PTRY(3) = PP(1,3)
      PTRY(4) = PP(1,4)

      WRITE(6,*) 'Calculating final results'

      DUM=EVALUATE(PTRY)


C     ***************** End of calculation final results ***************


  111 FORMAT(1X,27HINPUT DATA AFTER CORRECTION)
  112 FORMAT(1X,28HINPUT DATA BEFORE CORRECTION/)
  113 FORMAT(1X,28HALTOGETHER CORRECTION FACTOR, F12.8)
  114 FORMAT(1X,F12.5,F12.1)
```

```
5999 FORMAT (1X/,1X,33H ERROR IN SPECIFICATION - ABORTED,1X/)
 999 STOP
     END
     SUBROUTINE SIMPLEX(PP,PTRY,Y,MPP,EVALUATE)

     INTEGER I,J,MPP
     INTEGER NMAX,DATMAX,M,MAGCNT,FLAG,FLWR
     PARAMETER (NMAX=20,DATMAX=200)
     REAL PP(MPP,MPP-1),PTRY(NMAX),Y(MPP)
     REAL XX(DATMAX),YY(DATMAX),EVALUATE,START,CRYST
     REAL LEN(3),TL(3),T2(3),DW,DW1,DW2,TR(3)
     REAL L(3),HD(3),D(3),S(3),SUM,SUMAG(1005)
     DOUBLE PRECISION U(100),AA(100)
     INTEGER NT,NT1,NT2,GE(3),NP(3),R,R1,R2,RT,RT1,RT2,N,DIRE

     COMMON /ALAN/  D,TL,TR,L,HD,DIRE,FLAG,START,FLWR,CRYST
     COMMON /RES/   S,SUM,SUMAG,M,MAGCNT
     COMMON /PARAD/ U,AA,T2,XX,YY,DW,DW1,DW2,LEN
     COMMON /PARAI/ R,R1,R2,RT,RT1,RT2,NT,NT1,NT2,GE,NP,N

     EXTERNAL EVALUATE


     DO 20 I=1, MPP-1
      DO 30 J=1, MPP
        PP(J,I)=PP(1,I)
30    CONTINUE
20  CONTINUE

     DO 25 J=2, MPP
      PP(J,J-1)=PP(J,J-1)*1.15
25  CONTINUE

     DO 40 J=1, MPP
      DO 41 I=1, MPP-1
        PTRY(I)=PP(J,I)
41    CONTINUE
      Y(J)=EVALUATE(PTRY)
      WRITE(6,211) PTRY(1), PTRY(2), PTRY(3)
      WRITE(6,212) PTRY(4), PTRY(5), PTRY(6)
      WRITE(6,213) Y(J)
      WRITE(17,211) PTRY(1), PTRY(2), PTRY(3)
      WRITE(17,212) PTRY(4), PTRY(5), PTRY(6)
      WRITE(17,213) Y(J)
 40  CONTINUE
211 FORMAT('LEN`S= ', 3D10.4)
212 FORMAT('T1`s = ', 3F10.4)
213 FORMAT('SDD = ',  F10.4)
     RETURN
     END



     SUBROUTINE AMOEBA(PP,Y,MPP,NPP,NDIM,FTOL,EVALUATE,ITER)

     INTEGER ITER,MPP,NDIM,NPP,NMAX,ITMAX,DATMAX
     REAL FTOL,PP(MPP,NPP),Y(MPP),EVALUATE,AMOTRY
     PARAMETER (NMAX=20,ITMAX=5000,DATMAX=200)
     EXTERNAL EVALUATE
     INTEGER I,IHI,ILO,INHI,J
```

```
      REAL RTOL,SUM,SWAP,YSAVE,YTRY,PSUM(NMAX)
      INTEGER M,N


      ITER=0
    1 DO 12 N=1, NDIM
        SUM=0.
        DO 11 M=1, NDIM+1
          SUM=SUM+PP(M,N)
   11   CONTINUE
        PSUM(N)=SUM
   12 CONTINUE
    2 ILO=1
      IF (Y(1).GT.Y(2)) THEN
        IHI=1
        INHI=2
      ELSE
        IHI=2
        INHI=1
      ENDIF
      DO 13 I=1, NDIM+1
        IF(Y(I).LE.Y(ILO)) ILO=I
        IF(Y(I).GT.Y(IHI)) THEN
          INHI=IHI
          IHI=I
        ELSE IF(Y(I).GT.Y(INHI)) THEN
          IF(I.NE.IHI) INHI=I
        ENDIF
   13 CONTINUE
      RTOL=2.*ABS(Y(IHI)-Y(ILO))/(ABS(Y(IHI))+ABS(Y(ILO)))
      IF(RTOL.LT.FTOL) THEN
        SWAP=Y(1)
        Y(1)=Y(ILO)
        Y(ILO)=SWAP
        DO 14 N=1, NDIM
          SWAP=PP(1,N)
          PP(1,N)=PP(ILO,N)
          PP(ILO,N)=SWAP
   14   CONTINUE
        RETURN
      ENDIF
      IF(ITER.GE.ITMAX) PAUSE 'ITMAX EXCEEDED IN AMOEBA'
      ITER=ITER+2

      YTRY=AMOTRY(PP,Y,PSUM,MPP,NPP,NDIM,EVALUATE,IHI,-1.0)
      IF(YTRY.LE.Y(ILO)) THEN
        YTRY=AMOTRY(PP,Y,PSUM,MPP,NPP,NDIM,EVALUATE,IHI,2.0)
      ELSE IF(YTRY.GE.Y(INHI)) THEN
        YSAVE=Y(IHI)
        YTRY=AMOTRY(PP,Y,PSUM,MPP,NPP,NDIM,EVALUATE,IHI,0.5)
        IF(YTRY.GE.YSAVE) THEN
          DO 16 I=1, NDIM+1
            IF (I.NE.ILO) THEN
              DO 15 J=1, NDIM
                PSUM(J)=0.5*(PP(I,J)+PP(ILO,J))
                PP(I,J)=PSUM(J)
   15         CONTINUE
              Y(I)=EVALUATE(PSUM)
            ENDIF
   16     CONTINUE
          ITER=ITER+NDIM
          GOTO 1
```

```
 ENDIF
 ELSE
  ITER=ITER-1
 ENDIF
 GOTO 2
 END


 FUNCTION AMOTRY(PP,Y,PSUM,MPP,NPP,NDIM,EVALUATE,IHI,FAC)

 INTEGER IHI,MPP,NDIM,NPP,NMAX,DATMAX
 PARAMETER (NMAX=20,DATMAX=200)
 REAL AMOTRY,EVALUATE,FAC,PP(MPP,NPP),PSUM(NMAX),Y(MPP)
 EXTERNAL EVALUATE
 INTEGER J
 REAL FAC1,FAC2,YTRY,PTRY(NMAX)


 FAC1=(1.-FAC)/NDIM
 FAC2=FAC1-FAC
 DO 11 J=1, NDIM
  PTRY(J)=PSUM(J)*FAC1-PP(IHI,J)*FAC2
11 CONTINUE

 YTRY=EVALUATE(PTRY)

 IF (YTRY.LT.Y(IHI)) THEN
  Y(IHI)=YTRY
  DO 12 J=1, NDIM
   PSUM(J)=PSUM(J)-PP(IHI,J)+PTRY(J)
   PP(IHI,J)=PTRY(J)
12  CONTINUE
 ENDIF
 AMOTRY=YTRY
 RETURN
 END


 FUNCTION EVALUATE(PTRY)

 INTEGER NMAX,DATMAX,M,MAGCNT,FLAG,FLWR
 PARAMETER (NMAX=20,DATMAX=200)
 REAL XX(DATMAX),YY(DATMAX),DUM,EVALUATE,FUNK,PTRY(NMAX),START
 REAL LEN(3),TL(3),T2(3),DW,DW1,DW2,TR(3),CRYST
 REAL L(3),HD(3),D(3),MNEW,MOLD,S(3),SUM,SUMAG(1005)
 DOUBLE PRECISION U(100),AA(100)
 INTEGER NT,NT1,NT2,GE(3),NP(3),R,R1,R2,RT,RT1,RT2,N,DIRE

 COMMON /ALAN/  D,TL,TR,L,HD,DIRE,FLAG,START,FLWR,CRYST
 COMMON /RES/   S,SUM,SUMAG,M,MAGCNT
 COMMON /PARAD/ U,AA,T2,XX,YY,DW,DW1,DW2,LEN
 COMMON /PARAI/ R,R1,R2,RT,RT1,RT2,NT,NT1,NT2,GE,NP,N


 EXTERNAL FUNK

 MOLD=YY(1)
 R=R2
 RT=RT2
 DW=DW2
```

```
      NT=NT2
      FLAG=0
      DUM=FUNK(PTRY,MNEW)

      R=R1
      RT=RT1
      DW=DW1
      NT=NT1
      FLAG=1
      EVALUATE=FUNK(PTRY,MNEW)
      RETURN
      END



      FUNCTION FUNK(PTRY,MNEW)

C     !*************************************************************!
C     !                                                           !
C     !              RELAX                                        !
C     !                                                                 !
C     !*************************************************************!
C
C
C     SIMULATION OF NMR RELAXATION FOR AN INFINITE SYMMETRIC
C     HETEROGENEOUS SYSTEM CONSISTING OF LAMELLAE, RODS, OR SPHERULITES
C     EMBEDDED IN A MATRIX.  SAMPLE COMPRISES THREE LAYERS WITH
C     DISCRETE VALUES FOR SPIN LATTICE RELAXATION (IN BOTH THE
C     LABORATORY AND ON-RESONANCE ROTATING FRAMES), SPIN - SPIN
C     RELAXATION, PROTON DENSITY, AND SPIN DIFFUSION COEFFICIENT
C     IN EACH REGION. INTEGRATED MAGNETISATION CALCULATED.
C
C
      DOUBLE PRECISION A,B,TOUT,TS,ACC,TE,TCONST
      REAL L(3),TR(3),S(3),TL(3),D(3),P(3),LEN(3),HD(3),T2(3),FUNK
      REAL SUM,REP,DW,DW1,DW2,SUMAG(1005),TOT,CRYST
      INTEGER IFAIL,IMESH,IND,IWK,M,NPDE,NPTS,I,J,N,NT,NT1,NT2,MAGCNT
      INTEGER NMAX,DATMAX,FLAG,FLWR
      PARAMETER(NMAX=20,DATMAX=200)
      INTEGER DIRE,R,R1,R2,PULS,NP(3),GE(3),RT,RT1,RT2
      DOUBLE PRECISION X(100),U(100),WORK(2000),AA(100)
      REAL SSD,MNEW,XX(DATMAX),YY(DATMAX),PTRY(NMAX),START

      COMMON /ALAN/  D,TL,TR,L,HD,DIRE,FLAG,START,FLWR,CRYST
      COMMON /RES/  S,SUM,SUMAG,M,MAGCNT
      COMMON /PARAD/ U,AA,T2,XX,YY,DW,DW1,DW2,LEN
      COMMON /PARAI/ R,R1,R2,RT,RT1,RT2,NT,NT1,NT2,GE,NP,N


C
C     SUBROUTINE REFERENCES
C     D03PBF,DMESH,INTEG
C
      EXTERNAL BNDY,PDEF


C
C     REDEFINE LEN,TL WITH VERTEX
C

      LEN(1) = PTRY(1)
```

```
      LEN(3) = PTRY(2)
      LEN(2) = 0.5 * (1-CRYST) / CRYST * LEN(3)
       TL(1) = PTRY(3)
       TL(2) = PTRY(4)
       TL(3) = TL(2)
C
C CALCULATE DIMENSIONS USED IN REPEAT UNIT AND PUT IN
C CORRECTION FACTORS TO MAKE MODEL "SPACE FILLING"
C
      L(1)=LEN(1)/2
      L(2)=LEN(2)
      L(3)=LEN(3)/2
      IF (M.EQ.1) L(3)=(L(1)+L(2)+L(3))*1.050075136-(L(1)+L(2))
      IF (M.EQ.2) L(3)=(L(1)+L(2)+L(3))*1.1053389-(L(1)+L(2))
C
C     DEFINE INTEGRATION PARAMETERS
C
      ACC=1.0E-04
C
C     SIZE OF WORKSPACE
C
      IWK=2000
C
C     INTERVAL OF INTEGRATION
C
      A=0.0
      B=L(1)+L(2)+L(3)+A
C
C     ONE EQUATION
C
      NPDE=1
C
C     PERIODICITY
C
      REP=L(1)+L(2)+LEN(3)/2
C
C     CALCULATE PROPORTIONS OF VARIOUS COMPONENTS
C
      TOT=(B-A)**(M+1)
      P(1)=((L(1)**(M+1))/TOT)*100
      P(2)=(((L(2)+L(1))**(M+1))/TOT)*100-P(1)
      P(3)=100-(P(2)+P(1))
C
C     CALCULATE TOTAL NUMBER OF POINTS (INCLUDING BOUNDARIES)
C
      NPTS=NP(1)+NP(2)+NP(3)+4
C
C     PRINT PARAMETER VALUES
C
      IF (FLWR .EQ. 1) THEN
       WRITE (8,1100)
       IF (M.EQ.0) WRITE (8,1200)
       IF (M.EQ.1) WRITE (8,1201)
       IF (M.EQ.2) WRITE (8,1202)
       WRITE (8,1000)
       WRITE (8,1001) LEN(1),LEN(2),LEN(3)
       WRITE (8,1002) D(1),D(2),D(3)
       WRITE (8,1003) TL(1),TL(2),TL(3)
       WRITE (8,1004) TR(1),TR(2),TR(3)
       WRITE (8,2004) T2(1),T2(2),T2(3)
       WRITE (8,2006) GE(1),GE(2),GE(3)
       WRITE (8,1005) P(1),P(2),P(3)
```

```
      END IF
C
C NORMALISE PROTON DENSITIES AND CALCULATE %PROTONS IN EACH REGION
C
      SUM=0.
      TOT=HD(1)
      IF (HD(2).LT.TOT) TOT=HD(2)
      IF (HD(3).LT.TOT) TOT=HD(3)
      DO 11 I=1,3
      HD(I)=HD(I)/TOT
      P(I)=P(I)*HD(I)
      SUM=SUM+P(I)
   11 CONTINUE
      IF (FLWR.EQ.1) WRITE (8,2020) HD(1),HD(2),HD(3)
      TOT=100/SUM
      DO 12 I=1,3
      P(I)=P(I)*TOT
      HD(I)=HD(I)*TOT
   12 CONTINUE
C
C PRINT REST OF PARAMETER VALUES
C
      IF (FLWR.EQ.1) THEN
       WRITE (8,2010) P(1),P(2),P(3)
       WRITE (8,1006) NP(1),NP(2),NP(3)
       WRITE (8,1010) L(1),L(2),L(3)
       WRITE (8,1007) 2*REP
       WRITE (8,1008) NPTS
       WRITE (8,1009) ACC
       WRITE (8,4992)
      END IF

C     ********** begin check whether T2 or T1 *********

      IF (R.NE.3.AND.FLAG.EQ.0) THEN
C
C     DEFINE THE MESH
C
      IMESH=5
      CALL DMESH(L,NP,NPTS,X,A,B)
C
C     SET UP THE INITIAL CONDITIONS
C
      TE=0.0
      DIRE=0
      DO 20 I=1,NPTS
      U(I)=1
   20 CONTINUE

      ENDIF

C     ********** end check whether T2 or T1 *********


      PULS=R*90
      IF (FLWR.EQ.1) WRITE (8,4993) PULS
      IF (R.EQ.0) GOTO 65
      DO 40 J=1,R
      DIRE=DIRE+1
      IF (DIRE.GE.4) DIRE=DIRE-4
      IF (DIRE.NE.0.AND.DIRE.NE.2) GOTO 60
      DO 50 I=1,NPTS
```

```
      U(I)=-U(I)
   50 CONTINUE
   60 CONTINUE
   40 CONTINUE
   65 CONTINUE
      TS=0.0
      IF (DIRE.EQ.1.OR.DIRE.EQ.3) THEN
      IF (RT.NE.1.AND.RT.NE.2) THEN
      IF (FLWR.EQ.1) WRITE (8,5999)
      GOTO 999
      ELSE
      SUMAG(1003)=0
      ENDIF
      IF (RT.EQ.1) THEN
      IF (FLWR.EQ.1) WRITE (8,4995)
      ELSE
      IF (FLWR.EQ.1) WRITE (8,4005)
      ENDIF
      ELSE
      SUMAG(1003)=1
      IF (FLWR.EQ.1) WRITE (8,4994)
      ENDIF

      IF (R.NE.0) THEN
      MAGCNT=0
      SUMAG(1004)=0
      SUMAG(1005)=0
      ELSE
      MAGCNT=MAGCNT-1
      SUMAG(1004)=SUMAG(1001)
      SUMAG(1005)=SUMAG(1002)
      ENDIF
      SUMAG(1001)=NT
      SUMAG(1002)=DW
      IF (FLWR.EQ.1) THEN
       WRITE (8,7999) NT,DW
       WRITE (8,8990)
      END IF
      CALL INTEG(NP,NPTS,A,B,TS,X,U,TE,MNEW)
      SSD=0.

      IND=0
      DO 67 I=1,NPTS
      AA(I)=U(I)
   67 CONTINUE
      IFAIL=0
      DO 70 I=1,NT
      IF (R.NE.3.AND.FLAG.EQ.0) THEN
       TOUT=DW+TS
       TE=TE+DW
       TCONST=TE
      ELSE
       TOUT=DBLE(XX(I))
       TE=TOUT+TCONST
      ENDIF
      IF ((DIRE.EQ.1.AND.RT.EQ.2).OR.(DIRE.EQ.3.AND.RT.EQ.2)) THEN
      CALL TEETOO(NP,NPTS,TS,TOUT,U,GE,T2,AA)
      ELSE
C
C     CALL D03PBF TO COMPUTE SOLUTION AT TREL
C
      CALL D03PBF(NPDE,M,PDEF,BNDY,A,B,TS,TOUT,U,NPTS,IMESH,X,
```

```
     &ACC,WORK,IWK,IND,IFAIL)
      ENDIF
C
C     CHECK IF ERROR DETECTED
C
      IF (IFAIL.NE.0) GOTO 170
C
C     INTEGRATE THE MAGNETISATION AND OUTPUT THE RESULTS
C
      CALL INTEG(NP,NPTS,A,B,TS,X,U,TE,MNEW)

      IF (I.EQ.1) START=MNEW

      SSD=SSD+(YY(I)-MNEW)**2

   70 CONTINUE
      FUNK=SSD
      RETURN
C
C     ERROR IN D03PBF
C
  170 WRITE (8,8989)IFAIL,TOUT
  999 RETURN
C
C     FORMAT STATEMENTS
C
 1200 FORMAT (21X,34HLAMELLAR MORPHOLOGY          /)
 1201 FORMAT (21X,34HCYLINDRICAL MORPHOLOGY       /)
 1202 FORMAT (21X,34HSPHERICAL MORPHOLOGY         /)
 1010 FORMAT (1X,35HDIMENSIONS IN REPEAT UNIT (METRES):,5X,
     &3(1X,1PE11.4)/)
 1100 FORMAT (1X/,10X,24H1H RELAXATION SIMULATION,
     &22H FOR A 3 REGION SYSTEM,1X/)
 1000 FORMAT (43X,8HREGION 1,4X,8HREGION 2,4X,8HREGION 3/)
 1001 FORMAT (1X,30HTHICKNESS OF REGIONS (METRES):,10X,3(1X,1PE11.4)/)
 1002 FORMAT (1X,28HSPIN DIFFUSION COEFFS (MKS):,12X,3(1X,1PE11.4)/)
 2020 FORMAT (1X,28HNORMALISED PROTON DENSITIES:,12X,3(1X,1PE11.4)/)
 1003 FORMAT (1X,21HINTRINSIC T1'S (SEC):,19X,3(1X,1PE11.4)/)
 1004 FORMAT (1X,24HINTRINSIC T1RHO'S (SEC):,16X,3(1X,1PE11.4)/)
 2004 FORMAT (1X,21HINTRINSIC T2'S (SEC):,19X,3(1X,1PE11.4)/)
 1005 FORMAT (1X,'PROPORTIONS OF COMPONENTS (VOL%):',7X,3(3X,F6.3,3X)/)
 2010 FORMAT (1X,'PROPORTIONS OF COMPONENTS (1H%):',8X,3(3X,F6.3,3X)/)
 1006 FORMAT (1X,20HPOINTS DISTRIBUTION:,20X,3(5X,I3,4X)/)
 2006 FORMAT (1X,20HEXPO(1) OR GAUSS(2):,20X,3(5X,I3,4X)/)
 4999 FORMAT (1X/,1X,18H END OF SIMULATION,1X/)
 5999 FORMAT (1X/,1X,33H ERROR IN SPECIFICATION - ABORTED,1X/)
 4998 FORMAT (1X//,I3,2X,1PE11.4,2X,1PE11.4,2X,I3)
 4997 FORMAT (1X,I3)
 4995 FORMAT (1X/,4X,17H T1RHO SIMULATION,1X/)
 4005 FORMAT (1X/,4X,14H T2 SIMULATION,1X/)
 4994 FORMAT (1X/,4X,14H T1 SIMULATION,1X/)
 4993 FORMAT (1X/,4X,I3,13H DEGREE PULSE,1X/)
 4992 FORMAT (1X/,10X,30H START OF SIMULATION: M=1 (+Z),1X/)
 3999 FORMAT (1X,1PE11.4)
 3998 FORMAT (1X,I3)
 9999 FORMAT (1PE11.4)
 9998 FORMAT (I3)
 1007 FORMAT (1X,23HPERIODICITY (METRES) = ,1PE11.4/)
 1008 FORMAT (1X,24HNUMBER OF MESH POINTS = ,I3/)
 1009 FORMAT (1X,21HACCURACY PARAMETER = ,1PE11.4//)
 8990 FORMAT (1X/,2X,37H   TSIM      TMES    INTEGRAL 1,
     &38H  INTEGRAL 2  INTEGRAL 3   TOTAL M/)
```

```
 8989 FORMAT (1X,27H D03PBF FAILS WITH IFAIL = ,I3,
    &8H AT T = ,1PE11.4/)
 8987 FORMAT (1X/)
 8978 FORMAT (6(2X,1PE11.4))
 7999 FORMAT (1X,I3,' DATA POINTS WITH A DWELL OF ',
    &1PE11.4,' SECONDS'/)
      END


C     !*************************************************************!
C     !                                 !
C     !          SUBROUTINE TEETOO              !
C     !      ROUTINE TO SIMULATE T2 RELAXATION          !
C     !                                 !
C     !*************************************************************!

      SUBROUTINE TEETOO(NP,NPTS,TS,TOUT,U,GE,T2,AA)
      DOUBLE PRECISION TS,TOUT,U(NPTS),AA(NPTS)
      REAL T2(3),RFAC(3),GARBAGE
      INTEGER I,NPTS,NP(3),GE(3)
      TS=TOUT
      DO 10 I=1,NPTS
      U(I)=AA(I)
   10 CONTINUE
      DO 15 I=1,3
      GARBAGE=((-1/FLOAT(GE(I)))*(TS/T2(I))**FLOAT(GE(I)))
      RFAC(I)=ZEREXP(GARBAGE)
   15 CONTINUE
      DO 20 I=1,NP(1)+1
      U(I)=U(I)*RFAC(1)
   20 CONTINUE
      DO 30 I=NP(1)+3,NP(1)+NP(2)+2
      U(I)=U(I)*RFAC(2)
   30 CONTINUE
      DO 40 I=NPTS-NP(3),NPTS
      U(I)=U(I)*RFAC(3)
   40 CONTINUE
      U(NP(1)+2)=(U(NP(1)+1)+U(NP(1)+3))/2
      U(NP(1)+NP(2)+3)=(U(NP(1)+NP(2)+2)+U(NP(1)+NP(2)+4))/2
      RETURN
      END


C     !*************************************************************!
C     !                                 !
C     !          SUBROUTINE PDEF                !
C     !   ROUTINE TO DEFINE THE EQUATION IN EACH REGION      !
C     !                                 !
C     !*************************************************************!

      SUBROUTINE PDEF(NPDE,X,T,UX,DUX,F,G,C)
      DOUBLE PRECISION T,X,C(1),DUX(1),F(1),G(1),UX(1)
      REAL D(3),TD(3),L(3),TR(3),TL(3),DIFFAC,HD(3),START,CRYST
      INTEGER NPDE,RELTYP,DIRE,I,FLAG,FLWR
      COMMON/ALAN/D,TL,TR,L,HD,DIRE,FLAG,START,FLWR,CRYST
      COMMON/LOWT/TD
      IF (DIRE.EQ.3.OR.DIRE.EQ.1) THEN
      RELTYP=0
      DIFFAC=0.5
      ELSE
      RELTYP=1
      DIFFAC=1.0
```

```
      ENDIF
      DO 10 I=1,3
      IF (RELTYP.EQ.0) THEN
      TD(I)=TR(I)
      ELSE
      TD(I)=TL(I)
      ENDIF
   10 CONTINUE
      IF (X.LE.L(1)) GOTO 20
      IF (X.GE.L(1)+L(2)) GOTO 30
      G(1)=D(2)
      C(1)=HD(2)
      F(1)=TD(2)
      GOTO 40
   20 G(1)=D(1)
      C(1)=HD(1)
      F(1)=TD(1)
      GOTO 40
   30 G(1)=D(3)
      C(1)=HD(3)
      F(1)=TD(3)
   40 CONTINUE
      G(1)=G(1)*DIFFAC
      F(1)=C(1)*(RELTYP-UX(1))/F(1)
      RETURN
      END


C     !*********************************************************!
C     !                                                         !
C     !          SUBROUTINE BNDY                 !
C     !  ROUTINE TO DEFINE BOUNDARY CONDITIONS AT X=A AND X=B   !
C     !                                                         !
C     !*********************************************************!

      SUBROUTINE BNDY(NPDE,T,UX,IBND,P,Q,R)
      DOUBLE PRECISION T,P(NPDE),Q(NPDE),R(NPDE),UX(NPDE)
      INTEGER IBND,NPDE
      P(1)=0.0
      R(1)=0.0
      Q(1)=1.0
      RETURN
      END


C     !*********************************************************!
C     !                                                         !
C     !          SUBROUTINE DMESH                !
C     !     ROUTINE TO CALCULATE MESH POINTS          !
C     !                                                         !
C     !*********************************************************!

      SUBROUTINE DMESH(L,NP,NPTS,X,A,B)
      DOUBLE PRECISION A,B,X(NPTS)
      REAL L(3),PI
      INTEGER I1,I2,I3,I,NPTS,NP(3)
      PI=3.1415926535
C
C     INTERVAL FROM X=0 TO X=L(1)
C
      X(1)=A
      I1=NP(1)+1
```

```
      DO 20 I=2,I1
      X(I)=L(1)*SIN(PI*FLOAT(I-1)/(2*FLOAT(NP(1)+1)))
   20 CONTINUE
      X(NP(1)+2)=L(1)
C
C     INTERVAL FROM X>L(1) TO X=L(1)+L(2)
C
      I1=I1+2
      I2=NP(1)+NP(2)+2
      DO 30 I=I1,I2
      X(I)=L(1)+(L(2)/2)*(1-COS(PI*FLOAT(I-NP(1)-2)/
     &FLOAT(NP(2)+1)))
   30 CONTINUE
      X(NP(1)+NP(2)+3)=L(1)+L(2)
C
C     INTERVAL FROM X>L(1)+L(2) TO X=L(1)+L(2)+L(3)
C
      I2=I2+2
      I3=NP(1)+NP(2)+NP(3)+3
      DO 40 I=I2,I3
      X(I)=L(1)+L(2)+L(3)*(1-COS(PI*FLOAT(I-NP(1)-NP(2)-3)/
     &(2*FLOAT(NP(3)+1))))
   40 CONTINUE
      X(NPTS)=B
      RETURN
      END


C     !*********************************************************!
C     !                                 !
C     !         SUBROUTINE INTEG                !
C     !    ROUTINE TO INTEGRATE THE RESULTS             !
C     !                                 !
C     !*********************************************************!

      SUBROUTINE INTEG(NP,NPTS,A,B,TS,X,U,TE,MNEW)
      PARAMETER (DATMAX=200)
      DOUBLE PRECISION A,B,TS,TE,X(NPTS),U(NPTS)
      REAL DS,SUM,S(3),SUMAG(1005),HD(3),D(3),TR(3),TL(3),L(3),MNEW,
     &    START,CRYST
      INTEGER NPTS,I,M,NP(3),MAGCNT,DIRE,FLAG,FLWR

      COMMON /RES/  S,SUM,SUMAG,M,MAGCNT
      COMMON /ALAN/ D,TL,TR,L,HD,DIRE,FLAG,START,FLWR,CRYST

      MAGCNT=MAGCNT+1
C
C     INTEGRATE RESULTS IN REGION 1
C
      S(1)=0.0
      DO 10 I=1,NP(1)+1
      DS=(U(I+1)+U(I))*(X(I+1)**(M+1)-X(I)**(M+1))
      S(1)=S(1)+DS
   10 CONTINUE
C
C     INTEGRATE RESULTS IN REGION 2
C
      S(2)=0.0
      DO 20 I=NP(1)+2,NP(1)+NP(2)+2
      DS=(U(I+1)+U(I))*(X(I+1)**(M+1)-X(I)**(M+1))
      S(2)=S(2)+DS
   20 CONTINUE
```

```
C
C    INTEGRATE RESULTS IN REGION 3
C
     S(3)=0.0
     DO 30 I=NP(1)+NP(2)+3,NPTS-1
     DS=(U(I+1)+U(I))*(X(I+1)**(M+1)-X(I)**(M+1))
     S(3)=S(3)+DS
  30 CONTINUE
     DO 40 I=1,3
     S(I)=HD(I)*S(I)/(2*(B-A)**(M+1))
  40 CONTINUE
C
C    SUM THE RESULTS FOR THE THREE REGIONS
C
     SUM=S(1)+S(2)+S(3)
     SUMAG(MAGCNT)=SUM

C
C    PREPARE MAGNETISATION FOR LEAST SQUARES FIT
C    MNEW: MAGNETISATION IN MOBILE REGION
C

     MNEW=S(1)

C
C    OUTPUT THE NUMERICAL RESULTS
C
     IF (FLWR.EQ.1) WRITE (8,8978) TE,TS,S(1),S(2),S(3),SUM
     RETURN
 8978 FORMAT (6(2X,1PE11.4))
     END



C    !*************************************************************!
C    !                                   !
C    !          FUNCTION ZEREXP          !
C    !  FUNCTION TO RETURN THE EXPONENTIAL OF THE ARGUMENT;  !
C    !     RETURNS ZERO IF ANSWER LESS THAN 1.0E-30       !
C    !                                   !
C    !*************************************************************!

     FUNCTION ZEREXP(TEM)
     REAL TEM
     IF (TEM.LT.-70) THEN
     ZEREXP=0.0
     ELSE
     ZEREXP=EXP(TEM)
     ENDIF
     RETURN
     END
```

Appendix III TURBO PASCAL 6.0 PROGRAM "*LEAST.PAS*"

```
Program Least;

{$N+}

USES Crt,Dos,Dialog,Types,Complx,Fitpara,Theory,Fit2,Fadeunit;

var i,j,n,col: integer;
   dum     : double;
   ft      : text;
   filename,
   fl      : string[20];
   ch      : char;

begin
TextBackGround(LightGray);
TextColor(Black);
clrscr;
write('filename: ');
intenup(10);
readln(fl);

filename:= fl + '.dat';

assign (ft, filename);
reset (ft);
 WRITELN('How many columns? ');
ch:=ReadKey;
n:= ORD(Ch)-48;
 WRITELN('Data-modeling for which column? ');
ch:=ReadKey;
col:= ORD(Ch)-48;


i:= 0;
while not eof(ft) do
 begin
 i := i + 1;
 read (ft, x[i]);
 FOR j:= 1 TO n-1 DO
  BEGIN
   IF j<>col THEN BEGIN
    IF j < n-1 THEN
      READ(ft, dum)
    ELSE
      READLN(ft, dum);
   END
 ELSE
   BEGIN
    IF j < n-1 THEN
      READ(ft, y[i])
    ELSE
      READLN(ft, y[i]);
   END;
  END;
 yerr[i] := 1;
end;
```

```
close(ft);


Writeln('');
Writeln('');

Writeln('Which function?');
Writeln('');

Writeln(' 0: polynom a0+a1*t+a2*t^2+... ');
Writeln(' 1: error function');
Writeln(' 2: a*exp(-b*t)');
Writeln(' 3: Mehring equation for CP/MAS (Contact time) two components');
Writeln(' 4: 1-2*a*exp(-t/b); eg. T1 data');
Writeln(' 5: 1-2*a*exp(-t/b)+1-2*c*exp(-t/d)');
Writeln(' 6: Mehring equation for CP/MAS(Contact time) one components');
Writeln(' 7: Spin-depolarisation (one component) (Mueller, Kumar, Baummann, Ernst +');
Writeln('    modifiation by Wu for CH2-group');
Writeln(' 8: Spin-depolarisation (two components) (Mueller, Kumar, Baummann, Ernst +');
Writeln('    modifiation by Wu for CH2-group (application doubtful!)');
Writeln(' 9: Inversion-Recovery Cross-polarisation for non-protonated carbons');
Writeln('10: Cross-polarisation dynamics, advanced model');
Writeln('11: Spin-depolarisation (one component,Abragamian) (Mueller, Kumar, Baummann,');
Writeln('    Ernst');
Writeln('12: 1-2*a*exp(-t/b)+1-2*c*exp(-t/d) open for modifications');
Writeln('13: Spin-depolarisation (one component) (Mueller, Kumar, Baummann, Ernst +');
Writeln('    modifiation by Wu for CH-group');
Writeln('14: Cross-polarisation dynamics, more advanced model (based on 7)');
Writeln('15: Inverse-recovery Cross-polarisation dynamics (based on 14)');


intenup(10);

Ch:=ReadKey;

N_Theo:= ORD(Ch)-48;

clrscr;

If (N_Theo=2) or (N_Theo=4) then N_Par:= 2;
If (N_Theo=6) or (N_Theo=7) or (N_Theo=9) or (N_Theo=11) or (N_Theo=13) then N_Par:= 3;
If (N_Theo=5) or (N_Theo=10) or (N_Theo=12) or (N_Theo=14) or (N_Theo=15) or (N_Theo=16) then
N_Par:= 4;
If N_Theo=1 then N_Par:= 5;
If (N_Theo=3) or (N_Theo=8) then N_Par:= 6;
If N_Theo=0 then begin
  Write('How many elements (a0, a1, a2, ... ? ');
  Readln(N_Par);
end;

clrscr;

CTRL_PR := false;   { Do Control-Print on screen}
N_Fit  := 1024;    { Number of possible data max. 1024 }
F_lower :=  1;    { Uses only datapoints 1.....1024 }
F_upper :=  i;    { Upper data used in data file }
{N_Theo :=          Theory function: }
{N_Par  :=          Number of parameter }

pars[1]:= 1.0;
pars[2]:= 0.16;
pars[3]:= 0.997;
```

```
  pars[4]:= 0.16;
  pars[5]:= 0.15;
  pars[6]:= 7.0;

  Writeln('Parameter list:');
  FOR i:= 1 to N_Par do
    Writeln('pars[',i,']: ',pars[i]);
  Writeln('OK (y/n)?');
  Ch:=ReadKey;
  IF ch<>'y' THEN
   FOR i:= 1 to N_Par DO BEGIN
     WRITE('N_Par[',i,'] old-value: ', Pars[i], '  new-value:  ');
     READLN(Pars[i]);
   END;


  {calculates a fraction of pars for deviation (see UNIT theory.pas)}

  for i := 1 to N_Par do
  begin
   dpars[i]:= pars[i]/10000;
  end;


  {Output Result}

  Writeln('');
  Writeln('');
  Writeln('One moment please, I am thinking!');

  do_fit;

  intendown(10);
  clrscr;
  Writeln('Result:');
  Writeln('');
  Writeln('     Parameter              +-');
  Writeln('_____________________________________________________');

  for i := 1 to N_Par do
   writeln(pars[i],'  ',pars_err[i]); { ai +- err_ai }
  Writeln('');
  Writeln('');
  intenup(10);
  Writeln('press any key to continue!');

  repeat until keypressed;
  Writeln('');
  end.
```

Unit THEORY;

```
{$N+}

interface

Uses Types,Complx,FitPara;

function Theo(x: extended; pars: Sol_vec): double;
function Db (par,i: integer): double;
```

```
implementation

function Theo(x: extended; pars: Sol_vec): double;

{Fittable parameters are pars[i], with i ranging from 1 to 30; }
{unfittable, but variable parameters are par_fix[i], with i }
{ ranging fron 2 to 30. }

var t                    : extended;
  i                      : integer;
  lamb1,lamb2,lamb3,dlamb2,dlamb3,dlamb31,dlamb41: double;

const sqrttwo = 1.4142136;
    pi    = 3.141592654;

begin
 case N_Theo of
 0: begin
    { pars[1] : a0 }
    { pars[2] : a1 }
    { pars[3] : a2 }
    { ..... }
    { pars[N_par] : a(N_par+1) }
   t := pars[N_Par];            { Horner }
   for i := N_Par-1 downto 1 do
    t := t*x+pars[i];
   Theo := t;
  end;
 1: begin
    { pars[1] : t0 }

    { pars[2] : N }
    { pars[3] : lambda }
    { pars[4] : sigma }
    { pars[5] : back }
   t := x-pars[1]; { t-t0 }
   Theo := pars[2]/2*(fexp(sqr(pars[3]*pars[4])/2-pars[3]*t)*
        erfc((pars[3]*pars[4]-t/pars[4])/sqrttwo))+pars[5];
  end;

2: begin
   t:= x;
   Theo := pars[1]*exp(-1/pars[2]*t);
  end;

3: begin
   t := x;
   lamb1 := pars[2]/pars[3];
   lamb2 := pars[5]/pars[6];
   theo := pars[1]/(1-lamb1)*(1-exp(-(1-lamb1)/pars[2]*t))*exp(-t/pars[3])+
        pars[4]/(1-lamb2)*(1-exp(-(1-lamb2)/pars[5]*t))*exp(-t/pars[6]);
  end;
4: begin
   t:= x;
   Theo := 1-2*pars[1]*exp(-t/pars[2]);
  end;

5: begin
   t := x;
   theo := 1-(2*pars[1]*exp(-t/pars[2])+2*pars[3]*exp(-t/pars[4]));
  end;
```

```
6: begin
   t := x;
   lamb1 := pars[2]/pars[3];
   theo := pars[1]/(1-lamb1)*(1-exp(-(1-lamb1)/pars[2]*t))*exp(-t/pars[3]);
  end;

7: begin
   t := x;
   lamb2:= sqr(t/pars[3]);
   theo := pars[1]*(1/3*exp(-pars[2]*t)+2/3*exp(-3/2*pars[2]*t)*exp(-0.5*lamb2));
  end;

8: begin
   t := x;
   lamb2:= sqr(t/pars[3]);
   lamb3:= sqr(t/pars[6]);
   theo := pars[1]*(1/3*exp(-pars[2]*t)+2/3*exp(-3/2*pars[2]*t)*exp(-0.5*lamb2))+
        pars[4]*(1/3*exp(-pars[5]*t)+2/3*exp(-3/2*pars[5]*t)*exp(-0.5*lamb3));
  end;

9: begin
   t := x;
   lamb1 := pars[2]/pars[3];
   theo := (-pars[1]+2*pars[1]/(1-lamb1)*(1-exp(-(1-lamb1)/pars[2]*t)))*exp(-t/pars[3]);
  end;

10: begin
   t := x;
   lamb1:= pars[3]/pars[4];
   lamb2:= 0.5*sqr(t/pars[3]);
   if lamb2 < 300 then
    theo := pars[1]/(1-lamb1)*(1-1/3*exp(-pars[2]*t)-(exp(-(1-lamb1)/pars[3]*t)+exp(-lamb2)*
        2/3*exp(-3/2*pars[2]*t)))*exp(-t/pars[4])
   else
    theo := pars[1]/(1-lamb1)*(1-1/3*exp(-pars[2]*t)-exp(-(1-lamb1)/pars[3]*t))*exp(-t/pars[4]);
  end;

11: begin
   t := x;
   lamb2:= sqr(t/pars[3]);
   theo := pars[1]*(1/3*exp(-pars[2]*t)+2/3*exp(-3/2*pars[2]*t)*cos(1/2*pars[3]*t));
  end;

12: begin
   t := x;
   theo := 0.2-0.4*(pars[1]*exp(-t/pars[2])+pars[3]*exp(-t/pars[4]));
  end;


13: begin
   t := x;
   lamb2:= sqr(t/pars[3]);
   theo := pars[1]*(1/2*exp(-pars[2]*t)+1/2*exp(-3/2*pars[2]*t)*exp(-0.5*lamb2));
  end;

14: begin
   t := x;
   lamb2:= sqr(t/pars[3]);
   IF lamb2 < 400 then
    theo := pars[1]*(1-1/3*exp(-pars[2]*t)-2/3*exp(-3/2*pars[2]*t)*exp(-0.5*lamb2))*exp(-t/pars[4])
   ELSE
```

```
      theo:= pars[1]*(1-1/3*exp(-pars[2]*t))*exp(-t/pars[4]);
    end;

 15: begin
     t := x;
     lamb2:= 0.5*sqr(t/pars[3]);
     IF lamb2 < 400 then
      theo := (-pars[1]+2*pars[1]*(1-1/3*exp(-pars[2]*t)-2/3*exp(-3/2*pars[2]*t)*exp(-lamb2)))*exp(-
         t/pars[4])
     ELSE
      theo := (-pars[1]+2*pars[1]*(1-1/3*exp(-pars[2]*t)))*exp(-t/pars[4]);
    end;


 16: begin
     t := x;
     lamb1:= pars[3]/pars[4];
     lamb2:= 0.5*sqr(t/pars[3]);
     if lamb2 < 300 then
      theo := pars[1]*(1-1/3*exp(-pars[2]*t)-2/3*exp(-3/2*pars[2]*t)*exp(-lamb2))*exp(-t/pars[4])
     else
      theo := pars[1]*(1-1/3*exp(-pars[2]*t))*exp(-t/pars[4]);
    end;

 end; {case}
end;



function Db(par,i: integer): double;

{ Db = df(x[i],pars)/dpars[par] }

var e1,e2,e3,e4,e5,e6,t,efc,efc1,efc2,lamb1,lamb2,lamb3,dlamb2,dlamb3,dlamb31,dlamb41: double;

const sqrttwobypi = 0.7978845;
     sqrttwo    = 1.4142136;
     pi         = 3.141592654;

begin
 if fixed[par] then Db := 0
 else
 case N_Theo of
  0: if par=1 then Db := 1
    else Db := pot(x[i],pred(par));
  1: begin
     t  := x[i]-pars[1];
     e1  := fexp(sqr(pars[3]*pars[4])/2-pars[3]*t);
     e2  := fexp(-sqr(pars[3]*pars[4]-t/pars[4])/2);
     efc := erfc((pars[3]*pars[4]-t/pars[4])/sqrttwo);
     case par of
      1: Db := pars[2]/2*e1*(pars[3]*efc-sqrttwobypi/pars[4]*e2);
      2: Db := 0.5*e1*efc;
      3: Db := pars[2]/2*e1*((pars[3]*sqr(pars[4])-t)*efc-
           sqrttwobypi/pars[4]*e2);
      4: Db := pars[2]/2*e1*(sqr(pars[3])*pars[4]*efc-
           sqrttwobypi*(pars[3]/sqrttwo+t/sqr(pars[4]))*e2);
      5: Db := 1;
     end;
    end;

2: begin
```

```
    case par of
     1: Db := ((pars[1]+dpars[1])*exp(-1/pars[2]*x[i])-pars[1]*exp(-1/pars[2]*x[i]))/dpars[1];
     2: Db := (pars[1]*exp(-1/(pars[2]+dpars[2])*x[i])-pars[1]*exp(-1/pars[2]*x[i]))/dpars[2];
    end;
   end;

  3: begin
     t := x[i];
     lamb1 := pars[2]/pars[3];
     lamb2 := pars[5]/pars[6];
     dlamb2 := (pars[2]+dpars[2])/pars[3];
     dlamb3 := pars[2]/(pars[3]+dpars[3]);
     case par of
      1: Db := ((pars[1]+dpars[1])/(1-lamb1)*(1-exp(-(1-lamb1)/pars[2]*t))*exp(-t/pars[3])-
           (pars[1]/(1-lamb1)*(1-exp(-(1-lamb1)/pars[2]*t))*exp(-t/pars[3])))/dpars[1];

      2: Db := (pars[1]/(1-dlamb2)*(1-exp(-(1-(pars[2]+dpars[2])/pars[3])/
           (pars[2]+dpars[2])*t))*exp(-t/pars[3])-
           (pars[1]/(1-lamb1)*(1-exp(-(1-lamb1)/pars[2]*t))*exp(-t/pars[3])))/dpars[2];

      3: Db := (pars[1]/(1-dlamb3)*(1-exp(-(1-pars[2]/(pars[3]+dpars[3]))*
           t/pars[2]))*exp(-t/(pars[3]+dpars[3]))-
           (pars[1]/(1-lamb1)*(1-exp(-(1-lamb1)/pars[2]*t))*exp(-t/pars[3])))/dpars[3];

      4: Db := ((pars[4]+dpars[4])/(1-lamb2)*(1-exp(-(1-lamb2)/pars[5]*t))*exp(-t/pars[6])-
           (pars[4]/(1-lamb2)*(1-exp(-(1-lamb2)/pars[5]*t))*exp(-t/pars[6])))/dpars[4];

      5: Db := (pars[4]/(1-(pars[5]+dpars[5])/pars[6])*(1-exp(-(1-(pars[5]+dpars[5])/pars[6])/
           (pars[5]+dpars[5])*t))*exp(-t/pars[6])-
           (pars[4]/(1-lamb2)*(1-exp(-(1-lamb2)/pars[5]*t))*exp(-t/pars[6])))/dpars[5];

      6: Db := (pars[4]/(1-pars[5]/(pars[6]+dpars[6]))*(1-exp(-(1-pars[5]/(pars[6]+dpars[6]))*
           t/pars[5]))*exp(-t/(pars[6]+dpars[6]))-
           (pars[4]/(1-lamb2)*(1-exp(-(1-lamb2)/pars[5]*t))*exp(-t/pars[6])))/dpars[6];
     end;
    end;

  4: begin
     t:= x[i];
     case par of
      1: Db := (1-2*(pars[1]+dpars[1])*exp(-t/pars[2])-1+2*pars[1]*exp(-t/pars[2]))/dpars[1];
      2: Db := (1-2*pars[1]*exp(-t/(pars[2]+dpars[2]))-1+2*pars[1]*exp(-t/pars[2]))/dpars[2];
     end;
    end;

  5: begin
     t := x[i];
     case par of
      1: Db := -2*((pars[1]+dpars[1])*exp(-x[i]/pars[2])-(pars[1]*exp(-x[i]/pars[2])))/dpars[1];
      2: Db := -2*(pars[1]*exp(-x[i]/(pars[2]+dpars[2]))-(pars[1]*exp(-x[i]/pars[2])))/dpars[2];
      3: Db := -2*((pars[3]+dpars[3])*exp(-x[i]/pars[4])-(pars[3]*exp(-x[i]/pars[4])))/dpars[3];
      4: Db := -2*(pars[3]*exp(-x[i]/(pars[4]+dpars[4]))-(pars[3]*exp(-x[i]/pars[4])))/dpars[4];
     end;
    end;

 6: begin
     t := x[i];
     lamb1 := pars[2]/pars[3];
     case par of
      1: Db := ((pars[1]+dpars[1])/(1-lamb1)*(1-exp(-(1-lamb1)/pars[2]*t))*exp(-t/pars[3])-
           (pars[1]/(1-lamb1)*(1-exp(-(1-lamb1)/pars[2]*t))*exp(-t/pars[3])))/dpars[1];
```

```
    2: Db := (pars[1]/(1-(pars[2]+dpars[2])/pars[3])*(1-exp(-(1-(pars[2]+dpars[2])/pars[3])/
          (pars[2]+dpars[2])*t))*exp(-t/pars[3])-
          (pars[1]/(1-lamb1)*(1-exp(-(1-lamb1)/pars[2]*t))*exp(-t/pars[3])))/dpars[2];

    3: Db := (pars[1]/(1-pars[2]/(pars[3]+dpars[3]))*(1-exp(-(1-pars[2]/(pars[3]+dpars[3]))/
          pars[2]*t))*exp(-t/(pars[3]+dpars[3]))-
          (pars[1]/(1-lamb1)*(1-exp(-(1-lamb1)/pars[2]*t))*exp(-t/pars[3])))/dpars[3];
   end;
  end;

 7: begin
   t := x[i];
   lamb2:= sqr(t/pars[3]);
   case par of
    1: Db := ((pars[1]+dpars[1])*(1/3*exp(-pars[2]*t)+2/3*exp(-3/2*pars[2]*t)*exp(-0.5*lamb2))-
         (pars[1]*(1/3*exp(-pars[2]*t)+2/3*exp(-3/2*pars[2]*t)*exp(-0.5*sqr(t/pars[3])))))/dpars[1];

    2: Db := (pars[1]*(1/3*exp(-(pars[2]+dpars[2])*t)+2/3*exp(-3/2*(pars[2]+dpars[2])*t)*exp(-
0.5*lamb2))-
         (pars[1]*(1/3*exp(-pars[2]*t)+2/3*exp(-3/2*pars[2]*t)*exp(-0.5*sqr(t/pars[3])))))/dpars[2];

    3: Db := (pars[1]*(1/3*exp(-pars[2]*t)+2/3*exp(-3/2*pars[2]*t)*exp(-.5*sqr(t/(pars[3]+dpars[3])))))-
         (pars[1]*(1/3*exp(-pars[2]*t)+2/3*exp(-3/2*pars[2]*t)*exp(-0.5*sqr(t/pars[3])))))/dpars[3];
   end;
  end;

 8: begin
   t := x[i];
   lamb2:= sqr(t/pars[3]);
   lamb3:= sqr(t/pars[6]);
   case par of
    1: Db := ((pars[1]+dpars[1])*(1/3*exp(-pars[2]*t)+2/3*exp(-3/2*pars[2]*t)*exp(-0.5*lamb2))-
         (pars[1]*(1/3*exp(-pars[2]*t)+2/3*exp(-3/2*pars[2]*t)*exp(-0.5*lamb2)))))/dpars[1];

    2: Db := (pars[1]*(1/3*exp(-(pars[2]+dpars[2])*t)+2/3*exp(-3/2*(pars[2]+dpars[2])*t)*exp(-
        0.5*lamb2))-
         (pars[1]*(1/3*exp(-pars[2]*t)+2/3*exp(-3/2*pars[2]*t)*exp(-0.5*lamb2)))))/dpars[2];

    3: Db := (pars[1]*(1/3*exp(-pars[2]*t)+2/3*exp(-3/2*pars[2]*t)*exp(-.5*sqr(t/(pars[3]+dpars[3])))))-
         (pars[1]*(1/3*exp(-pars[2]*t)+2/3*exp(-3/2*pars[2]*t)*exp(-0.5*lamb2)))))/dpars[3];

    4: Db := ((pars[4]+dpars[4])*(1/3*exp(-pars[5]*t)+2/3*exp(-3/2*pars[5]*t)*exp(-0.5*lamb3))-
         (pars[4]*(1/3*exp(-pars[5]*t)+2/3*exp(-3/2*pars[5]*t)*exp(-0.5*lamb3)))))/dpars[4];

    5: Db := (pars[4]*(1/3*exp(-(pars[5]+dpars[5])*t)+2/3*exp(-3/2*(pars[5]+dpars[5])*t)*exp(-
        0.5*lamb3))-
         (pars[4]*(1/3*exp(-pars[5]*t)+2/3*exp(-3/2*pars[5]*t)*exp(-0.5*lamb3)))))/dpars[5];

    6: Db := (pars[4]*(1/3*exp(-pars[5]*t)+2/3*exp(-3/2*pars[5]*t)*exp(-.5*sqr(t/(pars[6]+dpars[6])))))-
         (pars[4]*(1/3*exp(-pars[5]*t)+2/3*exp(-3/2*pars[5]*t)*exp(-0.5*lamb3)))))/dpars[6];
  end;
 end;


9: begin
   t := x[i];
   lamb1 := pars[2]/pars[3];
   case par of
    1: Db := ((-(pars[1]+dpars[1])+2*(pars[1]+dpars[1])/(1-lamb1)*(1-exp(-(1-amb1)/pars[2]*t)))*exp(-
       t/pars[3])-((-pars[1]+2*pars[1]/(1-lamb1)*(1-exp(-(1-lamb1)/pars[2]*t)))*
       exp(-/pars[3])))/dpars[1];
```

```
    2: Db := ((-pars[1]+2*pars[1]/(1-(pars[2]+dpars[2])/pars[3])*(1-exp(-(1-(pars[2]+dpars[2])/pars[3])/
         (pars[2]+dpars[2])*t)))*exp(-t/pars[3])-
         ((-pars[1]+2*pars[1]/(1-lamb1)*(1-exp(-(1-lamb1)/pars[2]*t)))*exp(-t/pars[3])))/dpars[2];

    3: Db := ((-pars[1]+2*pars[1]/(1-pars[2]/(pars[3]+dpars[3]))*(1-exp(-(1-pars[2]/(pars[3]+dpars[3]))/
         pars[2]*t)))*exp(-t/(pars[3]+dpars[3]))-
         ((-pars[1]+2*pars[1]/(1-lamb1)*(1-exp(-(1-lamb1)/pars[2]*t)))*exp(-t/pars[3])))/dpars[3];
  end;
 end;


10: begin
   t := x[i];
   lamb1:= pars[3]/pars[4];
   lamb2:= 0.5*sqr(t/pars[3]);
   dlamb31:= (pars[3]+dpars[3])/pars[4];
   dlamb41:= pars[3]/(pars[4]+dpars[4]);
   dlamb2:= 0.5*sqr(t/(pars[3]+dpars[3]));
   if lamb2 < 300 then
   case par of
    1: Db := ((pars[1]+dpars[1])/(1-lamb1)*(1-1/3*exp(-pars[2]*t)-(exp(-(1-lamb1)/pars[3]*t)+exp(-
         lamb2)*2/3*exp(-3/2*pars[2]*t)))*exp(-t/pars[4])-
            (pars[1]/(1-lamb1)*(1-1/3*exp(-pars[2]*t)-(exp(-(1-lamb1)/pars[3]*t)+exp(-lamb2)*
            2/3*exp(-3/2*pars[2]*t)))*exp(-t/pars[4])))/dpars[1];

    2: Db := (pars[1]/(1-lamb1)*(1-1/3*exp(-(pars[2]+dpars[2])*t)-(exp(-(1-lamb1)/pars[3]*t)+exp(-
         lamb2)*
          2/3*exp(-3/2*(pars[2]+dpars[2])*t)))*exp(-t/pars[4])-
          (pars[1]/(1-lamb1)*(1-1/3*exp(-pars[2]*t)-(exp(-(1-lamb1)/pars[3]*t)+exp(-lamb2)*
          2/3*exp(-3/2*pars[2]*t)))*exp(-t/pars[4])))/dpars[2];


    3: Db := (pars[1]/(1-dlamb31)*(1-1/3*exp(-pars[2]*t)-(exp(-(1-lamb31)/(pars[3]+dpars[3])*t)+exp(-
         dlamb2)*2/3*exp(-3/2*pars[2]*t)))*exp(-t/pars[4])-
           (pars[1]/(1-lamb1)*(1-1/3*exp(-pars[2]*t)-(exp(-(1-lamb1)/pars[3]*t)+exp(-lamb2)*
           2/3*exp(-3/2*pars[2]*t)))*exp(-t/pars[4])))/dpars[3];

    4: Db := (pars[1]/(1-dlamb41)*(1-1/3*exp(-pars[2]*t)-(exp(-(1-dlamb41)/pars[3]*t)+exp(-lamb2)*
           2/3*exp(-3/2*pars[2]*t)))*exp(-t/(pars[4]+dpars[4]))-
           (pars[1]/(1-lamb1)*(1-1/3*exp(-pars[2]*t)-(exp(-(1-lamb1)/pars[3]*t)+exp(-lamb2)*
           2/3*exp(-3/2*pars[2]*t)))*exp(-t/pars[4])))/dpars[4];


   end
  else
   case par of

    1: Db := ((pars[1]+dpars[1])/(1-lamb1)*(1-1/3*exp(-pars[2]*t)-exp(-(1-lamb1)/pars[3]*t))*exp(-
         t/pars[4])-(pars[1]/(1-lamb1)*(1-1/3*exp(-pars[2]*t)-exp(-(1-lamb1)/pars[3]*t))*exp(-
         t/pars[4])))/dpars[1];

    2: Db := (pars[1]/(1-lamb1)*(1-1/3*exp(-(pars[2]+dpars[2])*t)-exp(-(1-lamb1)/pars[3]*t))*exp(-
         t/pars[4])-(pars[1]/(1-lamb1)*(1-1/3*exp(-pars[2]*t)-exp(-(1-lamb1)/pars[3]*t))*exp(-
         t/pars[4])))/dpars[2];


    3: Db := (pars[1]/(1-dlamb31)*(1-1/3*exp(-pars[2]*t)-exp(-(1-lamb31)/(pars[3]+dpars[3])*t))*exp(-
         t/pars[4])-(pars[1]/(1-lamb1)*(1-1/3*exp(-pars[2]*t)-exp(-(1-lamb1)/pars[3]*t))*exp(-
         t/pars[4])))/dpars[3];
```

```
      4: Db := (pars[1]/(1-dlamb41)*(1-1/3*exp(-pars[2]*t)-exp(-(1-dlamb41)/pars[3]*t))*exp(-
           t/(pars[4]+dpars[4]))-(pars[1]/(1-lamb1)*(1-1/3*exp(-pars[2]*t)-exp(-(1-
           lamb1)/pars[3]*t))*exp(-t/pars[4])))/dpars[4];

     end;
    end;

  11: begin
     t := x[i];
     lamb2:= sqr(t/pars[3]);
     case par of
      1: Db := ((pars[1]+dpars[1])*(1/3*exp(-pars[2]*t)+2/3*exp(-3/2*pars[2]*t)*cos(1/2*pars[3]*t))-
           (pars[1]*(1/3*exp(-pars[2]*t)+2/3*exp(-3/2*pars[2]*t)*cos(1/2*pars[3]*t))))/dpars[1];

      2: Db := (pars[1]*(1/3*exp(-(pars[2]+dpars[2])*t)+2/3*exp(-
           3/2*(pars[2]+dpars[2])*t)*cos(1/2*pars[3]*t))-
              (pars[1]*(1/3*exp(-pars[2]*t)+2/3*exp(-3/2*pars[2]*t)*cos(1/2*pars[3]*t))))/dpars[2];


      3: Db := (pars[1]*(1/3*exp(-pars[2]*t)+2/3*exp(-3/2*pars[2]*t)*cos(1/2*(pars[3]+dpars[3])*t))-
           (pars[1]*(1/3*exp(-pars[2]*t)+2/3*exp(-3/2*pars[2]*t)*cos(1/2*pars[3]*t))))/dpars[3];
     end;
    end;

  12: begin
     t := x[i];
     case par of
      1: Db := -0.4*((pars[1]+dpars[1])*exp(-x[i]/pars[2])-(pars[1]*exp(-x[i]/pars[2])))/dpars[1];
      2: Db := -0.4*(pars[1]*exp(-x[i]/(pars[2]+dpars[2]))-(pars[1]*exp(-x[i]/pars[2])))/dpars[2];
      3: Db := -0.4*((pars[3]+dpars[3])*exp(-x[i]/pars[4])-(pars[3]*exp(-x[i]/pars[4])))/dpars[3];
      4: Db := -0.4*(pars[3]*exp(-x[i]/(pars[4]+dpars[4]))-(pars[3]*exp(-x[i]/pars[4])))/dpars[4];
     end;
    end;

  13: begin
     t := x[i];
     lamb2:= sqr(t/pars[3]);
     case par of
      1: Db := ((pars[1]+dpars[1])*(1/2*exp(-pars[2]*t)+1/2*exp(-3/2*pars[2]*t)*exp(-0.5*lamb2))-
           (pars[1]*(1/2*exp(-pars[2]*t)+1/2*exp(-3/2*pars[2]*t)*exp(-0.5*sqr(t/pars[3])))))/dpars[1];

      2: Db := (pars[1]*(1/2*exp(-(pars[2]+dpars[2])*t)+1/2*exp(-3/2*(pars[2]+dpars[2])*t)*exp(-
           0.5*lamb2))-
              (pars[1]*(1/2*exp(-pars[2]*t)+1/2*exp(-3/2*pars[2]*t)*exp(-0.5*sqr(t/pars[3])))))/dpars[2];

      3: Db := (pars[1]*(1/2*exp(-pars[2]*t)+1/2*exp(-3/2*pars[2]*t)*exp(-.5*sqr(t/(pars[3]+dpars[3]))))-
           (pars[1]*(1/2*exp(-pars[2]*t)+1/2*exp(-3/2*pars[2]*t)*exp(-0.5*sqr(t/pars[3])))))/dpars[3];
     end;
    end;

  14: begin
     t := x[i];
     lamb2:= sqr(t/pars[3]);
     IF lamb2 < 400 THEN
     case par of
      1: Db := ((pars[1]+dpars[1])*(1-1/3*exp(-pars[2]*t)-2/3*exp(-3/2*pars[2]*t)*exp(-
           0.5*lamb2))*exp(-t/pars[4])-
              (pars[1]*(1-1/3*exp(-pars[2]*t)-2/3*exp(-3/2*pars[2]*t)*exp(-0.5*sqr(t/pars[3])))*exp(-
              t/pars[4])))/dpars[1];

      2: Db := (pars[1]*(1-1/3*exp(-(pars[2]+dpars[2])*t)-2/3*exp(-3/2*(pars[2]+dpars[2])*t)*exp(-
           0.5*lamb2))*exp(-t/pars[4])-
```

```
          (pars[1]*(1-1/3*exp(-pars[2]*t)-2/3*exp(-3/2*pars[2]*t)*exp(-0.5*sqr(t/pars[3])))*exp(-
        t/pars[4])))/dpars[2];

    3: Db := (pars[1]*(1-1/3*exp(-pars[2]*t)-2/3*exp(-3/2*pars[2]*t)*exp(-
        0.5*sqr(t/(pars[3]+dpars[3])))*exp(-t/pars[4])-
            (pars[1]*(1-1/3*exp(-pars[2]*t)-2/3*exp(-3/2*pars[2]*t)*exp(-0.5*sqr(t/pars[3])))*exp(-
        t/pars[4])))/dpars[3];

    4: Db := (pars[1]*(1-1/3*exp(-pars[2]*t)-2/3*exp(-3/2*pars[2]*t)*exp(-0.5*sqr(t/pars[3])))*exp(-
        t/(pars[4]+dpars[4]))-
            (pars[1]*(1-1/3*exp(-pars[2]*t)-2/3*exp(-3/2*pars[2]*t)*exp(-0.5*sqr(t/pars[3])))*exp(-
        t/pars[4])))/dpars[4];
   end
  ELSE
  case par of
    1: Db := ((pars[1]+dpars[1])*(1-1/3*exp(-pars[2]*t))*exp(-t/pars[4])-
            (pars[1]*(1-1/3*exp(-pars[2]*t))*exp(-t/pars[4])))/dpars[1];

    2: Db := (pars[1]*(1-1/3*exp(-(pars[2]+dpars[2])*t))*exp(-t/pars[4])-
            (pars[1]*(1-1/3*exp(-pars[2]*t))*exp(-t/pars[4])))/dpars[2];

    3: Db := (pars[1]*(1-1/3*exp(-pars[2]*t))*exp(-t/pars[4])-
            (pars[1]*(1-1/3*exp(-pars[2]*t))*exp(-t/pars[4])))/dpars[3];

    4: Db := (pars[1]*(1-1/3*exp(-pars[2]*t))*exp(-t/(pars[4]+dpars[4]))-
            (pars[1]*(1-1/3*exp(-pars[2]*t))*exp(-t/pars[4])))/dpars[4];

  end;
  end;


15: begin
   t := x[i];
   lamb2:= 0.5*sqr(t/pars[3]);
   IF lamb2 < 400 THEN
   case par of
    1: Db := ((-(pars[1]+dpars[1])+2*(pars[1]+dpars[1])*(1-1/3*exp(-pars[2]*t)-2/3*exp(-
        3/2*pars[2]*t)*exp(-lamb2)))*exp(-t/pars[4])-
            ((-pars[1]+2*pars[1]*(1-1/3*exp(-pars[2]*t)-2/3*exp(-3/2*pars[2]*t)*exp(-lamb2)))*exp(-
        t/pars[4])))/dpars[1];

    2: Db := ((-pars[1]+2*pars[1]*(1-1/3*exp(-(pars[2]+dpars[2])*t)-2/3*exp(-
        3/2*(pars[2]+dpars[2])*t)*exp(-lamb2)))*exp(-t/pars[4])-
            ((-pars[1]+2*pars[1]*(1-1/3*exp(-pars[2]*t)-2/3*exp(-3/2*pars[2]*t)*exp(-lamb2)))*exp(-
            t/pars[4])))/dpars[2];

    3: Db := ((-pars[1]+2*pars[1]*(1-1/3*exp(-pars[2]*t)-2/3*exp(-3/2*pars[2]*t)*exp(-
        0.5*sqr(t/(pars[3]+dpars[3])))))*exp(-t/pars[4])-((-pars[1]+2*pars[1]*(1-1/3*exp(-
        pars[2]*t)-2/3*exp(-3/2*pars[2]*t)*exp(-lamb2)))*exp(-t/pars[4])))/dpars[3];

    4: Db := ((-pars[1]+2*pars[1]*(1-1/3*exp(-pars[2]*t)-2/3*exp(-3/2*pars[2]*t)*exp(-lamb2)))*exp(-
        t/(pars[4]+dpars[4]))-((-pars[1]+2*pars[1]*(1-1/3*exp(-pars[2]*t)-2/3*exp(-
        3/2*pars[2]*t)*exp(-lamb2)))*exp(-t/pars[4])))/dpars[4];
   end
  ELSE
  case par of
    1: Db := ((-(pars[1]+dpars[1])+2*(pars[1]+dpars[1])*(1-1/3*exp(-pars[2]*t)))*exp(-t/pars[4])-
            ((-pars[1]+2*pars[1]*(1-1/3*exp(-pars[2]*t)))*exp(-t/pars[4])))/dpars[1];

    2: Db := ((-pars[1]+2*pars[1]*(1-1/3*exp(-(pars[2]+dpars[2])*t)))*exp(-t/pars[4])-
            ((-pars[1]+2*pars[1]*(1-1/3*exp(-pars[2]*t)))*exp(-t/pars[4])))/dpars[2];
```

```
      3: Db := ((-pars[1]+2*pars[1]*(1-1/3*exp(-pars[2]*t)))*exp(-t/pars[4])-
               ((-pars[1]+2*pars[1]*(1-1/3*exp(-pars[2]*t)))*exp(-t/pars[4])))/dpars[3];

      4: Db := ((-pars[1]+2*pars[1]*(1-1/3*exp(-pars[2]*t)))*exp(-t/(pars[4]+dpars[4]))-
               ((-pars[1]+2*pars[1]*(1-1/3*exp(-pars[2]*t)))*exp(-t/pars[4])))/dpars[4];

    end;
    end;


  16: begin
      t := x[i];
      lamb2:= 0.5*sqr(t/pars[3]);
      IF lamb2 < 400 THEN
      case par of
       1: Db := ((pars[1]+dpars[1])*(1-1/3*exp(-pars[2]*t)-2/3*exp(-3/2*pars[2]*t)*exp(-lamb2))*exp(-
          t/pars[4])-(pars[1]*(1-1/3*exp(-pars[2]*t)-2/3*exp(-3/2*pars[2]*t)*exp(-lamb2))*exp(-
          t/pars[4])))/dpars[1];

       2: Db := (pars[1]*(1-1/3*exp(-(pars[2]+dpars[2])*t)-2/3*exp(-3/2*(pars[2]+dpars[2])*t)*exp(-
          lamb2))*exp(-t/pars[4])-(pars[1]*(1-1/3*exp(-pars[2]*t)-2/3*exp(-3/2*pars[2]*t)*exp(-
          lamb2))*exp(-t/pars[4])))/dpars[2];

       3: Db := (pars[1]*(1-1/3*exp(-pars[2]*t)-2/3*exp(-3/2*pars[2]*t)*exp(-
          0.5*sqr(t/(pars[3]+dpars[3])))*exp(-t/pars[4])-
               (pars[1]*(1-1/3*exp(-pars[2]*t)-2/3*exp(-3/2*pars[2]*t)*exp(-lamb2))*exp(-
               t/pars[4])))/dpars[3];

       4: Db := (pars[1]*(1-1/3*exp(-pars[2]*t)-2/3*exp(-3/2*pars[2]*t)*exp(-lamb2))*exp(-
          t/(pars[4]+dpars[4]))-
               (pars[1]*(1-1/3*exp(-pars[2]*t)-2/3*exp(-3/2*pars[2]*t)*exp(-lamb2))*exp(-
               t/pars[4])))/dpars[4];
      end
      ELSE
      case par of
       1: Db := ((pars[1]+dpars[1])*(1-1/3*exp(-pars[2]*t))*exp(-t/pars[4])-
                (pars[1]*(1-1/3*exp(-pars[2]*t))*exp(-t/pars[4])))/dpars[1];

       2: Db := (pars[1]*(1-1/3*exp(-(pars[2]+dpars[2])*t))*exp(-t/pars[4])-
                (pars[1]*(1-1/3*exp(-pars[2]*t))*exp(-t/pars[4])))/dpars[2];

       3: Db := (pars[1]*(1-1/3*exp(-pars[2]*t))*exp(-t/pars[4])-
                (pars[1]*(1-1/3*exp(-pars[2]*t))*exp(-t/pars[4])))/dpars[3];

       4: Db := (pars[1]*(1-1/3*exp(-pars[2]*t))*exp(-t/(pars[4]+dpars[4]))-
                (pars[1]*(1-1/3*exp(-pars[2]*t))*exp(-t/pars[4])))/dpars[4];

      end;
      end;


   end;
  end; { of Db }
end.
```

Unit TYPES;

{$N+}

interface

```
  Uses DOS;

  Type StackType  = record
                Stack_setup : boolean;
                StackSize,
                StackPointer : word;
                Save_Area   : array [0..1] of integer;
               end;
     Str255 = string[255]; Str64 = string[64];
     Str32 = string[32]; Str16 = string[16];
     Screenpoint = record
                x,y:integer;
               end;
     Complex    = string[16];
     BezierType = (Smooth,Exact);
     Pal_Select = (Default, Natural_Spectrum, Mandelbrot, Colors3,
              Lightning, Shade_it, Back_foreground);
     Vector_Chars = record
                CharOfs: array [0..127] of integer;
                VChar  : array [0..1023] of byte;
               end;
     Stack_Area = ^StackType;

  Var Stack     : Stack_Area;
    MSrec     : Registers;
    VChars    : ^Vector_Chars;

  Const Month   : array [1..12] of String[3] =
             ('Jan','Feb','Mar','Apr','May',
             'Jun','Jul','Aug','Sep','Oct',
             'Nov','Dec');
     MaxStackSize : word = $FFEB;
     Actual_Page  : word = 0;
     Act_Page_Plot: word = 0;        { Actual_Page shl 8 }
     ActualXLength: Integer = 639;
     ActualYLength: integer = 199;
     MinXPos      : integer = 0;
     MaxXPos      : integer = 639;
     MinYPos      : integer = 0;
     MaxYPos      : integer = 349;
     Plotter      : boolean = false;
     VCharAvail   : boolean = false;
     Pal_Val      : array [0..16] of byte =
                ( 0, 1, 2, 3, 4, 5, 6, 7,
                 56, 57, 58, 59, 60, 61, 62, 63, 0 );

function RSTR (r: extended; a,b: integer): str255;
function ISTR (i: integer; a: integer): str255;
function STRR (s: str255; var ok: boolean): extended;
function STRI (s: str255; var ok: boolean): integer;
function FORMAT_NUM_STRING (st:str255): str255;

implementation

function FORMAT_NUM_STRING (st: str255): str255;

var pos: integer;
   len: byte absolute st;

begin
 pos := 1;
```

```
 if len>0 then
  while st[pos]=' ' do pos := succ(pos);
  st := copy(st,pos,len);              { new format }
  format_num_string := st;
end;

function RSTR (r: extended; a,b: integer): str255;
var s: str255;
begin
 str(r:a:b,s);
 rstr := s;
end;

function ISTR (i: integer; a: integer): str255;
var s: str255;
begin
 str(i:a,s);
 istr := s;
end;

function STRR (s:str255;var ok: boolean): extended;
var r: extended;
   k: integer;
begin
 s := format_num_string (s);
 val(s,r,k);
 ok := (k=0);
 if ok then strr := r else strr := 0;
end;

function STRI (s:str255; var ok: boolean): integer;
var i,k: integer;
begin
 s := format_num_string(s);
 val(s,i,k);
 ok := (k=0);
 if ok then stri := i else stri := 0;
end;
end.
```

Unit FITPARA;

```
{$N+}

interface

const N_Par_max     = 6;
    N_Par_max1    = 9;
    N_Data        =1024;
    Signif: integer =  0;
    N_Theo: integer =  1;

type Sol_Vec  = array [1..N_par_max] of double;  { Solution vector }
   Data_Vec = array [1..N_Data] of double;    { Data field }
   NLine    = array [1..N_par_max1] of double; { Matrix Line }
   Norm_eq  = array [1..N_par_max] of NLine;   { Normalized }
                                { equation system }

const Par_Fix: Sol_vec = (0.01,0,0,0,0,0);

   Fixed  : array [1..N_Par_max] of boolean =
```

```
                (false,false,false,false,false,
                 false);

      Lambdastart: extended = 1e-1;
      CTRL_PR: boolean = false;

  var ParsS,
      Pars,
      dPars,
      Pars_err,
      cont1,
      cont2  : Sol_Vec;
      x,y,
      yerr,
      xprim,
      yprim  : Data_Vec;
      A1     : Norm_eq;
      chi2   : extended;
      f_lower,
      f_upper,
      iter,
      N_Fit,
      N_Par,
      F_Error : integer;
      Fit_ok  : boolean;

implementation
end.
```

Unit FIT2;

```
{$N+}

interface

Uses CRT,DOS,Types,FitPara,Theory;

procedure DO_FIT;

implementation

const epsilon: extended = 1E-15; { Stop-accuracy Dpar/par}
      tau: extended = 1E-9; { par -> 0: Dpar/par -> Dpar/tau}

type MCol   = array [1..N_Par_max] of extended;
     Matrix = array [1..N_Data] of MCol;

var  w      : Data_Vec; { Weights }
     pars1,             { Test-vector for better Pars }
     d,                 { Correction-vector }
     d1     : Sol_Vec;  { Test-Correction-vector }
     A      : Norm_eq;  { A: P^(t)*P }
     ph,                { ph: calculated Phi }
     phold,             { phold : old Phi }
     lambda,            { Relaxationfactor }
     l,                 { l: Test-Lambda, Chi^2 }
     d_max,             { max. relative parameterchange }
     test: extended;    { Stop condition }
     N_Par1,            { N_Par + 1 }
     N,i,               { N: actual number of data to fit }
     lower,             { first fittet value }
```

```
    upper,                  { last fitted value }
    N_Par_free : integer;  { number of free parameters }
    converg    : boolean;   { convergence reached }
    q          : char;      { keyboard }

function PHI(b: Sol_Vec): extended;
var r: extended;
   i: integer;
begin
 r := 0;
 for i := 1 to N do
  r := r+w[i]*sqr(y[i]-Theo(x[i],b));
phi := r;
end;

procedure INIT;
label exit;
var i: integer;
   r: extended;

begin

 { Init parameters }

 if N_Theo=0 then
 begin
  lambdastart := 0;
  if N_par<2 then
   begin
    writeln('N_Par must be larger than 1 for linear fits!');
    halt;
   end;
 end;
N_par1 := succ(N_par);
move(Pars,ParsS,8*N_Par);
fillchar(d,8*N_Par,0);
epsilon := exp((signif-2)*ln(10));

{ Init data }

if f_upper>N_fit then f_upper := N_fit;
if f_lower>N_fit then f_lower := N_fit;
N := (f_upper-f_lower+1);
i := N_fit*8;
move(x[1],xprim[1],i);          { Save original data }
move(y[1],yprim[1],i);
i := N*8;
move(xprim[f_lower],x[1],i);    { Shift data correctly }
move(yprim[f_lower],y[1],i);
for i := 1 to N do
 begin
  if yerr[f_lower+i-1]=0 then w[i] := 1
  else w[i] := 1/sqr(yerr[f_lower+i-1]);
 end;

N_par_free := N_par;            { # of free parameters }
for i := 1 to N_par do
if fixed[i] then N_par_free := pred(N_Par_free);

if N<N_par_free+1 then
 begin
  Fit_ok := false;
```

```
    F_Error := 5;
    goto exit;
   end;

  converg := false;
  iter := 0;
  lambda := par_fix[1]*lambdastart;
  d_max := 0;
  ph := phi(pars);              { Phi for start-values }
 exit:
 end;

 procedure SET_IT_UP;
 var i,j,l   : integer;
    P      : ^Matrix;
    r      : extended;
    Diag   : array [1..N_Par_max] of extended;

 begin
  new(P);
  for i := 1 to N do       { Calculate the derivation matrix P }
   for j := 1 to N_Par do
    P^[i,j] := Db(j,i);

  for i := 1 to N_par do  { Calculate diagonal elements of A }
  begin                   { and store standard deviation Diag }
   r := 0;
   for l := 1 to n do
    r := r+w[l]*sqr(P^[l,i]);
   if r = 0 then r := 1; { Check paraneter fixed }
   A[i,i] := r;
   Diag[i] := sqrt(r);
   r := 0;                { Calculate g and Store it in A and }
   for l := 1 to n do     { normalized in A1 }
    r := r+P^[l,i]*w[l]*(y[l]-Theo(x[l],Pars));
   A[i,N_Par1] := r;
   A1[i,N_Par1] := r/Diag[i];
  end;

 for i := 1 to N_par do  { Calculate A = P^tP and }
                         { A1 = P^tP/sqrt(Aii*Ajj) }
  for j := i+1 to N_Par do
   begin
    r := 0;
    for l := 1 to n do
     r := r+w[l]*P^[l,i]*P^[l,j];
    A[i,j] := r;
    A1[i,j] := r/(Diag[i]*Diag[j]);
   end;

 dispose(P);
end; { of SET_IT_UP }

procedure CHOLESKY (var A: norm_eq; var x: Sol_Vec);
label exit;
var l      : norm_eq;
   i,j,k,
   N,N1    : integer;
   h       : extended;

begin
N := N_Par;
```

```
 N1 := succ(N);

 for i := 1 to n do      { Calculate the solution to L(n-1)c=b }
  for j := 1 to i do
  begin
   h := A[j,i];              { h=b[j] }
   for k := 1 to j-1 do
    h := h-l[i,k]*l[j,k];     { h=b[j]-Sum(l[i,k]*c[k])) }
    if i=j then
    begin
     if h<0 then
     begin
      Fit_ok := false;
      F_Error := 2;
      goto exit;
     end;
     l[i,i] := sqrt(h);   { Diagonalelement l[i,i] }
    end
   else l[i,j] := h/l[j,j];  { c(j) := h/l[j,j] }
  end;

 for i := 1 to N do         { Solve Ly=b }
  begin
   h := A[i,N1];           { h := b[i] }
   for k := 1 to i-1 do     { y[i] := L^(-1)*b }
    h := h-l[i,k]*x[k];
    x[i] := h/l[i,i];
  end;

 for i := N downto 1 do   { Solve L(t)x=y }
  begin
   h := x[i];
   for k := i+1 to n do   { x[i] := L(t)^(-1)*y }
    h := h-l[k,i]*x[k];
    x[i] := h/l[i,i];
  end; { i }
 exit:
end; { Cholesky }

procedure INV_CHOLESKY;
label exit;
var l    : norm_eq;
   i,j,k,
   N,N1  : integer;
   h     : extended;

begin
 N := N_Par;
 N1 := succ(N);

 for i := 1 to n do      { Calculate the solution to L(n-1)c=b }
  for j := 1 to i do
  begin
   h := A[j,i];              { h=b[j] }
   for k := 1 to j-1 do
    h := h-l[i,k]*l[j,k];     { h=b[j]-Sum(l[i,k]*c[k])) }
   if i=j then
    begin
     if h<0 then
      begin
       Fit_ok := false;
       F_Error := 2;
```

```
        goto exit;
       end;
      l[i,i] := sqrt(h);      { Diagonalelement l[i,i] }
     end
    else l[i,j] := h/l[j,j];  { c(j) := h/l[j,j] }
  end;

 for i := 1 to N do           { Invert L }
  for j := i to N do
   begin
    if j>i then
    begin
     h := 0;
      for k := i to j-1 do
       h := h-L[j,k]*L[k,i];
    end
    else h := 1;
    L[j,i] := h/L[j,j];
   end;

 for j := 1 to N do           { L^(-1)^T*L^(-1) }
  for i := j to N do
   begin
    h := 0;
     for k := i to N do
      h := h+L[k,i]*L[k,j];
     L[i,j] := h;
     A1[i,j] := h;           { Store solutions in public A1 }
     A1[j,i] := h;
   end;
 exit:
end; { inverse Cholesky }


procedure SOLVE_IT (lambda: extended; var b, delta: Sol_Vec);
label exit;
var i: integer;
begin
 for i := 1 to N_Par do
  A1[i,i] := 1+lambda;         { A1+lambda*I; A1[i,i] is always 1 }

 cholesky(A1,delta);           { Determine Correction-vector delta }
 if not Fit_ok then goto exit;

 for i := 1 to N_par do        { New Pars }
  begin
   if fixed[i] then delta[i] := 0 { Parameter fixed }
   else                    { else Re-renorm delta }
    delta[i] := delta[i]/sqrt(A[i,i]);
   b[i] := b[i]+delta[i];      { New parameter-vector b }
  end;
exit:
end; { of SOLVE_IT }

procedure EVAL_ERRORS;
label exit;
var  i,j: integer;
     d,
   parsT: Sol_vec;
   zsoll,
    zist: extended;
```

```
  begin
  parsT := pars;              { Init parsT }
  zsoll := phi(pars);         { Gauge value Zsoll for optimum Pars }
  chi2  := zsoll/(N-N_par_free-1);
  set_it_up;                  { Calculate final matrix A }

  inv_cholesky;
  if not Fit_ok then goto exit;

  for i := 1 to N_Par do      { Test i-th axis }
   begin
   for j := 1 to N_par do
    begin
     d[j] := A1[j,i];
     A1[j,i] := d[j]*Chi2;    { Covariance-matrix in A1 }
    end;

  if not fixed[i] then
   begin
   Pars_err[i] := sqrt(A1[i,i]); { Error=SDev }
   for j := 1 to N_par do { Controlstep = Normed column-vector }
    begin            { of A1*SDev = d/error[i] }
     d[j] := Chi2*d[j]/Pars_err[i];
     parsT[j] := pars[j]-d[j];
    end;

   Zist := phi(parsT);        { Control 1 }
   Cont1[i] := (Zist-Zsoll)/Zsoll*(N-N_par_free);

   for j := 1 to N_par do
    parsT[j] := pars[j]+d[j];

   Zist := phi(parsT);        { Control 2 }
   Cont2[i] := (Zist-Zsoll)/Zsoll*(N-N_Par_free);
  end
  else
   begin
    pars_err[i] := 1;         { Parameter was fixed }
    cont1[i] := 1;
    cont2[i] := 1;
   end;
  end; { of Test i-th axis }

 for i := 2 to N_par do       { Normalize Corvariance-Matrix }
  for j := 1 to i-1 do        { to Correlation-matrix }
   begin
    A1[i,j] := A1[i,j]/(Pars_err[i]*Pars_err[j]);
    Fit_ok := ((1-abs(A1[i,j]))>1E-8);
    if not Fit_ok then
     begin
      F_Error := 3;
      goto exit;
     end;
   end;
 exit:
end; { of EVAL_ERRORS }

function NORM_STRING(s: str255; len: byte): str255;
begin
 if ord(s[0])>len then s[0] := chr(len);
 norm_string := s;
end;
```

```
procedure DO_FIT;
var st: str255;
label exit;
begin
 F_Error := 0;
 Fit_ok := true;
 if (N_par>N_Par_max) or (N_Fit>N_Data) then
  begin
   Fit_ok := false;
   F_Error := 1;
   goto exit;
  end;

 init;
 if not Fit_ok then goto exit;
repeat                    { Iteration loop }
 phold := ph;             { Save old phi}
 pars1 := pars;           { Save old pars, use pars1 instead }
 set_it_up;               { Calculate A1 }
 solve_it(lambda,pars1,d1);  { Solve systen for current lambda }
 if not Fit_ok then goto exit;
 ph := phi(pars1);        { Calculate new phi }
 if ph<=phold then        { Is it less than the old one ? }
  lambda := par_fix[1]*sqrt(abs((phold-ph)/(N-N_par_free-1)))
 else                     { If not, restore pars1 }
  begin                   { and repeat procedure for }
   pars1 := pars;         { 10*lambda }
   solve_it(10*lambda,pars1,d1);
   if not Fit_ok then goto exit;
   ph := phi(pars1);      { Calculate new phi }
   if (ph>phold) then     { Is it larger than the old one ? }
    begin                 { if yes, then repeat this procedure }
     l := lambda;         { Save lambda }
     repeat
      l := l*10;          { l = 10*l }
      pars1 := pars;      { Restore pars1 }
      solve_it(l,pars1,d1);  { Solve systen for lambda=l }
      if not Fit_ok then goto exit;
      ph := phi(pars1);   { New phi }
      if keypressed then  { allow an interrupt }
     begin
      Fit_ok := false;
      F_Error := 4;
      goto exit;
     end;
 until (ph<phold) or (l>=1E8);

 if l>=1E8 then           { No better phi was found up to }
  begin                   { l >= 1E8 }
   d1 := d;               { Last correction step was to large }
   for i := 1 to N_Par do { Go back by Delta/2 }
    begin
     d1[i] := d1[i]/2;
     pars1[i] := pars[i]-d1[i];
    end;
   ph := phi(pars1);      { Calculate new phi }
   if ph>phold then
    pars1 := pars;        { mininum already found }
  end
 else lambda := l;        { A better phi was found }
end                       { of if ph>phold }
```

```
 else ph := phold;        { Minimum already found }
 end;                  { of else ... }
 converg := true;
 d_max := 0;
 for i := 1 to N_par do
 begin
  test := abs(d1[i])/(tau+abs(pars[i])); { Old pars, new delta }
  if test>d_max then d_max := test;
  converg := converg and (test<epsilon);
 end;
 converg :=    converg and (iter>0)
         and (abs((phold-ph)/(N-N_Par_free-1))<1E-6)
         or (iter=40)
         or (lambdastart=0);   { Linear fit }

 pars := pars1;          { Store new parameters in Pars }
 d := d1;              { Save old delta too, if step is too far }
 iter := iter+1;         { Next iteration }
 chi2 := ph/(N-N_par_free-1);
 if keypressed then
 begin
  fit_ok := false;
  F_Error := 4;
  goto exit;
 end;

 until converg;

 eval_errors;

 exit:
  i := N_fit*8;
  move(xprim[1],x[1],i);          { Restore original data }
  move(yprim[1],y[1],i);
 end;

 end.
```

Unit COMPLX;

```
{$N+}

interface

Uses Types;  { Msp contains table for FAK(n) }

function Z_COMPLEX (re ,im: extended): complex;
function RE (z:complex):extended;
function IM (z:complex):extended;
function FEXP (r: extended):extended;
function POT (x: extended; n: integer): extended;
function ERFC (z: extended): extended;
function IERFC (z: extended): extended;
function FACU (n: integer): extended;

implementation

type cmplx = record
         len : byte;
         im,re: extended;
```

```
        end;

  function Z_COMPLEX(re,im: extended): complex;

  var z: complex;
  begin
   z[0] := #16;
   move(im,z[1],16);
   Z_Complex := z;
  end;

  function RE (z:complex):extended;
  var r: cmplx absolute z;
  begin
   re := r.re;
  end;

  function IM (z:complex):extended;
  var r: cmplx absolute z;
  begin
   IM := r.im;
  end;

  function FEXP (r: extended):extended;
  begin
   if r< -5.75E2 then fexp := 0
   else fexp := exp(r);
  end;


  function POT (x: extended; n: integer): extended;
  begin
   if (x=0) then pot := 0
   else
    if x<0 then pot := -fexp(n*ln(abs(x)))
    else pot := fexp(n*ln(x));
  end;

  function ERFC (z: extended): extended;

  const p = 0.327591;
  var y,e: extended;

  begin
   y := 1/(1+p*abs(z));
   e := (((1.06141*y-1.45315)*y+1.42141)*y-0.284497)*y+0.25483;
   if z>7396 then e := 0
    else e := e*y*fexp(-z*z);
   if z<0 then e := 2-e;
   erfc := e;
  end;

  function IERFC (z:extended): extended;

  const pi = 3.141692654;
        q = 0.88623;
       eps = 5e-19;

  var   i,k : integer;
        res,
       res1,
       res2,
```

```
    sum1,
    sum2,
   tempres: extended;

 begin
  sum1:= 0;
  sum2:= 0;
  res:= 0;
  k:= -1;
  repeat
   k:= k+1;
   res1:= (k+0.5)*pi/q*pot(z,round(2*k))/facu(k);
   res2:= pot(z,round(2*k))/facu(k);
   writeln('k1: ',k,' res1 ', res1,' res2:  ',res2);
   sum1:= sum1+res1;
   sum2:= sum2+res2;
   tempres:= res-sum1;
   res:= sum1;
  until abs(tempres) < eps;

  ierfc:= exp(-sqr(z))/(2*q)*sum1-z*exp(-sqr(z))*sum2;
 end;


 function FACU (n: integer): extended;

 var i : integer;
    j : extended;
 begin
  j:= n;
  if n=0 then facu:= 1
  else
   begin
    for i:= n downto 2 do
     j:= j*(i-1);
    facu:= j;
   end;
 end;
 end.


 UNIT FadeUnit;

 INTERFACE

 PROCEDURE IntenDown(d:BYTE);
 PROCEDURE IntenUp  (d:BYTE);
 { senkt/erhöht die Helligkeit - d ist die
   Wartezeit zwischen zwei Einstellungen }

 PROCEDURE SetInten(b:BYTE);
 { setzt die Helligkeit auf b/63-tel }

 IMPLEMENTATION

 USES Crt,DOS;

 CONST PelIdxR =$3C7;  { Port zum Lesen }
     PelIdxW =$3C8;  { Port zum Schreiben }
     PelData =$3C9;  { Datenport }
     MaxReg  =63;    { bei Grafik auf 255 ändern }
     MaxInten=63;
```

```
 VAR  col:ARRAY[0..MaxReg] OF RECORD r,g,b:BYTE END;
 { originale Farbregister-Werte }

 PROCEDURE GetCol(ColNr:BYTE;VAR r,g,b:BYTE);
 { ermittelt die Zusammensetzung einer Farbe }
 BEGIN
  Port[PelIdxR]:=ColNr;
  r:=Port[PelData];g:=Port[PelData];b:=Port[PelData];
 END;

 PROCEDURE SetCol(ColNr,r,g,b:BYTE);
 { setzt die Zusammensetzung einer Farbe }
 BEGIN
  Port[PelIdxW]:=ColNr;
  Port[PelData]:=r;Port[PelData]:=g;Port[PelData]:=b;
 END;

 PROCEDURE InitCol;
 { Übernahme des Anfangsbelegung }
 VAR i:BYTE;
 BEGIN
  FOR i := 0 TO MaxReg DO
    GetCol(i,col[i].r,col[i].g,col[i].b);
 END;

 PROCEDURE SetInten(b:BYTE);
 { setzt die Helligkeit auf b/63-tel }
 VAR i:BYTE; fr,fg,fb:BYTE;
 BEGIN
  FOR i:=0 TO MaxReg DO BEGIN
    fr:=col[i].r*b DIV MaxInten;
    fg:=col[i].g*b DIV MaxInten;
    fb:=col[i].b*b DIV MaxInten;
    SetCol(i,fr,fg,fb);
  END;
 END;

 PROCEDURE IntenDown(d:BYTE);
 VAR i:BYTE;
 BEGIN
  FOR i:=MaxInten DOWNTO 0 DO BEGIN
    SetInten(i); Delay(d)
  END;
 END;

 PROCEDURE IntenUp(d:BYTE);
 VAR i:BYTE;
 BEGIN
  FOR i:=0 TO MaxInten DO BEGIN
    SetInten(i); Delay(d)
  END;
 END;

 BEGIN
  InitCol
 END.


 UNIT Dialog;
```

```
INTERFACE

USES CRT, DOS;

Procedure warten;
Procedure Piepton;
Function Tab (Spalte: BYTE): CHAR;
Function Vtab (Zeile: BYTE): CHAR;
Function xy (x, y: BYTE): CHAR;
Procedure Vln (Zeile, Spalte, Laenge: BYTE);
Procedure Hln (Zeile, Spalte, Laenge: BYTE);
Procedure Kreuz (Zeile, Spalte, HBreite, Laenge:Byte);
Function inv: CHAR;
Function invinv: Char;
Function bli: Char;
Function blioff: Char;
Function _: CHAR;
Function dkl: Char;
Function nrm: Char;
Procedure Fenster (Zeile, Spalte, breit, tief: BYTE);
Procedure Rahmen (Zeile, Spalte, Breite, Tiefe: BYTE);
Procedure invscr;
Var
 Eingabe_beendet: BOOLEAN;
Procedure zEingabe (var r: REAL);
 TYPE
  Information = String[79];
Procedure Statuszeile (Info: Information);
Procedure loesch_Statuszeile;
Function Zeit: real;
VAR
 alta, altc: BYTE;

IMPLEMENTATION

PROCEDURE warten;
 var a:char;
 Begin a:= Readkey end;

Procedure Piepton;
 Begin Write (chr(7)) end;

FUNCTION Tab (Spalte: Byte): Char;
 Begin
  Write(' '); Tab:= CHR(8);
  GotoXY(Spalte+1, WhereY)
 end;

FUNCTION Vtab (Zeile: BYTE): CHAR;
 Begin
  Write(''); Vtab:= chr(10);
  GotoXY (WhereX, Zeile-1)
 end;

FUNCTION xy (x, y: BYTE): CHAR;
 Begin Write (''); GotoXY(x+1,y); xy:= CHR(8) end;

Procedure Vln (Zeile, Spalte, Laenge: BYTE);
 Var
 i: BYTE;
Begin
 For i:= 0 to Laenge-1 Do Begin
```

```
    Gotoxy (Spalte, Zeile + i);
    Write(CHR(179))
   end
  end;

 Procedure Hln (Zeile, Spalte, Laenge: BYTE);
  Var
  i: BYTE;
 Begin
  Gotoxy (Spalte, Zeile);
  For i:= 1 to Laenge Do Write(CHR(196))
 end;

 Procedure Kreuz (Zeile, Spalte, HBreite, Laenge:Byte);
  var
   i: byte;
 Begin
   Vln(Zeile, Spalte, Laenge);
   Hln(Zeile+1, Spalte-HBreite, 2*HBreite+1);
   GotoXY(Spalte, Zeile+1);Writeln(chr(197));
 end;


 Function Inv: CHAR;
  Begin
   Write(''); TEXTCOLOR (BLACK);
   TEXTBACKGROUND(WHITE); Inv:= XY(WhereX, WhereY);
  end;

 Function InvInv: CHAR;
  Begin
   Write(''); TEXTCOLOR (WHITE);
   TEXTBACKGROUND(BLACK); InvInv:= XY(WhereX, WhereY);
  end;

 FUNCTION Bli: CHAR;
  Begin
   Write(''); TEXTCOLOR (15+16); Bli:= XY(WhereX, WhereY);
  end;

 FUNCTION BliOff: CHAR;
  Begin
   Write(''); TEXTCOLOR (15); BliOff:= XY(WhereX, WhereY);
  end;

 FUNCTION _: CHAR;
  Begin
   Write(''); TEXTCOLOR (9); _:= XY(WhereX, WhereY);
  end;

 FUNCTION dkl: CHAR;
  Begin
   Write(''); LOWVIDEO; dkl:= XY(WhereX, WhereY);
  end;

 FUNCTION nrm: CHAR;
  Begin
   Write(''); TEXTCOLOR(WHITE);
   TEXTBACKGROUND(BLACK); nrm:= XY(WhereX, WhereY);
  end;

Procedure Fenster (Zeile, Spalte, breit, tief: BYTE);
```

```
  var
   i: BYTE;
  Begin
   WINDOW(Spalte, Zeile, Spalte+breit-1, Zeile+tief-1);
  end;

 Procedure Rahmen (Zeile, Spalte, Breite, Tiefe: BYTE);
  CONST
   obenlinks  =#218;
   obenrechts =#191;
   untenlinks =#192;
   untenrechts=#217;

  var
   x,y,sx,sy: BYTE;
  Begin
   x:= Spalte; Y:= Zeile; sx:= Breite; sy:= Tiefe;
   GotoXY(x,y+sy-1); Write(untenlinks);
   GotoXY(x+sx-1,y+sy-1); Write(untenrechts);
   GotoXY(x,y);
   if (x+sx-1=80) and (y+sy-1=25) then INSLINE;
   Write (obenlinks);
   GotoXY(x+sx-1,y); Write(obenrechts);
   hln(y,x+1,sx-2); hln(y+sy-1,x+1,sx-2);
   vln(y+1,x,sy-2); vln(y+1,x+sx-1,sy-2); Write(obenrechts);
   GotoXY (x+1,y+1)
  end;

PROCEDURE invscr;
 Begin Write (inv, CHR(8)); clrscr end;

PROCEDURE zEingabe (var r:real);
 var
  c,p,q,l: Integer;
  s: String[18];
 Begin
  p:= WhereX; q:= WhereY;
  REPEAT
   s:= ''; Readln(s); VAL (s,r,c); l:= LENGTH(s);
   if (c<>0) and (l<>0) then Begin
    GotoXY(p,q); Write(' ':l); GotoXY(p,q);
   end
  UNTIL (c=0) or (l=0);
  IF l = 0 then Eingabe_beendet:= true
  ELSE Eingabe_beendet:= false;
  GotoXY (p+l+2,q)
 end;

PROCEDURE Statuszeile (Info: Information);
 VAR
  Zeile, Spalte, l, d: Integer;
 Begin
  l:= LENGTH (Info); d:= (79-l) DIV 2;
  TEXTCOLOR(0); TEXTBACKGROUND(15);
  Zeile:= WhereY; Spalte:= WhereX;
  GotoXY(1,25); Write(' ':d, Info, ' ':d);
  NORMVIDEO; GotoXY(Spalte, Zeile)
 end;

PROCEDURE LOESCH_STATUSZEILE;
 VAR
  Zeile, Spalte: Integer;
```

```
   Begin
    Zeile:= WhereY; Spalte:= WhereX;
    GotoXY(1,25); Write(' ':79);
    GotoXY(Spalte, Zeile)
   end;

FUNCTION Zeit: Real;
 Var
  Std, min, sec, hsec: Word;
 Begin
  Gettime (Std, min, sec, hsec);
  Zeit:= std*3600+min*60+sec+hsec/100
 end;
end.
```

Appendix IV Colloquia, Lectures and Seminar from Invited Speakers

1991

January 15	Dr. B.J. Alder, Lawrence Livermore Labs., California Hydrogen in all its Glory
January 31	Dr. P. Sarre Nottingham University Comet Chemistry
January 24	Dr. P.J. Sadler, Birkbeck College London Design of Inorganic Drugs: Precious Metals, Hypertension + HIV
January 31	Dr. D. Lacey, Hull University Liquid Crystals
February 6	Dr. R. Bushby, Leeds University Biradicals and Organic Magnets
February 6	Dr. M.C. Petty, Durham University Molecular Electronics
February 20	Prof. B.L. Shaw, Leeds University Syntheses with Coordinated, Unsatturated Phosphine Ligands
February 28	Dr. J. Brown, Oxford University Can Chemistry Provide Catalysts Superior to Enzymes
March 6	Dr. C.M. Dobson, Oxford University NMR Studies of Dynamics in Molecular Crystals
March 7	Dr. J. Markam, ICI Pharmaceuticals DNA Fingerprinting
April 24	Prof R.R. Schrock, Massachusetts Instutute of Technology Metal-ligand Multiple Bonds and Metathesis Initiator
June 20	Prof. M.S. Brookhart, University of N. Carolina Olefin Polymerisations, Oligomerisations and Dimerisations Using Electrophilic Late Transition Metal Catalysts
July 29	Dr. M.A. Brimble, Massey University, New Zealand

Synthesis Studies Towards the Antibiotic Griseusin-A

September 16 Dr. A.C. Griffin, University of Cambridge
Photoactive Liquid Crystalline Polyacrylcinnamates

October 17 Dr. J.A. Salthouse, University of Manchester
Son et Lumiere - a demonstration lecture

October 31 Dr. R. Keeley, Metropolitan Police
Forensic Science Modern forensic sience

November 6 Prof. B.F.G. Johnson, Edinburgh University
Cluster-surface analogies

November 7 Dr. A.R. Butler, St. Andrews University
Traditional Chinese herbal drugs: a different w ay of treating disease

November 13 Prof. D. Gani, St. Andrews University
The chemistry of PLP-dependent enzymes

November 20 Dr. R. More O'Ferrall, University College, Dublin Some acid-catalysed rearrangements in organic chemistry

November 28 Prof. I.M. Ward, IRC in Polymer Science, University of Leeds
The SCI lecture: the science and technology of orientated polymers

December 4 Prof. R. Grigg, Leeds University
Palladium-catalysed cyclisation and ion-capture processes

December 5 Prof. A.L. Smith, ex Unilever
Soap, detergents and black puddings

December 11 Dr. W.D. Cooper, Shell Research
Colloid science: theory and practice

1992

January 22 Dr. K.D.M. Harris, St. Andrews University
Understanding the properties of solid inclusion compounds

January 29 Dr. A. Holmes, Cambridge University
Cycloaddition reactions in the service of the synthesis of piperidine and indolizidine natural products

January 30 Dr. M. Anderson, Sittingbourne Research

Centre Shell Research
Recent Advances in the Safe and Selective Chemical Control of Insect Pests

February 12 Prof. D.E. Fenton, Shefield University
Polynuclear complexes of molecular clefts as models for copper biosites

February 13 Dr. J. Saunders, Glaxo Group Research Limited
Molecular Modelling in Drug Discovery

February 19 Prof. E.J. Thomas, Manchester University
Applications of organostannanes to organic synthesis

February 20 Prof. E.Vogel, University of Cologne
The Musgrave Lecture
Porphyrins: Molecules of Interdisciplinary Interest

February 25 Prof. J.F. Nixon, Univessity of Sussex
The Tilden Lecture
Phosphaalkynes: new building blocks in inorganic and organometallic chemistry

February 26 Prof. M.L. Hitchman, Strathclyde University
Chemical vapour deposition

March 5 Dr. N.C. Billingham, University of Sussex
Degradable Plastics - Myth or Magic?

March 11 Dr. S.E. Thomas, Imperial College
Recent advances in organoiron chemistry

March 12 Dr. R.A. Hann, ICI Imagedata
Electronic Photography - An Image of the Future

March 18 Dr. H. Maskill, Newcastle University
Concerted or stepwise fragmentation in a deamination-type reaction

March 25 Prof. H. Cherdron, Hoechst AG, Centrale Polymerforschung, Frankfurt a. M.
Structural Concepts and Synthetic Methods in Industrial Polymer Science

April 7 Prof. D.M. Knight, Philosophy Department, University of Durham
Interpreting experiments: the beginning of electrochemistry

May 13	Dr. J-C Gehret, Ciba Geigy, Basel Some aspects of industrial agrochemical research
September 17	Prof. D. Fisher, University of Hamburg From Organo-f-element Systems to Organo-main-group Polymers
September 17	Prof. E.L. Thomas, Massachusetts Instutute of Technology, Cambridge, Massachusetts Interface Structures in Copolymer/ Homopolymer Blends
October 15	Dr M. Glazer & Dr. S. Tarling, Oxford Universitv & Birbek College, London It Pays to be British! - The Chemist's Role as an Expert Witness in Patent Litigation
October 20	Dr. H.E. Bryncza, Du Pont Central Research Synthesis, Reactions and Thermochemistry of Metal (Alkyl) Cyanide Complexes and Their Impact on Olefin Hydrocyanation Catalysis
October 22	Prof. A. Davies University College London The lngold-Albert Lecture The Behaviour of Hydrogen as a Pseudometal
October 28	Dr. J.K. Cockcroft, Universitv of Durham Recent Developments in Powder Diffraction
October 29	Dr. J. Emsley, Imperial College, London The Shocking History of Phosphorus
November 4	Dr. T.P. Kee, University of Leeds Synthesis and Coordination Chemistry of Silylated Phosphites
November 5	Dr. C.J. Ludman, University of Durham Explosions, A Demonstration Lecture
November 11	Prof. D. Robins, Glasgow Universitv Pyrrolizidine Alkaloids: Biological Activity, Biosynthesis and Benefits
November 12	Prof. M.R. Truter, University College,London Luck and Logic in Host - Guest Chemistry
November 18	Dr. R. Nix, Queen Mary College, London Characterisation of Heterogeneous Catalysts
November 25	Prof. L. D. Quin, University of Massachusetts, Amherst Fragmentation of Phosphorous Heterocycles as

a Route to Phosphoryl Species with Uncommon Bonding

November 26 Dr. D. Humber, Glaxo, Greenford
AIDS - The Development of a Novel Series of Inhibitors of HIV

December 2 Prof. A.F. Hegarty, University College, Dublin
Highly Reactive Enols Stabilised by Steric Protection

December 2 Dr. R.A. Aitken, Universitv of St. Andrews
The Versatile Cycloaddition Chemistry of $Bu_3P{\cdot}CS_2$

December 3 Prof. P. Edwards, Birmingham University
The SCI Lecture - What is Metal?

December 9 Dr. A.N. Burgess, ICf Runcorn
The Structure of Perfluorinated Ionomer Membranes

1993

January 20 Dr. D. C. Clary, University of Cambridge
Energy Flow in Chemical Reactions

January 21 Prof. L. Hall, Cambridge
NMR - Window to the Human Body

January 27 Dr. W. Kerr, University of Strathclyde
Development of the Pauson-Khand ,Annulation Reaction : Organocobalt Mediated Synthesis of Natural and Unnatural Products

January 28 Prof. J. Mann, University of Reading
Murder, Magic and Medicine

February 3 Prof. S.M. Roberts, University of Exeter
Enzymes in Organic Synthesis

February 10 Dr. D. Gillies, University of Surrey
NMR and Molecular Motion in Solution

February 11 Prof. S. Knox, Bristol University
The Tilden Lecture Organic Chemistry at Polynuclear Metal Complexes

February 17 Dr. R.W. Kemmitt, University of Leicester
Oxatrimethylenemethane Metal Complexes

February 18 Dr. I. Fraser, ICI Wilton
Reactive Processing of Composite Materials

February 22 Prof. D.M. Grant, University of Utah
Single Crystals, Molecular Structure, and Chemical-Shift Anisotropy

February 24 Prof. C.J.M. Stirling, University of Sheffield
Chemistry on the Flat-Reactivity of Ordered Systems

March 10 Dr. P.K. Baker, University College of North Wales, Bangor
'Chemistry of Highly Versatile 7-Coordinate Complexes $[MI_2(CO)_3(NCMe)_2]$ (M=Mo,W)'

March 11 Dr. R.A.Y. Jones, University of East Anglia
The Chemistry of Wine Making

March 17 Dr. R.J.K. Taylor, University of East Anglia
Adventures in Natural Product Synthesis

March 24 Prof. I.O. Sutherland, University of Liverpool
Chromogenic Reagents for Cations

April 1 Prof. H. Spiess, Max Planck Institut für Polymerforschung
Multidimensional NMR Study of Structure and Dynamics of Polymers

May 13 Prof. J.A. Pople, Carnegie-Mellon University, Pittsburgh, USA
The Boys-Rahman Lecture
Applications of Molecular Orbital Theory

May 21 Prof. L. Weber, University of Bielefeld
Metallo-phospha Alkenes as Synthons in Organometallic Chemistry

June 1 Prof. J.P. Konopelski, University of California, Santa Cruz
Synthetic Adventures with Enantiomerically Pure Acetals

June 2 Prof. F. Ciardelli, University of Pisa
Chiral Discrimination in the Stereospecific Polymerisation of Alpha Olefins

June 7 Prof. R.S. Stein, University of Massachusetts
Scattering Studies of Crystalline and Liquid Crystalline Polymers

June 16 Prof. A.K. Covington, University of Newcastle
Use of Ion Selective Electrodes as Detectors in lon Chromatography

June 17 Prof. O.F. Nielson, H.C. Ørsted Institute, University of Copenhagen
Low-Frequency IR- and Raman Studies of Hydrogen Bonded Liquids